Simulation of hydration and microstructure development of blended cements

Gao, Peng

DOI
10.4233/uuid:5bb2f97b-55f7-4afa-b6f4-f18f16543273

Publication date
2018

Document Version
Final published version

Citation (APA)
Gao, P. (2018). *Simulation of hydration and microstructure development of blended cements*. [Dissertation (TU Delft), Delft University of Technology]. https://doi.org/10.4233/uuid:5bb2f97b-55f7-4afa-b6f4-f18f16543273

Simulation of hydration and microstructure development of blended cements

Dissertation

for the purpose of obtaining the degree of doctor
at Delft University of Technology
by the authority of the Rector Magnificus prof.dr.ir. T.H.J.J van der Hagen
chair of the Board for Doctorates
to be defended publicly on
Tuesday 12 June 2018 at 10:00 o'clock

by

Peng GAO

Master of Science in Materialogy, South China University of Technology, China
born in Chongqing, China

This dissertation has been approved by the promotors.

Composition of the doctoral committee:

Rector Magnificus	chairman
Prof. dr. ir. K. van Breugel	Delft University of Technology, promotor
Prof. J.X. Wei	South China University of Technology, China, promotor
Dr. G. Ye	Delft University of Technology, copromotor

Independent membranes

Prof. dr. ir. T.J.H. Vlugt	Delft University of Technology
Prof. dr. ir. G. De Schutter	Ghent University, Belgium
Dr. J.S. Dolado	TECNALIA Research & Innovation, Spain
Prof. dr. ir. E. Schlangen	Delft University of Technology

The doctoral research has been carried out in the context of an agreement on joint doctoral supervision between South China University of Technology, China and Delft University of Technology, the Netherlands.

ISBN: 978-94-6366-045-7

Keywords: hydration, microstructure, simulation, pore solution chemistry, porosity, slag, fly ash.

Printing: Gildeprint Drukkerijen, The Netherlands.

Cover design: Peng GAO and Wenhao GUO

Printed in the Netherlands.

To my parents

List of contents

Summary

For optimization of the use of Supplementary Cementitious Materials (SCMs), i.e. blast furnace slag (BFS) and fly ash (FA), in cementitious system a numerical model for simulating the hydration and microstructure development of blended cements can be used. Several models have been proposed in recent years to simulate the hydration and microstructure development of blended cements. However, most of these models need further development. For example, the nucleation and growth of calcium hydroxide (CH) particles were often not simulated explicitly in these models. Moreover, the influence of pore solution chemistry on the reaction rate of SCMs was not quantified (see Chapter 2). This study aims to extend one of the previously proposed numerical models for pure Portland cement (PC), i.e. HYMOSTRUC3D, to simulate the hydration and microstructure development of blended cement pastes. HYMOSTRUC3D is based on the original HYMOSTRUC model developed by Van Breugel *[1991]* and later extended by Koenders *[1997]* and Ye *[2003]* to simulate the reaction process and formation of microstructure in hydrating pure PC. The rate of cement hydration was simulated as a function of the chemistry and particle size distribution of the cement, the water content and distribution of water in the pore system and the temperature of the system. HYMOSTRUC3D has been used to simulate the evolution of materials properties of cement-based materials, such as strength and stiffness of cement paste, autogenous shrinkage and transport properties of cement paste (see Chapter 2). The extended HYMOSTRUC3D model is called HYMOSTRUC3D-E. HYMOSTRUC3D-E comprises two routes: the *cement hydration route* (see Chapter 3) and the *microstructure development route* (see Chapter 4).

The *cement hydration route* concentrates on the extension of the hydration module of HYMOSTRUC3D. The stoichiometry of the reactions of PC, BFS and FA particles in blended cement pastes is dealt with. The reaction kinetics of PC, BFS and FA particles in blended cement pastes are discussed. At early age all the particles of PC, BFS and FA are assumed to follow a *phase-boundary reaction*. At later-ages all the particles of PC, BFS and FA are assumed to follow a *diffusion-controlled reaction.* With the reaction kinetic of *phase-boundary reaction* and *diffusion-controlled reaction*, the reaction rates of PC, BFS and FA particles are calculated as a function of the chemistry and particle size distribution of these powders, the water content, the pore solution chemistry and the temperature of the system.

In *the cement hydration route* a module is proposed for simulating the pore solution chemistry of blended cement pastes (see section 3.3). The concentrations of Na^+ and K^+ ions are calculated using Taylor's method. The concentrations of Ca^{2+}, SO_4^{2-} and OH^- ions are calculated from the solubility equilibria of CH and gypsum and the electrical neutrality of the pore solution.

The *microstructure development route* deals with the extension of the microstructure module of HYMOSTRUC3D. A representative elementary volume (REV) of cement paste is defined. Next, the initial spatial distribution of particles in the fresh paste is simulated by

random packing the PC, BFS and FA particles in the REV. Then, by letting these PC, BFS and FA particles grow, the microstructure development of blended cement paste is simulated. The thickness of the growing shell of reaction product depends on the degree of hydration of blended cement obtained in the *cement hydration route*. A module is proposed to simulate the nucleation and growth of CH particles (see section 4.2.3). In the *microstructure development route* the evolution of the capillary porosity is simulated as well (see section 4.3.2). Specific porosities are assigned to the inner and outer products. By determining the volume evolution of the inner and outer products in cement paste, the contribution of gel pores to total porosity of cement paste is quantified.

In chapter 5 the HYMOSTRUC3D-E model for simulating the hydration process and microstructure development of PC paste (section 5.2), the hydration process, pore solution chemistry and porosity of slag cement pastes (section 5.2), the hydration process, porosity and CH contents of fly ash cement pastes (section 5.3) and the chemical shrinkage of PC, slag cement and fly ash cement (section 5.4) are validated. From this study the following conclusions can be drawn:

1. Degree of hydration

For the mixtures with different w/c and different initial content of BFS and FA, the simulated degree of hydration (or reaction) of PC, BFS and FA is compared with experimental data. In HYMOSTRUC3D-E, the influence of the mineral composition of PC on the hydration of PC is taken into account using the initial penetration rates of the reaction front K_0 and the transition thicknesses δ_{tr} for each mineral, i.e. C_3S, C_2S, C_3A and C_4AF, in PC particles. In addition, the influence of BFS or/and FA on the hydration of PC and the effect of the w/b on the hydration, or reaction, of PC, BFS, and FA are quantified by further detailing of the reduction factors Ω_1, Ω_2 and Ω_3 of HYMOSTRUC3D, which factor allows for the changes of the water distribution and changes in pore water chemistry in the system. The effect of the pore solution chemistry on the pozzolanic reaction of BFS and FA is quantified using a pH-factor M_{pH}. With these extensions of the original simulation model, the hydration process of cements with different components, such as different amounts of PC, BFS and FA, and different w/b, could be simulated.

2. Pore structure

For pure Portland cement paste (w/c = 0.4), the simulated capillary pore size distributions at the age from 1 day to 28 days are in good agreement with those obtained using SEM image analysis. The simulated total porosity is larger than the porosity measured using MIP. This is because the small gel pores, i.e. gel pores < 4 nm, cannot be measured by MIP, whereas in HYMOSTRUC3D-E all pores are considered. The second reason is that MIP cannot detect the isolated pores, whereas HYMOSTRUC3D-E gives all pores. This difference also occurs in slag cement systems (w/b = 0.4 and BFS content from 30% to 70%), fly ash cement systems (w/b = 0.4 initial FA content ranges from 30% to 50%).

3. Pore solution chemistry

For a pure Portland cement paste (w/c = 0.4) and slag cement pastes (w/b = 0.4, BFS content ranges from 30% to 70%), the simulated concentrations of alkali ions (Na^+ and K^+) in

the pore solution are close to the experimental data. However, the simulated concentrations of Ca^{2+} and SO_4^{2-} differ from the experimental data. This is probably because the actual Ca^{2+} in the pore solution are supersaturated at early age (see section 4.2.3), which cannot be calculated accurately with *only* the concept of solubility equilibrium. Another possible reason is an inadequate consideration of the solubility equilibria of hydration products containing calcium. In HYMOSTRUC3D-E it is assumed that the concentration of Ca^{2+} ions *only* depends on the solubility equilibria of gypsum and CH. In reality, the concentration of Ca^{2+} ions is also affected by the solubility equilibria of other phases in the cement paste, such as AFt, AFm, CSH. The concentrations of Ca^{2+} and SO_4^{2-} are much lower than the concentrations of alkali ions. The relatively low accuracy of the simulated concentrations of Ca^{2+} and SO_4^{2-} will not significantly affect the accuracy of the simulated pH values. Hence, the trends of the simulated evolution of the pH of the pore solution and the experimental data are in fairly good agreement.

4. Chemical shrinkage

The chemical shrinkage of PC pastes with w/c = 0.3 and 0.4, slag cement paste with w/b = 0.31 and fly ash cement paste with w/b = 0.33 are simulated with HYMOSTRUC3D-E. The simulated chemical shrinkage of the PC-pastes is in good agreement with the experimental results at early age, i.e. during the first 1 day. At later age, i.e. after 1 day, the simulated chemical shrinkage is larger than the experimental results. The reason for this is that for measuring chemical shrinkage transport of water into the cement paste is needed, which becomes difficult at later age (see section 5.5.4). This difference also occurs in the slag cement paste and the fly ash cement paste. For the same total degree of hydration of (the blended) cement (i.e. degree of conversion of the powders into reaction product), both slag cement and fly ash cement show larger chemical shrinkage than pure PC, because the chemical shrinkage of PC for complete hydration is smaller than the chemical shrinkage BFS and FA for complete reaction (see Table 5.12).

5. Nucleation and growth of CH particles

For a pure Portland cement system (w/c = 0.4), the cumulative particle size distribution of CH particles simulated by HYMOSTRUC3D-E is close to the experimental data, at least for small CH-particle, i.e. < 3.4 μm. For large CH-particles, i.e. > 3.4 μm, the cumulative particle size distribution of CH particles simulated by HYMOSTRUC3D-E differs from the experimental data. This is because the pore structure simulated by HYMOSTRUC3D-E does not contain the big pores, i.e. the pores > 10 μm (limitation due to the size of the REV of cement paste). In reality these big pores exist in the cement paste, and they provide room for the growth of large CH particles.

There is still further room to improve and extend HYMOSTRUC3D-E model:

1. Simulation of pore solution chemistry

The concentrations of Na^+, K^+, OH^- simulated by HYMOSTRUC3D-E show trends similar to experimental data. However, the accuracy of the simulation of the concentrations of Ca^{2+} and SO_4^{2-} is relatively low. Moreover, the concentrations of the ions, such as Mg^{2+}, $Al(OH)^{4-}$,

$SiO(OH)^{3-}$, are not simulated in HYMOSTRUC3D-E. It is recommended to further consider the equilibrium of hydration products, such as AFt, AFm and CSH gel etc., in the pore solution to simulate the concentrations of the ions like Ca^{2+}, SO_4^{2-}, Mg^{2+}, $Al(OH)^{4-}$, $SiO(OH)^{3-}$, etc., more accurately.

2. Nucleation and growth of hydration products, such as AFt and AFm

In the 3D microstructure simulated by HYMOSTRUC3D the hydration products, such as CSH gel, CH, AFt, AFm, etc., are considered as one gel phase. In comparison with HYMOSTRUC3D, HYMOSTRUC3D-E distinguishes between CSH and CH, and explicitly simulates the nucleation and growth of CH particles in the pore space. In further study, it is recommended to simulate the nucleation and growth of AFt and AFm particles in the pore space.

Samenvatting

Voor optimalisatie van het gebruik van cement vervangende poeders (Supplementary Cementitious Materials; SCM's), zoals hoogovenslakken (BFS) en vliegas (FA), kan gebruik worden gemaakt van een numeriek model voor het simuleren van het hydratatieproces en microstructuurontwikkeling van samengestelde cementen. Verschillende modellen zijn de afgelopen jaren voorgesteld om de hydratatie en microstructuurontwikkeling van cementgebonden materialen te simuleren. De meeste van deze modellen moeten echter verder worden ontwikkeld. Kiemvorming en groei van calciumhydroxide(CH)-deeltjes worden bijvoorbeeld in deze modellen vaak niet expliciet gesimuleerd. Bovendien wordt de invloed van de chemische samenstelling van het poriewater op de reactiesnelheid van SCM's niet gekwantificeerd (zie hoofdstuk 2). Deze studie beoogt een van de eerder voorgestelde numerieke simulatiemodellen voor Portlandcement (PC), te weten HYMOSTRUC3D, uit te breiden om de hydratatie en microstructuurontwikkeling van samengestelde cementen te simuleren. HYMOSTRUC3D is gebaseerd op het originele HYMOSTRUC-model, ontwikkeld door Van Breugel *[1991]* en later uitgebreid door Koenders *[1997]* en Ye *[2003]*, om het reactieproces en de vorming van microstructuur bij het hydrateren van Portlandcement te simuleren. In dit model wordt de snelheid van het hydratatieproces gesimuleerd als functie van de chemie en korrelverdeling van het cement, het watergehalte en de verdeling van water in het poriënsysteem en de temperatuur van het systeem. HYMOSTRUC3D is gebruikt om de ontwikkeling van materiaaleigenschappen van cementgebonden materialen te simuleren, zoals sterkte en stijfheid van cementsteen, autogene krimp en transporteigenschappen van cementsteen (zie hoofdstuk 2). Het uitgebreide HYMOSTRUC3D-model wordt HYMOSTRUC3D-E genoemd. HYMOSTRUC3D-E omvat twee routes: de cementhydratatieroute (zie hoofdstuk 3) en de route voor de ontwikkeling van microstructuren (zie hoofdstuk 4).

De *cementhydratatieroute* concentreert zich op de uitbreiding van de hydratatiemodule van HYMOSTRUC3D. De stoichiometrie van de reacties en de reactiekinetiek van PC-, BFS- en FA-korrels in samengestelde cementen worden behandeld. Aangenomen wordt dan in het begin van de reactie alle PC-, BFS- en FA-korrels reageren volgens een oppervlaktereactie, terwijl op latere leeftijd de reacties verlopen volgens een diffusie-gecontroleerde reactie. Uitgaande van de oppervlaktereacties en de diffusie-gecontroleerde reacties, worden de reactiesnelheden van PC-, BFS- en FA-korrels berekend als functie van de chemie en korrelverdeling van deze poeders, het watergehalte, de chemie van het poriënwater en de temperatuur van het systeem.

In de *cementhydratatieroute* wordt een module voorgesteld voor het simuleren van de chemische samenstelling van het poriënwater van samengestelde cementen (zie paragraaf 3.3). De concentraties van Na^+- en K^+-ionen worden berekend met behulp van de Taylor-methode. De concentraties van Ca^{2+}, SO_4^{2-} en OH^--ionen worden berekend uit de oplosbaarheidsevenwichten van CH en gips en de elektrische neutraliteit van het poriënwater.

De *microstructuurontwikkelingsroute* heeft betrekking op de uitbreiding van de microstruc-tuurmodule van HYMOSTRUC3D. Een representatief elementair volume (REV) van cementsteen wordt gedefinieerd. Vervolgens wordt de initiële ruimtelijke verdeling van korrels in de verse cementpasta gesimuleerd door de PC-, BFS- en FA-korrels willekeurig in de REV te plaatsen. Door de korrels te laten 'groeien', wordt de microstructuurontwikkeling gesimuleerd en ontstaat een cementsteen. De dikte van de groeiende schil van het reactieproduct hangt af van de mate van hydratatie van het samengestelde cement zoals berekend in de *cementhydratatieroute*. Verder is een module ontwikkeld om de kiemvorming en groei van CH-deeltjes te simuleren (zie paragraaf 4.2.3).

In de *microstructuurontwikkelingsroute* wordt ook de ontwikkeling van de *capillaire* porositeit gesimuleerd (zie paragraaf 4.3.2). Aan het zogenaamde 'inner product' en 'outer product' worden karakteristieke porositeiten toegekend. Door de volumetoename te bepalen van het inner en outer product in de cementsteen wordt de bijdrage van *gelporiën* aan de totale porositeit van cementpasta gekwantificeerd.

In hoofdstuk 5 wordt het HYMOSTRUC3D-E-model gevalideerd voor het simuleren van het hydratatieproces en de microstructuurontwikkeling van PC-steen (sectie 5.2), de hydratatie en de chemische samenstelling van het poriënwater en de porositeit van hoogovencement (sectie 5.2), het hydratatieproces, de porositeit en CH-gehalte van vliegascementsteen (punt 5.3) en de chemische krimp van Portlandcement, hoogovencement en vliegascement (paragraaf 5.4). Uit deze studie kunnen de volgende conclusies worden getrokken.

1. Hydratatiegraad

Voor mengsels met verschillende w/c factoren en verschillende percentages hoogovenslak (BFS) en vliegas (FA), is de gesimuleerde hydratatiegraad (of reactiegraad) van PC, BFS en FA vergeleken met experimentele resultaten. In HYMOSTRUC3D-E wordt de invloed van de minerale samenstelling van Portlandcement op de hydratatiesnelheid in aanmerking genomen met behulp van de initiële penetratiesnelheden van het reactiefront K_0 en de overgangsdiktes δ_{tr} voor elk van de klinkercomponenten, t.w. C_3S, C_2S, C_3A en C_4AF. Daarnaast worden de invloed van BFS en/of FA op de hydratatie van PC en het effect van de w/b op de hydratatie, of reactie, van PC, BFS en FA gekwantificeerd door verdere 'verfijning' van de reductiefactoren Ω_1, Ω_2 en Ω_3 van HYMOSTRUC3D, i.c. de factoren die het effect beschrijven van veranderingen in de waterverdeling en de poriewaterchemie in het systeem op de reactiesnelheid. Het effect van de poriewaterchemie op de puzzolane reactie van BFS en FA wordt gekwantificeerd met behulp van een pH-factor M_{pH}. Met deze uitbreidingen van het oorspronkelijke simulatiemodel kan het hydratatieproces van samengestelde cementen met verschillende hoeveelheden PC, BFS en FA, en met verschillende w/b-factoren worden gesimuleerd.

2. Poriënstructuur

Voor zuivere Portlandcementpasta (w/c = 0,4) komen de gesimuleerde capillaire poriëngrootteverdelingen van cementsteen met een ouderdom van 1 dag tot 28 dagen goed overeen met resultaten van SEM-beeldanalyse. De gesimuleerde totale porositeit is groter dan

de porositeit gemeten met behulp van MIP. Dit komt omdat de kleine *gelporiën*, d.w.z. gelporiën <4 nm, niet met MIP kunnen worden gemeten, terwijl in HYMOSTRUC3D-E alle poriën worden beschouwd. De tweede reden is dat MIP de *geïsoleerde* poriën niet kan detecteren, terwijl HYMOSTRUC3D-E ook deze poriën geeft. Dit verschil treedt ook op in hoogovencementen (w/b = 0,4 en BFS-gehalte van 30% tot 70%), vliegascementen (w/b = 0,4 en initieel FA-gehalte variërend van 30% tot 50%).

3. Chemische samenstelling poriewater

Voor een Portlandcementpasta (w/c = 0,4) en een hoogovencementpasta (w/b = 0,4 en slakgehalte variërend van 30% tot 70%), liggen de gesimuleerde concentraties van alkali-ionen (Na^+ en K^+) in de poriënoplossing dicht bij de experimentele resultaten. De gesimuleerde concentraties van Ca^{2+} en SO_4^{2-} verschillen echter van de experimentele resultaten. Dit komt waarschijnlijk omdat de werkelijke Ca^{2+}-concentraties in het poriewater op jonge leeftijd oververzadigd zijn (zie paragraaf 4.2.3) en niet nauwkeurig kan worden berekend uit het oplosbaarheidsevenwicht. Een andere mogelijke reden is een niet adequate beschrijving van de oplosbaarheidsevenwichten van hydratatieproducten die calcium bevatten. In HYMOSTRUC3D-E is de concentratie van Ca^{2+}-ionen alleen afhankelijk van de oplosbaarheidsevenwichten van gips en CH. In werkelijkheid wordt de concentratie van Ca^{2+}-ionen ook beïnvloed door de oplosbaarheidsevenwichten van andere fasen in de cementsteen, zoals AFt, AFm, CSH. De concentraties van Ca^{2+} en SO_4^{2-} zijn veel lager dan de concentraties alkali-ionen. De relatief lage nauwkeurigheid van de gesimuleerde concentraties van Ca^{2+} en SO_4^{2-} zal de nauwkeurigheid van de gesimuleerde pH-waarden niet significant beïnvloeden. Vandaar dat de trends van het gesimuleerde verloop van de pH van het poriënwater vrij goed overeenkomen.

4. Chemische krimp

De chemische krimp van PC-pasta's met w/c = 0,3 en 0,4, hoogovencementpasta's met w/b = 0,31 en vliegascementpasta met w/b = 0,33 zijn gesimuleerd met HYMOSTRUC3D-E. De gesimuleerde chemische krimp van de PC-pasta's komt goed overeen met de experimentele resultaten op jonge leeftijd, d.w.z. gedurende de eerste 1 dag. Op latere leeftijd, d.w.z. na 1 dag, is de gesimuleerde chemische krimp groter dan de experimentele resultaten. De reden hiervoor is dat voor het meten van chemische krimp transport van water in de cementsteen nodig is, wat op latere leeftijd moeilijker wordt (zie paragraaf 5.5.4). Dit verschil treedt ook op bij de hoogovencementen en de vliegascementen. Voor dezelfde 'totale' hydratatie van (het samengestelde) cement (d.w.z. de mate van omzetting van de poeders in reactieproduct), vertonen zowel hoogovencement als vliegascement grotere chemische krimp dan puur PC, omdat de chemische krimp van PC bij volledige hydratatie kleiner is dan de chemische krimp BFS en FA. (zie Tabel 5.12).

5. Nucleatie en groei van CH-deeltjes

Voor een zuiver Portlandcementsysteem (w/c = 0,4) ligt de cumulatieve deeltjesgrootteverdeling van CH-deeltjes, gesimuleerd met HYMOSTRUC3D-E, dicht bij de experimentele resultaten, ten minste voor kleine CH-deeltjes, d.w.z. deeltjes <3,4 μm. Voor grote CH-deeltjes, d.w.z. deeltjes > 3,4 μm, verschilt de cumulatieve deeltjesgrootteverdeling

van CH-deeltjes gesimuleerd met HYMOSTRUC3D-E van de experimentele resultaten. Dit komt omdat de poriënstructuur gesimuleerd met HYMOSTRUC3D-E de grote poriën, d.w.z. poriën > 10 μm, niet meeneemt (beperking vanwege de grootte van de REV). In werkelijkheid zijn deze grote poriën in de cementsteen aanwezig en bieden ze ruimte voor de groei van grote CH-deeltjes.

Het model HYMOSTRUC3D-E kan worden verbeterd en/of uitgebreid op de volgende punten:

1. Simulatie van chemie van het poriewater

De concentraties van Na^+, K^+, OH^- in het poriewater, gesimuleerd door HYMOSTRUC3D-E, vertonen trends die vergelijkbaar zijn met experimentele resultaten. De nauwkeurigheid van de simulatie van de concentraties van Ca^{2+} en SO_4^{2-} is echter relatief laag. Bovendien worden de concentraties van de ionen, zoals Mg^{2+}, $Al(OH)^{4-}$, $SiO(OH)^{3-}$, niet gesimuleerd in HYMOSTRUC3D-E. Het wordt aanbevolen om het evenwicht van hydratatieproducten, zoals AFt, AFm en CSH gel, in het poriewater mee te nemen ten einde de concentraties van ionen zoals Ca^{2+}, SO_4^{2-} , Mg^{2+}, $Al(OH)^{4-}$, $SiO(OH)^{3-}$, etc., nauwkeuriger te simuleren.

2. Nucleatie en groei van hydratatieproducten, zoals AFt en AFm

In de 3D-microstructuur gesimuleerd door HYMOSTRUC3D worden de hydratatieproducten, zoals CSH-gel, CH, AFt, AFm, enz., als één gelfase beschouwd. In vergelijking met HYMOSTRUC3D maakt HYMOSTRUC3D-E onderscheid tussen CSH en CH en simuleert expliciet de nucleatie en groei van CH-deeltjes in de porieruimte. Aanbevolen wordt om in verder onderzoek de nucleatie en groei van AFt- en AFm-deeltjes in de porieruimte te simuleren.

Acknowledgement

I would like to thank the people who have helped me for my PhD study.

Firstly, I am appreciated for the help from my supervisors, viz., Prof. Klaas van Breugel and Assoc. Prof. Guang Ye from Delft University of Technology (TUDelft), and Prof. Qijun Yu and Prof. Jiangxiong Wei from South China University and Technology (SCUT), China. Each supervisor knows a great deal and has good reputation in the research field of cement-based materials.

Prof. Klaas van Breugel is the founder of HYMOSTRUC3D model. He has a deep insight into the simulation related to cement-based materials. When I was doing the extension of HYMOSTRUC3D model, he gave me a lot of valuable suggestion. Also he helped me a lot for the writing of my PhD thesis manuscript, like revising the language and the logical of writing. Prof. Klaas van Breguel is an interesting and humorous person. His attitude of life is optimistic and positive, which infects me.

Assoc. Prof. Dr. Guang Ye is my guide of doing modelling work. He recruited me to study the "dual PhD degree between TUDelft and SCUT"，which provided me the opportunity to do modelling work in TUDelft. Dr. Guang Ye is also familiar with HYMOSTRUC3D model, and gave me a lot of valuable advice on how to do the modelling work, and how to improve the HYMOSTRUC3D model. He also helped me a lot when I was writing the manuscript of my PhD thesis.

Prof. Qijun Yu is my guide of doing PhD study. In 2009, he recruited me to join his research group and carry on the program of one year's master study and four years' PhD study. He is a wise man, and always gives me a lot of valuable suggestion when I must make a decision, like the application of "joint PhD study supported by China Scholarship Council" and "dual PhD degree between TUDelft and SCUT".

Prof. Jiangxiong Wei also gave me a lot of meaningful guidance on the selection of the topic of my PhD study, the methods of doing experiments and data analysis, and the writing of thesis. Prof. Jiangxiong Wei has deep insights on all topics of cement-based materials. I have learned a lot from the discussion between him and me. In addition, Prof. Jiangxiong Wei has a deep understanding of mathematical algorithms and simulations.

I would like to thank my dissertation committee of Prof. dr. T.J.H. Vlugt, Prof. dr. ir. G. De Schutter, Dr. J.S. Dolado and Prof. dr. ir. E. Schlangen.

Many thanks to Prof. Jie Hu from SCUT for linking me and Microlab of TUDelft. He also played an important role in my application of "dual PhD degree between TUDelft and SCUT". Besides, his wife, Assoc. Dr. Yuwei Ma helped me a lot when I came to TUDelft. Wish everything goes well with Prof. Jie Hu and Assoc. Dr. Yuwei Ma.

I took four years to do PhD study in SCUT. The people in SCUT are friendly and helpful. I would like to thank Assoc. Dr. Tongsheng Zhang, Pingping Zhang, Peixin Chen, Pinghai Gao, Ruifeng Luo and Ya Gao for their help when I was doing experiments. Many thanks to Dr. Jianxin Li, Dr. Sun Li, Dr. Dong Lin, Dr. Chenchen Gong, Dr. Hui Guo, Liang Zheng,

Hengchang Wang, Mo Yang, Pengfei Peng, Gen Zhong, Hu Sun, Xueli Jiang, Yajun Ji, etc. and Dr. Feifei Long, Liang Ma, Mingjun Wang, Xianyuan Zhang, Ni Zhang, Zhaoheng Li, Yang Chen, Chun Lin, Chuan Shi, Dr. Zhiyong Ai, Yapo Tian, Xiansu Gao, An Li, Shanmei Gao, Zhengmou Guo, Guangyao Yang, Zhenshan Chen, Xiangyang Liu, Pengfei Yang, Binghua Xie, Shaolong Liu, Yiqun Guo and Yubo Nong. Many thanks to Prof. Xuhong Yin, Dr. Fangxian Li, Prof. Datong Zhang, Mr. Weixian Guo, Mr. Jianqin Lin and Ms. Jieru Zheng. Special thanks to Wenhao Guo.

I also took four years to do PhD study in TUDelft. During this period, many people helped me a lot. First, I would like to thank Dr. Hua Dong. In the first few months when I arrived in TUDelft, Dr. Hua Dong helped me to become familiar with the life in the Netherlands. He is a skilled driver and provides us much convenience. I also want to thank Dr. Zhuqing Yu. She is a nice friend.

I would like to the friends in Microlab, like Dr. Zhiwei Qian, Assoc. Dr. Haoliang Huang, Dr. Chunping Gu, Dr. Xiaowei Ouyang, Jiayi Chen, Xuliang Hou, Tianshi Lu, Zhipei Chen, Bei Wu, Yibing Zuo, Hongzhi Zhang, Leyang Lv, Wenjuan Lv, Xu Ma, Zhenming Li, Shizhe Zhang, Shi Xu andYong Zhang. Also many thanks to the friends like Ms. Marija Nedeljković, Farhad Pargar, Stefan Chaves Figuieredo, Ms. Renee Mors, Dr. Damian Palin, Dr. Branko Šavija, Dr. Mladena Luković, Ms. Claudia Romero Rodrguez, Ms. Nynke Verhulst and Ms. Claire de Bruin, etc.

Many thanks to Prof. Yingzi Yang from Harbin Institute of Technology, Assoc. Dr. Fuhai Li from Southwest Jiaotong University, Assoc. Dr. Yun Huang from Wuhan University of Technology.

Many thanks to my office mates in TUDelft, viz., Dr. Virginie Wiktor, Mr. Gerrit Nagtegaal, Mr. Maiko van Leeuwen and Mr. Bart Hendrix.

This PhD study was financially supported by China Scholarship Council and the Doctoral visiting scholar program of SCUT.

Many thanks to Ms. Xiaomei Cao and Ms. Wanting Yu. Wish everything goes well with them.

Many thanks to Ms. Xiaoqin Yin.

Many thanks to Mr. Guotao Wang.

I would like to thank my brother Dr. Zhengdong Gao, because he supported me for many years. Wish everything goes well with him and his family.

Many thanks to my parents, wish everything goes well with you.

Peng Gao
May 2018, Guangzhou, China

Chapter 1

General Introduction

1.1 Background

Portland cement is a material widely used in construction and civil engineering. The annual global demand of Portland cement is huge, especially for the developing countries, such as Brazil, China, and India, etc. According to *USGS [2015],* in 2015 the worldwide production of Portland cement was around 3.6 billion tons. The CO_2 emissions of the cement industry are also huge. As reported by Worrell et al. *[2001]*, the cement industry is responsible for about 5% of the global anthropogenic CO_2 emissions. Hence, a main concern of the cement industry is how to reduce CO_2 emissions. Past studies have demonstrated that the use of supplementary cementitious materials (SCMs) in cementitious system is an efficient method for reducing CO_2 emissions.

In cement-based materials, SCMs often take part in the hydration reactions and contribute to the hydration product *[Taylor, 1997]*. The most commonly used SCMs are ground granulated blast furnace slag (BFS), fly ash (FA), and natural pozzolans *[Ramezanianpour, 2014]*. Other SCMs, such as rice husk ash and metakaolin, are also increasingly used *[Siddique et al., 2011; Ramezanianpour, 2014]*. The use of SCMs in cementitious systems has many advantages. In the first place, many SCMs are industrial wastes, which have to be disposed of or recycled. For example, BFS is a by-product from the production of steel and iron and FA is a by-product of power plants burning pulverized coal. The annual worldwide productions of BFS and FA have been estimated at 360 million tonnes *[USGS, 2015]* and 500 million tonnes *[Ahmaruzzaman, 2010]*, respectively. Furthermore, the CO_2 emissions per ton of concretes made with large quantities of SCMs are less than that of concretes made with pure Portland cement (CO_2 emissions of SCMs can be regarded very small, since most of them are industrial wastes) *[Taylor, 1997; Lothenbach et al., 2011]*. Besides, the incorporation of SCMs can improve the performance of concrete structures. For example, BFS can be used to improve the long-term performance of marine concrete structures and FA can be used to reduce the heat evolution of concrete in massive structures *[Taylor, 1997]*.

Although information about the use of SCMs in cementitious systems is available, the utilization of SCMs still suffers from a gap in knowledge. Systems of cement-based materials blended with SCMs are much more complex than that of pure Portland cement *[Lothenbach et al., 2011]*. With the addition of SCMs the properties of cement-based materials, such as workability, strength, different types of shrinkage and durability, will change.

Numerical models are helpful tools for engineers and researchers to simulate and describe the properties of cement-based materials. In the past decades, numerical models, such as

HYMOSTRUC3D *[Van Breugel, 1991; Koenders, 1997; Ye, 2003]*, CEMHYD3D *[Bentz, 1995; 1997]*, DuCOM *[Maekawa et al., 1999]*, HydraticCA *[Bullard, 2007a, 2007b]* and μic *[Bishnoi et al., 2009a]*, have been proposed to simulate the hydration and microstructure development of Portland cement. For optimization the use of blended cements containing SCMs, a number of numerical models for simulating the hydration and microstructure development of blended cements were also proposed in recent years (Table 1.1). Some of these models were extensions of models for pure PC systems. For example, CEMHYD3D was extended to simulate the hydration process and microstructure development of fly ash cements *[Bentz et al., 1997]*, and slag cements *[Bentz, 2005]*.

Table 1.1 Numerical models for blended cements proposed in recent years

Models for fly ash cements	Bentz et al. *[1997]* Wang et al. *[2009, 2010a]*
Models for slag cements	Bentz *[2005]* Chen *[2007a, 2007b, 2007c]* Kolani et al. *[2012]* Merzouki et al. *[2013]* Wang et al. *[2010a, 2010b]* Tan *[2015]*

Most of the numerical models for simulating the hydration and microstructure development of blended cement-based materials need modification to allow for the complexity of blended cement systems. Two main research issues will be dealt with in this study:

(1) Nucleation and growth of calcium hydroxide (CH) particles

In pure PC systems, the hydration of PC will produce CH. The nucleation and growth of CH particles will contribute to the microstructure and strength development. In blended cement systems, CH formed in the hydration of PC will be consumed by the pozzolanic reactions of SCMs. This consumption of CH will alter the performance of cement-based materials. For instance, the carbonation resistance of blended cement concretes will decrease if the CH content in the systems decreases. Hence it is important to determine the nucleation and growth of CH particles in blended cement systems more precisely.[1]

[1] In recent models, e.g. those of Wang et al. *[2009, 2010a, 2010b]*, Kolani et al. *[2012]*, Merzouki et al*[2013]* and Tan *[2015]*, the nucleation and growth of CH particles in blended cement systems were not simulated.

(2) Effect of pore solution chemistry on the reaction rates of SCMs particles

In blended cement systems the reaction rates of SCMs are affected by the pore solution chemistry. In these models, such as Wang's model *[Wang, et al., 2009, 2010a, 2010b]*, Kolani's model *[Kolani et al., 2012]*, Merzouki's model *[Merzouki, 2013]* and Tan's model *[Tan, 2015]*, the pore solution chemistry of blended cement systems was not simulated, and its influence on the reaction rates of SCMs was not quantified. In CEMHYD3D *[Bentz et al., 1997; Bentz, 2005]*, the pore solution chemistry of blended cement systems was simulated and its effect on the reaction rates of SCMs was quantified as function of pH and the concentration of SO_4^{2-}. However, this simulation was not validated with experimental data at that time.

1.2 Objectives

HYMOSTRUC3D is a numerical model for simulating the hydration process and the microstructure development of PC paste *[Van Breugel, 1991; Koenders, 1997; Ye, 2003]*. The main input parameters of HYMOSTRUC3D are clinker composition and particle size distribution of cement, water-to-cement ratio (w/c) of cement paste and temperature. Meanwhile HYMOSTRUC3D has been used to simulate the properties of cement-based materials, such as autogenous shrinkage of cement paste *[Koenders, 1997]*, transport properties of cement paste *[Ye, 2006; Zhang, 2013]* and strength and stiffness of cement paste *[Qian et al., 2010]*, etc. However the simulation for blended cement-based materials was not dealt with in HYMOSTRUC3D.

This study aims to extend HYMOSTRUC3D for simulating the hydration and microstructure development of blended cement systems. In the extended model, the pore solution chemistry of blended cement systems and its effect on the reactions of SCMs will be particularly dealt with. The nucleation and growth of CH particles in blended cement systems will also be simulated. The extended model can be used to simulate the chemical shrinkage, pore solution chemistry, pore structure development of blended cement paste, which provides possible inputs for investigating the influence of SCMs on the properties of blended cement-based materials, such as strength and shrinkage.

Two typical SCMs, i.e., BFS and FA, are chosen for this investigation. The use of BFS and FA in cementitious system is very common. The annual worldwide production of BFS and FA is huge, which makes them good candidates for replacing PC. Moreover, the addition of BFS and FA can improve the performance of cement-based materials, such as workability and durability.

1.3 Outline of this thesis

As shown in Fig. 1.1, this thesis has 6 chapters.

- Chapter 1 deals with the background, objective and outline of this thesis.
- Chapter 2 contains the literature survey of the numerical models for the hydration process

and microstructure development of hydrating Portland and blended cements.

- In chapter 3 and chapter 4, HYMOSTRUC3D is extended to simulate the hydration process and microstructure development of blended cement pastes, in which the pore solution chemistry, nucleation and growth of CH particles, and pore structure of blended cement pastes are also simulated. This extended HYMOSTRUC3D is called HYMOSTRUC3D-E
- Chapter 5 presents the validation of HYMOSTRUC3D-E in view of the hydration process, pore solution chemistry, chemical shrinkage and microstructure development of blended cements.
- Chapter 6 summarizes the conclusions and outlooks of this thesis.

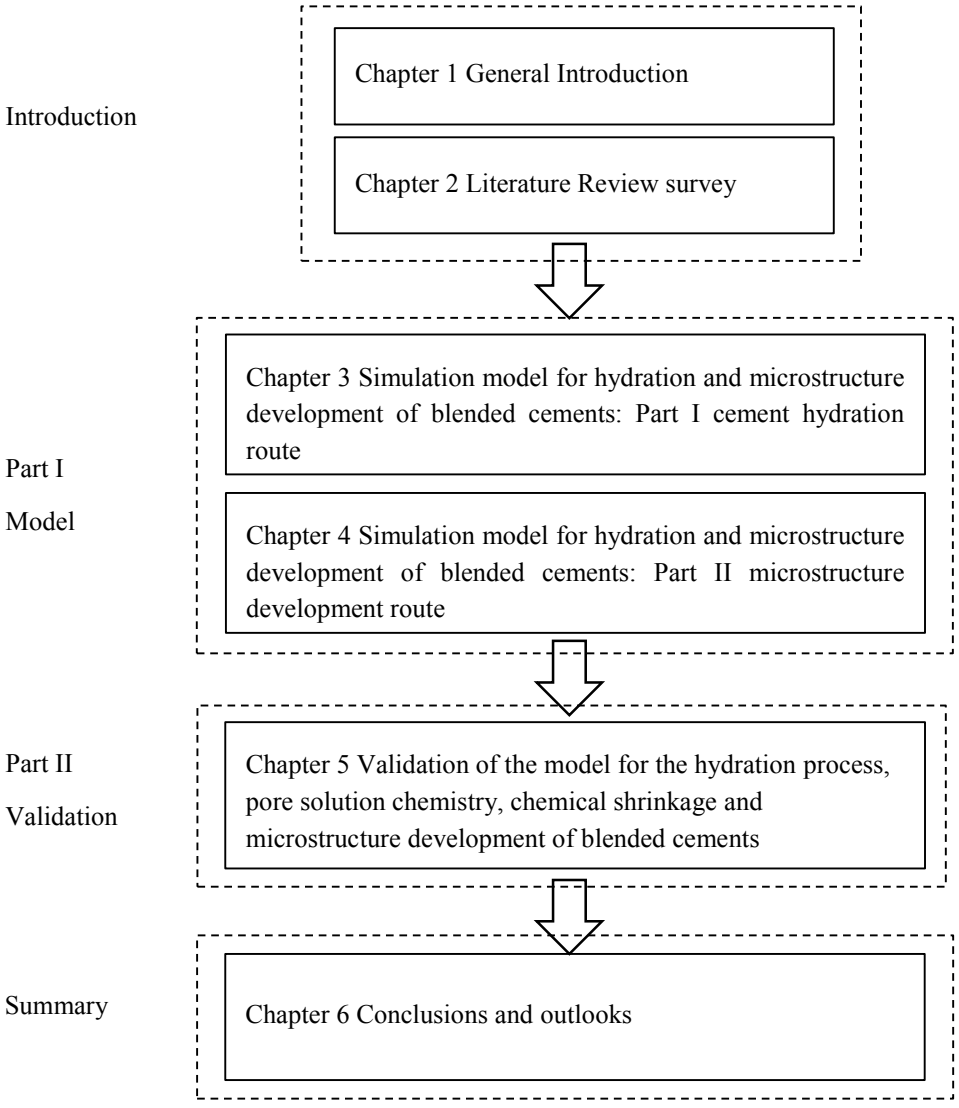

Fig. 1.1 Outline of this thesis

Chapter 2

Numerical models for hydration and microstructure of Portland and blended cements – A Literature survey

2.1 Introduction

Numerical models are helpful tools for engineers and researchers to simulate the properties of hardened cement-based materials. In the past decades, a number of numerical models were proposed to simulate the properties of pure Portland cement-based materials. These numerical models can be categorized as macro-level and meso-level models for concretes and mortars, micro-level for cement pastes and sub-micro-level for CSH gels *[Wittmann, 1983; Dolado et al., 2011]*. For optimization the use of supplementary cementitious materials (SCMs), such as blast furnace slag (BFS) and fly ash (FA), in blended cement-based materials, an increasing number of numerical models were proposed in recent years to simulate the hydration and microstructure of hardening blended cements.

This chapter will deal with the literature survey of numerical models for the hydration and microstructure of hardening Portland cement and blended cements[2]. This literature survey concentrates on the micro-level models, and comprises two topics:

1. Numerical models for hardening pure Portland cement and cement components
2. Numerical models for hardening blended cements

2.2 Numerical models for hydration and microstructure of hardening pure cement components and Portland cements

2.2.1 Categorisation of models

A number of models have been proposed in the past three decades to simulate the hydration and microstructure of cement-based materials. There are several extensive reviews about these numerical models, e.g. Ye *[2003],* Van Breugel *[2004],* Pignat et al. *[2005]*, Dolado et al. *[2011]* and Thomas et al. *[2011]*.

As listed in Table 2.1, cement hydration models can be categorized into four groups, i.e., overall kinetics, particle kinetics, hybrid kinetics and integrated kinetics *[Van Breugel, 2004;*

[2] In this thesis, blended cement = Portland cement blended with blast furnace slag or/and fly ash

Dolado et al., 2011]. The details of these four hydration kinetics can be found in the aforementioned reviews. In comparison with other three kinetics models, integrated kinetic models are capable of simulating the 3D microstructure of cement pastes. This chapter will focus on the literature survey of integrated kinetic models.

Regarding the algorithm for describing the particle shape, integrated kinetic models can be categorized as vector models (also called continuum model) and pixel models *[Ye, 2003; Bishnoi et al., 2009a; Thomas et al., 2011]*. In vector models cement particles are normally represented as spheres, while in pixel models cement particles with irregular shape can be modelled. These irregular shapes consist of uniform cubic cells. Recently Qian et al. *[2010]* proposed a vector model called Anm materials model to simulate the packing of concrete aggregate particles. It is noted that in Anm materials model concrete aggregate particles were considered with irregular shapes. Table 2.2 lists the main integrated kinetic cement hydration models.

Table 2.1 Categories of numerical models for cement hydration [see also Van Breugel,1991]

Categories	Features
Overall kinetics	Hydration process is a function of time without addressing the mechanisms at particle level; Chemical composition of cement, w/c, and temperature, etc. are considered
Particle kinetics	The mechanisms at particle level are considered; The interaction between particles is not taken into account
Hybrid kinetics	The mechanisms at particle level are considered; The interaction between particles is involved
Integrated kinetics	The mechanisms at particle level are considered; The interaction between particles is involved; The formation of the microstructure is simulated

Table 2.2 Categories of main integrated kinetic cement hydration models

Categories	Names
Vector model (Continuum model)	Model of Jennings et al. *[1986]* HYMOSTRUC3D *[Van Breugel, 1991; Koenders, 1997; Ye, 2003]* Model of Navi et al. *[1996]* Model of Nothnagel et al. *[2008]* μic *[Bishnoi et al., 2009a]* Model of Wang et al. *[2009, 2010a, 2010b]*
Pixel model	CEMHYD3D *[Bentz, 1995]* DuCom *[Maekawa, et al., 1999; 2003]* HydraticCA *[Bullard, 2007a]*

2.2.2 Continuum models

(1) Model of Jennings et al.

In 1986 Jennings et al. *[1986]* proposed a model for hydration of individual components of PC, i.e. C_3S. In this model the C_3S particles were represented as spheres (Fig. 2.1). With progress of the hydration process CSH gel was formed on the surface of the shrinking cores of hydrating C_3S particles (Fig. 2.1b). In the formation of microstructure, the CSH gel between growing C_3S particles would overlap. An algorithm was used in this model to redistribute the overlapped CSH gels on available surface of the C_3S particles which are hydrating. The model of Jennings et al. *[1986]* was not widely used due to the limited computer power at that time. However, it paved the road for most of the integrated kinetic models, such as HYMOSTRUC3D, CEMHYD3D, and Navi's model and μic model *[Thomas et al., 2011]*.

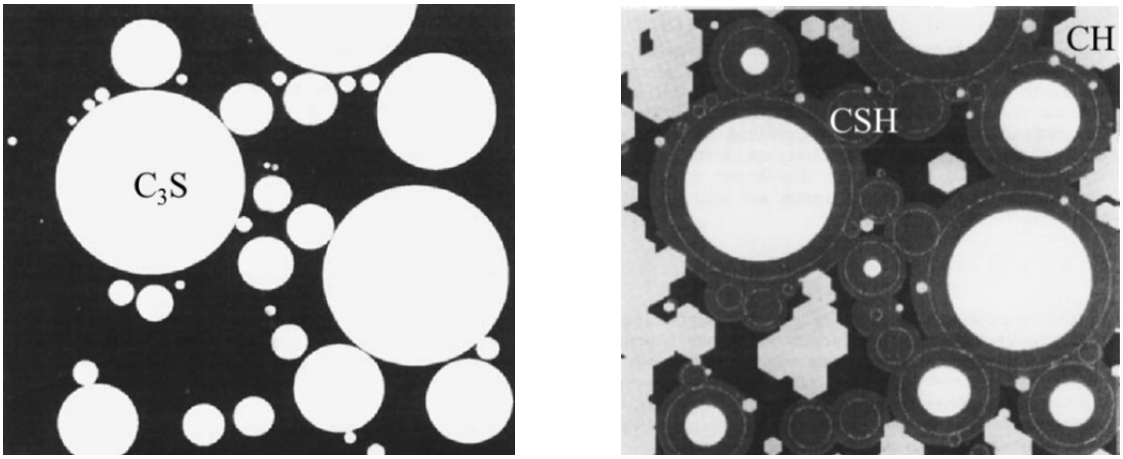

(a) Hydration degree = 0 % *(d) Hydration degree = 42 %*

Fig. 2.1 Simulated microstructure of C_3S paste with w/c = 0.5 by Jennings and Johnson model in 2D [After Jennings et al., 1986]

(2) HYMOSTRUC3D

In 1991 Van Breugel *[1991]* proposed a numerical cement hydration model called HYMOSTRUC, the acronym for HYdration, MOrphology and STRUCture formation. In this model, cement particles were homogenously distributed in a 3D cell (Fig. 2.2a). With progress of the hydration process, hydration products were formed on the surface of the shrinking cores of hydrating cement particles. The hydration process of cement particles was divided into two stages: *phase boundary reaction* stage and *diffusion-controlled reaction* stage. During both stages the reaction rate of cement particles was calculated as a function of the chemical composition and particle size distribution of the cement, water content, temperature of the system.

HYMOSTRUC focused on simulating the hydration process of Portland cements. It also simulated the microstructure of cement pastes by distributing the cement particles homogenously in the 3D cell (Fig. 2.2a). Using this 3D cell microstructure, the contact areas between hydrating cement particles were calculated. The calculated contact areas were used to predict the mechanical properties of cement paste, such as strength and stiffness.

Koenders *[1997]* incorporated an algorithm in HYMOSTRUC to simulate the *random* spatial distribution of cement particles in the representative elementary volume (REV) of cement paste. (see Fig. 2.2b). Ye *[2003]* incorporated a pixel-based algorithm in HYMOSTRUC to analyse the pores of the simulated microstructure. Since the extensions of HYMOSTRUC concentrated on the 3D microstructure simulation, the new version of HYMOSTRUC was called HYMOSTRUC3D.

Up to now, HYMOSTRUC3D has been used for predicting many properties of cement-based materials, including autogenous shrinkage of cement pastes *[Koenders, 1997]*, transport properties of cement pastes *[Ye et al., 2006; Zhang, 2013]* and tensile strength and stiffness of cement pastes *[Qian et al., 2010]*, etc. However, HYMOSTRUC3D still needs further development. For example, all the hydration products of cement, including CSH gel and calcium hydroxide (CH), are considered as one gel phase. This is a shortcoming, particularly in case of blended cements, because CH is an essential reactant for the pozzolanic reactions of BFS and FA particles.

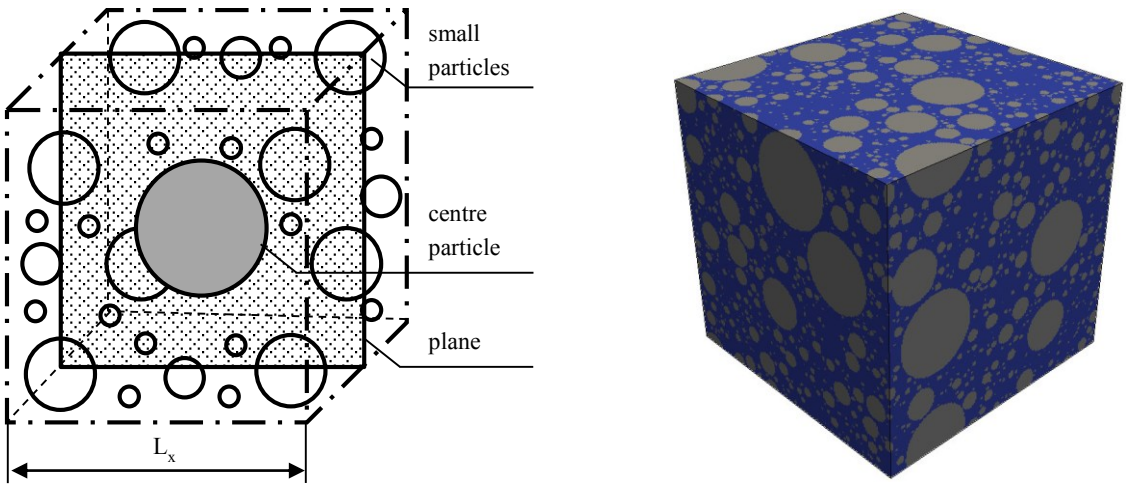

(a) homogenously distribution (HYMOSTRUC) *(b) spatial distribution (HYMOSTRUC3D)*

Fig. 2.2 Method to distribute cement particles in HYMOSTRUC and HYMOSTRUC3D

(3) Model of Navi et al. and μic microstructural modelling platform

In 1996, Navi et al. *[1996]* proposed a numerical model to simulate the hydration and microstructure development of C_3S pastes. C_3S was assumed to consist of spherical particles with the same particle size distribution as PC. Also in the model of Navi et al. *[1996]* the hydration of C_3S is assumed to develop from phase boundary stage to diffusion-controlled stage.

Based on the model of Navi et al., Bishnoi et al. *[2009a]* developed a new cement hydration platform, μic (pronounce "mike"). The advantage of μic is that it allows users to define the reactions by themselves. In comparison with Navi's model, μic contains an improved algorithm for packing cement particles and reduces the computing time. Furthermore, an algorithm is incorporated in μic to describe the pore size distribution of cement paste. Fig. 2.3 shows an example of the simulated microstructure of C_3S paste. In past years, μic was used to investigate the properties of cementitious systems, such as the hydration of C_3S, the nucleation and growth kinetics of the C_3S hydration *[Bishnoi et al., 2009b]* and the effect of sodium and potassium hydroxide on the C_3S hydration *[Kumar et al., 2012]*. In those studies, μic was also used to simulate the concentrations of calcium and silicium ions in the pore solution of C_3S paste. Fig. 2.4 shows an example of the simulated calcium and ions in the pore solution with different contents of NaOH from mixing time up to 8 hours.

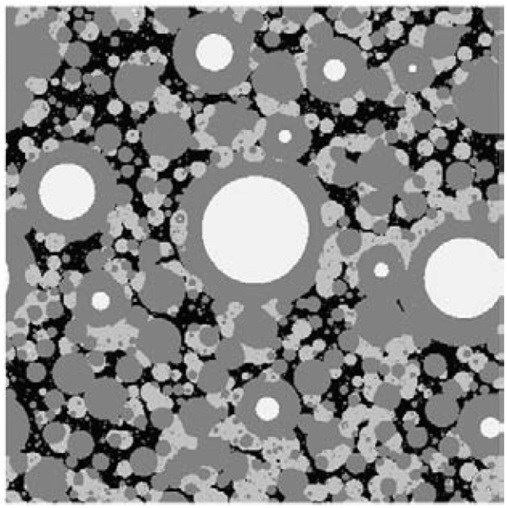

Fig. 2.3 Microstructures at 80% hydration for C_3S paste simulated by μic platform [After Bishnoi et al. 2009a] (C_3S is in lightest grey-scale, followed by CH and CSH and pores in black.)

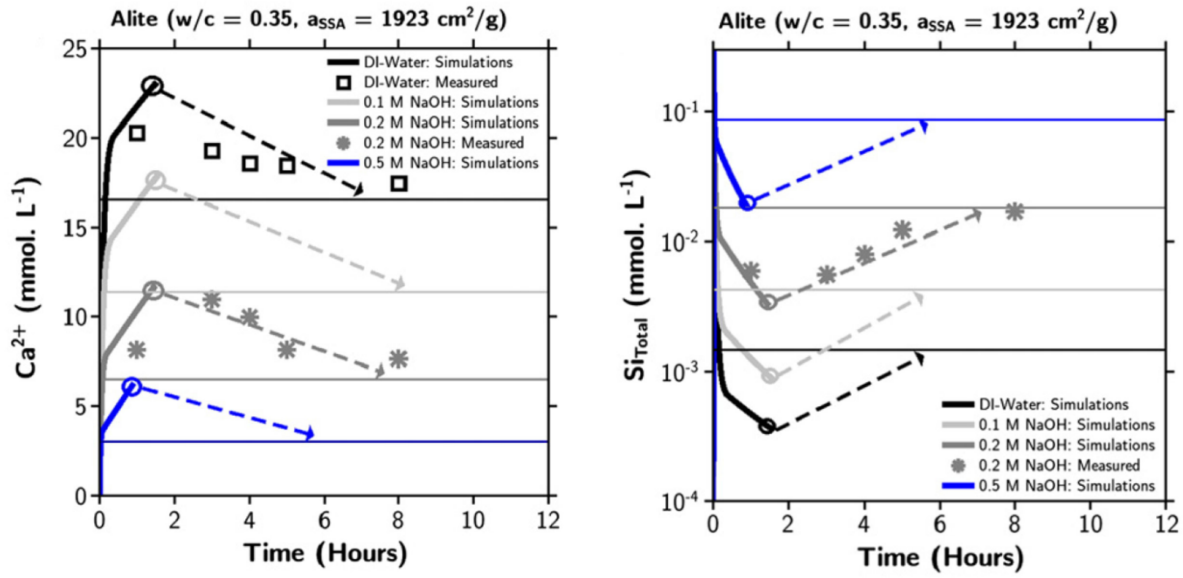

(a) Ca^{2+} ions *(b) Total silicium ions*

Fig. 2.4 Evolution of calcium and silicium ions in the pore solution with different contents of NaOH. [After Kumar et al., 2012]

(4) DuCOM model

Maekawa et al. *[1999; 2003]* proposed the model: **Du**rability of **Co**ncrete **Mo**del (DuCOM), to evaluate the durability of concrete structures. Fig. 2.5 shows the structure of the DuCOM model. This model comprised many modules, such as hydration module, microstructure module, O_2 transport module and corrosion module. Using these modules, the DuCOM model traces the development of concrete hardening (hydration), formation of microstructure and several associated phenomena.

In the DuCOM model, the cement particles were assumed to be spherical and have similar composition and same particle size. Arrhenius's law was used to simulate the hydration and heat release of cement particles. A particle expansion approach was used to simulate microstructure development (Fig. 2.6). Inner product was considered as a shell. This shell formed inside the original spherical geometry of the grains (see number 2 in Fig. 2.6). Outer product was assumed to consist of CSH gel grains. These outer CSH gel grains were distributed outside the original spherical geometry (see number 3 in Fig. 2.6). The space between the outer CSH gel grains was considered as capillary pores (see number 4 in Fig. 2.6).

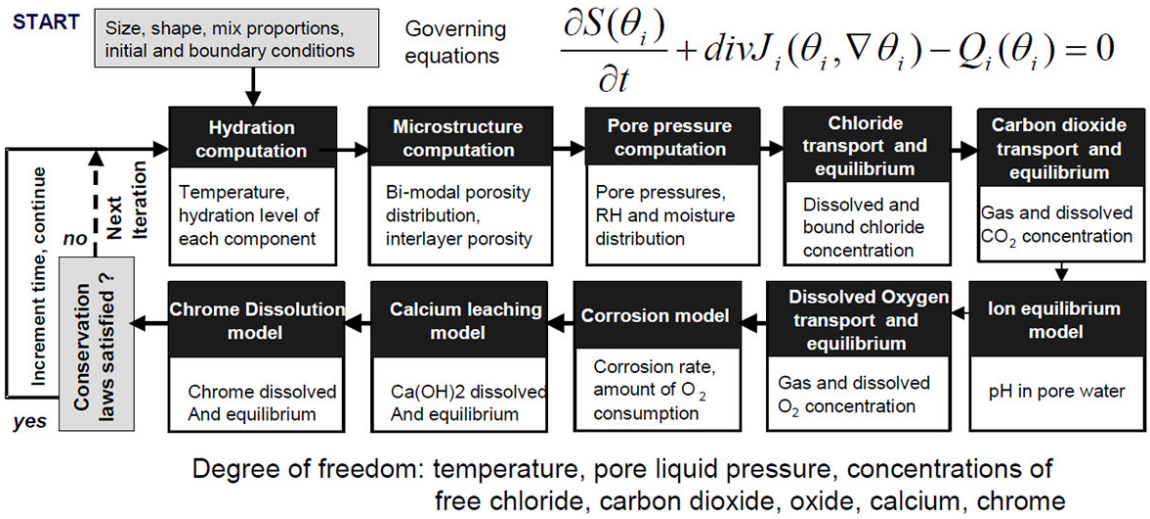

*Fig. 2.5 Sub-structure of **Du**rability of **Co**ncrete **Mo**del – DuCOM [Maekawa et al., 1999]*

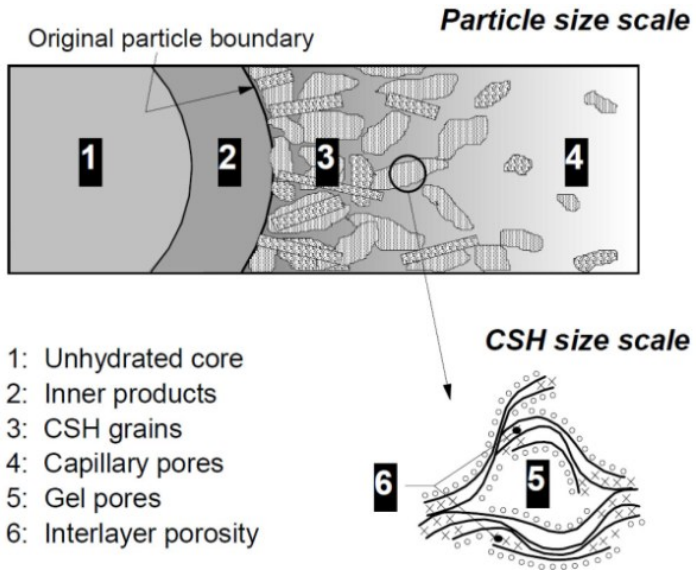

Fig. 2.6 Statistical modelling of micro-pore geometry and pore size for hardening cement paste [Maekawa et al., 2003]

(4) SPACE and XIPKM models

In 1999, Stroeven *[1999]* proposed a model called SPACE to simulate the hydration and microstructure development of PC paste. The hydration of PC particles was also assumed to develop from a *phase boundary reaction* and a *diffusion-controlled reaction*. In the simulation of the rate of hydration of PC particles the interaction between growing particles were considered.

In 2013, Le et al. *[2013]* proposed a model called Extended Integrated Particle Kinetics model (XIPKM) to simulate the hydration and microstructure development of cement containing pozzolans (SiO_2). In this model the hydration of PC particles and the reaction of pozzolan particles were also assumed to develop from a *phase boundary reaction* and a *diffusion-controlled reaction*. In the simulation of the rate of hydration of PC particles and the rate of reaction of pozzolans, the interaction between particles, the CSH gel was considered as a shell forming on the surface of the shrinking cores of reacting cement and pozzolan particles (see the bottom of Fig. 2.7). The CH, CAH and FH were randomly placed in the pore space.

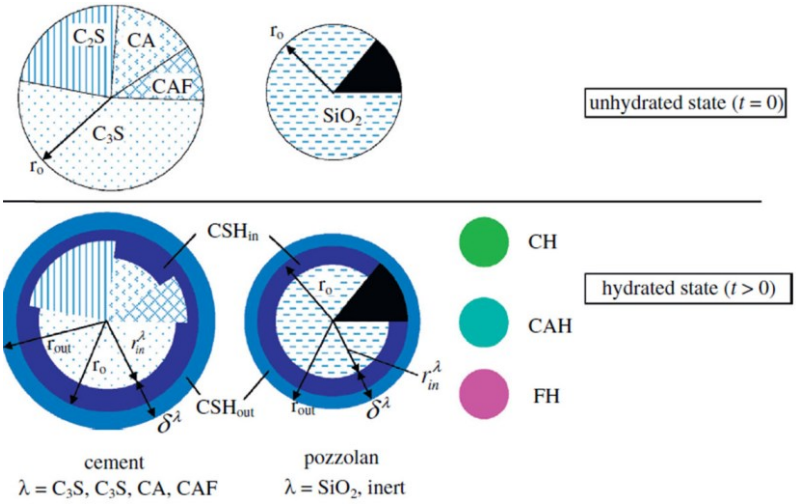

Fig. 2.7 Particle models of cement, pozzolan and hydration products in the unhydrated state (top) and hydrated state (bottom) in XIPKM (after [Le et al., 2013])

(5) Model of Nothnagel et al.

In 2008, Nothnagel et al. *[2008]* proposed a model to simulate the hydration and microstructure development of PC paste. In this model two algorithms were used to simulate the spatial distribution of cement particles in the REV of cement paste. In the first algorithm, the cement particles were random distributed (Fig. 2.8a). In another algorithm, the cement particles were flocculated (Fig. 2.8b). In comparison with the random particle distribution, the flocculation distribution was more close to the real situation, because cement particles are normally flocculated unless they are dispersed by superplasticizer *[Diamond, 2007; Nothnagel et al., 2008]*.

The hydration of cement was simulated with several interacting processes. A core-shell model was used to describe the formation of inner product and outer product (Fig. 2.9). This core-shell model is different from that used in HYMOSTRUC, because the outer shell (outer product) of this core-shell model was not a homogenous layer of uniform porosity.

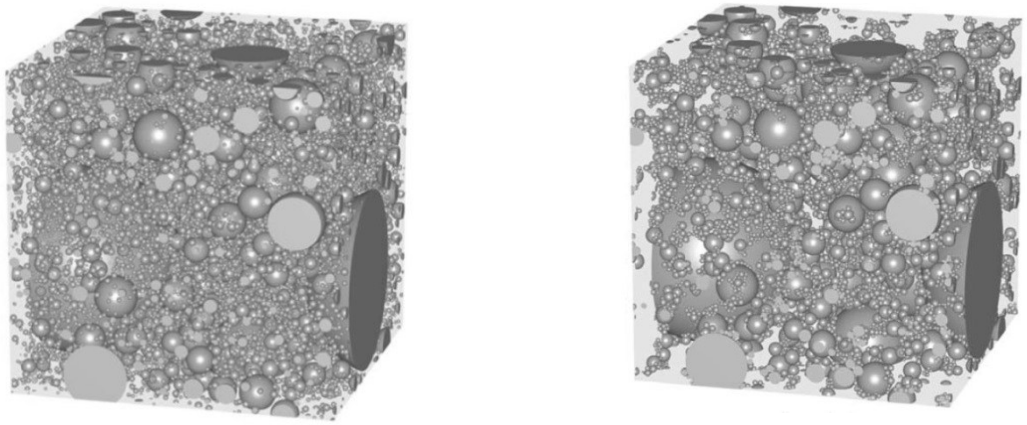

(a) particles are random distributed *(b) particles are flocculated*

Fig. 2.8 Two types of spatial distribution of cement particles in fresh cement paste in the model of Nothnagel et al. [2008].

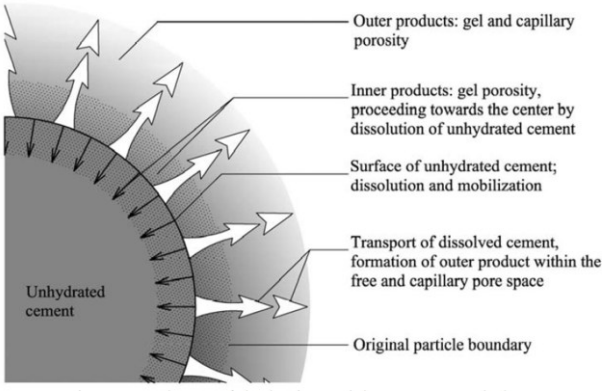

Fig. 2.9 Schematic picture of the basic model processes and phases in the model of Nothnagel et al. [2008]

2.2.3 Pixel models

(1) CEMHYD3D

CEMHYD3D is a cement hydration model proposed by Bentz et al. *[Bentz et al. 1991, 1994; Bentz 1995, 1997]*. In this model, the microstructure of cement paste was digitalized into uniform cubic voxels. The cubic voxels represented some phases of cement pastes, e.g., unhydrated C_3S, water-filled capillary pores, CSH gel, etc. A lattice-based approach was used to simulate the dissolution, diffusion and reaction of cement voxels. This model simulated the spatial distribution of different minerals in cement particles (Fig. 2.10). CEMHYD3D has been used for simulating many properties of cement-based materials, including heat of hydration, chemical shrinkage, setting time, capillary porosity, diffusivity, etc. *[Bentz et al., 2000; Thomas et al., 2011]*.

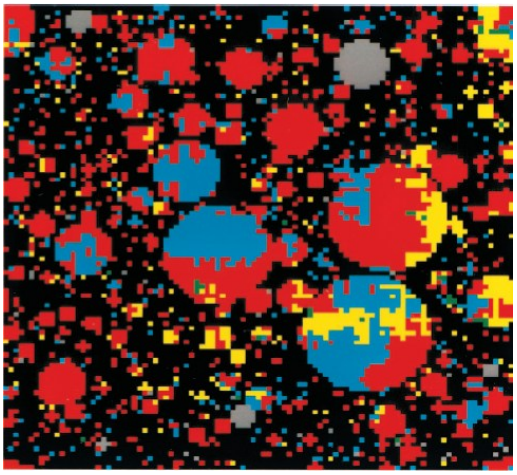

Fig. 2.10 2D slices from 3D model of the initial microstructure for Portland cement paste with fineness of 387 m^2/kg simulated by CEMHYD3D (colour assignments: red-C_3S, blue-C_2S, green-C_3A, yellow-C_4AF grey-hemihydrate, and black-capillary porosity; original images were 100 μm by 100 μm) [Bentz et al., 2001].

CEMHYD3D has shown to be very successful. However, it has some limitations. The first limitation is that the time scale of CEMHYD3D is not defined as the physical time scale, although the hydration process simulated by CEMHYD3D can be calibrated with experimental data, such as chemical shrinkage and non-evaporable water content *[Thomas et al., 2011]*. Another limitation is the size of the cell for representing different phases in the microstructure of cement paste. In CEMHYD3D the size of the cell is normally at the microscale, i.e., 1 μm. In consequence, some specific features of the microstructure of cement paste will be lost. The gel pores at the nanoscale, for example, are difficult to obtain.

(2) HydratiCA

To overcome the limitations of CEMHYD3D, Bullard *[Bullard 2007a, 2007b]* proposed a model called HydratiCA, based on more fundamental principles of reaction kinetics and thermodynamics. HydratiCA can simulate the dissolution of minerals, the transport of ions and the precipitation of hydration products. In this model the solid phase, water and ions were discretized into cells located in a regular cubic lattice. With progress of the hydration process, probabilistic rules were used to determine chemical and structural changes of the system. Fig. 2.11 shows the simulated process of the dissolution of MO particles and the precipitation of $M(OH)_2$. An advantage of HydratiCA is that there is no need to adjust the reaction parameters for the system with different mixture design, e.g. chemical composition of cement, w/c, etc. This model has a great potential, but is still in development.

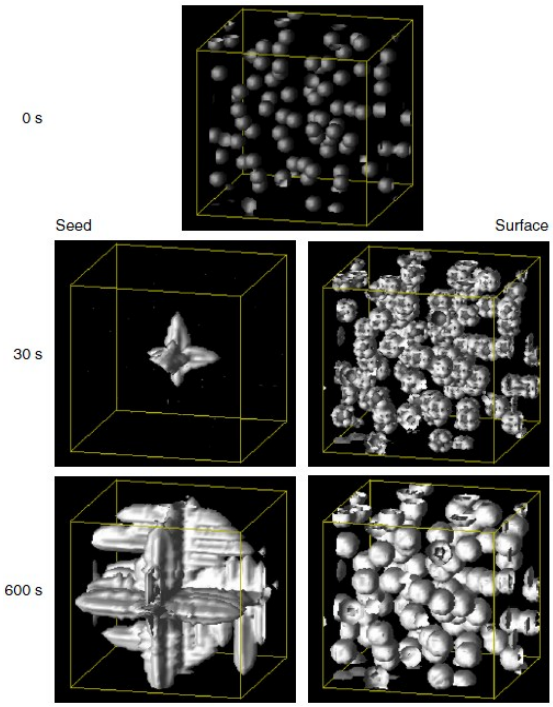

Fig. 2.11 Predicted microstructure development as MO particles dissolve in water and $M(OH)_2$ nucleates either on a single inert seed (left) or on the surfaces of the dissolving particles (right).The temperature is kept constant at 298 K. Other than the difference in nucleation sites, all model parameters are identical in both simulations. [After Bullard, 2007a]

2.3 Numerical models of hydration and microstructure of blended cements

For optimization the use of SCMs in blended cement-based materials, a number of numerical models for blended cements were proposed in recent years (Table 2.3).

Table 2.3 Numerical models for blended cements (see also Table 1.1)

Models for fly ash cements	Bentz et al *[1997]* Wang et al. *[2009, 2010a]*
Models for slag cements	Bentz *[2005]* Chen *[2007a, 2007b, 2007c]* Kolani et al. *[2012]* Merzouki et al. *[2013]* Wang et al. *[2010a, 2010b]* Tan *[2015]*

Bentz et al. *[1997]* extended CEMHYD3D to simulate the hydration and microstructure development of fly ash cement pastes. As shown in Fig. 2.12, the fly ash (FA) particles were assumed to consist of cells of silica (S), aluminosilicate (AS), anhydrite ($C\bar{S}$), calcium aluminosilicate (CAS_2), tricalcium aluminate (C_3A), inert phases, etc. To simulate the pozzolanic reaction of FA particles, these phases were considered to react individually. Bentz et al. *[1997]* indicated that the rate of reaction of FA particles should be a function of pH of the pore solution. However, this function wasn't incorporated at that time.

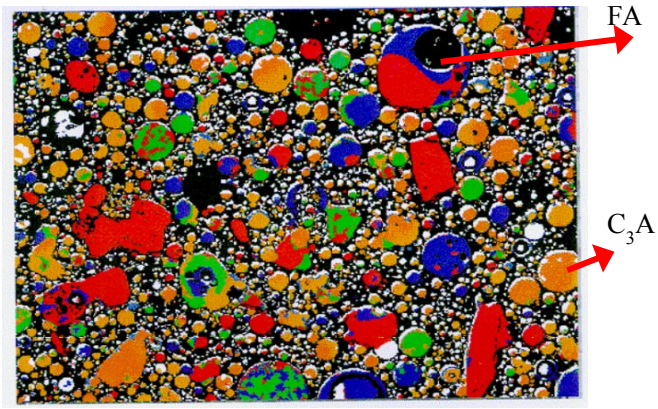

Fig. 2.12 Segmented two-dimensional image of Class C fly ash containing C_3A. Red = S, Blue = AS, Green = CAS_2, Orange = C_3A, Aqua = anhydrite, White = inert phase. Size = 250 μm ×200 μm [After Bentz et al., 1997]

In 2005, Bentz *[2005]* released the version 3.0 of CEMHYD3D. In this version hydration reactions for blast furnace slag (BFS) particles were incorporated. The stoichiometry of the reaction of BFS particles in this version of CEMHYD3D is given in Table 2.4. In this version of CEMHYD3D the pore solution chemistry was simulated. The effect of pore solution chemistry on the reaction rates of FA and BFS particles was quantified as a function of the pH and the concentration of SO_4^{2-} ions. However, these extensions could not be validated by sufficient experimental data at that time.

Table 2.4 Compositions of BFS particles (in mass percentages) and the stoichiometry of the reaction of BFS particles in CEMHYD3D v 3.0. [After Bentz, 2005]

Weight mass (%)					Slag composition	Hydration product composition	Extra C_3A in slag
SiO_2	Al_2O_3	CaO	MgO	SO_3			
39.2	7.9	36.3	10.3	3.1	$C_{16.5}S_{17}M_{6.5}A_2\bar{S}$	$C_{21.25}S_{17}M_{6.5}A_2\bar{S}H_{86}$	No
34.7	11.4	45.5	8.5	3.0	$C_{21.5}S_{15}M_{5.5}A_3\bar{S}$	$C_{20.25}S_{15}M_{5.5}A_2\bar{S}H_{83}$	Yes

Inspired by CEMHYD3D, Chen et al. *[2007a; 2007b; 2007c]* proposed a model to simulate the hydration and microstructure of slag cement pastes. In this model, slag pixels were used to represent slag particles. It was assumed that MgO (M) and some part of Al_2O_3 (A) in BFS will react with water to produce an hydrotalcite-like phase (M_5AH_{13}), some part of CaO (C), Al_2O_3 (A) and SO_3 ($\bar{S}$) in BFS will react with water to produce AFt phase ($C_6A\bar{S}_3H_{32}$), and some part of C, A and $\bar{S}$ in BFS will react with C_3S and C_2S in PC to produce CSH gel and CH. Chen et al. also took into account the effect of the chemical composition of BFS on the reaction rate of BFS. In addition, the influence of the pore solution chemistry on the reactivity of BFS was quantified as a function of pH in the pore solution.

Recently, Wang et al. *[2009, 2010a, 2010b]* used the stoichiometric data of the pozzolanic reaction of BFS proposed by Maekawa et al. *[1999]* to simulate the hydration and microstructure of slag cement pastes, and the stoichiometric data of the pozzolanic reaction of FA proposed by Papadakis et al. *[1999, 2000]* to simulate the hydration and microstructure of fly ash cement pastes. Kolani et al. *[2012]* used the stoichiometry of the pozzolanic reaction of BFS proposed by Chen et al. *[2007a; 2007b; 2007c]* to simulate the hydration and heat release of slag cements. Merzouki et al. *[2013]* simulated the hydration and chemical shrinkage of slag cements using the stoichiometry of the pozzolanic reaction of BFS proposed by Richardson et al. *[2002]*. Inspired by HYMOSTRUC3D, also Tan *[2015]* proposed a model for the hydration and microstructure development of slag cement pastes. The progress of the pozzolanic reaction process of BFS was assumed to develop from *phase boundary reaction* and *diffusion-controlled reaction*. Similar to the reaction rate of PC in HYMOSTRUC3D, the reaction rate of BFS was described as a function of the curing temperature and the reduction factor allowing for the change of water distribution in the system, etc.

2.4 Summary of this chapter

In this chapter, the numerical models for the hydration and microstructure development of pure Portland cements and blended cements are briefly surveyed. Based on this literature survey, the following conclusions can be drawn.

A number of integrated kinetic models have been proposed in past decades to simulate the hydration and microstructure of pure Portland cements and cement components. These models not only take into account the cement composition, w/c, temperature, but also consider the interaction mechanisms between cement particles. These integrated kinetics models show many successes to simulate the properties of cement-based materials like strength, heat release, transport properties, etc.

For optimization of the use of SCMs, such as BFS and FA, in cementitious systems, an increasing number of numerical models have been proposed in recent years to simulate the hydration and microstructure of blended cements. These models, like those of Wang et al. *[2009, 2010a, 2010b]*, Kolani et al. *[2012]*, Merzouki et al. *[2013]* and Tan *[2015]*, can predict the degree of reaction of SCMs, the heat release and the 3D microstructure of blended

cement pastes. However, because of the complexity of blended cement systems, there is still room for improving these models. For example, the nucleation and growth of CH particles will contribute to the microstructure and strength development of cement pastes. In hardening blended cement pastes, the pozzolanic reaction of BFS and FA particles will consume the CH formed during the hydration of PC. Hence, the addition of BFS and FA will affect the microstructure and strength development of blended cement pastes. In a study of the effects of BFS and FA on microstructure and strength development of blended cement pastes, it is important to take into account the nucleation and growth of CH particles. In addition, the rates of reaction of BFS and FA particles in blended cement pastes are sensitive to the pore solution chemistry. To simulate the hydration process of blended cements containing BFS and FA particles, the effect of the pore solution chemistry on the reaction rates of BFS and FA particles should be considered.

Chapter 3

Simulation model for hydration and microstructure development of blended cements: Part I Cement hydration route

3.1 Introduction

For optimization the use of supplementary cementitious materials (SCMs) in cementitious systems, a numerical model for simulating the hydration and microstructure development of blended cements is helpful. A lot of models, such as the models of Wang et al. *[2009, 2010a, 2010b]*, Kolani et al. *[2012]*, Merzouki et al. *[2013]* and Tan *[2015]*, have been proposed in recent years to simulate the hydration and microstructure of blended cements. However, most of these models need further development. For example, the nucleation and growth of CH particles were not simulated. Moreover, the influence of the pore solution chemistry on the reaction rate of SCMs was not quantified (see Chapter 2). The limitations of these model will be dealt with in this study.

In this study, HYMOSTRUC3D (see introduction of HYMOSTRUC3D in section 2.2.2) will be extended for simulating the hydration and microstructure development of PC blended with blast furnace slag (BFS) or/and fly ash (FA). The pore solution chemistry of blended cement system and its influence on the reaction of BFS or/and FA are particularly dealt with. The nucleation and growth of CH particles will be simulated. In addition, a pore structure module will be proposed to simulate the evolution of the porosity of capillary pores and gel pores of blended cement paste. This model is an extension of HYMOSTRUC3D. Hence, it is called HYMOSTRUC3D-E.

Fig. 3.1 shows the structure of Chapter 3. First the chemistry of reactants will be discussed. Then the structure of HYMOSTRUC3D-E will be explained. In the last part one of the two routes of HYMOSTRUC3D-E, i.e. *cement hydration route*, will be described.

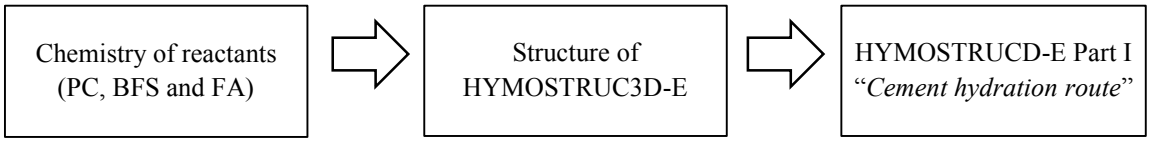

Fig. 3.1 Structure of Chapter 3

3.1.1 Chemistry of reactants (PC, BFS and FA)

The hydration and microstructure development of blended cements involve a variety of physical and chemical aspects. Fig. 3.2 shows a schematic picture for these aspects.

1. Initial mixing stage

Fig. 3.2a shows the initial stage when PC, BFS and FA are mixed with water. The particles of PC, BFS have irregular shapes, and the particles of FA are more spherical. PC is rich in CaO and SiO_2, BFS is rich in CaO, SiO_2 and Al_2O_3, and FA is rich in SiO_2 and Al_2O_3. The oxides in PC particles are present mainly in crystalline form, such as C_3S, C_2S, C_3A, and C_4AF, and the oxides in both BFS and FA particles are mainly present in glassy form.

2. Hydration of PC

Fig. 3.2b illustrates an arbitrary stage of the hydration process of PC. The oxides (CaO, SiO_2, Al_2O_3, Na_2O, and K_2O, etc.) of PC and the gypsum will dissolve in the water at first. Then, the Ca^{2+}, Na^+, K^+, OH^- , SO_4^{2-}, $Al(OH)_4^-$ and $SiO(OH)_3^-$ ions will form in the pore solution, and the pH of the pore solution will increase. Because the solubility of anhydrous phases is higher than that of hydration products, the hydration products will form when their solubility equilibria in the pore solution are reached. For example, when the concentrations of Ca^{2+} and OH^- ions increase to the solubility equilibrium of calcium hydroxide (CH), CH will form. When the concentrations of Ca^{2+}, $SiO(OH)_3^-$ and OH^- ions reach the solubility equilibrium of calcium silicate hydrate (CSH) gel, CSH gel will form. CH particles normally form in the pore space. CSH gel is normally categorized as inner CSH gel and outer CSH gel. Inner CSH gel is produced in the space originally occupied by unhydrated PC, while the outer product is produced in the water-filled pore space *[Taylor, 1997]*. Because the volume of hydration products is smaller than that of the reactants, chemical shrinkage will occur with progress of the hydration process and empty capillary pores will form.

3. Pozzolanic reaction of BFS and FA

Fig. 3.2c illustrates an arbitrary stage of the pozzolanic reactions of BFS and FA. BFS particles will partially dissolve in the pore solution very fast and a Ca^{2+}-rich protective film at the surface of BFS particles is formed (see Taylor *[1997]* and Mehta *[1989]*) and will inhibit its further dissolution. With ongoing hydration, the pH in the pore solution will reach a critical value. Beyond this critical pH, the Ca^{2+}-rich protective film will break, and the oxides in BFS will gradually dissolve in the pore solution. Unlike BFS particles, the FA particles probably will not form a Ca^{2+}-rich protective film when they dissolve in the pore solution because the amount of CaO in FA particles is small. With increasing the pH in the pore solution, both the dissolution rates of BFS and FA will increase. It is noted that the amount of CaO in BFS and FA is much smaller than in PC, and is insufficient to form CSH gel. The Ca^{2+} released from PC and CH, however, will contribute to the formation of CSH gel. This process is called pozzolanic reaction. The CSH gel produced by pozzolanic reactions of BFS and FA differs

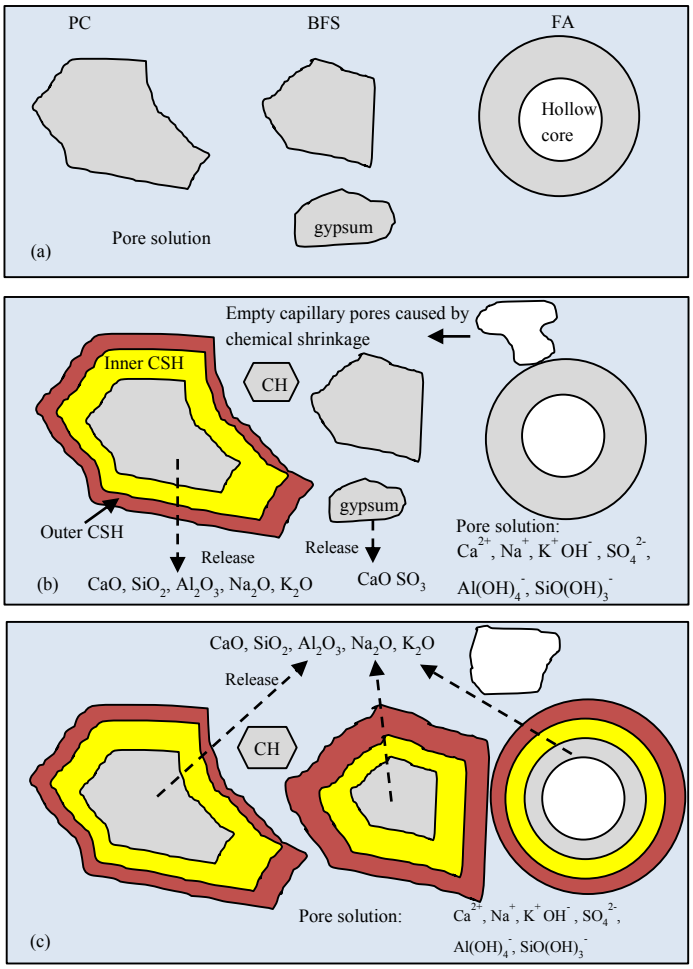

Fig. 3.2 Schematic picture of the hydration in sealed blended cement system. (a) Initial stage; (b) PC starts to hydrate; (c) BFS and FA start to react.

from that produced by the hydration of PC. For example, the CSH gel formed by the pozzolanic reaction of BFS will contain a small amount of Al_2O_3, and less CaO *[Richardson, 1999; 2002]*. This CSH gel, that contains Al_2O_3, is also called CASH gel.

4. Formation of microstructure

The volume of hydration products is larger than that of solid reactants. Hence, the system will become denser. The CSH gel will bind the cement or/and other particles. A solid skeleton will form, and the cement paste will get strength. The remaining space of cement paste is the capillary pore system. The CSH gel will contain small pores at the nanoscale. These pores are defined as gel pores.

3.1.2 Structure of the simulation model

The dissolution of cementitious particles and the formation of hydration products are two processes of the hydration and microstructure development of blended cements. Several aspects of these two processes should be addressed for simulating the hydration and microstructure development of blended cement. These aspects are:

1. Stoichiometry of the hydration of blended cement
2. Kinetics of the reaction of blended cement
3. Pore solution chemistry
4. Interactions between PC, BFS and FA particles
5. Multi-scale pore structure

By considering these aspects, the structure of the model for hydration and microstructure development of blended cements is proposed (Fig. 3.3). This structure comprises two routes: the *cement hydration route* and the *microstructure development route*.

In the *cement hydration route* (see the left part of Fig. 3.3), the rate of hydration of blended cement is simulated as a function the water content, clinker composition, particles size distribution of the cement and temperature of the system. The effect of the pore solution chemistry on the reaction rate of blended cement is quantified. The obtained degree of hydration is used to simulate the pore solution chemistry and to calculate the volume evolution of different phases in the system based on the stoichiometry of the chemical reactions of PC, BFS and FA.

In the *microstructure development route* (see the right part of Fig. 3.3), a representative elementary volume (REV) of cement paste is built first. Next, the initial spatial distribution of particles in the fresh paste is simulated by random packing of the PC, BFS and FA particles in the REV. Then, by letting these PC, BFS and FA particles grow, the microstructure development of blended cement paste is simulated. In the algorithm for particle growth, the thickness of the shell of reaction product depends on the degree of hydration of the blended cement obtained in the *cement hydration route*. An additional module is proposed to simulate the nucleation and growth of CH particles in the pore space. After simulating the microstructure, the volume evolution of different phases in the 3D microstructure can be calculated. In addition the evolution of the gel porosity in cement paste is determined using a pore structure module.

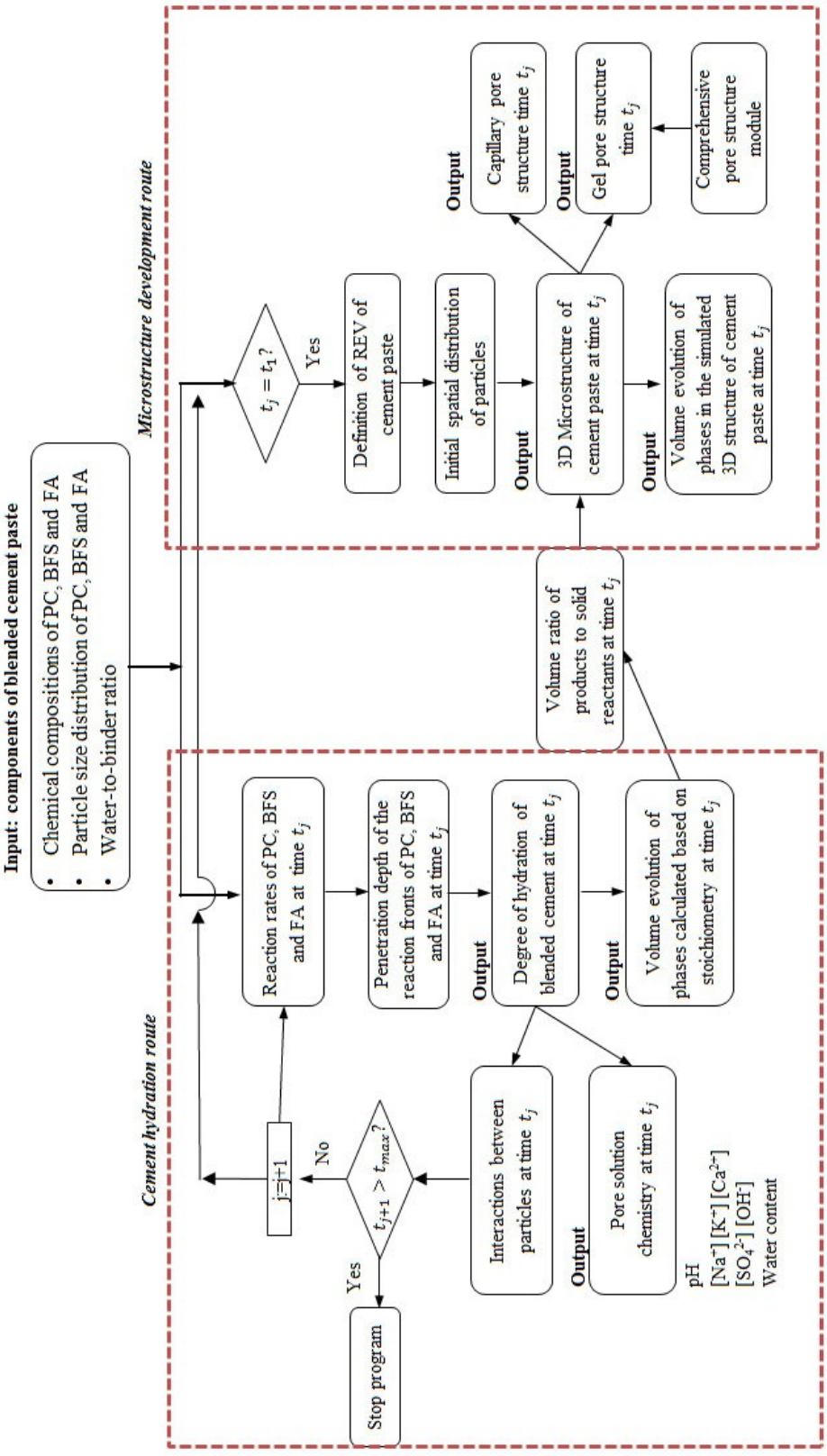

Fig. 3.3 Two routes in the model for hydration and microstructure development of blended cement pastes. REV = representative elementary volume

This chapter will concentrate on the *cement hydration route*. Because of the importance of the pore solution chemistry, this chapter is divided in two sections: 1) Section 3.2 will deal with the *cement hydration route*. 2) Section 3.3 will deal with the simulation of the pore solution chemistry of blended cement paste. The *microstructure development route* will be discussed in the next chapter (Chapter 4).

3.2 The cement hydration route

3.2.1 Stoichiometry of the chemical reactions of blended cements

The stoichiometry of the hydration of blended cements is a fundamental aspect for the simulation model. Based on the stoichiometry of the hydration of blended cement, the evolution of different phases, i.e., the reactants and hydration products, in the system can be calculated. The following paragraphs will deal with the stoichiometry of the hydration and pozzolanic reactions of PC, BFS and FA in HYMOSTRUC3D-E.

3.2.1.1 Stoichiometry of the hydration of PC

Portland cement comprises four main minerals, i.e. C_3S, C_2S, C_3A, C_4AF. These minerals can react with water to form hydration products. The hydration products of C_3S and C_2S are CSH gel and CH. The hydration products of C_3A and C_4AF are more complex because the chemical reactions of C_3A and C_4AF depend on the actual contents of gypsum ($C\bar{S}H_2$) and ettringite ($C_6A\bar{S}_3H_{32}$) in the system *[Bentz et al, 1994; Merzouki et al., 2013]*. C_3A and C_4AF will react with gypsum and water to form ettringite. If gypsum is used up and ettringite is present in the system, C_3A and C_4AF will react with ettringite and water to form AFm phase ($C_4A\bar{S}H_{12}$). If the system doesn't have gypsum or ettringite, C_3A and C_4AF will react with water to produce C_3AH_6. In comparison with other hydration products, such as CH, CSH gel does not have one specific composition. Taylor *[1997]* summarized that the mole ratio of Ca to Si (Ca/Si ratio) in CSH gel ranges from 1.6 to 2.0. A lower Ca/Si ratio was also observed during the first few hours of reaction. Young et al. *[1986]* calculated the stoichiometry of the hydration of C_3S. In this calculation, the composition of CSH was assumed as $C_{1.7}SH_4$. Similarly, in models, such as the models of Bentz et al. *[1994]* and Merzouki et al. *[2013]*, the composition of CSH was also assumed as $C_{1.7}SH_4$.

In HYMOSTRUC3D-E, the chemical composition of CSH gel produced by the hydration of C_3S and C_2S is also assumed as $C_{1.7}SH_4$. The chemical reactions of C_3S and C_2S are *[Young et al., 1986; Bentz et al., 1994; Merzouki et al., 2013]:*

$$C_3S+5.3H\rightarrow C_{1.7}SH_4+1.3CH \quad (3.1)$$

$$C_2S+4.3H\rightarrow C_{1.7}SH_4+0.3CH \quad (3.2)$$

The chemical reactions of C_3A and C_4AF are classified according to the actual amount of gypsum ($C\bar{S}H_2$) and ettringite ($C_6A\bar{S}_3H_{32}$) in the system *[Bentz et al, 1994; Merzouki et al., 2013]*:

1. If gypsum is present in the system:

$$C_3A+3C\bar{S}H_2+26H\rightarrow C_6A\bar{S}_3H_{32} \quad (3.3)$$

$$C_4AF+3C\bar{S}H_2+30H\rightarrow C_6A\bar{S}_3H_{32}+CH+FH_3 \quad (3.4)$$

2. If gypsum is used up and ettringite is present in the system:

$$2C_3A+C_6A\bar{S}_3H_{32}+4H\rightarrow 3C_4A\bar{S}H_{12} \quad (3.5)$$

$$2C_4AF+C_6A\bar{S}_3H_{32}+12H\rightarrow 3C_4A\bar{S}H_{12}+2CH+2FH_3 \quad (3.6)$$

3. If gypsum is used up and ettringite is used up:

$$C_3A+6H\rightarrow C_3AH_6 \quad (3.7)$$

$$C_4AF+10H\rightarrow C_3AH_6+CH+FH_3 \quad (3.8)$$

With progress of the hydration process of PC, the actual contents of gypsum and ettringite will change. Accordingly the stoichiometry of the hydration of PC will change, which will affect the chemically bound water of PC and the evolution of phases in the cement paste (see Appendix C). In HYMOSTRUC3D-E, these aspects will be taken into account in the simulation of the hydration process and microstructure development of hardening blended cement.

3.2.1.2 Stoichiometry of the pozzolanic reaction of BFS

In the presence of moisture BFS particles will react with CH at ordinary temperatures to form compounds with cementitious properties. As proposed by Maekawa et al. *[1999]*, the chemically-bound water, gel water and consumed CH per 1 g reacted BFS are 0.30 g, 0.15 g, 0.22 g, respectively. Wang et al. *[2010a, 2010b]* used these stoichiometric data to simulate the hydration and microstructure of slag cement pastes. Also Richardson et al. *[2002]* investigated the stoichiometry of the reaction of BFS in the presence of moisture and CH. Based on experimental data, they used the following chemical reaction to describe the reaction of BFS with water and CH:

$$C_{7.88}S_{7.39}M_3A+2.6CH+bH\rightarrow 7.39C_{1.42}SH_mA_{0.046}+0.66M_{4.6}AH_d \quad (3.9)$$

where $C_{7.88}S_{7.39}M_3A$ represents BFS. $C_{1.42}SH_mA_{0.046}$ is the CSH gel produced by the reaction of BFS with CH and water. $M_{4.6}AH_d$ is the chemical formula of hydrotalcite. In this equation b, m and d are stoichiometric coefficients.

Merzouki et al. *[2013]* used the stoichiometry of the pozzolanic reaction of BFS proposed by Richardson et al. *[2002]* (Eq. (3.9)) to simulate the hydration and chemical shrinkage of slag cements. This stoichiometry of the pozzolanic reaction of BFS is suitable for the specified BFS with a chemical composition $C_{7.88}S_{7.39}M_3A$. However for other BFS with different chemical composition whether this chemical reaction is suitable needs further study.

Chen et al. *[2007a, 2007b, 2007c]* quantified the reaction products of BFS formed in the presence of alkalis and water, based on the molar balances of the oxides between the BFS and the reaction products. This method can be used for determining the stoichiometry of the pozzolanic reaction of BFS with different chemical compositions. Kolani et al. *[2012]* also used the stoichiometry of the reaction of BFS proposed by Chen et al. *[2007a, 2007b, 2007c]* to simulate the hydration of slag cements.

Similar to the model of Merzouki et al. *[2013],* the HYMOSTRUC3D-E model uses the stoichiometry of the reaction of BFS proposed by Richardson et al. *[2002]*. The stoichiometric coefficients b, m and d in Eq. (3.9) are identified as follows:

As summarized by Chen et al. *[2007a, 2007b, 2007c]*, the H/S ratio of CSH gel can be linked to the C/S ratio of CSH gel: H/S = C/S +1.5 at 100% relative humidity (RH). Using this relationship, stoichiometric coefficient m for CSH gel $C_{1.42}SH_mA_{0.046}$ is calculated with Eq. (3.10):

$$m = 1.42 + 1.5 = 2.92 \quad (3.10)$$

where 1.42 is the C/S ratio of CSH gel $C_{1.42}SH_mA_{0.046}$.

The stoichiometric coefficient d for the pozzolanic reaction product $M_{4.6}AH_d$ is set at 19 according to the research of Chen et al. *[2007a, 2007b, 2007c]*. Then, according to the molar balance of water in Eq. (3.9), the stoichiometric coefficient b is calculated at 31.5. Accordingly, the stoichiometry of the pozzolanic reaction of BFS used in the HYMOSTRUC3D-E model is:

$$C_{7.88}S_{7.39}M_3A+2.6CH+31.5H\rightarrow 7.39C_{1.42}SH_{2.92}A_{0.046}+0.66M_{4.6}AH_{19} \quad (3.11)$$

3.2.1.3 Stoichiometry of pozzolanic reactions of FA

Bentz et al. *[1997]* used $C_{1.1}SH_{3.9}$ to represent the CSH gel produced by the pozzolanic reaction of FA. The reactants of the pozzolanic reaction of FA were assumed to be CH, water, SiO_2 (S, released from fly ash) and Al_2O_3+SiO_2 (AS, aluminosilicate glass, released from

FA). The main reaction products were assumed to be $C_{1.1}SH_{3.9}$ and strätlingite (C_2ASH_8). The main chemical reactions are:

1. CSH gel formation:

$$1.1CH+S+2.8H\rightarrow C_{1.1}SH_{3.9} \quad (3.12)$$

2. strätlingite formation:

$$2CH+AS+6H\rightarrow C_2ASH_8 \quad (3.13)$$

According to Biernacki et al. *[2001]* the consumption of CH per unit of FA calculated based on experimental data was not consistent with Eq. (3.12) to Eq. (3.13). In contrast, the consumption of CH was closer to the value calculated based on the chemical equations proposed by Helmuth *[1987]*:

$$xCH+yS+zH\rightarrow C_xS_yH_{x+z} \quad (3.14)$$

$$AS_2+3CH+zH\rightarrow CSH_{x-5}+C_2ASH_8 \quad (3.15)$$

$$A+3CH+C\bar{S}H_2+7H\rightarrow C_4A\bar{S}H_{12} \quad (3.16)$$

In Eq. (3.14) to Eq. (3.16) the reactants are CH, water, gypsum ($C\bar{S}H_2$), SiO_2 (S, released from FA), Al_2O_3 (A, released from FA) and $Al_2O_3+2SiO_2$ (AS_2, aluminosilicate glass, released from FA). The products are CSH gel ($C_xS_yH_{x+z}$ and CSH_{x-5}), strätlingite (C_2ASH_8), and monosulphate ($C_4A\bar{S}H_{12}$).

According to Papadakis *[1999]* the products of the pozzolanic reaction of FA contain CSH gel, tetracalcium aluminate hydrate (C_4AH_{13}) and monosulfate ($C_4A\bar{S}H_{12}$). For the pozzolanic reactions of FA he proposed:

$$S+1.5CH\rightarrow C_{1.5}SH_{1.5} \quad (3.17)$$

$$A+C\bar{S}H_2+3CH+7H\rightarrow C_4A\bar{S}H_{12} \quad (3.18)$$

$$A+4CH+9H\rightarrow C_4AH_{13} \quad (3.19)$$

The main differences between the chemical equations proposed by Bentz et al. *[1997],* Helmuth *[1987],* Papadakis *[1999]* are found in the formation of hydration products (Table 3.1). First of all, the C/S ratio of the CSH gel produced by the reaction of FA in different studies is different. In addition, Bentz et al. *[1997]* and Biernacki et al. *[2001]* considered that

Table 3.1 Reactants and products of the pozzolanic reaction of FA reported in literature

Reference	Reactants	Products
Helmuth *[1987]*	S, AS_2, A, CH, $C\bar{S}H_2$, water	$C_xS_yH_{x+z}$, CSH_{x-5} C_2ASH_8, $C_4A\bar{S}H_{12}$
Bentz et al. *[1997]*	S, AS, CH, water	$C_{1.1}SH_{3.9}$, C_2ASH_8
Papadakis *[1999]*	S, A, $C\bar{S}H_2$,CH, water	$C_{1.5}SH_{1.5}$, $C_4A\bar{S}H_{12}$ C_4AH_{13}

strätlingite could be produced, whereas Papadakis *[1999]* indicated that aluminate hydrate could be produced. These differences are probably due to differences in the chemical compositions of FA in their studies.

In HYMOSTRU3D-E the stoichiometry of pozzolanic reactions of FA proposed by Bentz et al. *[1997]* are used. By combining Eq. (3.12) and Eq. (3.13) it holds:

$$AS{\cdot}xS{\cdot}yC+(2+1.1x-y)CH+(6+2.8x+y)H\rightarrow xC_{1.1}SH_{3.9}+C_2ASH_8 \quad (3.20)$$

where AS·xS·yC is the chemical formula for FA. x and y are stoichiometry coefficients. x and y can be calculated from the chemical composition of FA.

3.2.2 Reaction rates of PC, BFS and FA particles

3.2.2.1 Reaction rate of PC particles and PC clinker components

1. Reaction kinetics of PC

In HYMOSTRUC, the hydration process of PC was assumed to change from *phase-boundary reaction* to *diffusion-controlled reaction [Van Breugel, 1991]*. These two reaction periods were simulated with a core-shell model (Fig. 3.4). At the beginning the reaction of the particle is controlled by a *phase-boundary reaction*. During this period, the reaction rate will not be affected by the formation of hydration products. With progress of the hydration process the cement particle gradually dissolves. The inner product will form in the place originally occupied by unhydrated PC. The outer product will form on the outer surface of the particle, which will lead to an outward growth of the outer shell. When the total thickness of the inner product and outer product reaches a threshold value, the hydration will become *diffusion-controlled reaction*. This threshold value is defined as *transition thickness*. During the aforementioned reaction period, the reaction rate is affected by the total thickness of the inner product and outer product.

With increasing thickness of outer shell the adjacent small particles will be embedded in the outer shell of bigger particles. The encapsulation of adjacent small particles will result in an extra growth of the outer shell (Fig. 3.4). In addition, if the embedded small cement particles are not fully hydrated yet, they will further react, consuming water. In consequence, the rate of reaction of the bigger particles will further decrease.

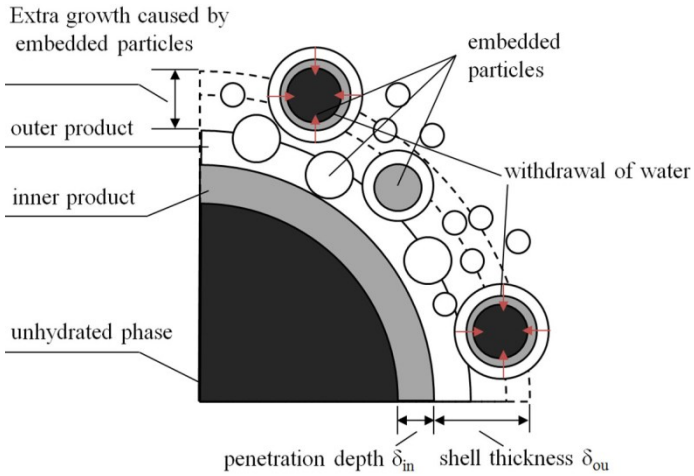

Fig. 3.4 Schematic representation of the core-shell model of a hydrating PC particle in HYMOSTRUC

Based on the above growth process, Van Breugel *[1991]* simulated the rate of hydration of PC particles with Eq. (3.21):

$$\frac{\Delta\delta_{in,x_i,j+1}}{\Delta t_{j+1}} = K_0 \times \Omega_1(.) \times \Omega_2(.) \times \Omega_3(.) \times F_1(.) \times \left[F_2(.) \times \left(\frac{\delta_{tr}}{\delta_{x_i,j}}\right)^{\beta_1}\right]^{\lambda} \qquad (3.21)$$

where $\Delta\delta_{in,x_i,j+1}$ is an incremental increase of the penetration depth of the reaction front of PC particle x_i during a time increment $\Delta t_{j+1} = t_{j+1} - t_j$. K_0 is the initial penetration rate of the reaction front of a hydrating PC particle [μm/hour]. Ω_1, Ω_2 and Ω_3 are reduction factors allowing for the change of water distribution and change in pore water chemistry in the system. F_1 represents the influence of temperature on the rate of reaction. F_2 represents the influence of temperature on the morphology and structure of hydration products. δ_{tr} is the *transition thickness* of the shell of hydration products when the hydration mechanism of PC particle changes from *phase boundary reaction* to *diffusion-controlled reaction*. λ is a coefficient to control the types of reaction (from *phase boundary reaction* ($\lambda = 0$) to *diffusion-controlled reaction* ($\lambda = 1$)). β_1 is a calibration parameter.

PC normally consists of four clinker components (C_3S, C_2S, C_3A and C_4AF). As summarized by Van Breugel *[1991]*, these clinker components will hydrate independently at early age (Fig. 3.5a), while at later age when the hydration is in the *diffusion-controlled* period, the hydrations of these clinker components are at equal fraction rate (Fig. 3.5b). The concept of independent hydration seems to be more realistic to describe the hydration of PC particularly at early age, because the solubility of these minerals is different.

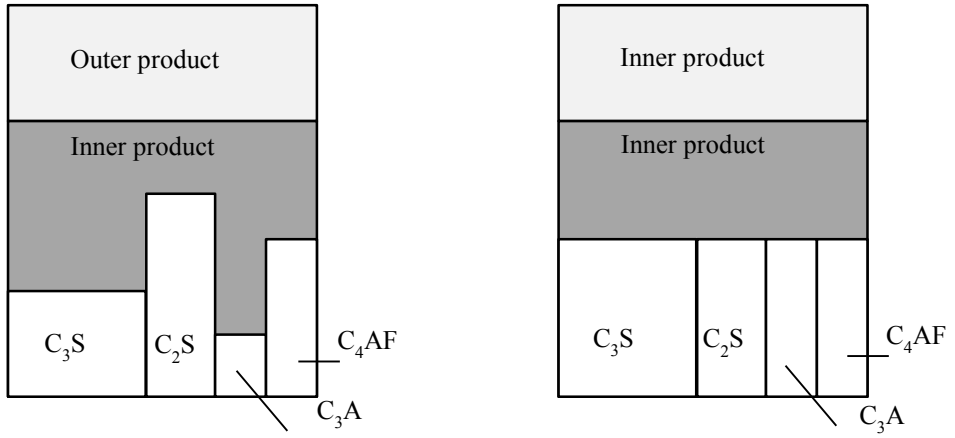

Fig. 3.5 Schematic representation of independent hydration concept and hydration at equal fractional rates [after Van Breugel, 1991]

2. Reaction rates of PC particles and PC clinker components in HYMOSTRUC3D-E

In this thesis, the concept of independent hydration of the components of PC particles (C_3S, C_2S, C_3A and C_4AF) will be used for simulating the hydration process of PC particles. Similar to Eq. (3.21), the reaction rates of the components of PC particles can be described with Eq. (3.22):

$$\frac{\Delta\delta_{in,x_i,j+1,M_k}}{\Delta t_{j+1}} = K_{0,M_k} \times \Omega_1(.) \times \Omega_2(.) \times \Omega_3(.) \times F_1(.) \times \left[F_2(.) \times \left(\frac{\delta_{tr,M_k}}{\delta_{x_i,j,M_k}} \right)^{\beta_1} \right]^{\lambda_{M_k}} \quad (3.22)$$

where $\Delta\delta_{in,x_i,j+1,M_k}$ is an incremental increase of the penetration depth of the reacted part of component M_k ($M_{k=1}$ = C_3S; $M_{k=2}$ = C_2S; $M_{k=3}$ = C_3A; $M_{k=4}$ = C_4AF) during a time increment $\Delta t_{j+1} = t_{j+1} - t_j$. K_{0,M_k} is the initial penetration rate of the reaction front of component M_k (μm/hour). δ_{tr,M_k} is the transition thickness of the shell of hydration products when the hydration mechanism of M_k changes from *phase boundary reaction* (λ_{M_k} = 0) to *diffusion-controlled reaction* (λ_{M_k} = 0). The definitions and calculations of K_0, Ω_1, Ω_2, Ω_3, F_1, F_2 are described in Appendix A.7. The values of K_0 and δ_{tr} for C_3S, C_2S, C_3A, C_4AF are calculated according to the equations suggested by Nguyen *[2011]*. Nguyen *[2011]* summarized the values of K_0 and δ_{tr} for C_3S, C_2S, C_3A, C_4AF in PC particles with different clinker compositions. He found that the values of K_0 and δ_{tr} for C_3S, C_2S, C_3A, C_4AF depend on the mass fraction of clinker components in PC particles. Using linear regression he obtained the equations listed in Table 3.2 to calculate the values of K_0 and δ_{tr} for C_3S, C_2S, C_3A, C_4AF in PC particles.

Table 3.2 Equations to calculate the hydration parameters K_0 and δ_{tr} for different components of PC [after Nguyen, 2011]

No.	Phase	K_0 [μm/h]	δ_{tr} [μm]
1	C_3S	0.064 + 0.020×(1 - % C_3S)	2.12 + 1.47×(1 - % C_3S)
2	C_2S	0.003 + 0.002×(1 - % C_2S)	2.07 + 1.15×(1 - % C_2S)
3	C_3A	1.212 - 1.171×(1 - % C_3A)	2.33 + 1.28×(1 - % C_3A)
4	C_4AF	0.02	1.19

3.2.2.2 Reaction rates of BFS and FA particles

1. Reaction kinetics of BFS and FA

To investigate the reaction kinetics of BFS, Biernacki et al. *[2002]* determined the CH consumption in the system of BFS mixed with CH and water. Using the measured CH consumption, they calculated the degree of reaction of BFS. They found that the reaction rate of BFS at early age is very fast and then gradually slows down (Fig. 3.6). The fast reaction rate at early age follows the *phase boundary reaction*, and the slow reaction rate at later age follows the *diffusion-controlled reaction*.

Biernacki et al. *[2001]* investigated the reaction kinetics of FA in the presence of CH and water. They determined the CH consumed by the reaction of FA. As shown in Fig. 3.7, the consumption rate of CH is very fast at early age and slows down at later age. The fast consumption of CH at early age illustrates that the reaction of FA follows the *phase boundary reaction* at early age. The slow consumption rate of CH at later age suggests that the reaction of FA the follows the *diffusion-controlled reaction*.

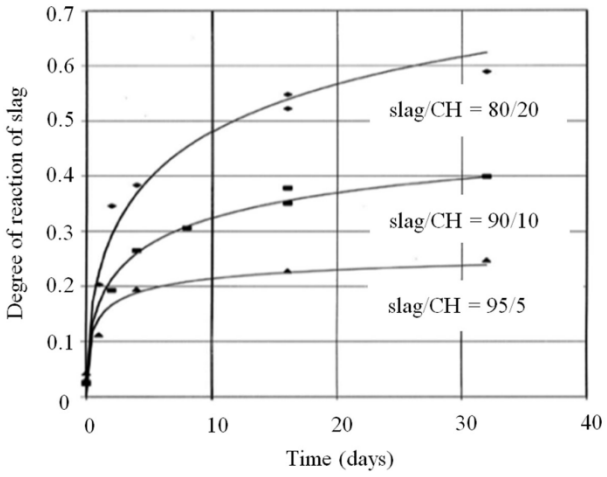

Fig. 3.6 Extent of slag hydration versus time at 25 ºC for various slag to CH ratios: slag/CH = 80/20, 90/10 and 95/5 [after Biernacki et al., 2002]. Note: water-to-solid ratio is 0.55 for all samples

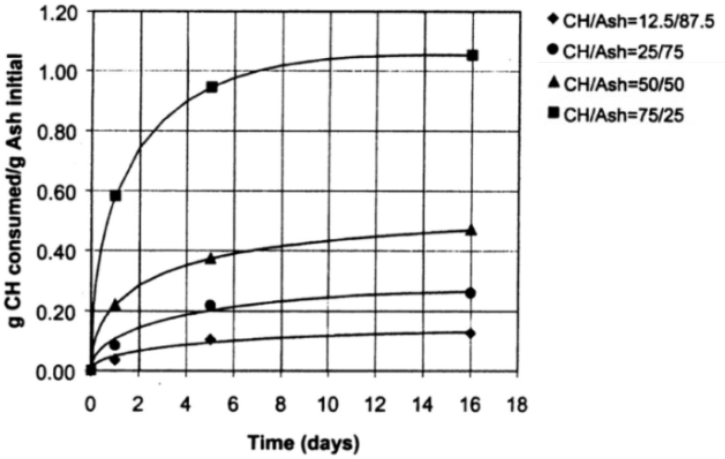

Fig. 3.7 Mass of CH consumed per unit mass of fly ash as a function of time for various CH to fly ash ratios at 25 ºC [Biernacki et al., 2001] Note: water-to-solid ratio is 1.25 for all samples

It should be noted that some FA particles are hollow. For solid FA particles the change from *phase boundary reaction* to *diffusion-controlled reaction* is applicable. However, for hollow FA particles the change from the *phase boundary reaction* to *diffusion-controlled reaction* is less obvious and needs further study. Fig. 3.8 schematically shows the core-shell model of a reacting hollow FA particle, while Fig. 3.9 shows the schematic diagram of the reaction rate versus the total thickness of product shell of the reacting hollow FA particle. At early age, the dissolution rate $d\delta_{in}/dt$ of the hollow FA particle is constant (K_0) at a certain temperature and for a certain pore solution chemistry. The hollow core of the FA particle will not affect this dissolution rate. As long as the total thickness of the product shell δ_{tot} does not reach a critical thickness δ_{tr}, the reaction of the follow FA particle will follow a *phase boundary reaction*. When δ_{tot} reaches the transition thickness δ_{tr}, the reaction of the hollow FA particle will follow a *diffusion-controlled reaction*. The dissolution rate $d\delta_{in}/dt$ of the hollow FA particle will be affected by the total thickness of the product shell, while the penetration rate will change from K_0 to $K_0 \times \delta_{tr}/\delta_{tot}$. The hollow core of the FA particle will not affect this dissolution rate. Hence, for hollow FA particles the change from *phase boundary reaction* to *diffusion-controlled reaction* is also adopted.

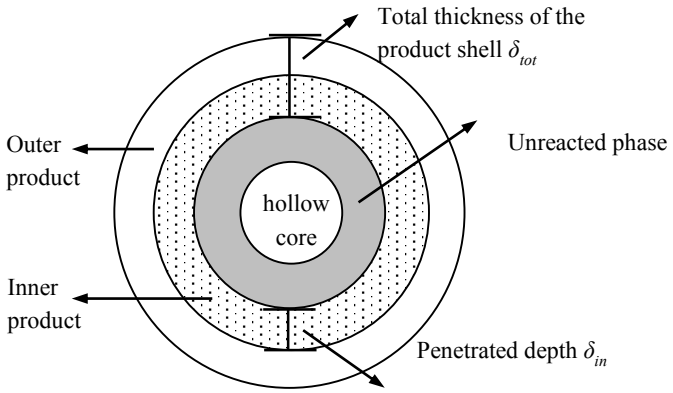

Fig. 3.8 Schematic representation of the core-shell model of a reacting hollow FA particle

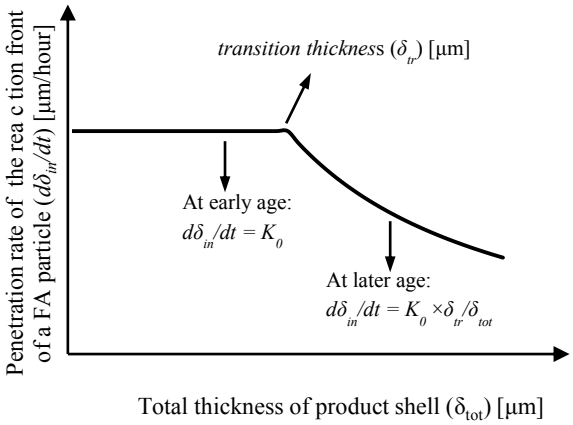

Fig. 3.9 Schematic diagram of the dissolution rate versus the total thickness of product shell of a reacting hollow FA particle

2. Reaction rates of BFS and FA particles

In HYMOSTRUC3D-E the reaction rates of BFS and FA particles are simulated with functions similar to Eq. (3.21). However, there are several modifications:

2a Critical pH

As mentioned in section 3.1.1, BFS particles mainly consist of glassy phases. The glassy phases will initially dissolve in the pore solution very fast and form a Ca^{2+}-rich protective film that inhibits further dissolution of the BFS particles (see Taylor *[1997]* and Mehta *[1989]*). When the pH in the pore solution reaches a critical value, the Ca^{2+}-rich protective film will break, and the glassy phases will gradually dissolve in the pore solution. This value of the pH in the pore solution is called critical pH. FA particles also mainly consist of glassy phases. Unlike BFS particles, the FA particles will probably not form a Ca^{2+}-rich protective film when they dissolve in the pore solution because the amount of CaO in FA particles is small. In

HYMOSTRUC3D-E the critical pH for the pozzolanic reaction of BFS is set at 11.5, a value that has been reported by Song et al. *[1999]*. For the pozzolanic reaction of FA no critical pH is used.

2b Dissolution rate versus pH

For glassy phases, the dissolution rate is normally a function of the pH *[Abraitis et al., 2000; Brantley, 2008; Maeda et al., 2004; Oelkers et al., 1994; Oelkers, 2001]*. Since both BFS and FA particles mainly consist of glassy phases the dissolution rates of BFS and FA particles should be a function of the pH. Fig. 3.10 shows that for the pH from 7 up to 14 the dissolution rate of BFS linearly increases with increasing pH (y axis is log scale, x axis is linear scale).

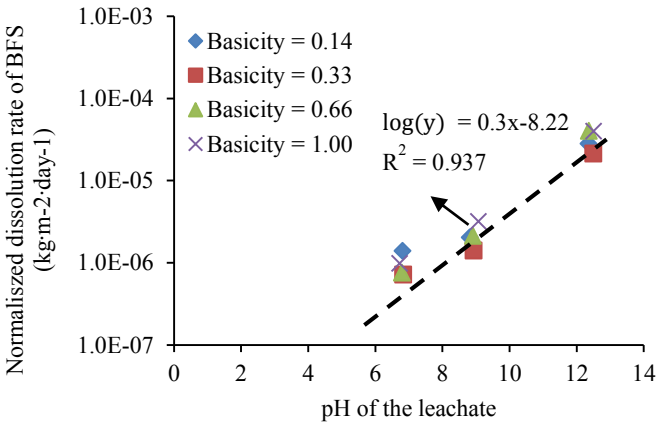

Fig. 3.10 Dissolution rates of BFS particles with different basicity (basicity = mass ratio of CaO+MgO to SiO_2+Al_2O_3) as a function of the pH (temperature = 40 ºC) [after Maeda et al., 2004]

2c Influence of CH

It is possible that CH, produced by the hydration of PC, will be used up by the pozzolanic reactions of BFS and FA. In this case, the pozzolanic reactions of BFS and FA particles will stop, since CH is an essential reactant of the pozzolanic reactions of BFS and FA particles.

Based on the foregoing reasoning, there are three assumptions and conditions for the pozzolanic reactions of BFS and FA particles:

I. The BFS particles will not react until the pH of the pore solution reaches 11.5;
II. The reaction rates of BFS and FA particles are a function of pH of the pore solution;
III. The pozzolanic reaction of BFS and FA particles will stop if no CH is present in the system.

Accordingly, the reaction rates of BFS and FA particles can be simulated using Eq. (3.23):

$$\frac{\Delta\delta_{in,x_i,j+1,S_k}}{\Delta t_{j+1}} = K_{0,S_k} \times \Omega_1(.) \times \Omega_2(.) \times \Omega_3(.) \times F_1(.) \times \left[F_2(.) \times \left(\frac{\delta_{tr,S_k}}{\delta_{x_i,j,S_k}}\right)^{\beta_1}\right]^{\lambda} \times M_{pH} \qquad (3.23)$$

where $\Delta\delta_{in,x_i,j+1,S_k}$ is an incremental increase of the penetration depth of S_k ($S_{k=1}$ = BFS; $S_{k=2}$ = FA) particle during a time increment $\Delta t_{j+1} = t_{j+1} - t_j$. K_{0,S_k} is the initial penetration rate of the reaction front of BFS and FA particle [μm/hour], respectively. δ_{tr,S_k} is the transition thickness of the shell of hydration products when the hydration mechanism of BFS and FA particle changes from *phase boundary reaction* to *diffusion-controlled reaction*. See the calculation of K_{0,S_k} and δ_{tr,S_k} in Appendix A.7.2. M_{pH} is the pH-factor that represents the influence of the pH on the penetration rates of BFS and FA particles. The value of M_{pH} is derived as follows:

The value of M_{pH} for the reaction of BFS particles at time t_j

As shown in Fig. 3.10, for the pH from 7 up to 14, the log dissolution rate [kg·m^{-2}·day^{-1}] of BFS particles increases linearly with increasing the pH. It holds:

$$log(\gamma_{BFS}) = A_{BFS} \times pH + B_{BFS} \qquad (3.24)$$

where A_{BFS} and B_{BFS} are the coefficients of the linear relationship between the pH and $log(\gamma_{BFS})$. For the linear relationship shown in Fig. 3.10, A_{BFS} = 0.3, and B_{BFS} = -8.22.

According to Eq. (3.24), the dissolution rate of BFS particles $\gamma_{BFS,j}$ at time t_j in the pore solution with a certain pH value pH_j is calculated as:

$$\gamma_{BFS,j} = 10^{A_{BFS} \times pH + B_{BFS}} \qquad (3.25)$$

The dissolution rate of BFS particles ($\gamma_{BFS,ref}$) in the pore solution that is used to determine the initial penetration rate of the reaction front of BFS particles ($K_{0,BFS}$) also follows Eq. (3.24):

$$\gamma_{BFS,ref} = 10^{A_{BFS} \times pH_{ref,BFS} + B_{BFS}} \qquad (3.26)$$

where $pH_{ref,BFS}$ is the pH in the pore solution that is used to determine the initial penetration rate of the reaction front of BFS particles.

By combining Eq. (3.25) and Eq. (3.26), we get:

$$\gamma_{BFS,j}/\gamma_{BFS,ref} = 10^{A_{BFS} \times (pH_j - pH_{ref,BFS})} \qquad (3.27)$$

The ratio $\gamma_{BFS,j}/\gamma_{BFS,ref}$ is called the pH-factor M_{pH}, which determines the effect of pH on the reaction rate of a BFS particle at time t_j. Fig. 3.11 shows the value of M_{pH} versus the pH of the pore solution. For pH = $pH_{ref,BFS}$ the factor M_{pH} = 1; for pH < pH_{ref} the factor M_{pH} < 1; for pH > pH_{ref} the factor M_{pH} >1.

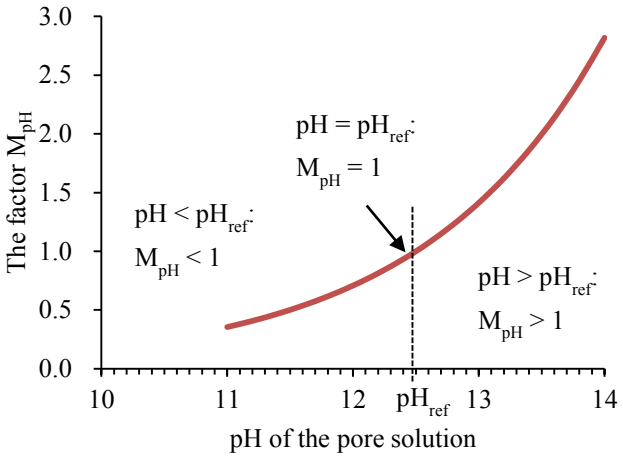

Fig. 3.11 Value of the pH-factor M_{pH} versus the pH of the pore solution. (A_{BFS} = 0.3; pH_{ref} = 12.5)

In Eq. (3.27) A_{BFS} can be determined experimentally. Maeda et al. *[2004]* measured the dissolution rate of BFS particles with different basicity as a function of the pH (temperature = 40 ºC). They found that A_{BFS} is around 0.3 (see the slope of the fit line in Fig. 3.10). Maeda et al. *[2004]* did not measure the dissolution rate of BFS particles at other temperatures. Since BFS particles normally contain over 95 wt. % glassy phase, A_{BFS} should be similar with that for glass (A_{glass}). According to the experiments of McGrail et al. *[1997]* A_{glass} was around 0.4 and did not change significantly with temperature in the range 20-90 ºC (Fig. 3.12). In HYMOSTRUC3D-E it is assumed that A_{BFS} will not change with temperature and A_{BFS} is set at 0.3 according to the experimental data of Maeda et al. *[2004]*.

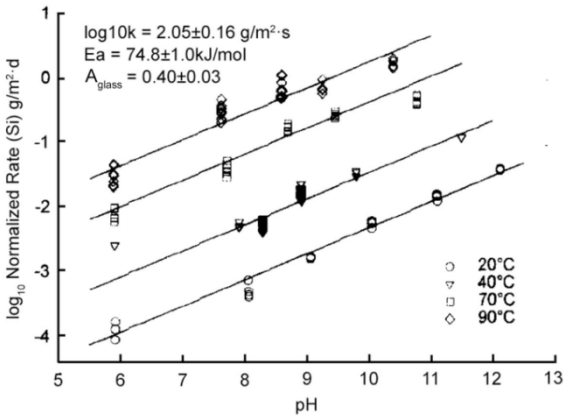

Fig. 3.12 Si release rate as a function of pH and temperature for a Na-Ca-Al borosilicate glass [after McGrail et al., 1997]

The value of M_{pH} for the reaction of FA particles at time t_j

Like the calculation for BFS particles, the factor M_{pH} for determining the effect of pH on the reaction rate of FA particles at time t_j is calculated as:

$$M_{pH,j,FA} = 10^{A_{FA}\times(pH_j - pH_{ref,FA})} \tag{3.28}$$

where $pH_{ref,FA}$ is the pH of pore solution used to determine the initial penetration rate of the reaction front of FA particles $K_{0,FA}$. pH_j is the pH of the pore solution at time t_j. A_{FA} is the slope in the linear relationship between the pH and the log of the dissolution rate of FA. For FA particles the value of A_{FA} is assumed to equal to the value of A_{BFS} (0.3) for the slag cement system.

3.2.3 Degree of hydration of PC and degree of pozzolanic reaction of BFS and FA

The degree of hydration of a particle depends on the ratio of the volume of the reacted part of the particle to the volume of the original particle. The penetrated depth (δ_{in}) can be calculated using Eq. (3.22) and Eq. (3.23). For a PC and BFS particles with radius r and penetrated depth δ_{in} (Fig. 3.13a), the degree of hydration (or reaction) can be calculated with Eq. (3.29). For a hollow FA particle with radius r, the hollow core radius r_{hollow} and the penetrated depth δ_{in} (Fig. 3.13b), the degree of reaction can be calculated with Eq. (3.30).

The overall degrees of hydration can be calculated by considering the particle size distribution in the system. In Appendix B details of procedures for obtaining the degree of hydration of PC and the degrees of pozzolanic reaction of BFS and FA are presented.

$$\alpha(PC\ or\ BFS) = \frac{r^3 - (r - \delta_{in})^3}{r^3} \tag{3.29}$$

$$\alpha(FA) = \frac{r^3 - (r - \delta_{in})^3}{r^3 - r_{hollow}^3} \tag{3.30}$$

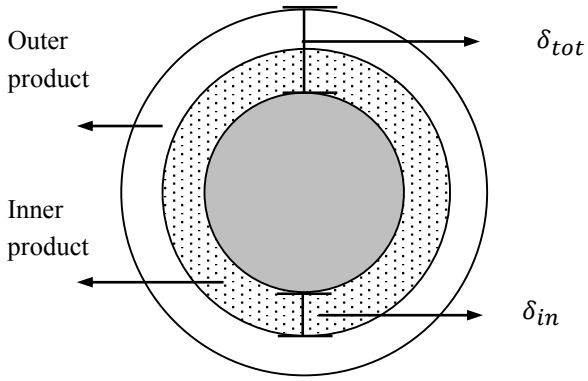

(a) Calculation of the degree of hydration or reaction of a PC and BFS particles

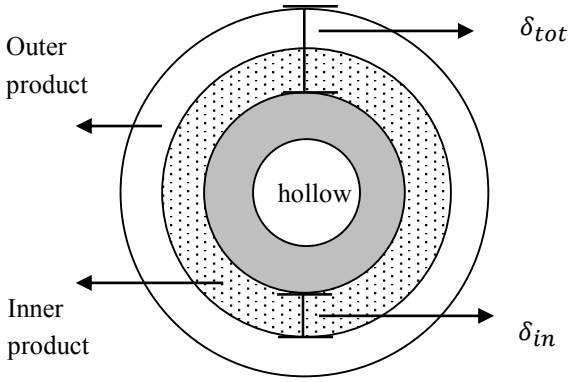

(b) Calculation of the degree of reaction of a FA particle

Fig. 3.13 Schematic representation of the calculation of degree of hydration (or reaction) of a PC, BFS or FA particle.

3.2.4 Interactions between PC, BFS and FA particles

The presence of BFS and FA in a blended cement system will affect the hydration process of PC. Meanwhile, the pozzolanic reactions of BFS and FA will also influence each other. In HYMOSTRUC3D-E, these interactions are considered using the factors Ω_1, Ω_2, Ω_3 and M_{pH} in the equations Eq. (3.22) and Eq. (3.23) for calculating the reaction rates of PC, BFS and FA particles.

3.2.4.1 Reduction factor Ω_1

In HYMOSTRUC, small particles are assumed to become embedded in the growing outer shell of bigger particles. If the embedded small particles are not fully hydrated yet, they will further react, consuming water. In consequence, the amount of water for further reaction of

the bigger particles will reduce. As a result, the rate of reaction of the bigger particles will decrease. This so called water withdrawal effect is accounted for factor Ω_1. The reduction factor Ω_1 is also considered in HYMOSTRUC3D-E for the hydration of blended cements (Fig. 3.14).

1. Reduction factor Ω_1 for the hydration of a PC particle

For a PC particle in blended cement system the water for its further hydration will be partially consumed by the embedded PC, BFS and FA particles as shown in Fig. 3.14a. The reduction factor Ω_1 for the hydration of this PC particle is calculated with Eq. (3.31):

$$\Omega_{em;x_i,j+1,PC} = \frac{\Delta w_{x_i,j,PC}}{\Delta w_{x_i,j,PC} + \Delta w_{em;x_i,j,PC,PC} + \Delta w_{em;x_i,j,BFS,PC} + \Delta w_{em;x_i,j,FA,PC}} \quad (3.31)$$

where $\Omega_{em;x_i,j+1,PC}$ is the reduction factor Ω_1 at time t_{j+1} of a PC particle with diameter of x_i μm. $\Delta w_{x_i,j,PC}$ is the water consumption of this PC particle between time t_{j-1} and t_j. $\Delta w_{em;x_i,j,PC,PC}$, $\Delta w_{em;x_i,j,BFS,PC}$, $\Delta w_{em;x_i,j,FA,PC}$ are the water consumption of embedded PC, BFS, and FA particles between time t_{j-1} and t_j, respectively. For the calculation of $\Delta w_{x_i,j,PC}$, $\Delta w_{em;x_i,j,PC,PC}$, $\Delta w_{em;x_i,j,BFS,PC}$, $\Delta w_{em;x_i,j,FA,PC}$ see Appendix E.1.

2. Reduction factor Ω_1 for the reaction of a BFS particle

For a BFS particle in blended cement system, the water for its further reaction will be partially consumed by the embedded PC, BFS and FA particles as shown in Fig. 3.14b. The reduction factor Ω_1 for the hydration of this BFS particle is calculated with Eq. (3.32):

$$\Omega_{em;x_i,j+1,BFS} = \frac{\Delta w_{x_i,j,BFS}}{\Delta w_{x_i,j,BFS} + \Delta w_{em;x_i,j,PC,BFS} + \Delta w_{em;x_i,j,BFS,BFS} + \Delta w_{em;x_i,j,FA,BFS}} \quad (3.32)$$

where $\Omega_{em;x_i,j+1,BFS}$ is the reduction factor Ω_1 at time t_{j+1} of a BFS particle with diameter of x_i μm. $\Delta w_{x_i,j,BFS}$ is the water consumption of this BFS particle between time t_{j-1} and t_j. $\Delta w_{em;x_i,j,PC,BFS}$, $\Delta w_{em;x_i,j,BFS,BFS}$, $\Delta w_{em;x_i,j,FA,BFS}$ are the water consumption of embedded PC, BFS, and FA particles between time t_{j-1} and t_j, respectively. For the calculation of $\Delta w_{x_i,j,BFS}$, $\Delta w_{em;x_i,j,PC,BFS}$, $\Delta w_{em;x_i,j,BFS,BFS}$ and $\Delta w_{em;x_i,j,FA,BFS}$ see Appendix E.2.

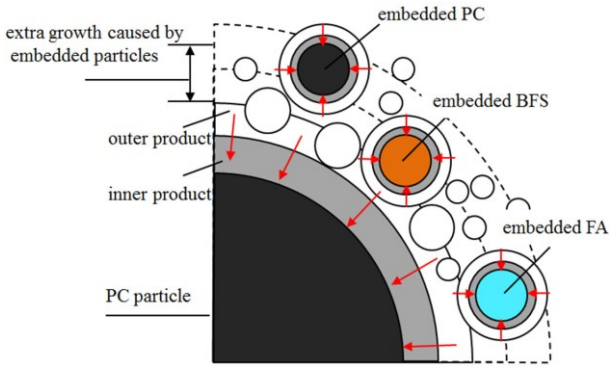

(a) the reduction factor Ω_1 for the hydration of a PC particle

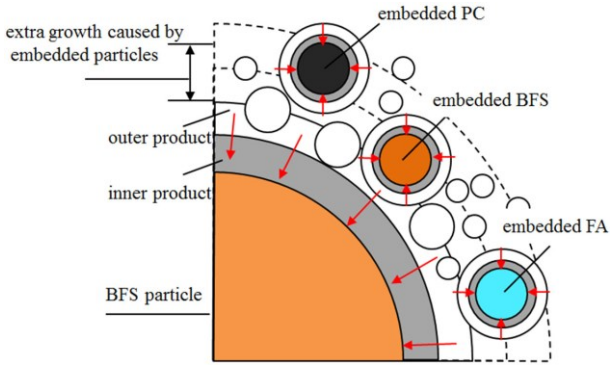

(b) the reduction factor Ω_1 for the reaction of a BFS particle

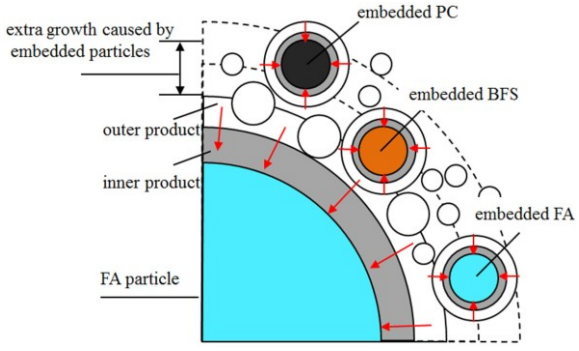

(c) the reduction factor Ω_1 for the reaction of a FA particle

Fig. 3.14 Schematic pictures of the reduction factor Ω_1 for the hydration of a PC,BFS or FA particle

3. Reduction factor Ω_1 for the reaction of a FA particle

For a FA particle in blended cement system, the water for its further reaction will be partially consumed by the embedded PC, BFS and FA particles as shown in Fig. 3.14c. The reduction

factor Ω_1 for the hydration of this FA particle is calculated with Eq. (3.33):

$$\Omega_{em;x_i,j+1,FA} = \frac{\Delta w_{x_i,j,FA}}{\Delta w_{x_i,j,FA} + \Delta w_{em;x_i,j,PC,FA} + \Delta w_{em;x_i,j,BFS,FA} + \Delta w_{em;x_i,j,FA,FA}} \quad (3.33)$$

where $\Omega_{em;x_i,j+1,FA}$ is the reduction factor Ω_1 at time t_{j+1} of a FA particle with diameter of x_i μm. $\Delta w_{x_i,j,FA}$ is the water consumption of this FA particle time t_{j-1} and t_j. $\Delta w_{em;x_i,j,PC,FA}$, $\Delta w_{em;x_i,j,BFS,FA}$, $\Delta w_{em;x_i,j,FA,FA}$ are the water consumption of embedded PC, BFS, and FA particles time t_{j-1} and t_j, respectively. For the calculation of $\Delta w_{x_i,j,FA}$, $\Delta w_{em;x_i,j,PC,FA}$, $\Delta w_{em;x_i,j,BFS,FA}$ and $\Delta w_{em;x_i,j,FA,FA}$ see Appendix E.3.

According to the concept of embedded particles, the particles with different size will embed different volumes of small particles. Hence, Ω_1 will be different for particles with different size.

3.2.4.2 Reduction factor Ω_2

With ongoing hydration water is continuously consumed and the internal relative humidity (RH) will decrease if the system is sealed. As a result, the rate of reaction of the cement particles will decrease. In HYMOSTRUC this effect of water shortage is allowed for with the reduction factor Ω_2. It is calculated with Eq. (3.34):

$$\Omega_2(\alpha) = \frac{A_{wat}(\alpha)}{A_{por}(\alpha)} \quad (3.34)$$

where $A_{wat}(\alpha)$ is the pore wall area of capillary pores filled with water. $A_{por}(\alpha)$ is the total capillary pore wall area.

This reduction factor Ω_2 is also considered in HYMOSTRUC3D-E for the hydration of blended cements (Fig. 3.15). The chemical shrinkage caused by the hydration or reaction of PC, BFS and FA particles will lead to the formation of empty capillary pores in the system and a decrease of the RH. The value of Ω_2 will be identical for all the particles in a certain system. Using the algorithm similar to HYMOSTRUC the reduction factor Ω_2 in HYMOSTRUC3D-E for the hydration of blended cements is calculated as:

$$\Omega_2(\alpha) = \frac{A_{wat}(\alpha)}{A_{por}(\alpha)} = \frac{\phi_{wat;\alpha} - \phi_0}{\phi_{por;\alpha} - \phi_0} \times \frac{\phi_{por;\alpha}}{\phi_{wat;\alpha}} \quad (3.35)$$

where ϕ_0 is the diameter of the smallest capillary pore. $\phi_{por;\alpha}$ is the diameter of the largest capillary pore. $\phi_{wat;\alpha}$ is the diameter of largest capillary pore filled with water. ϕ_0, $\phi_{por;\alpha}$, and $\phi_{wat;\alpha}$ are calculated in the Appendix A.7.4.

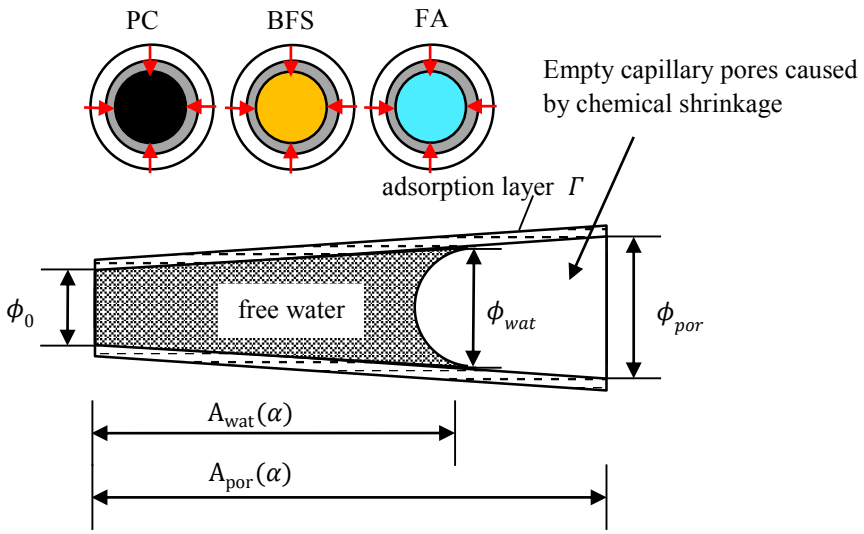

Fig. 3.15 Schematic representation of the reduction factor Ω_2 for the hydration of a PC, BFS or FA particle. Note: ϕ_0 is the diameter of smallest capillary pore and ϕ_{pot} is the diameter of largest capillary pore. ϕ_{wat} is the diameter of largest capillary pore filled with water.

3.2.4.3 Reduction factor Ω_3

With continuing hydration the amount of capillary water available for accommodating Ca^{2+} ions will decrease. When assuming a constant concentration of Ca^{2+} ions, the total amount of Ca^{2+} ions in capillary water will decrease because of the shortage of capillary water. Because Ca^{2+} is important for the formation of hydration products, such as CSH gel and CH, etc., it was estimated that the rate of reaction in the paste will decrease because of the decreasing total amount of Ca^{2+} ions in capillary water *[Van Breugel, 1991]*. In HYMOSTRUC this effect is described with Ω_3:

$$\Omega_3(\alpha) = \frac{V_{wat,j}}{V_{wat,0}} \tag{3.36}$$

where $V_{wat,0}$ is the initial water volume in the system. $V_{wat,j}$ is the capillary water volume at time t_j. This reduction factor Ω_3 is also considered in HYMOSTRUC3D-E for the hydration of blended cements. Ω_3 is calculated with Eq. (3.36). In this equation the capillary water volume $V_{wat,j}$ at time t_j is calculated as:

$$V_{wat,j} = V_{paste,0} - V_{solid,j} - V_{chsh,j} - V_{ad,j,wat} \tag{3.37}$$

where $V_{paste,0}$ is the volume of cement paste with 1 g blended cement and a given w/c [cm^3], $V_{chsh,j}$ is the chemical shrinkage at time t_j for the cement paste with 1 g blended cement [cm^3], $V_{solid,j}$ is the volume of the solid phase of the cement paste [cm^3] at time t_j and $V_{ad,j,wat}$ is the volume of water adsorbed by CSH gel [cm^3] .

3.2.4.3 pH-factor M_{pH}

In the simulation of the evolution of the pH the parameters, such as the degree of reaction of PC, BFS and FA, the alkali proportions in PC, BFS and FA, the gypsum content in the system and the w/c are taken into account (Fig. 3.16). The simulated evolution of the pH is used to quantify the effect of the pH on the reaction rate of BFS and FA particles using the pH-factor M_{pH} (see section 3.2.2.2). Section 3.3 will deal with the module for simulating the pore solution chemistry.

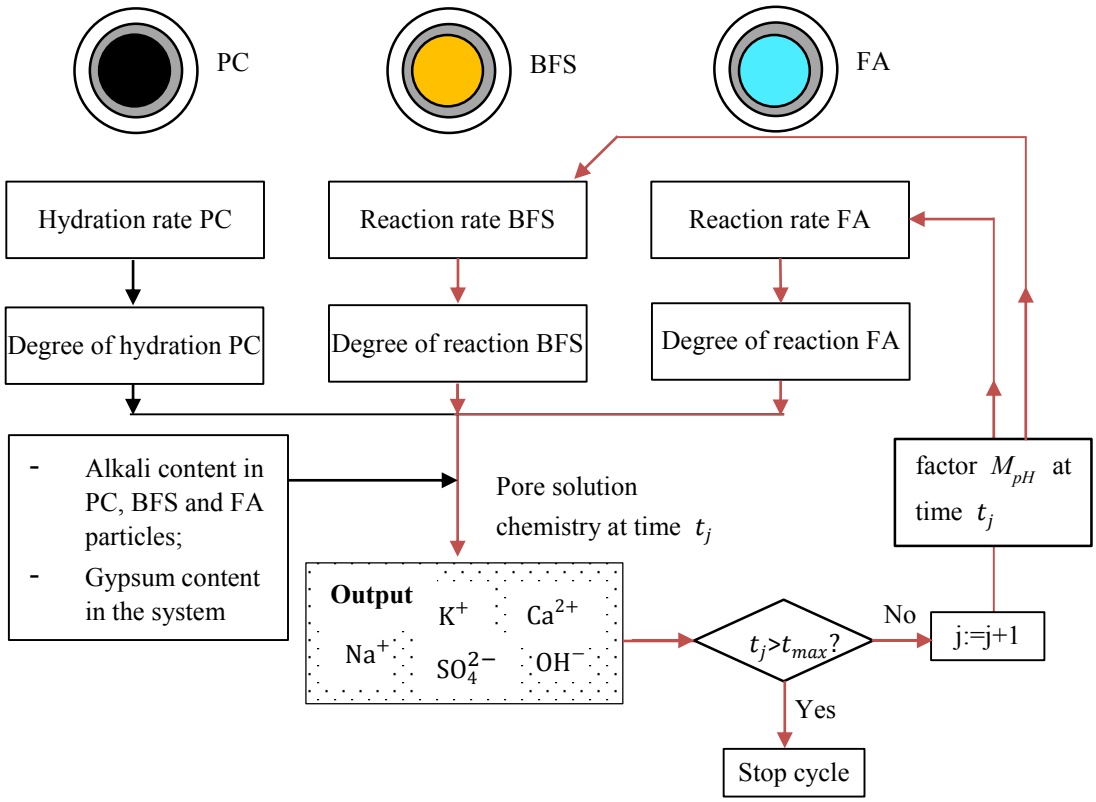

Fig. 3.16 Schematic representation of the relationship between the pore solution chemistry, the factor M_{pH} and the reaction rate of BFS and FA. Note: The value of M_{pH} at time t=0 is assumed to be 1. t_{max} is the maximum duration of the simulation period.

3.2.5 Volume evolution of different phases calculated based on stoichiometry

With progress of the hydration process the shell of reaction product around hydrating particles grows. This results in the microstructure of the cement paste. Without considering the influence of other particles, the thickness of the shell of reaction product around a particle is a function of the radius of the particle, the penetrated depth and the ratio of volumes of reaction products to the volumes of the reactants. In HYMOSTRUC3D, the volume increase ratio is denoted υ. Van Breugel *[1991]* summarized that for Portland cement, the υ-value is a function of curing temperature and the degree of hydration of PC (Fig. 3.17). At room temperature the factor υ decreases from approximate 2.2 to around 1.88 with progress of the hydration process (see the data at room temperature in Fig. 3.17).

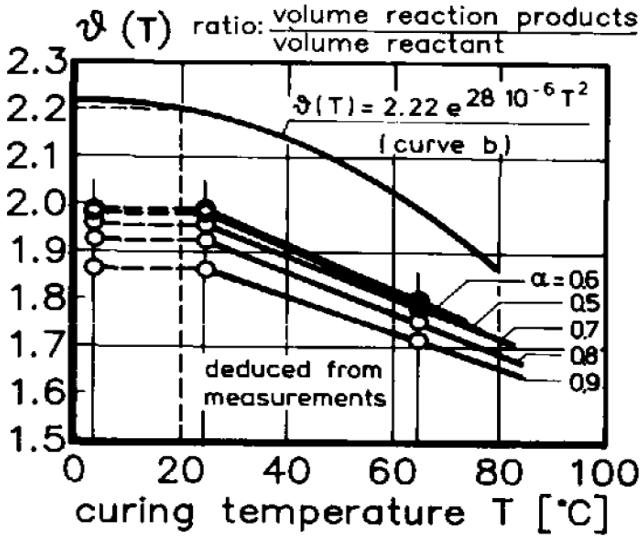

Fig. 3.17 The volume ratio of products to reactants of PC at different degrees of hydration and temperatures [Van Breugel, 1991]

For blended cements, the volume increase ratio υ can be calculated if the evolution of different phases in the blended cement system is obtained. In HYMOSTRUC3D-E the evolution of different phases in the blended cement system is calculated based on the stoichiometry of blended cement hydration. To illustrate how to calculate the volume of different phases based on stoichiometry, the calculation for the volume evolution of hydrating C_3S is taken as an example (Table 3.3). There are four steps:

Table 3.3 Calculation of the volume evolution of hydrating of C_3S

Stoichiometric:	C_3S	+	5.3H	→	$C_{1.7}SH_4$	+	1.3CH
Molar mass (g/mole):	228.3		18		227.4		74.1
Density (g/cm^3):	3.21		1.00		2.05		2.24
Weight (g):	m_{con,j,C_3S}		m_{con,j,H,C_3S}		m_{re,j,CSH,C_3S}		m_{re,j,CH,C_3S}
Amount (in mole):	n_{con,j,C_3S}		n_{con,j,H,C_3S}		n_{re,j,CSH,C_3S}		n_{re,j,CH,C_3S}
Volume (cm^3):	V_{con,j,C_3S}		V_{con,j,H,C_3S}		V_{re,j,CSH,C_3S}		V_{re,j,CH,C_3S}

Note: the weight of reacted C_3S (the value in the grey cell) can be calculated from the degree of reaction of C_3S; using the calculated value in the grey cell, the values in the yellow grid can be obtained based on the stoichiometry of the hydration of C_3S.

Step 1: Weight of reacted C_3S

For the cement paste with 1 g blended cement and a given w/b, the weight of reacted C_3S is calculated from the degree of hydration of C_3S as follows:

$$m_{con,j,C_3S} = \alpha_{j,C_3S} \times f_{C_3S} \times m_{PC} \quad [g] \tag{3.38}$$

where α_{j,C_3S} is the degree of hydration of C_3S at time t_j. m_{PC} is the initial weight of PC [g]. f_{C_3S} is the initial weight fraction of C_3S in PC.

Step 2: Amount (in mole) of hydrated C_3S, consumed water, formed CSH and formed CH.

The amount (in mole) of hydrated C_3S is calculated as:

$$n_{con,j,C_3S} = m(C_3S)/228.3 \quad [mole] \tag{3.39}$$

where 228.3 is the molar mass of C_3S [g/mole].

Based on the stoichiometry of the hydration of C_3S (row 1 in Table 3.3) the amount (in mole) of reacted water, formed CSH and formed CH are calculated as:

$$n_{con,j,H,C_3S} = 5.3 \times n_{con,j,C_3S} \quad [mole] \tag{3.40}$$

$$n_{re,j,CSH,C_3S} = 1 \times n_{con,j,C_3S} \quad [mole] \tag{3.41}$$

$$n_{re,j,CH,C_3S} = 1.3 \times n_{con,j,C_3S} \quad [mole] \tag{3.42}$$

where 5.3, 1, 1.3 are the stoichiometric coefficients (see line 1 of Table 3.3).

Step 3: Weight of consumed water, formed CSH and formed CH

The weight of reacted water, formed CSH and formed CH are calculated as:

$$m_{con,j,wat,C_3S} = 18 \times n_{con,j,wat,C_3S} \quad [g] \quad (3.43)$$

$$m_{re,j,CSH,C_3S} = 227.4 \times n_{re,j,CSH,C_3S} \quad [g] \quad (3.44)$$

$$m_{re,j,CH,C_3S} = 74.1 \times n_{re,j,CH,C_3S} \quad [g] \quad (3.45)$$

where 18, 227.4 and 74.1 are the molar mass of water, CSH and CH, respectively [g/mole].

Step 4: Volume evolution of hydrating C_3S

The volumes of hydrated C_3S, reacted water, formed CSH and formed CH are:

$$V_{con,j,C_3S} = m_{con,j,C_3S}/3.21 \quad [cm^3] \quad (3.46)$$

$$V_{con,j,wat,C3S} = m_{con,j,wat,C_3S}/1.00 \quad [cm^3] \quad (3.47)$$

$$V_{re,j,CSH,C_3S} = m_{re,j,CSH,C_3S}/2.05 \quad [cm^3] \quad (3.48)$$

$$V_{re,j,CH,C_3S} = m_{re,j,CH,C_3S}/2.24 \quad [cm^3] \quad (3.49)$$

where 3.21, 1.00, 2.05 and 2.24 are the density of C_3S, water, CSH and CH, respectively [cm^3/g].

Fig. 3.18 shows the calculated volume evolution of hydrating C_3S. (Initial PC weight = 1 g, initial C_3S weight = 0.5 g and w/c = 0.4)

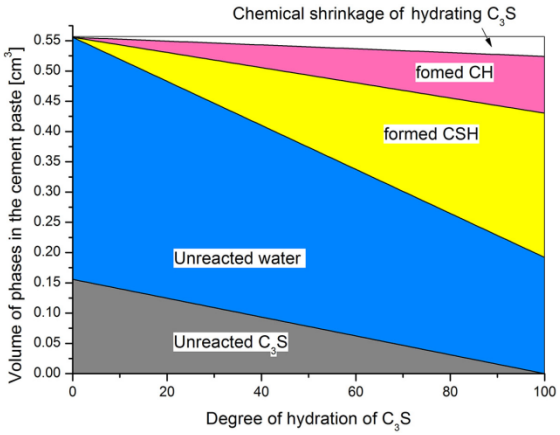

Fig. 3.18 Calculated volume evolution of hydrating C_3S as function of the degree of hydration

3.2.6 Growth of the shell of reaction product at particle level

As mentioned in section 3.2.5, the volume increase ratio υ is important to simulate the 3D microstructure development of a cement paste. In HYMOSTRUC3D-E the υ-value of PC, BFS and FA is calculated from the volume evolution of different phases. For example, for the hydration products of PC are CSH, AFt, AFm, CH, C_3AH_6 and FH_3, the υ-value of PC (at temperature 20 ºC) is calculated with Eq. (3.50):

$$\nu_{j,20,PC} = \frac{\begin{pmatrix} V_{re,j,CSH,PC} + V_{re,j,AFt,PC} + V_{re,j,AFm,PC} + V_{re,j,CH,PC} + \\ V_{re,j,C_3AH_6,PC} + V_{re,FH_3,PC} \end{pmatrix}}{V_{con,j,C_3S} + V_{con,j,C_2S} + V_{con,j,C_3A} + V_{con,j,C_4AF} + V_{con,j,gyp}} \tag{3.50}$$

where $V_{re,j,CSH,PC}$, $V_{re,j,AFt,PC}$, $V_{re,j,AFm,PC}$, $V_{re,j,CH,PC}$, $V_{re,j,C_3AH_6,PC}$, $V_{re,FH_3,PC}$ are the volumes of CSH, AFt, AFm, CH, C_3AH_6, FH_3 formed by the hydration of PC at time t_j respectively. V_{con,j,C_3S}, V_{con,j,C_2S}, V_{con,j,C_3A}, V_{con,j,C_4AF}, $V_{con,j,gyp}$ are the volumes of reacted C_3S, C_2S, C_3A, C_4AF, gypsum, respectively.

As will be discussed in Chapter 4, in the simulation of the 3D microstructure of blended cement paste the CH phase will be separated from the CSH gel phase and distributed in the pore structure. To calculate the shell thickness of a hydrating PC particle for simulating the 3D microstructure of blended cement paste, a υ-value of PC without considering CH phase should be determined. In this thesis the υ-value of PC, without considering CH phase $\nu_{j,20,PC,excl\ CH}$, is calculated by removing the volume of CH phase in Eq. (3.50). It holds:

$$\nu_{j,20,PC,excl\ CH} = \nu_{j,20,PC} - \frac{V_{re,j,CH,PC}}{\left(V_{con,j,C_3S} + V_{con,j,C_2S} + V_{con,j,C_3A} + V_{con,j,C_4AF} + V_{con,j,gyp}\right)} \tag{3.51}$$

An example of the calculated evolution of the υ-value of PC with time ($t = t_j$), including all hydration products and without considering CH phase, is shown in Fig. 3.19. The υ-value of PC including CH is around 2.2 at early age, and decreases to approximate 2.0 with progress of the hydration process. Using this calculated υ-value of PC, the simulated capillary porosity of PC paste is in good agreement with the experimental data (Fig. 3.20)

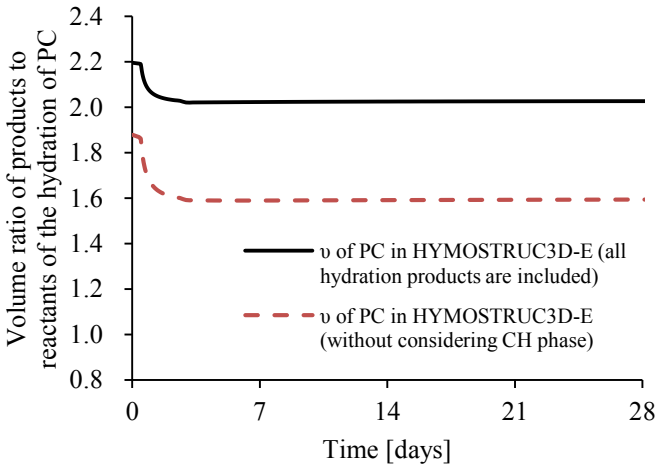

Fig. 3.19 The volumes ratios of products to reactants of PC in HYMOSTRUC3D and HYMOSTRUC3D-E. (w/c = 0.4, temperature = 20 ºC and for the properties of PC used as input in the simulation see section 5.2)

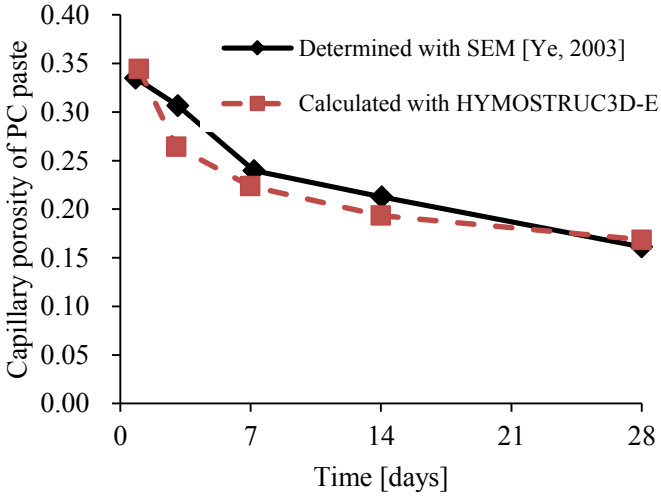

Fig. 3.20 Evolution of capillary porosity of PC paste. Values obtained with SEM and calculated with HYMOSTRUC3D-E (w/c = 0.4, temperature = 20 ºC and for the properties of PC used as input in the simulation see section 5.2)

3.3 Simulation module for pore solution chemistry of blended cements

3.3.1 General

In the past decades, an increasing number of investigations have been conducted on the simulation of the pore solution chemistry of cement-based materials. Taylor *[1987]* predicted the concentrations of Na^+ and K^+ in the pore solution of Portland cement paste. In the work of Taylor *[1987]*, the relationship between the concentrations of alkali ions in the pore solution and the amount of alkali ions bound by the hydration product was introduced. Van Eijk et al. *[2000]* simulated the concentrations of Na^+, K^+, Ca^{2+} and OH^- in the Portland cement system. In their study the concentrations of Na^+ and K^+ were simulated with Taylor's method and the relationship between the concentrations of Ca^{2+} and OH^- was introduced based on the dissolution equilibrium of the CH in the pore solution. Although the concentrations of Na^+ and K^+ were in agreement with the experimental data, the concentration of Ca^{2+} and the pH were not fully consistent with experiments. A possible reason for this is inadequate consideration of SO_4^{2-}. Bentz *[2005]* considered the concentration of SO_4^{2-}, and simulated the pore solution chemistry of slag and fly ash cement pastes. Up to now, only a few studies have been performed on the simulation of the pore solution chemistry of blended cement pastes.

In HYMOSTRUC the reduction factor Ω_3 was used to quantify the influence of the decreasing amount Ca^{2+} in the pore solution on the hydration of PC particles (see section 3.2.4.3). However the concentrations of the ions like Na^+, K^+, Ca^{2+}, SO_4^{2-} were not simulated in HYMOSTRUC model.

In HYMOSTRUC3D-E a module is proposed to simulate the pore solution chemistry of blended cement pastes. In this simulation module for the pore solution chemistry of blended cement pastes five types of ions, i.e. Na^+, K^+, Ca^{2+}, SO_4^{2-} and OH^-, are considered. Other ions, such as $Al(OH)_4^-$ and $SiO(OH)_3^-$ are not incorporated because their concentrations are much less than of these five ions.

3.3.2 Modelling approach for the pore solution chemistry of blend cement paste

The main ions in the pore solution are Na^+, K^+, Ca^{2+}, SO_4^{2-} and OH^-. Normally the pore solution is electroneutral. The amount of positive charges is equal to the amount of negative charges. It holds:

$$Q_{Na^+} + Q_{K^+} + Q_{Ca^{2+}} = Q_{SO_4^{2-}} + Q_{OH^-} \tag{3.52}$$

where Q_{Na^+}, Q_{K^+}, $Q_{Ca^{2+}}$, $Q_{SO_4^{2-}}$ and Q_{OH^-} are the electrical charges caused by Na^+, K^+, Ca^{2+}, SO_4^{2-} and OH^- ions. For a pore solution with a certain volume V [L], Q_{Na^+}, Q_{K^+}, $Q_{Ca^{2+}}$, $Q_{SO_4^{2-}}$ and Q_{OH^-} depends on the concentrations of Na^+, K^+, Ca^{2+}, SO_4^{2-} and OH^- ions:

$$Q_{Na^+} = N_A \times V \times e \times c_{Na^+} \tag{3.53}$$

$$Q_{K^+} = N_A \times V \times e \times c_{K^+} \tag{3.54}$$

$$Q_{Ca^{2+}} = 2N_A \times V \times e \times c_{Ca^{2+}} \tag{3.55}$$

$$Q_{SO_4^{2-}} = 2N_A \times V \times e \times c_{SO_4^{2-}} \tag{3.56}$$

$$Q_{OH^-} = N_A \times V \times e \times c_{OH^-} \tag{3.57}$$

where $c_{Na^+}, c_{K^+}, c_{Ca^{2+}}, c_{SO_4^{2-}}$ and c_{OH^-} are the concentrations of Na^+, K^+, Ca^{2+}, SO_4^{2-} and OH^- ions [mole/L]. N_A is Avogadro constant. e is the charge of a proton. By combining Eq. (3.52) to Eq. (3.57), it holds:

$$c_{Na^+} + c_{K^+} + 2c_{Ca^{2+}} = 2c_{SO_4^{2-}} + c_{OH^-} \tag{3.58}$$

If the concentrations of Na^+, K^+, Ca^{2+} and SO_4^{2-} are determined, the value of pH of the pore solution can be calculated. In HYMOSTRUC3D-E the concentrations of Na^+, K^+, Ca^{2+} and SO_4^{2-} are calculated step by step to simulate the value of pH. The main simulation steps are shown in Fig. 3.21. Firstly, the volume of capillary water is calculated based on the evolution of phases in the cement paste. Then, the concentrations of Na^+ and K^+ ions are calculated using Taylor's method. Next, the concentrations of Ca^{2+}, SO_4^{2-} and OH^- ions are calculated with the solubility equilibria of CH and gypsum, and the electrical neutrality of pore solution (Eq. (3.58)).

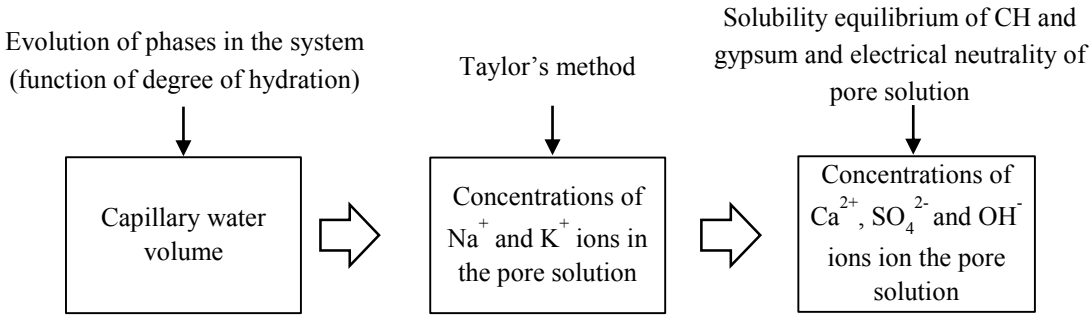

Fig. 3.21 Main steps to simulate the pore solution chemistry of blended cement pastes

3.3.2.1 Volume of free capillary water

With progress of the hydration process, the water in capillary pores will be gradually consumed by the hydration of PC and the pozzolanic reactions of BFS and FA. Besides, a part of water in capillary pores will be adsorbed by CSH gel *[Thomas et al., 2012]*. For the cement paste with 1 g blended cement and a given w/b, the volume of free water [cm^3] in the capillary pores at time t_j can be calculated as:

$$V_{fr,j,wat,tot} = V_{wat,in} - V_{con,j,wat,PC} - V_{con,j,wat,BFS} - V_{con,j,wat,FA} - V_{ab,j,wat} \quad (3.59)$$

where $V_{wat,in}$ is the volume of initial capillary water [cm^3]. $V_{con,j,wat,PC}$, $V_{con,j,wat,BFS}$ and $V_{con,j,wat,FA}$ are the volumes of the water consumed by the hydration of PC, and the pozzolanic reactions of BFS, and FA, respectively [cm^3]. $V_{ab,j,wat}$ is the volume of water adsorbed by CSH gel [cm^3] (See the calculation of these water volumes in Appendix C).

3.3.2.2 Concentrations of Na^+ and K^+

For pure Portland cement paste, the alkalis in the Portland cement particles supply the Na^+ and K^+ ions in the pore solution. Taylor *[1987]* categorized two categories of the alkalis in PC (Fig. 3.22). The first category is in the form of sulphates that can dissolve completely in the pore solution immediately after mixing. The second category is bound in C_3S, C_2S, C_3A and C_4AF will be released with progress of the hydration process. Hence, the total amount of alkalis released from PC is a function of the degree of hydration of PC (Fig. 3.23).

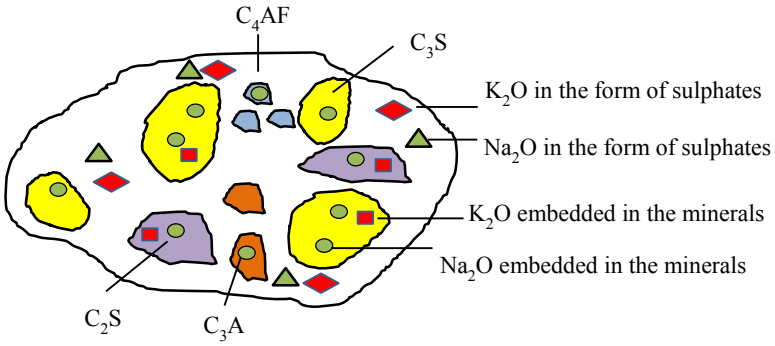

Fig. 3.22 Schematic picture of the categories of alkalis in a PC particle

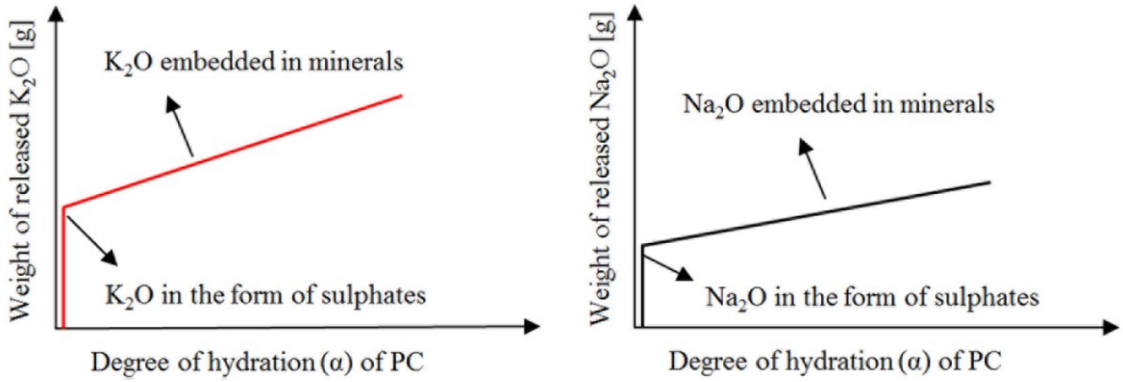

(a) released K_2O *(b) released Na_2O*

Fig. 3.23 Schematic diagram of the weight [g] of released alkalis versus the degree of hydration of PC. Note: The solubility of alkalis is very high in water. Hence, it is assumed that all the released alkalis can dissolve in the pore solution.

It is noted that not all the released alkalis are present in the pore solution, because some alkali ions will be bound by hydration products, such as CSH gel and AFm (Fig. 3.24). To calculate the concentrations of alkali ions in the pore solution, the amount of alkali ions bound by the hydration products has to be known. According to Taylor *[1987]* the amount of alkalis bound by a given mass of hydration products m_p [g] is proportional to the concentration:

$$m_p = b \times P \times c \tag{3.60}$$

where P is the weight of the hydration products able to take up alkali ions [g]. c is the concentration of the alkali ions in the pore solution [mole/L]. The slope of this linear relationship b is defined as binding factor and is determined experimentally. A schematic diagram of this linear relationship is shown in Fig. 3.25.

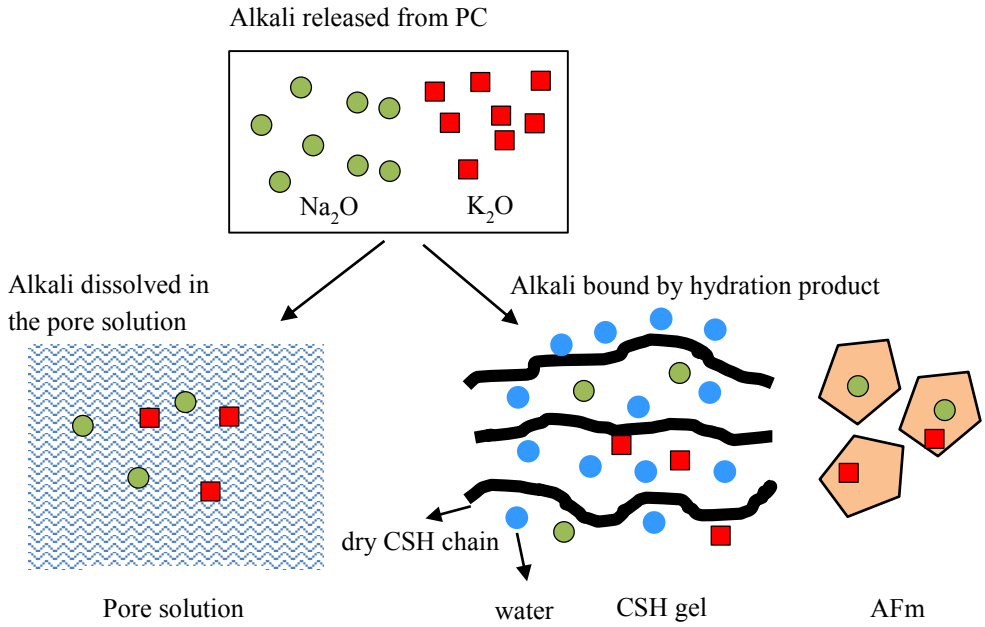

Fig. 3.24 Schematic picture of the distribution of the released alkalis in pure Portland cement paste

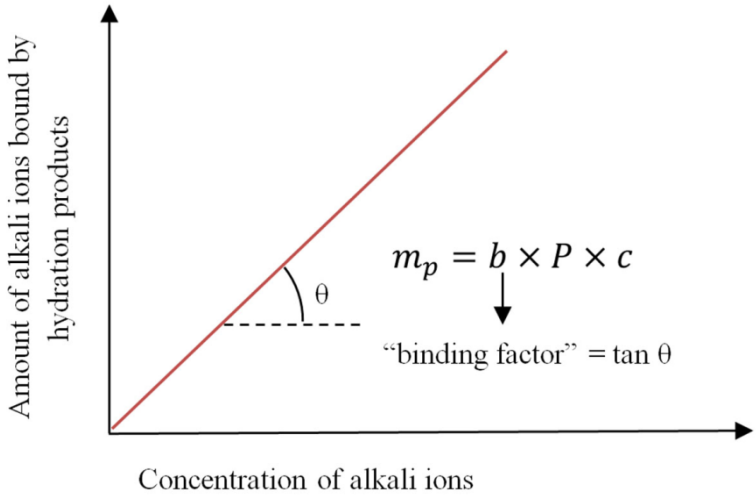

Fig. 3.25 Schematic relationship between the concentrations of alkali ions in the pore solution and the amount of alkali ions bound by hydration products. Note: m_p is the amount of alkali ions bound by hydration products. P is the mass of the hydration products able to take up alkali ions. c is the concentration of the alkali ions in the pore solution.

In HYMOSTRUC3D-E, Taylor's method will be followed to simulate the concentrations of Na^+ and K^+ ions in the pore solution of blended cement pastes. The simulation process comprises two steps (Fig. 3.26) viz.:

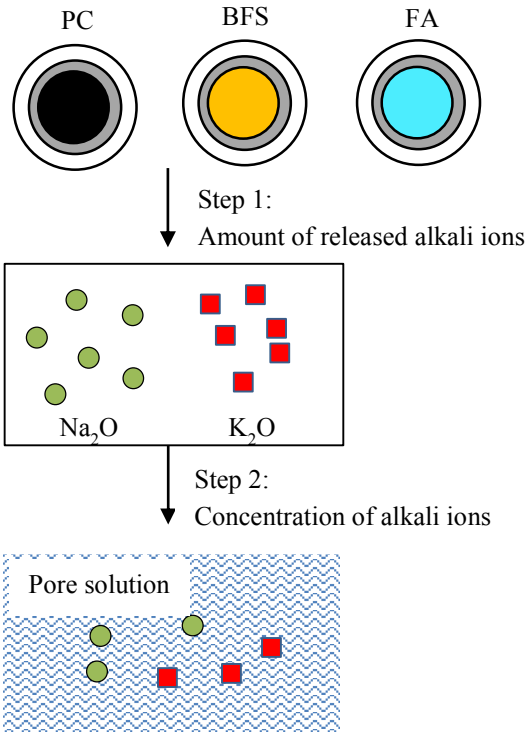

Fig. 3.26 Schematic representation of the steps to calculate the concentration of alkali ions in the pore solution of blended cement paste in HYMOSTRUC3D-E.

Step 1: Amount of released alkali ions
In blended cement system, alkalis can be released from PC, BFS and FA.

1. Amount of alkali released from PC
According to Taylor *[1987],* 35% of the total Na_2O and 70% of the total K_2O are present as Na_2SO_4 and K_2SO_4. These alkalis will dissolve immediately after mixing. The still remaining alkalis will release with ongoing hydration. The amount of alkalis released from PC, $n_{Na,j,PC}$ [mole] and $n_{K,j,PC}$ [mole], are functions of the degree of hydration of PC:

$$n_{Na,j,PC} = \frac{2 \times m_{PC} \times f_{Na_2O,PC} \times \left(\alpha_{PC} \times k_{Na_2O,PC} + \left(1 - k_{Na_2O,PC}\right)\right)}{M_{Na_2O}} \tag{3.61}$$

$$n_{K,j,PC} = \frac{2 \times m_{PC} \times f_{K_2O,PC} \times \left(\alpha_{PC} \times k_{K_2O,PC} + \left(1 - k_{K_2O,PC}\right)\right)}{M_{K_2O}} \tag{3.62}$$

where m_{PC} is the mass of PC in 1 g blended cement [g], α_{PC} is the degree of hydration of PC, $f_{Na_2O,PC}$ and $k_{Na_2O,PC}$ are the mass fractions of Na_2O and K_2O in PC, respectively. M_{Na_2O} and M_{K_2O} are the molar mass of Na_2O and K_2O [g/mole], respectively. $k_{Na_2O,PC}$,

$k_{K_2O,PC}$ are the weight fractions of Na_2O and K_2O present as Na_2SO_4 and K_2SO_4, respectively. According to the research of Taylor *[1987]* the values of $k_{Na_2O,PC}$ and $k_{K_2O,PC}$ are set at 0.65 and 0.30, respectively.

2. Amount of alkalis released from BFS and FA

Different from PC both BFS and FA contain a huge amount of glassy phases. It is assumed that the alkalis are homogenously embedded in the glassy phases of BFS and FA. With this assumption the alkalis in BFS and FA will be gradually released to the pore solution with the progress of the pozzolanic reactions of BFS and FA. The amount of alkalis released from BFS, $n_{Na,j,BFS}$ [mole] and $n_{K,j,BFS}$ [mole], are functions of the degree of reaction of BFS (Eq. (3.63) and (3.64)):

$$n_{Na,j,BFS} = \left(2 \times m_{BFS} \times \alpha_{BFS} \times f_{Na_2O,BFS}\right)/M_{Na_2O} \quad \text{[mole]} \quad (3.63)$$

$$n_{K,j,BFS} = \left(2 \times m_{BFS} \times \alpha_{BFS} \times f_{K_2O,BFS}\right)/M_{K_2O} \quad \text{[mole]} \quad (3.64)$$

where m_{BFS} is the mass of BFS [g] in 1 g blended cement, α_{BFS} is the degree of reaction of BFS, $f_{Na_2O,BFS}$ and $f_{K_2O,BFS}$ are the mass fractions of Na_2O and K_2O in BFS, respectively.

The amount of the alkalis released from FA, $n_{Na,j,FA}$ [mole] and $n_{K,j,FA}$ [mole], are functions of the degree of reaction of FA (Eq. (3.65) and (3.66)):

$$n_{Na,j,FA} = \left(2 \times m_{FA} \times \alpha_{FA} \times f_{Na_2O,FA}\right)/M_{Na_2O} \quad \text{[mole]} \quad (3.65)$$

$$n_{K,j,FA} = \left(2 \times m_{FA} \times \alpha_{FA} \times f_{K_2O,FA}\right)/M_{K_2O} \quad \text{[mole]} \quad (3.66)$$

where m_{FA} is the mass of FA [g] in 1 g blended cement. α_{FA} is the degree of reaction of FA. $f_{Na_2O,FA}$ and $f_{K_2O,FA}$ are the weight fractions of Na_2O and K_2O in FA, respectively.

Fig. 3.27 shows an example of the calculated amount of the Na released from PC, BFS and FA.

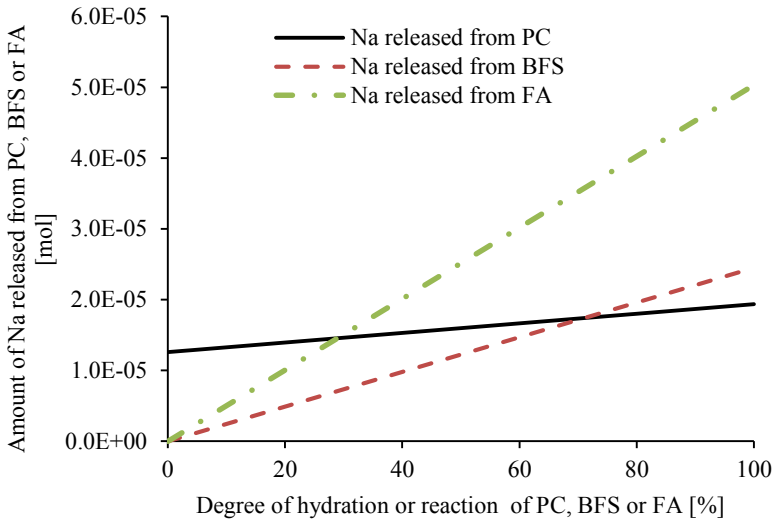

Fig. 3.27 An example of the released Na as a function of the degree of hydration of 1g blended cement (60% PC, 20% BFS, and 20% FA. Na_2O mass fractions in PC, BFS and FA are 0.14%, 0.21% and 0.72%, respectively. For the properties of PC, BFS and FA used as input for the simulation, see section 5.5)

Step 2: Concentration of alkali ions

In step 1 the amount of released alkalis was calculated from the degree of hydration of blended cements. A certain amount of the released alkalis will be bound by the hydration products, such as CSH gel and AFm. The remaining alkalis are present in the pore solution.

In the pure Portland cement system both CSH gel and AFm phase can bind alkalis *[Taylor, 1987]*. In the slag cement system the hydrotalcite-like phase (M_5AH_{13}) can also bind alkalis *[Chen et al, 2011]*. In HYMOSTRUC3D-E the alkalis are assumed to be bound by the CSH gel and the AFm phase formed by the hydration of PC, the CSH gel and hydrotalcite-like phase formed by the reaction of BFS, and the CSH gel formed by the reaction of FA (Fig. 3.28).

Taylor *[1987]* suggested that the binding factors b in Eq. (3.60), Na^+ and K^+ bound by CSH gel, are 0.31 and 0.20 ml/g, respectively. Hong et al. *[1999, 2002]* indicated that the binding factors b in Eq. (3.60), Na^+ and K^+ bound by CSH gels containing Al, are related to the C/S ratio. Van Eijk et al. *[2000]* suggested the binding factors b in Eq. (3.60), Na^+ and K^+ bound by CSH gel, are 0.30 and 0.27, respectively. Table 3.4 shows the binding factors b in Eq. (3.60), Na^+ and K^+ bound by reaction products of PC (CSH_{PC} and AFm_{PC}) and of blended cements (CSH_{BFS}, HT_{BFS} and CSH_{FA}), used in HYMOSTRUC3D-E.

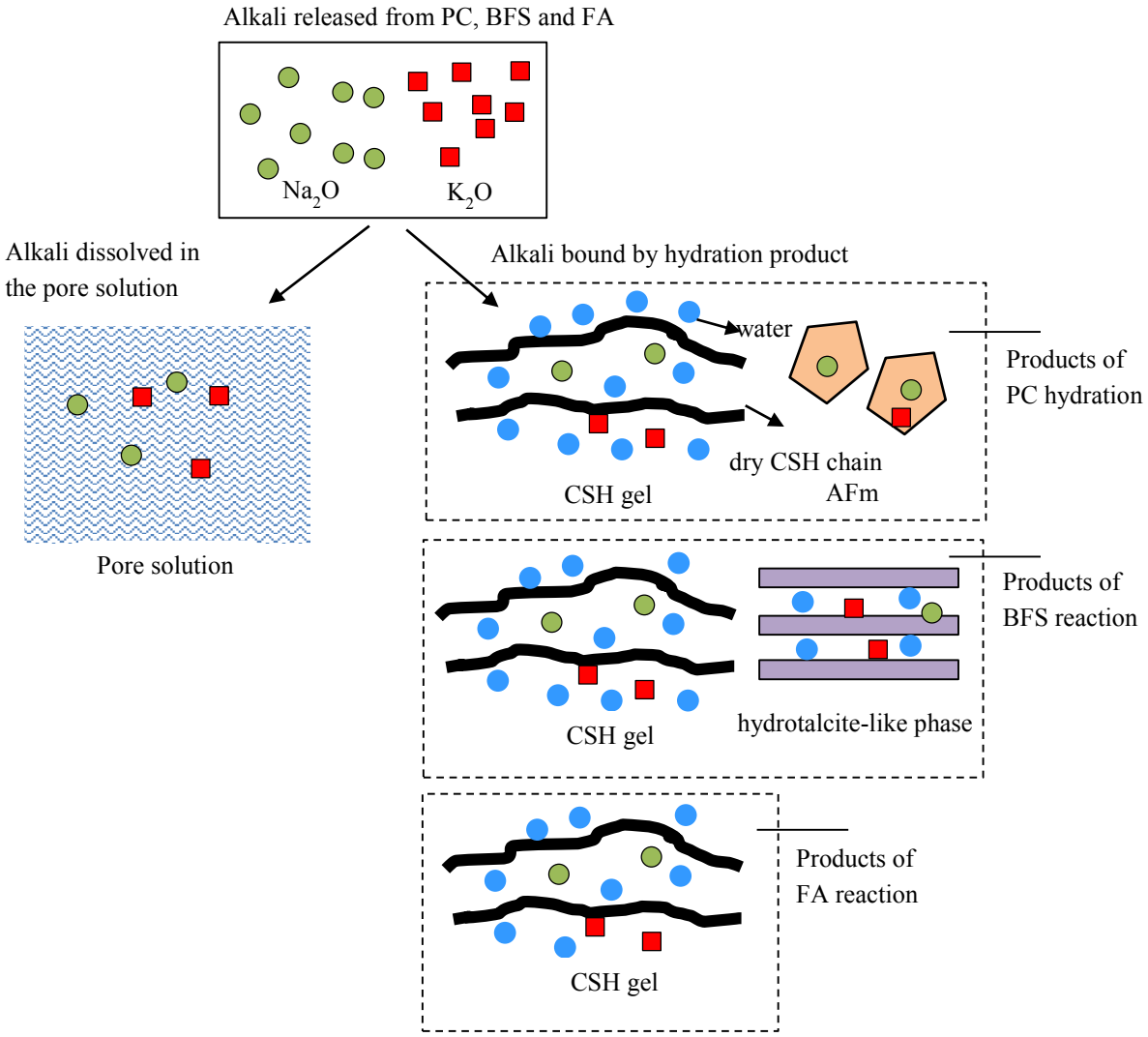

Fig. 3.28 Schematic picture of the distribution of the released alkalis in blended cement paste

Table 3.4 Binding factors b in Eq. (3.60) (Na^+ and K^+ bound by reaction products of PC (CSH_{PC} and AFm_{PC}) and of blended cements (CSH_{BFS}, HT_{BFS} and CSH_{FA})) used in HYMOSTRUC3D-E

Ions	Binding factors [ml/g]				
	CSH_{PC}	AFm_{PC}	CSH_{BFS}	HT_{BFS}	CSH_{FA}
Na+	0.39	0.10	0.30	0.30	0.30
K+	0.30	0.10	0.30	0.30	0.30

Note: CSH_{PC} and AFm_{PC} are the CSH and AFm produced by the hydration of PC, CSH_{BFS} and HT_{BFS} are the CSH and HT produced by the reaction of BFS, CSH_{FA} is the CSH produced by the reaction of FA.

It is also assumed that the concentrations of alkali ions in the pore solution and the amount of alkali ions bound by hydration products follow the linear relationship shown in Fig. 3.25. Accordingly, the concentrations of alkali ions in the pore solution of blended cement paste can be calculated with the same way as proposed by Taylor *[1987]*.

For the concentration of Na^+ ions it holds (Eq. (3.67)):

$$c_{Na^+} = \frac{n_{Na,j,PC} + n_{Na,j,BFS} + n_{Na,j,FA}}{\begin{pmatrix} V_{fr,j,wat,tot} + b_{Na,CSH,PC} \times m_{CSH,j,PC} + b_{Na,AFm,PC} \times m_{AFm,PC+} \\ b_{Na,CSH,BFS} \times m_{CSH,j,BFS} + b_{Na,HT,BFS} \times m_{HT,j,BFS} + \\ b_{Na,CSH,FA} \times m_{CSH,j,FA} \end{pmatrix}} \quad (3.67)$$

For the concentration of K^+ ions it holds (Eq. (3.68)):

$$c_{K^+} = \frac{n_{K,j,PC} + n_{K,j,BFS} + n_{K,j,FA}}{\begin{pmatrix} V_{fr,j,wat,tot} + b_{K,CSH,PC} \times m_{CSH,j,PC} + b_{K,AFm,PC} \times m_{AFm,j,PC} + \\ b_{K,CSH,BFS} \times m_{CSH,j,BFS} + b_{K,HT,BFS} \times m_{HT,j,BFS} \\ + b_{K,CSH,FA} \times m_{CSH,j,FA} \end{pmatrix}} \quad (3.68)$$

where $V_{fr,j,wat,tot}$ is the volume of free capillary water [cm^3]. $m_{CSH,j,PC}$, $m_{AFm,PC}$, $m_{CSH,j,BFS}$, $m_{HT,j,BFS}$, $m_{CSH,j,FA}$ are the mass of CSH gel and AFm produced by the hydration of PC, CSH gel and HT hydrotalcite-like phase produced by the reaction of BFS, CSH gel produced by the pozzolanic reaction of FA at time t_j, respectively [g]. $b_{Na,CSH,PC}$, $b_{Na,AFm,PC}$, $b_{Na,CSH,BFS}$, $b_{Na,HT,BFS}$ and $b_{Na,CSH,FA}$ are the binding factors (Na^+ bound by CSH gel and AFm produced by the hydration of PC, CSH gel and HT hydrotalcite-like phase produced by the reaction of BFS, CSH gel produced by the pozzolanic reaction of FA, respectively [cm^3/g]). $b_{K,CSH,PC}$, $b_{K,AFm,PC}$, $b_{K,CSH,BFS}$, $b_{K,HT,BFS}$ and $b_{K,CSH,FA}$ are the binding factors (K^+ bound by CSH gel and AFm produced by the hydration of PC, CSH gel and HT hydrotalcite-like phase produced by the reaction of BFS, CSH gel produced by the pozzolanic reaction of FA, respectively [cm^3/g]).

Fig. 3.29 shows an example of the simulated concentrations of Na^+ and K^+ ions in the pore solutions of PC paste, slag cement paste and fly ash cement paste as functions of time. (For the properties of the blended cement used as input for the simulation, see in section 5.5).

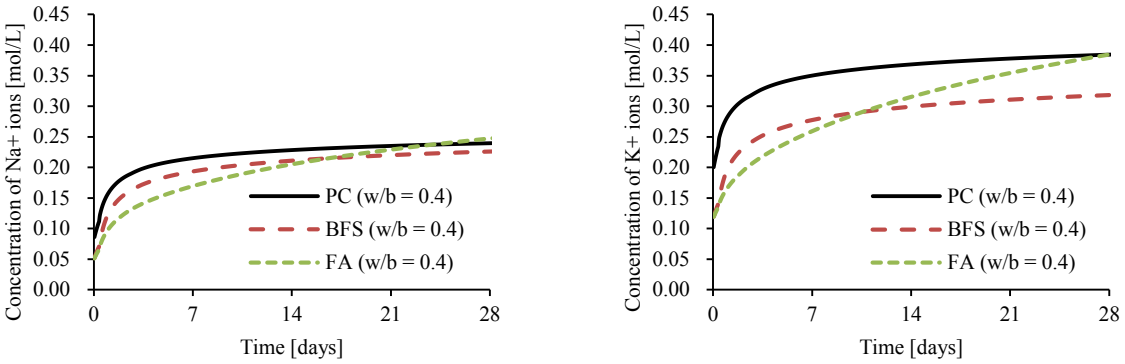

(a) concentration of Na^+ ions *(b) concentration of K^+ ions*

Fig. 3.29 Simulated concentrations of Na^+ and K^+ ions in the pore solution of cement pastes. BFS content in slag cement = 40% and FA content in fly ash cement = 40%. (For the properties of PC, BFS and FA used as input for the simulation, see section 5.5)

3.3.2.3 Concentrations of Ca^{2+}, SO_4^{2-} and OH^-

With progress of the hydration process of blended cements, PC, BFS and FA will partially dissolve in the pore solution and form the ions such as Ca^{2+}, Al^{3+}, $SiO(OH)_3^-$, SO_4^{2-}, OH^-. (Fig. 3.30). When the concentrations of these ions increase towards the solubility equilibria of hydration products, then hydration products will be formed. For example, when the concentrations of Ca^{2+} and OH^- reach the solubility equilibrium of CH, the CH will form. These solubility equilibria can be maintained if these hydration products, such as CSH gel, CH, AFt and AFm, are present in the system. Using these solubility equilibria, the concentrations of ions can be calculated.

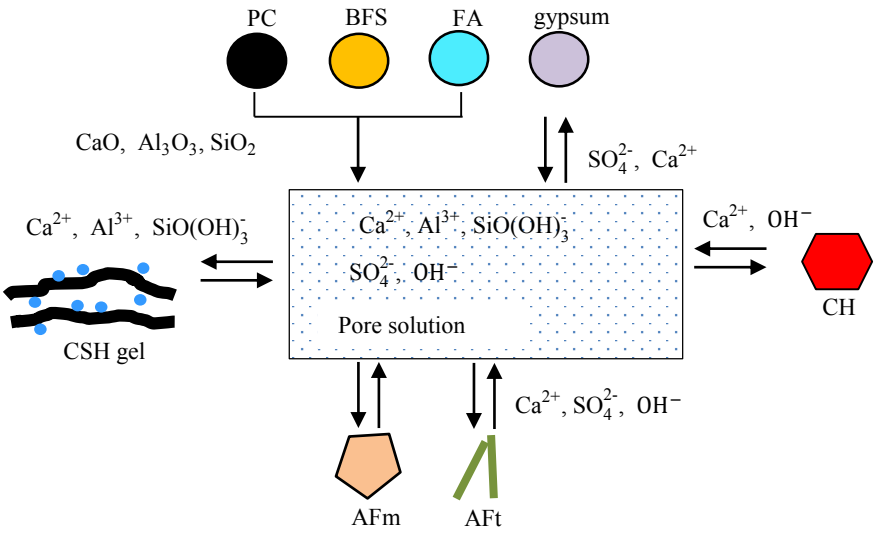

Fig. 3.30 Schematic representation of the solubility equilibria of hydration products in the blended cement system.

In blended cement systems the concentration of SO_4^{2-} ions mainly depends on the solubility equilibria of gypsum, AFt and AFm, while the concentration of Ca^{2+} ions mainly depends on the solubility equilibria of gypsum, CH, AFt, AFm and CSH. According to the thermodynamic data base *[Lothenbach et al., 2006; Blanc et al., 2010]*, the solubility constant of gypsum and CH are much lower than that of hydration products, such as CSH gel and AFt. For this reason, in HYMOSTRUC3D-E only the solubility equilibria of CH and gypsum (Eq. (3.69) and Eq. (3.70)) are used to calculate the concentrations of Ca^{2+} and SO_4^{2-}.

$$CH \Leftrightarrow Ca^{2+} + 2OH^- \tag{3.69}$$

$$C\bar{S}H_2 \Leftrightarrow Ca^{2+} + SO_4^{2-} + 2H_2O \tag{3.70}$$

where $\bar{S}$ represents SO_3 and $C\bar{S}H_2$ represents gypsum.

If the solid phase of CH is present in the system, the concentrations of Ca^{2+} and OH^- in the pore solution depend on the solubility constant of CH *[Damidot et al., 2011]*:

$$\frac{\{CH^0\}}{\{Ca^{2+}\} \times \{OH^-\}^2} = \frac{1}{c_{Ca^{2+}} \times \gamma_{Ca^{2+}} \times (c_{OH^-})^2 \times (\gamma_{OH^-})^2} = K_{sp,CH} \tag{3.71}$$

where $\{CH^0\}$, $\{Ca^{2+}\}$, $\{OH^-\}$ are the activities of ions, $\gamma_{Ca^{2+}}$ and γ_{OH^-} are the activity

coefficients of ions[3]. $K_{sp,CH}$ is the solubility constant of CH. Using the thermodynamic data summarized by Blanc et al. *[2010]* its value is calculated at $10^{5.2}$.

Similarly, if gypsum is present in the system, the concentrations of Ca^{2+} and SO_4^{2-} in the pore solution depend on the solubility constant of gypsum. For the solubility constant of gypsum, $K_{sp,gyp}$, it holds:

$$\frac{\left\{C\bar{S}H_2{}^0\right\}}{\{Ca^{2+}\}\times\{SO_4^{2-}\}\times\{H_2O\}^2}=\frac{1}{c_{Ca^{2+}}\times\gamma_{Ca^{2+}}\times c_{SO_4^{2-}}\times\gamma_{SO_4^{2-}}}=K_{sp,gyp} \tag{3.72}$$

where $K_{sp,gyp}$ is the solubility constant of gypsum. Its value is calculated at $10^{4.65}$ using on the thermodynamic data summarized by Blanc et al. *[2010]*.

The activity coefficients of ions, Ca^{2+}, SO_4^{2-} and OH^-, are calculated based on Davies equations *[Hummel et al., 2002]*:

$$log_{10}\gamma_{Ca^{2+}}=4\times A\times\left(C_D\times I_m-\frac{\sqrt{I_m}}{1+\sqrt{I_m}}\right) \tag{3.73}$$

$$log_{10}\gamma_{OH^-}=A\times\left(C_D\times I_m-\frac{\sqrt{I_m}}{1+\sqrt{I_m}}\right) \tag{3.74}$$

$$log_{10}\gamma_{SO_4^{2-}}=4\times A\times\left(C_D\times I_m-\frac{\sqrt{I_m}}{1+\sqrt{I_m}}\right) \tag{3.75}$$

where A and C_D are constant. A = 0.510 $kg^{1/2}\cdot mole^{-1/2}$ and C_D = 0.2. I_m is the ionic strength of pore solutions.

By solving Eq. (3.58) and Eq. (3.69) to Eq. (3.75), the concentrations of Ca^{2+}, SO_4^{2-}, and OH^- in the pore solution can be obtained. The equation solving process is described in detail in Appendix F.

Fig. 3.31 shows an example of the simulated concentrations of Ca^{2+} and SO_4^{2-} ions, and evolution of pH in cement pastes. (The properties of blended cement used as input in the simulation are presented in section 5.5).

[3] The activity coefficient of ions is a factor used in thermodynamics to account for deviations from ideal behaviour in a mixture of chemical substances *[Hummel et al., 2002]*.

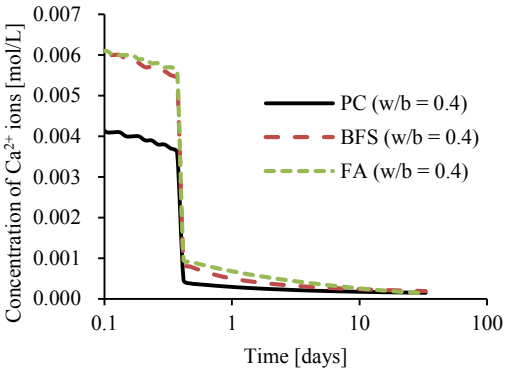

(a) concentration of Ca^{2+} ions

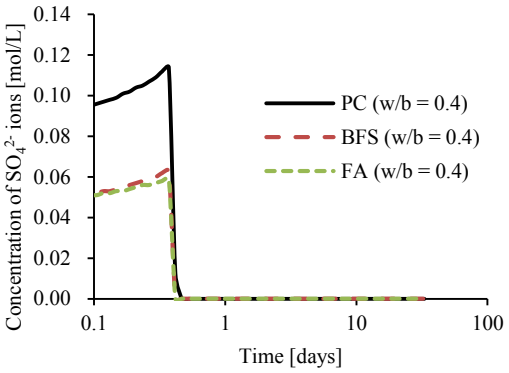

(b) concentration of SO_4^{2-} ions

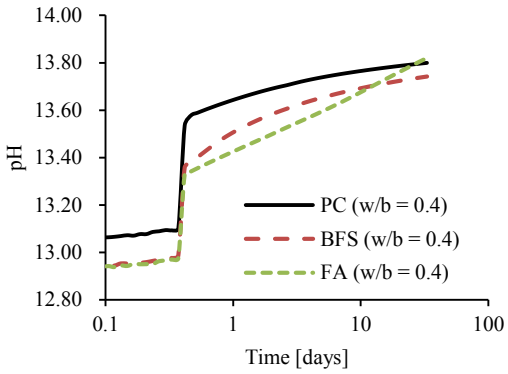

(c) evolution of pH

Fig. 3.31 Simulated concentrations of Ca^{2+} and SO_4^{2-} ions, and evolution of pH in cement pastes. BFS content in slag cement = 40% and FA content in fly ash cement = 40%. For the properties PC, BFS and FA of the blended cement used as input in the simulation, see section 5.5.

3.4 Summary of this chapter

This study aims to extend HYMOSTRUC3D to simulate the hydration and microstructure development of PC blended with BFS or/and FA. The extended model is called HYMOSTRUC3D-E. HYMOSTRUC3D-E consists of the *cement hydration route* and the *microstructure development route* (Fig. 3.32). Chapter 3 dealt with the *cement hydration route*, in which the stoichiometry of the hydration of blended cements, reaction rates of PC, BFS and FA particles, interaction between particles in the system and the pore solution chemistry and its influence on the reaction rates of PC, BFS and FA particles are considered.

The *microstructure development route* will be discussed detail in the next chapter (Chapter 4). In that route, the nucleation and growth of CH particles in blended cement pastes will be simulated. In addition, a pore structure module will be proposed to determine the evolution of capillary porosity and gel porosity of blended cement pastes.

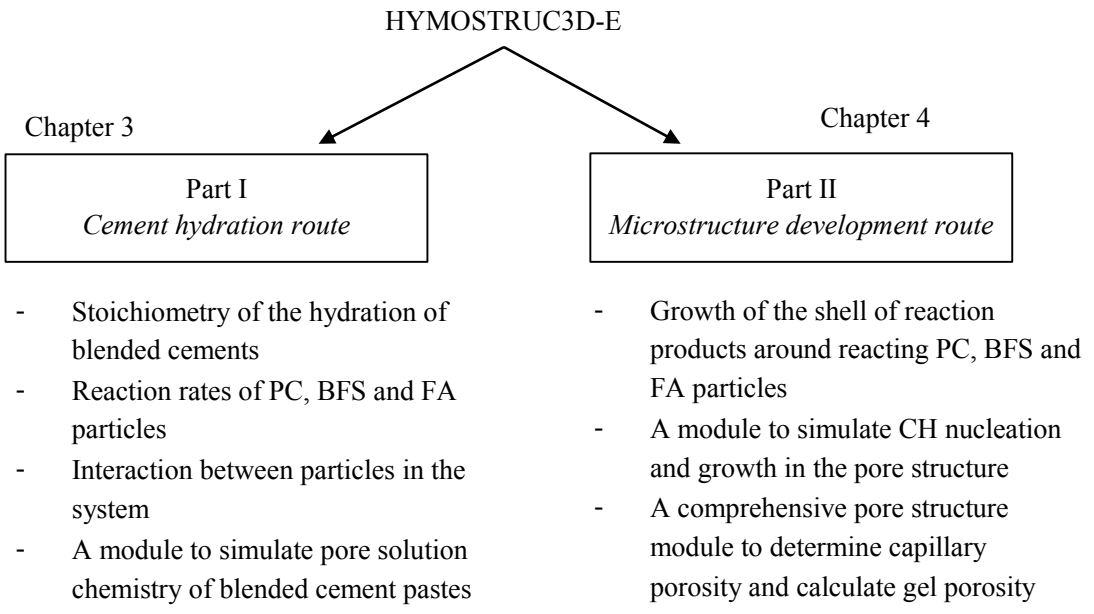

Fig. 3.32 Main contents in Chapter 3 and Chapter 4

Chapter 4

Simulation model for hydration and microstructure development of blended cements: Part II Microstructure development route

4.1 Introduction

HYMOSTRU3D is extended to simulate the hydration and microstructure development of blended cements (PC blended with BFS or/and FA). This extended HYMOSTRUC3D, called HYMOSTRU3D-E, consists of two routes: *the cement hydration route* and *the microstructure development route*. The *cement hydration route* has been discussed in Chapter 3. In Chapter 3 the degree of hydration of blended cements was simulated based on the kinetics of the hydration of the different components of blended cements. The pore solution chemistry of blended cement pastes and its influence on the reaction of BFS or/and FA were particularly dealt with. In addition, the simulated degree of hydration was used to calculate the evolution of volumes of individual phases in cement paste using the stoichiometry of the chemical reactions of PC, BFS and FA. This chapter, Chapter 4, deals with *the microstructure development route*. It consists of two sections:

Section 4.2: The microstructure development route
This section deals with the packing of PC, BFS and FA particles and the hydration-related growth of these particles in the representative elementary volume (REV) of cement paste. The nucleation and growth of CH particles are explicitly simulated.

Section 4.3: Pore structure module
In this section a pore structure module is proposed to determine the evolution of the pore structure, including the contribution of the gel pores to the porosity.

4.2 Microstructure development route

The *microstructure development route* mainly consists of four parts, viz.:
1. Presentation of the main assumptions in the *microstructure development route*
2. The initial spatial distribution and growth of PC, BFS and FA particles.
3. The nucleation and growth of CH particles.
4. Identification of the volumes of individual phases in the simulated 3D microstructure.

4.2.1 Main assumptions

The microstructure of blended cement pastes comprises several phases. The main phases are the particles of unreacted PC, BFS and FA; the hydration products including CSH gel, CH, AFt ($C_6A\bar{S}_3H_{32}$), and AFm ($C_4A\bar{S}H_{12}$) phases; capillary water and air bubbles. In HYMOSTRUC3D-E the main phases of the virtual 3D microstructure are:

1. Unreacted PC, BFS and FA particles,
2. Hydration products of PC: CSH gel and CH,
3. Reactions products of BFS and FA: CSH gel,
4. Pore space, including water and empty capillary pores

In HYMOSTRUC3D-E the CSH gel produced by the hydration of PC and the pozzolanic reactions of BFS and FA is subdivided in high density gel (inner product) and low density gel (outer product). Other hydration products, such as AFt and AFm phases, are considered the part of CSH gel. Different from HYMOSTRUC3D, the CH produced during the hydration of PC is separated from the gel phase in HYMOSTRUC3D-E.

In the microstructure development route, the main assumptions are:

a. The shape of PC, BFS and FA particles

In practical, PC and BFS particles are obtained by grinding the raw materials of PC (e.g. clinker) and BFS (e.g. iron slag) into a fine powder. As a result, the PC and BFS particles are normally irregular. FA particles are formed in the cooling process of fused materials in the air. As a consequence, the FA particles are normally spherical. Zuo et al. *[2018]* investigate the influence of the shape of particles on the 3D pore structure development of cement paste using the numerical models. They found that the particle shape does not significantly influence the pore size distribution of the simulated initial particle parking structure. In the simulation of the 3D microstructure development of cement paste, the use of the spherical particle shape can reduce the computing time in comparison with the use of the irregular particle shape. For above reasons, the PC, BFS and FA particles are all assumed to be spherical in HYMOSTRUC3D-E.

b. The shape of CSH gel and CH particles

In HYMOSTRUC3D-E the hydration products, such as AFt and AFm, are considered as the part of CSH gel. The CSH gel is classified as inner product and outer product. At the microscale CSH gel is considered to form shells around the PC, BFS and FA particles.

CH in the cement paste occurs as massive clusters or/and as isolated hexagonal crystals. However, some CH particles in cement pastes are irregular *[Ye, 2003; Gallucci et al., 2007]* (Fig. 4.1). In HYMOSTRUC3D-E the CH particles are also considered, initially, as spherical. At later age the shape of the CH particles become irregular if they overlap.

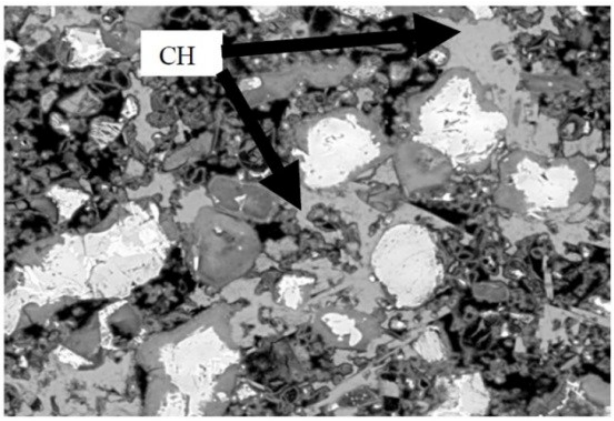

Fig. 4.1 Morphology of CH in PC paste (w/c = 0.5, time = 28days) [Ye, 2003]

c. The growth of a PC particle

As shown in the top part of Fig. 4.2, the hydration products of a PC particle are classified as inner product, outer product and CH particles. The inner product and outer product represent CSH gel, AFt, AFm, hydrogarnet (C_3AH_6) and iron hydroxide (FH_3). The inner product[4] is assumed to form in the space originally occupied by unhydrated cement, while the outer product[5] is assumed to form on the outer surface of the inner product. Different from hydration products, like CSH gel and AFt, CH particles are assumed to form in the water-rich pore space.

d. The growth of a BFS or FA particle

As shown in the middle and bottom parts of Fig. 4.2, the products of the pozzolanic reactions of BFS and FA particles are classified as inner product and outer product. Both BFS and FA particles react with CH particles. Similar to that in the system of PC, it is assumed that the inner product is formed in the space originally occupied by unreacted BFS or FA, and the outer product is formed on the outer surface of the inner product.

[4] inner product – high density gel

[5] outer product – low density gel

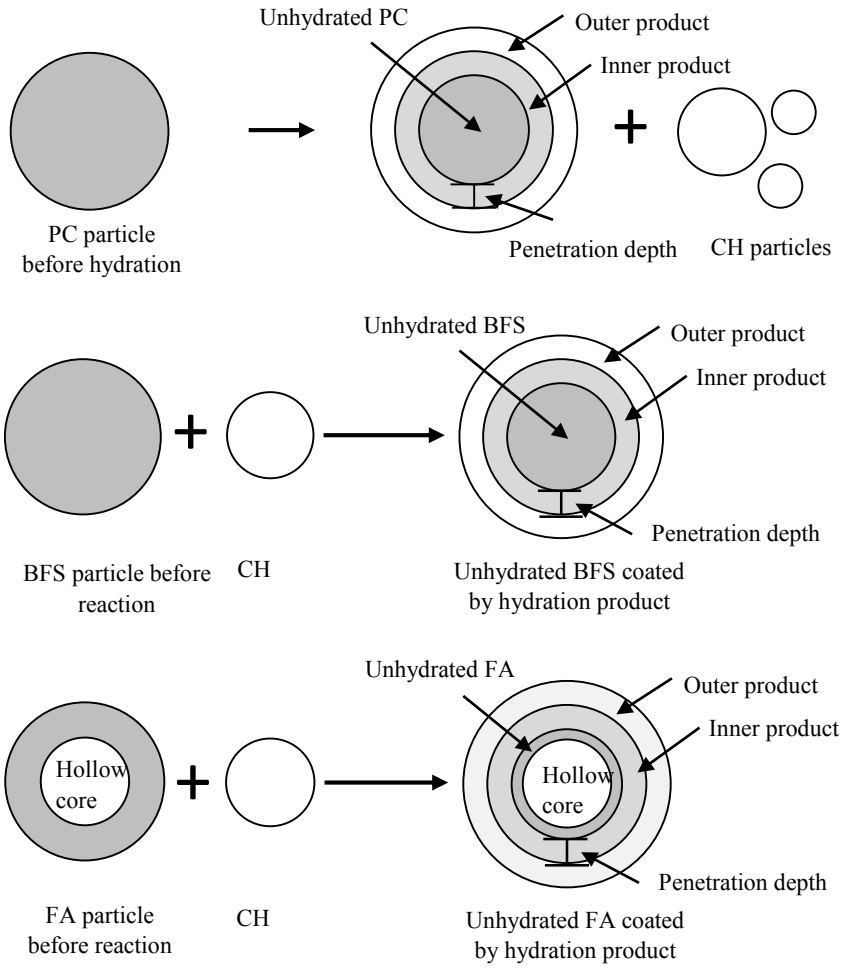

Fig. 4.2 Schematic representation of the growth of a PC, BFS or FA particle in the microstructure development route

4.2.2 Initial spatial distribution and growth of PC, BFS and FA particles

4.2.2.1 Initial spatial distribution of PC, BFS and FA particles

The initial spatial distribution of particles in the fresh paste is the starting point for simulating the microstructure development. A packing algorithm is used to simulate the initial spatial distribution of PC, BFS and particles in the fresh paste. This algorithm comprises two steps:

Step 1 - Calculation of the number of particles in the REV of cement paste

The size of the REV of cement paste might be different for different research purposes. In HYMOSTRUC3D-E, the size of the REV of cement paste is fixed at $100\times100\times100$ μm^3. The number of particles that should be packed in the REV of cement paste is calculated from the content of PC, BFS and FA particles in the REV and the particle size distribution of the PC, BFS and FA particles. The details of this algorithm is described in Appendix A.4.

Step 2 - Packing of PC, BFS and FA particles

The PC, BFS and FA particles are distributed in the REV of cement paste using a random packing algorithm. In this random packing algorithm, the particles with sizes from big to small are randomly placed, and no overlap exists between particles. Fig. 4.3 shows an example of the packing process.

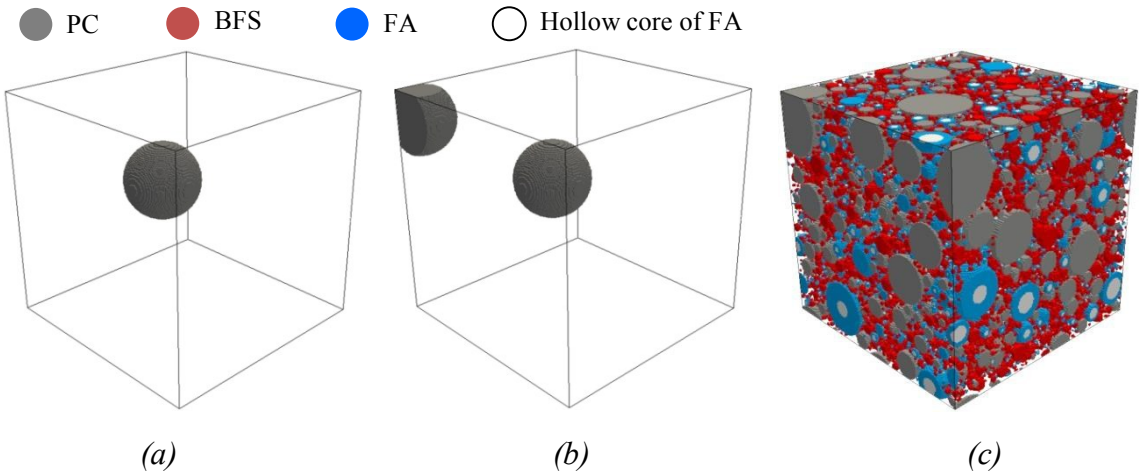

Fig. 4.3 Schematic diagram of the random packing algorithm (w/b = 0.4. 60% PC, 20% BFS, 20% FA. For the properties of PC, BFS and FA, see section 5.5). (a) Largest PC particle is packed, (b) Second PC particle is packed, (c) All PC, BFS and FA particles are packed.

4.2.2.2 Growth of PC, BFS and FA particles

The thickness of the shell of reaction product of PC, BFS and FA (without taking into account the physical interactions with adjacent particles) has been calculated in section 3.2.6. However, this thickness cannot be directly used in the *microstructure development route*, because the physical interaction between particles will affect the growth of particles. For example, as shown in Fig. 4.4, the small particles may become embedded in the shell of hydration products of big particles with progress of the hydration process. Due to the embedded particles in the outer shell of bigger particles, the outer shell of the bigger particles will experience an extra growth. In HYMOSTRUC *[Van Breugel, 1991]*, the total volume of the outer shell of particles (taking into account the volume of embedded particles) is called *the volume of the expanded outer shell*. To quantify this *the volume of expanded outer shell*, Van Breugel *[1991]* introduced a concept of "shell density" ζ and proposed an iteration algorithm.

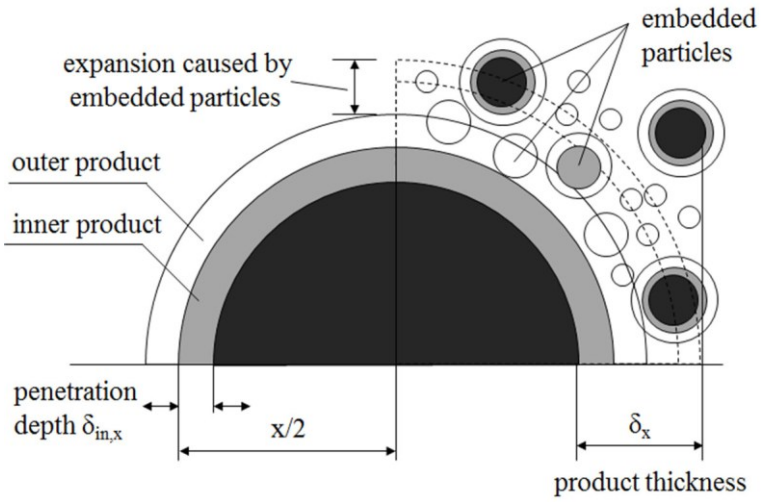

Fig. 4.4 The concept of embedded particles in HYMOSTRUC [after Van Breugel, 1991]

Using this iteration algorithm, *the volume of the expanded outer shell* follows:

$$V_{ou,ex;x,j} = \frac{V_{ou;x,j}}{1-\zeta(\chi \cdot \delta_{ou;x,j}) \times \{1+(\upsilon-1) \times \alpha_{<x,j}\}} \tag{4.1}$$

where $V_{ou;x,j}$ is the volume of outer product that corresponds to the degree of hydration $\alpha_{<x,j}$. χ is a *stereometric conversion factor*. It is equal to $(4\pi/3)^{1/3}$ (see definition in *[Van Breugel, 1991]*). $\delta_{ou;x,j}$ is the thickness of the outer shell. υ is the volume increase ratio (see section 3.2.5). ζ is the shell density, which stands for the amount of cement in a shell around a cement particle *[Van Breugel, 1991]*.

A similar algorithm is used in HYMOSTRUC3D-E to calculate the *volume of the expanded outer shell* in case PC, BFS and FA particles become embedded in the outer shell (see Appendix E).

4.2.3 Nucleation and growth of CH particles

4.2.3.1 General

CH is an important hydration product of PC. In cement paste, CH is generally present in crystalline form *[Taylor, 1997]*. The formation of CH in cement-based materials can be divided in two periods: the nucleation period and the period of growth of crystals *[Kjellsen et al., 2004; Gallucci et al., 2007]*.

a. Nucleation period

Fig. 4.5 schematically shows the nucleation of CH particles in a blended cement paste. As shown in Fig. 4.5a, the PC and gypsum particles will partially dissolve in the pore solution

and ions, such as Na^+, K^+ Ca^{2+},OH^-, will be released. The concentrations of Ca^{2+} and OH^- will increase beyond the solubility equilibrium of CH. The supersaturation ratio of Ca^{2+} and OH^- ions (the ratio of ion product (IP) to equilibrium constant (K_{sp}) of CH) will increase. The thermodynamic driving force for the nucleation of CH particles will also increase. As a consequence, a CH nucleus will form. During the formation of the CH nucleus a free energy ΔG^* will be consumed (Fig. 4.5b). It is noted that in cement-based materials the gypsum particles could also act as a nucleus for the growth of CH particles *[Gallucci et al., 2007]*. To sum up, the nuclei of CH particles in cement-based materials come from two possible resources: 1) the supersaturation ratio of Ca^{2+} and OH^- ions; 2) the gypsum particles.

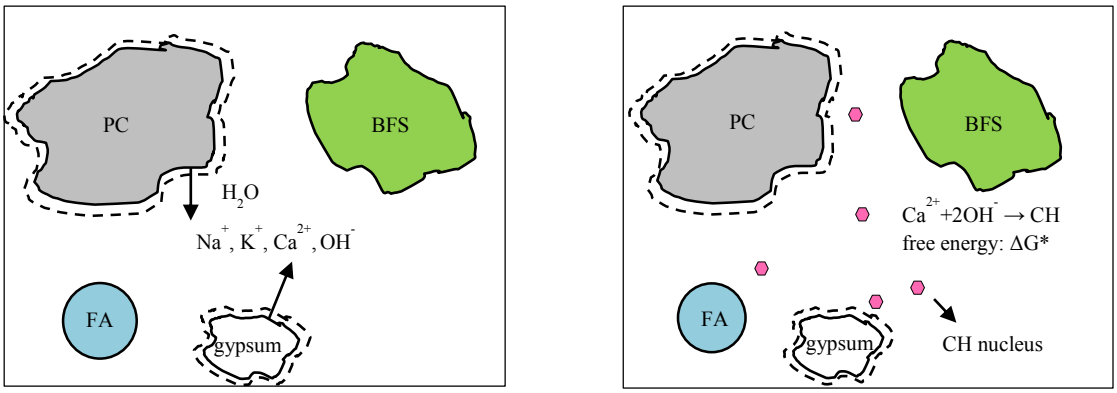

(a) Formation of Ca^{2+} and OH^- *(b) nucleation of CH particles*

Fig. 4.5 Schematic representation of the nucleation of CH particles

b. Crystal growth period

In a homogenous solution, the growth rate of CH particles is also a function of the supersaturation ratio of Ca^{2+} and OH^- ions *[Harutyunyan et al., 2009]*. In cement-based materials the growth of CH particles in the pore space will be hindered by the pore walls. Fig. 4.6 schematically shows the growth of a crystal in a cylindrical pore. When the crystal is still relatively small, it can grow freely (Fig. 4.6a). When the crystal reaches to pore wall, the growth of the crystal will be hindered by the pore wall. (Fig. 4.6b). However, as shown in Fig. 4.6c, the crystal can also grow in the direction parallel with the pore wall leading to a more cylindrical crystal *[Steiger, 2005]*. This is consistent with the observations of Diamond *[2001]* and Gallucci et al. *[2007]*, who observed long thin CH crystals randomly distributed in the microstructure of cement paste.

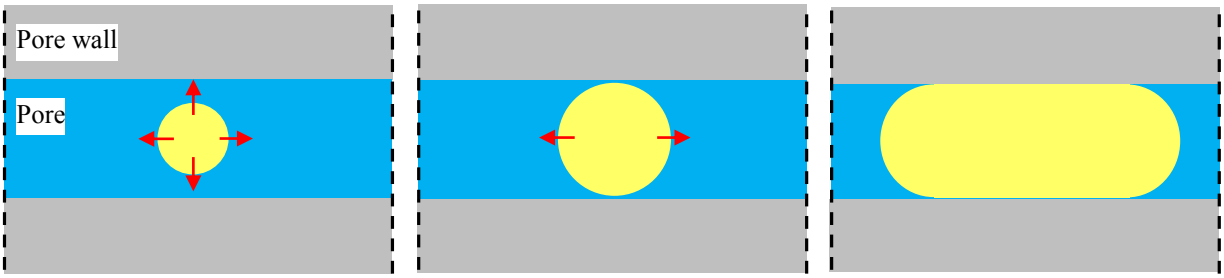

(a) *(b)* *(c)*

Fig. 4.6 Schematic representation of the growth of a crystal in a cylindrical pore (yellow represents crystals) [After Steiger, 2005]

The growth of crystals depends on the pore size. Based on the relationship between crystallization pressure and crystal growth, Scherer *[2002]* proposed that "*if there is a path connecting small and large pores, small crystals will dissolve and the solute will diffuse to a larger pore where the chemical potential of the crystal will be lower*". Fig. 4.7 shows a schematic representation of the dissolution of crystals in small pores and the growth of a crystal in a bigger pore. First, the nucleation of crystals can occur in pores of all sizes (Fig. 4.7a). The growth of crystals in big pores will reduce the supersaturation ratio. If this supersaturation ratio is lower than the supersaturation ratio for the equilibrium of the crystals in small pores, the crystals in small pores will dissolve and feed the growth of the larger one (Fig. 4.7b and Fig. 4.7c). In other words, a small crystal is metastable as long as no crystals have nucleated in the larger accessible pores; once a larger crystal appears, the smaller crystal is unstable.

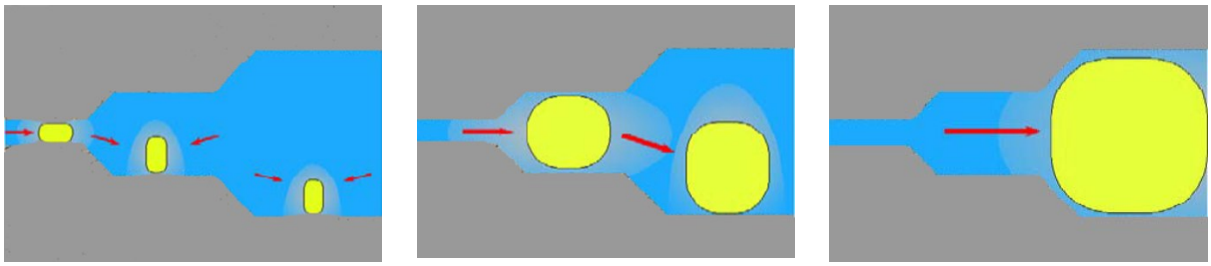

(a) *(b)* *(c)*

Fig. 4.7 Crystals nucleate in pores of all sizes (a), but growth is quickly constrained in the smallest, which dissolves (b) and transfers its solute to a larger crystal in an adjacent pore; the process continues until crystals only exist in the largest accessible pores (c). [After Scherer, 2002]

4.2.3.2 Modelling approach for the growth of CH particles

In HYMOSTRU3D-E, the simulation of the 3D spatial distribution of CH particles in the REV of cement paste comprises two parts: *nucleation of CH particles* and *growth of CH particles*.

a. Nucleation of CH particles

In the simulation of the nucleation process of CH particles, first the number of CH nuclei is calculated. There are two resources for the formation of CH nuclei in the cement paste:

Resource 1

In cementitious systems gypsum particles could also act as CH nuclei *[Gallucci et al., 2007]*. In HYMOSTRUC3D-E each gypsum particle is assumed to act as one CH nucleus in the REV of cement paste. Gypsum is normally milled together with PC in the cement production process. It is also assumed that gypsum has a similar particle size distribution to PC. Hence the number of gypsum particles can be calculated from the number of PC particles (Eq. (4.2)):

$$N_{gyp} = N_{PC} \times \frac{V_{gyp}}{V_{gyp} + V_{PC}} = N_{PC} \times \frac{f_{gyp}/\rho_{gyp}}{f_{gyp}/\rho_{gyp} + (1 - f_{gyp})/\rho_{PC}} \quad (4.2)$$

where N_{PC} is the number of PC particles in the REV of cement paste calculated in section 4.2.2.1 and Appendix A.4, and f_{gyp} is the mass fraction of gypsum in PC. ρ_{gyp} and ρ_{PC} are the densities of gypsum and PC, respectively. V_{gyp} and V_{PC} are the volume of gypsum and PC, respectively.

Resource 2

Resource 2 comes from the increasing supersaturation ratio of Ca^{2+} and OH^- ions in the pore solution. According to Klein et al. *[1968]*, the number of CH nuclei can be calculated from the supersaturation ratio in the pore solution (Eq. (4.3)):

$$dN_{CH}/dt = (D_{Ca,OH}/{d_{CH}}^2 v_0)\sqrt{\frac{2ln(IP/K_{sp,CH})}{3\pi n^*}}\, exp(-\Delta G^*/kT) \quad (4.3)$$

where $D_{Ca,OH}$ is the mean diffusion coefficient of Ca^{2+} and OH^- ions in the solution. d_{CH} the diameter of a CH molecule. n^* is the number of CH molecules in a CH nucleus. v_0 is the molecular volume of water. $IP/K_{sp,CH}$ is the supersaturation ratio. $K_{sp,CH}$ is equilibrium constant (also called solubility constant) for saturated solution and solid formation. IP is the ion product. k is the Boltzmann constant. T is the temperature (K) and ΔG^* is the free energy of forming the CH nuclei. is the For the values of $D_{Ca,OH}$, d_{CH}, n^*, $K_{sp,CH}$, k and ΔG^*, see Klein et al. *[1968]*. The ion product is calculated with Eq. (4.4):

$$IP = c_{Ca^{2+},S} \times \left(c_{OH^-,S}\right)^2 \quad (4.4)$$

where $c_{Ca^{2+},S}$ is the concentration of Ca^{2+} ions in the supersaturated pore solution and $c_{OH^-,S}$ is the concentration of OH^- ions in the supersaturated pore solution.

Because the rate of reaction of PC particles is relatively much higher than that of BFS and FA particles at very early age, the OH^- ions are mainly from the dissolution of Na_2O and K_2O of PC particles in the pore solution. The concentration of OH^- ions $c_{OH^-,S}$ [mole/L] in the supersaturated pore solution is calculated with Eq. (4.5):

$$c_{OH^-,S} = c_{Na^+} + c_{K^+} \quad (4.5)$$

where c_{Na^+} is the concentration of Na^+ ions [mole/L] and c_{K^+} is the concentration of K^+ ions [mole/L]. For the calculation of c_{Na^+} and c_{K^+}, see section 3.3.2.2.

The Ca^{2+} ions mainly come from the dissolution of C_3S, C_2S, C_3A, C_4AF and gypsum. At very early age a very few reaction products are formed. Gallucci et al. *[2007]* observed that the first emerge of CH particles is at 4 hours after mixing and very little CSH gel has precipitated at 8 hours after mixing. Based on this observation, the nucleation period of CH particles in HYMOSTRUC3D-E is assumed to be from mixing time up to 4 hours. It is also assumed that all the Ca^{2+} ions released from the dissolution of C_3S, C_2S, C_3A, C_4AF and gypsum are present in the pore solution during the nucleation period of CH particles. Hence, the concentration of Ca^{2+} ions $c_{Ca^{2+},S}$ [mole/L] in the supersaturated pore solution is calculated with Eq. (4.6):

$$c_{Ca^{2+},S} = \frac{m_{PC} \times \begin{bmatrix} 3 \times f_{C3S} \times \alpha_{j,C3S} + 2 \times f_{C2S} \times \alpha_{j,C2S} + 4 \times f_{C4AF} \times \alpha_{j,C4AF} \\ +3 \times f_{C3A} \times \alpha_{j,C3A} + f_{gyp} \times \alpha_{j,gyp} \end{bmatrix}}{V_{fr,j,wat,tot}} \quad (4.6)$$

where m_{PC} is the mass of PC particles in 1 g blended cement. f_{C3S}, f_{C2S}, f_{C4AF}, f_{C3A}, f_{gyp} are the mass fraction of C_3S, C_2S, C_4AF, C_3A and gypsum in PC, respectively. $\alpha_{j,C3S}$, $\alpha_{j,C2S}$, $\alpha_{j,C4AF}$, $\alpha_{j,C3A}$, $\alpha_{j,gyp}$ are the degree of hydration of C_3S, C_2S, C_4AF, C_3A and gypsum, respectively. $V_{fr,j,wat,tot}$ is the volume of free capillary water. These parameters have been calculated in the *cement hydration route*.

Fig. 4.8 shows an example of the calculated number of CH nuclei in the REV of cement pastes with different BFS contents (w/b = 0.4). The calculated number of CH nuclei decreases with increasing BFS content. For the same BFS content, the calculated number of CH nuclei from resource 1 (Fig. 4.8a) is much more than that from resource 2 (Fig. 4.8b).

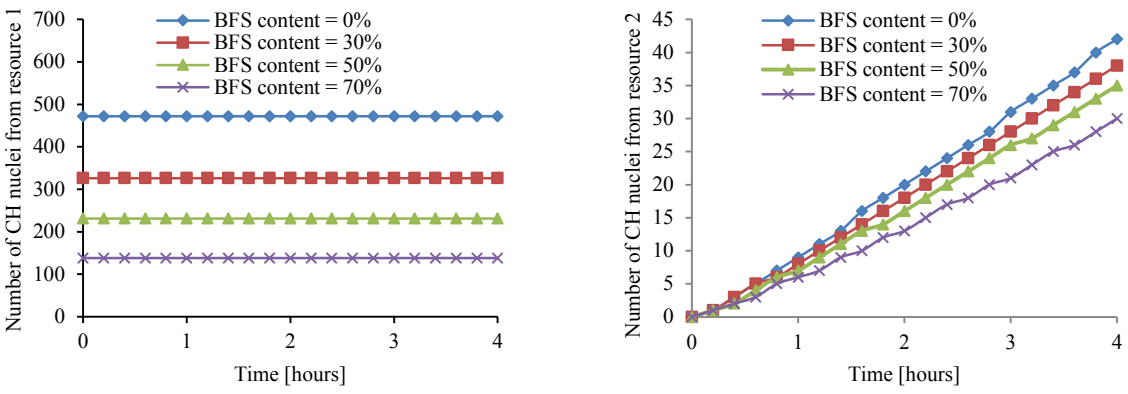

(a) *(b)*

Fig. 4.8 An example of calculated number of CH nuclei in the REV of cement paste from mixing time up to 4 hours. Note: w/b = 0.4, REV size = 100×100×100 μm³, the properties of PC and BFS are presented in section 5.5. (a) number of CH nuclei calculated with Eq. (4.2), (b) number of CH nuclei calculated with Eq. (4.3). Degree of hydration of PC is less than 10%.

b. Growth of CH particles

In section 4.2.3.1 Scherer *[2002]* was quoted, who said that "*if there is a path connecting small and large pores, small crystals will dissolve and the solute will diffuse to a larger pore where the chemical potential of the crystal will be lower*". In HYMOSTRUC3D-E this rule for the crystal growth in porous materials as proposed by Scherer *[2002]* will be followed to simulate the growth of CH particles in the pore structure of cement paste. Fig. 4.9 shows the schematic representation of the simulation of the growth process of CH particles in HYMOSTRUC3D-E. The simulation of the growth process of CH particles contains the following three steps:

Step 1 - Number of CH nuclei in the pore space

The number of CH nuclei in the pore space is calculated in the previous paragraphs, viz., *a. Nucleation of CH particles*

Step 2 - Distribution of CH nuclei in the pore space

The CH nuclei are placed in the centre of pores with size from big to small, until all the CH nuclei are placed. For example, if there are 10 CH nuclei, all these CH nuclei are placed in the centre of pores with size from big to small (Note: the number in Fig. 4.9a represents the sequence to place CH nuclei).

Step 3 - Growth of CH particles in the pore space

First the CH nucleus in the "big" pores grows until the CH particle is hindered by the pore

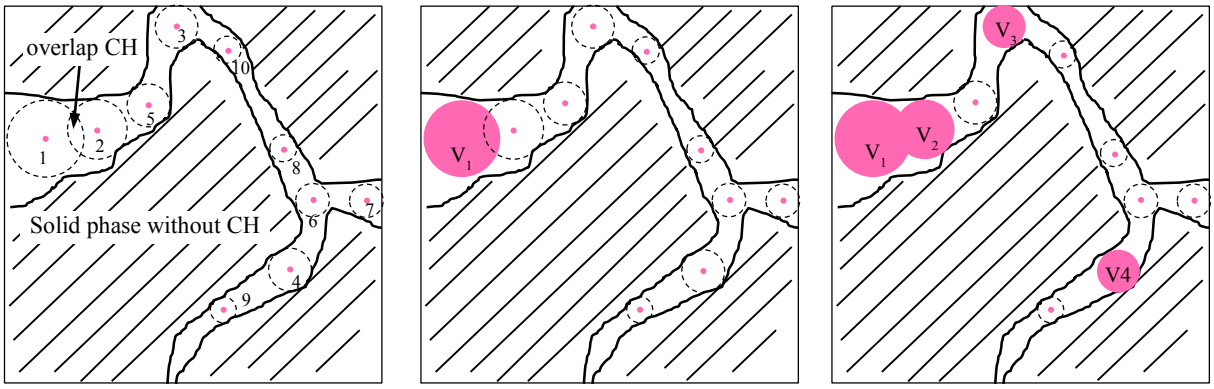

(a) *(b)* *(c)*

Fig. 4.9 Schematic representation of the growth of CH particles in HYMOSTRUC3D-E: (a) Placing CH nuclei in big pores to small pores; (b) Growth of CH nuclei in "biggest" pore; (c) Growth of other CH nuclei until the total volume in the 3D pore space (V_1+V_2+V_3+⋯V_i) has reached the volume of CH particles calculated based on the stoichiometry of cement hydration. Note: the number in Fig. 4.9a represents the sequence to place CH nuclei.

wall (e.g. the CH particle V_1 in Fig. 4.9b). Then, the CH nuclei in smaller pores grow one by one until the total volume of CH particles has reached the CH volume calculated based on the stoichiometry of cement hydration, $V_{j,CH,tot}$ (see section 3.2.5 and Appendix C.4). For example, if the total volume of CH particles ($V_1 + V_2 + V_3 + V_4$) in the pore space (Fig. 4.9c) has reached $V_{j,CH,tot}$, the growth of CH particles will stop.

In the growth process of CH particles shown in Fig. 4.9 it is possible that CH particles overlap (e.g. the CH particles V_1 and V_2 in Fig. 4.9c). Fig. 4.10 shows the schematic representation of the algorithm to consider the overlap. First step is to check whether CH particles overlap. If two CH particles overlap (Fig. 4.10a), the part of overlapped CH phases will be redistributed on the surface of these two CH particles (Fig. 4.10b). The next step is to check whether the redistributed CH phase and the pore wall overlap. If the redistributed CH phase and the pore wall overlap, the overlapped CH phase will redistributed on the surface of CH particles again (Fig. 4.10c). This iteration from Fig. 4.10b to Fig. 4.10c continues until the volume of CH phases in Fig. 4.10c equals to V_1+V_2.

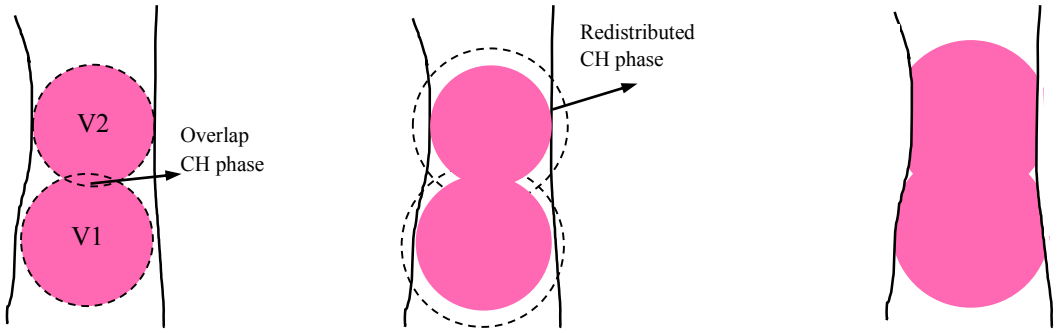

Fig. 4.10 Schematic representation of the algorithm to consider the overlap between two CH particles. (a) Check whether two CH particle overlap. (b) Redistribute the overlapped CH phase between CH particles. (c) Redistribute the overlapped CH phase between CH particles and pore wall.

Fig. 4.11 shows three stages of the growth process of CH particles in pore structure of PC paste (w/c = 0.4, time =1 day). The pore space, with pore size from big to small, is filled with CH particles. Fig. 4.12 shows the simulated 3D distribution of CH particles in PC paste up to 28 days.

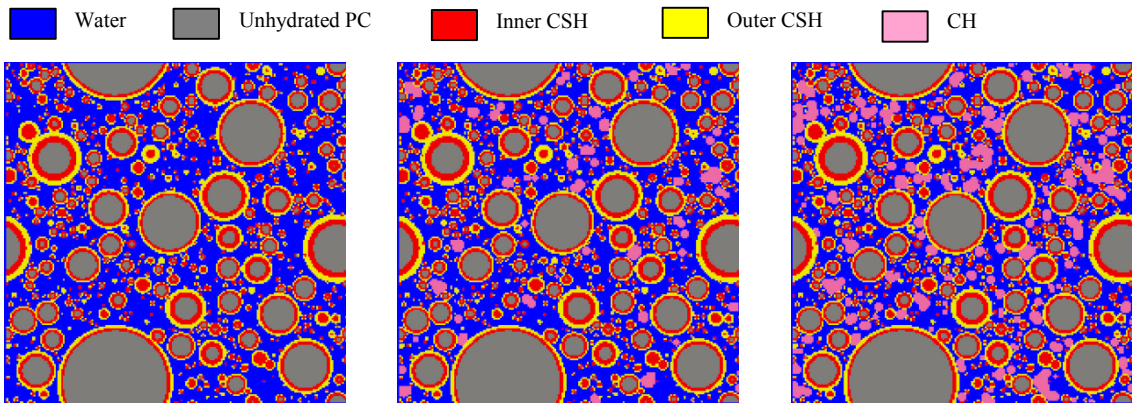

Fig. 4.11 The simulation of the growth process of CH particles in pore structure of PC paste visualized in 2D (w/c = 0.4, time =1 day, see the properties of PC as input of simulation in [Gallucci et al., 2007]). Note: Volume fraction of CH in cement paste = 7.29 %.

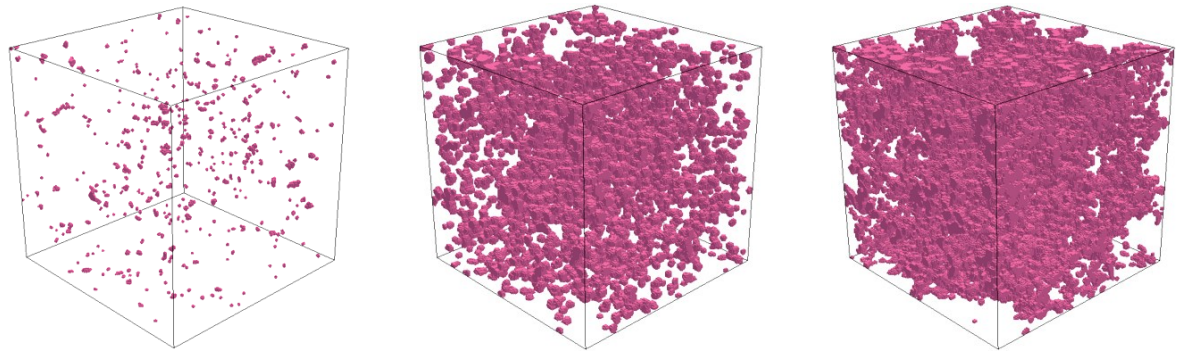

(a) time = 0 day *(b) time = 1 day* *(c) time = 28 days*

Fig. 4.12 An example of the growth of CH particles in the REV of PC paste (w/c = 0.4; REV size = 100×100×100 μm³, see the properties of PC as input of simulation in [Gallucci et al., 2007]).

Fig. 4.13 shows the cumulative size distribution of CH particles. The cumulative size distribution of CH particles simulated by HYMOSTRUC3D-E is close to the experimental data published by Gallucci et al. *[2007]*, at least for small particle sizes, i.e. < 3.4 μm. For large particle sizes, i.e. > 3.4 μm, the simulated cumulative size distribution of CH particles differs from the experimental data. The main reason for this discrepancy is that the pore structure simulated by HYMOSTRUC3D-E with an REV = *100×100×100* μm³ does not contain the very big pores, i.e. the pores > 10 μm. In reality these big pores exist in the cement paste, and they provide room for the growth of large CH particles.

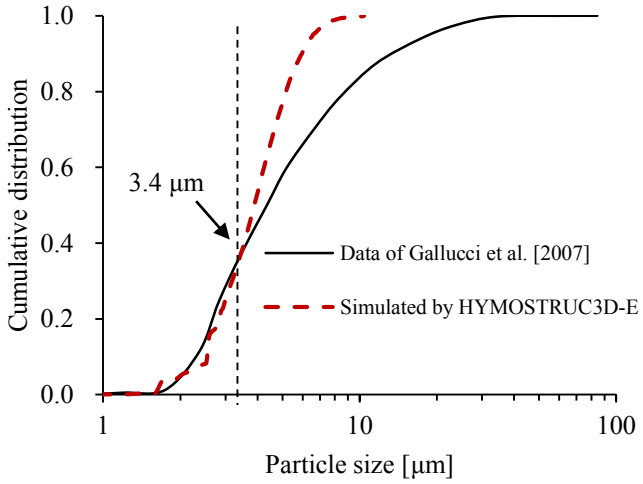

Fig. 4.13 Cumulative size distribution of CH particles in the PC paste (w/c = 0.4; time = 1 day). REV size = 100×100×100 μm³.

4.2.4 Volumes of individual phases in the 3D microstructure of cement paste

For determining the evolution of the pore structure (including the contribution of the gel pores to the porosity), it is necessary to identify the evolution of the volume propositions of inner and outer CSH gels. In this section, section 4.2.4, the volumes of individual phases, including PC, BFS, FA, inner product, outer product, etc., in the 3D microstructure of cement paste are identified.

The simulated 3D microstructure is digitalized into small voxels $1\times1\times1$ μm^3. An example is shown in Fig. 4.14. The digitalized cement paste consists of $100\times100\times100$ μm^3 voxels. By counting the number of these voxels, the volume proportions of individual phases in the REV of cement paste can be calculated with Eq. (4.7):

$$f_{dig,j,X_k} = N_{dig,X_k}/N_{dig,tot} \tag{4.7}$$

where f_{dig,j,X_k} is the volume fraction of a phase (X_k) in the simulated 3D microstructure at time t_j. $X_{k=1}$ = capillary pores, $X_{k=2}$ = PC, $X_{k=3}$ = BFS, $X_{k=4}$ = FA, $X_{k=5}$ = inner product, $X_{k=6}$ = outer product, $X_{k=7}$ = CH, $X_{k=8}$ = FA hollow core, N_{dig,X_k} is the number of voxels of X_k in the REV of cement paste. The volume proportions of inner and outer CSH gels, i.e. $f_{dig,j,in,gel}$ and $f_{dig,j,ou,gel}$, as used later for Eq. (4.13) and Eq. (4.14) are obtained with Eq. (4.7).

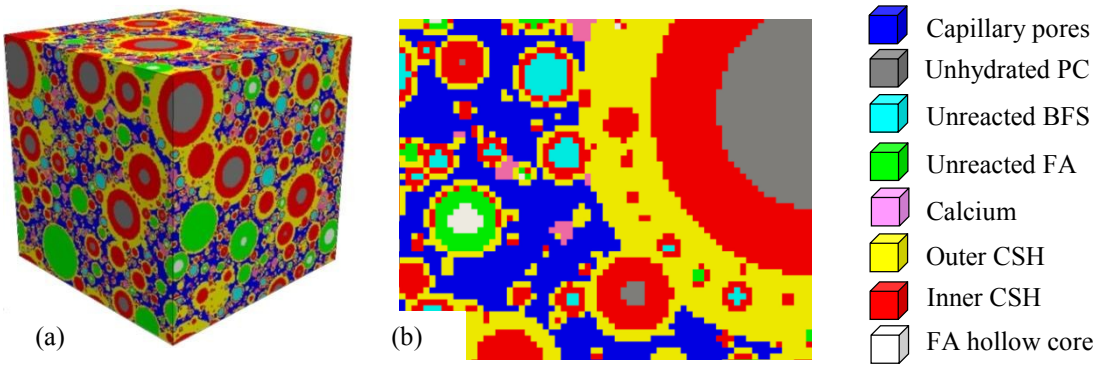

Fig. 4.14 The digitalization of the simulated 3D microstructure of cement paste: (a) Simulated microstructure visualized in 3D (b) Digitalized microstructure visualized in 2D (time = 28 days, w/b = 0.4, 60% PC, 20% BFS, 20% FA, see the properties of PC, BFS and FA in section 5.5)

4.3 Module for determining the evolution of the pore structure of blended cement pastes

4.3.1 General

Cement paste is a multi-scale porous material that comprises capillary pores at the microscale and gel pores at the nanoscale. Capillary pores are commonly considered as the remnants of the initially water-filled space *[Taylor, 1997; Mindess et al., 2003]*, and gel pores are defined as an intrinsic part of CSH gel *[Jennings, 2004]*.

The sizes of capillary pores and gel pores are different due to different formation mechanisms. Classifications of capillary pores and gel pores have been proposed by different researchers *[Mindess et al., 2003; Jennings, 2004]*. Mindess et al. *[2003]* indicated that capillary pores are in the range of 10 nm to 10 μm and gel pores are smaller than 10 nm (Table 4.1). Jennings *[2004]* indicated that capillary pores are around 75 nm, and gel pores are smaller than 5 nm (Table 4.2).

Table 4.1 Classification of pore sizes in hydrated cement paste by Mindess et al. [2003]

Designation	Diameter	Description
Capillary Pores	10-0.05 μm	Large capillaries (macroposes)
	50-10 nm	Medium capillaries (large mesopores)
Gel Pores	10-2.5 nm	Small isolated capillaries (small mesopores)
	2.5-0.5 nm	Micropores
	≤ 0.5 nm	Interlayer spaces (space between CSH sheets)

Table 4.2 Classification of pores in cement paste by Jennings [2004]

Pore category	New pore category	Size of pore within structure	RH Pores Empty % by Kelvin
Capillary	Capillary	75 nm	90
Large Gel	Inter low density (LD) CSH	2-5 nm	40
Small gel	Inter-globule	1.2-2 nm	20
Inter layer	Intra-globule or globule	<0.5 nm	0

Identifying the capillary pore structure and gel pore structure of cement-based materials is relevant for some specific research topics. There are two examples:

(1) Potential for investigating creep

The origin of creep of cement-based materials is the creep of hydration products, such as CSH gel. Knowing the CSH gel pore structure provides a basis for better understanding of creep of cement-based materials and its consequence.

(2) Potential for investigating drying shrinkage

Being exposed to the atmosphere at air temperature, the relative humidity (RH) of cement-based materials can drop from 100% to 50%. Both the capillary pores and the large gel pores will dry out at this RH range. The simulation of capillary pores and gel pores can be helpful to describe the drying process of cement-based materials.

At the microscale numerical cement hydration models e.g. HYMOSTRUC3D *[Van Breugel, 1991; Koenders, 1997; Ye, 2003]*, CEMHYD3D *[Bentz et al. 1991, 1994; Bentz 1995, 1997]* and μic microstructural modelling platform *[Bishnoi et al., 2009]*, etc., are available to simulate the microstructures of cement paste. The capillary pore structures can be obtained from the simulated microstructures *[Ye, 2003]*. The gel pore structures, however, are difficult to be obtained from these numerical cement hydration models because of the limited resolution of these models.

At the nanoscale (< 100 nm), Bentz et al. *[1995]* applied the hard core and soft shell model to simulate the nanostructures of CSH gel. Fonseca et al. *[2011]* used random close packing, and close packing of mono-sized spheres for simulating the nanostructures of outer CSH gel and inner CSH gel, respectively. Masoero et al. *[2012]* employed random close packing of multi-sized spheres to represent the nanostructures of CSH gel. However, the aforementioned research didn't give detailed information about gel pore structures, such as pore size distribution of gel pores.

In HYMOSTRUC3D-E a pore structure module is proposed to determine the evolution of the pore structure of blended cement pastes, including the contribution of the gel pores to the porosity capillary.

4.3.2 Modelling of the pore structure of blended cement pastes

4.3.2.1 Levels of the pore structure module

This pore structure module distinguishes three levels:

Level I:

At the nanoscale, ＜5 nm, the concept of CSH globules proposed by Jennings *[2000; 2004; 2008]* is adopted. As shown in the top part of Fig. 4.15, this CSH globule consists of layers of CSH chains and interlayer water. The pore space between CSH chains are defined as interlayer gel pores.

Level II:

Also at the nanoscale, but now in the range from 5 nm to 100 nm, the nanostructures of inner and outer CSH gels are determined by the packing of CSH globules, respectively (see the middle part of Fig. 4.15). The packing density of inner CSH gels is higher than that of outer CSH gels. Gel pores are defined as the space between the CSH globules. The nanostructures of inner and outer CSH gels are assigned to the inner and outer products calculated with HYMOSTRUC3D-E.

Level III:

At the microscale, from 100 nm to 100 μm, capillary pores form between solid phases (see the bottom part of Fig. 4.15). It is noted that at this scale CSH gels are considered as one porous phase, consisting of inner and outer products.

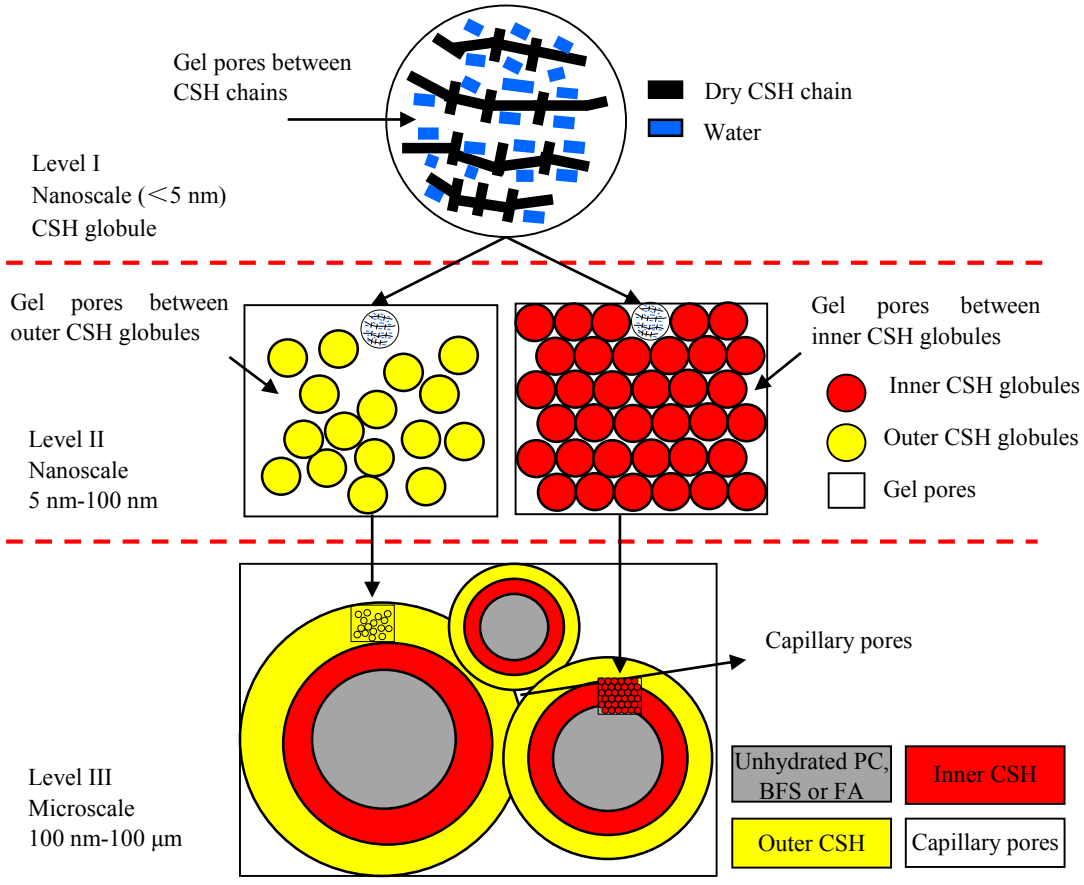

Fig. 4.15 Schematic representation of the multi-scale pore structures of blended cement paste. The concept of CSH globules is from Jennings [2000; 2004; 2008].

4.3.2.2 Nanostructures of outer and inner CSH gel

At the scale from 5 nm to 100 nm the nanostructures of outer CSH gel and inner CSH gel are determined by the packing of the CSH globules.

a. Nanostructure of outer CSH gel

Jennings et al. *[2007]* proposed that the packing density of outer CSH gel is approximate 0.64. This packing density is almost equal to that of *random close packing of mono-size spheres*. *Random close packing of mono-size spheres* means "*the maximum density that a large, random collection of spheres can attain and this density is a universal quantity*" *[Torquato et al., 2000]*. The *random close packing of mono-size spheres* has been applied in many studies to represent the structure of materials. For example, Fonseca et al. *[2011]* used it to represent the nanostructure of outer CSH gel.

In HYMOSTRUC3D-E the *random close packing of mono-size spheres* is adopted to represent the nanostructure of outer CSH gel. To generate the *random close packing of mono-size spheres* a program of Skoge et al. *[2006]* is used in HYMOSTRUC3D-E. The program of Skoge et al. is based on molecular dynamic mechanism. The following paragraphs describe how to obtain the *random close packing of mono-size spheres.*

A cube with a length = 100 nm is defined as the representative elementary volume (REV) of outer CSH gel. The number of CSH globules $N_{ou,glo}$ in the REV of outer CSH gel is calculated with Eq. (4.8) :

$$N_{ou,globule} = V_{REV,CSH} \times \rho_{pack,ou}/V_{globule} \quad (4.8)$$

where $N_{ou,globule}$ is the number of mono-size spheres for the nanostructure of outer CSH gel in the REV, $V_{REV,CSH}$, [nm^3], of outer CSH gel. $V_{globule}$ [nm^3] is the volume of one CSH globule. Jennings *[2000, 2004, 2008]* proposed that the diameter of CSH globules is around 5 nm. Hence, $V_{globule}$ is equal to $\pi\times5^3/6$ nm^3. $\rho_{pack,ou}$ is the packing density of outer CSH gel. For $V_{REV,CSH}$ = *100×100×100* nm^3, $\rho_{pack,ou}$ = 0.64, $V_{globule}$ = $\pi\times5^3/6$ nm^3, Eq. (4.8) gives $N_{ou,globule}$ = 9778. Fig. 4.16 shows a 3D picture of the random close packing of 9778 globules with diameter = 5 nm in the REV of outer CSH gel with size = *100×100×100* nm^3.

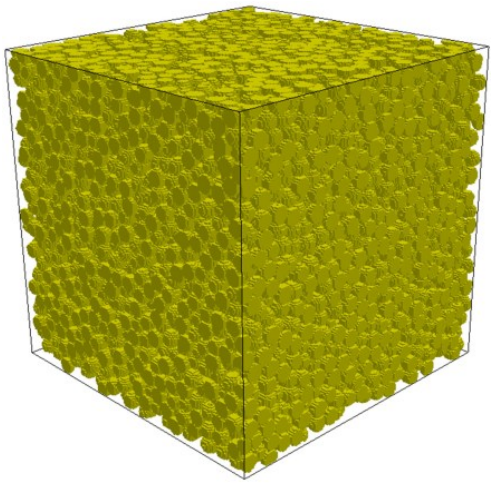

Fig. 4.16 The random close packing of CSH globules in the REV of outer CSH gel simulated using the program of Skoge et al. [2006] (The REV size = 100×100×100 nm^3, the number of CSH globules = 9778)

(2) Nanostructure of inner CSH gel

The nanostructure of inner CSH gel is determined using the *close packing of mono-size spheres*. The *close packing of mono-size spheres* can be realized by the dense arrangement of mono-size spheres with packing density of 0.74 *[Hales, 1998]*. There are two types of mono-size close packing: face-centred cubic (FCC) and hexagonal close-packed (HCP). The FCC of close packing of mono-sized spheres is used in this study. Fig. 4.17b shows the nanostructure of inner CSH gel simulated with FCC packing.

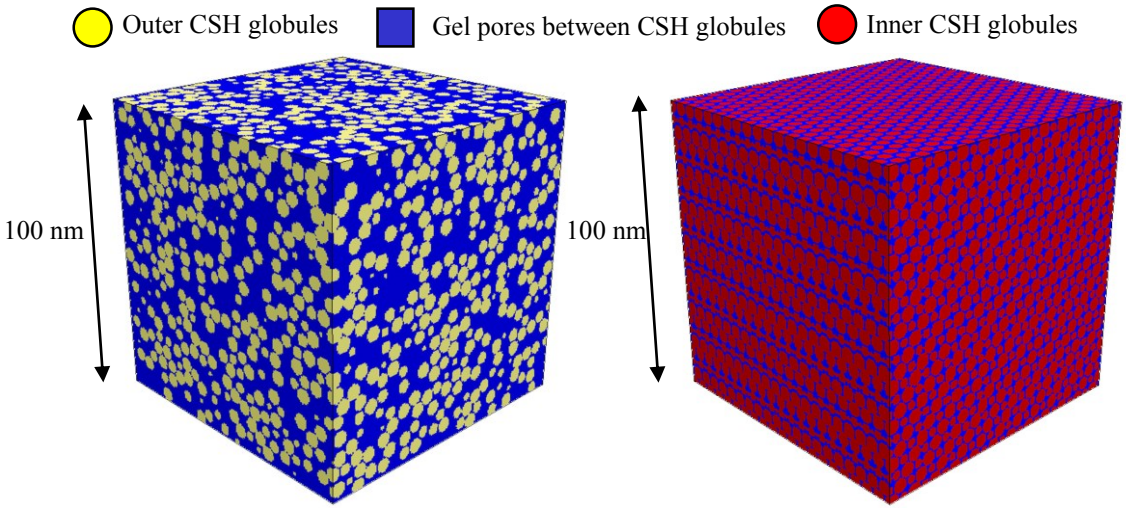

Fig. 4.17 Nanostructures of CSH gel: (a) Nanostructure of outer CSH gel, (b) Nanostructure of inner CSH gel.

4.3.2.3 Incorporating nanostructures of CSH to microstructures of blended cement paste

In HYMOSTRUC3D-E the microstructure of blended cement paste is simulated by distributing the inner CSH gel and outer CSH gel on the surfaces of PC, BFS and FA particles and distributing CH particles in the pore space (the left part of Fig. 4.18). Both inner CSH and outer CSH have a porous nanostructure (the middle part of Fig. 4.18). These nanostructures consists of CSH globules (the right part of Fig. 4.18) and gel pores between CSH globules.

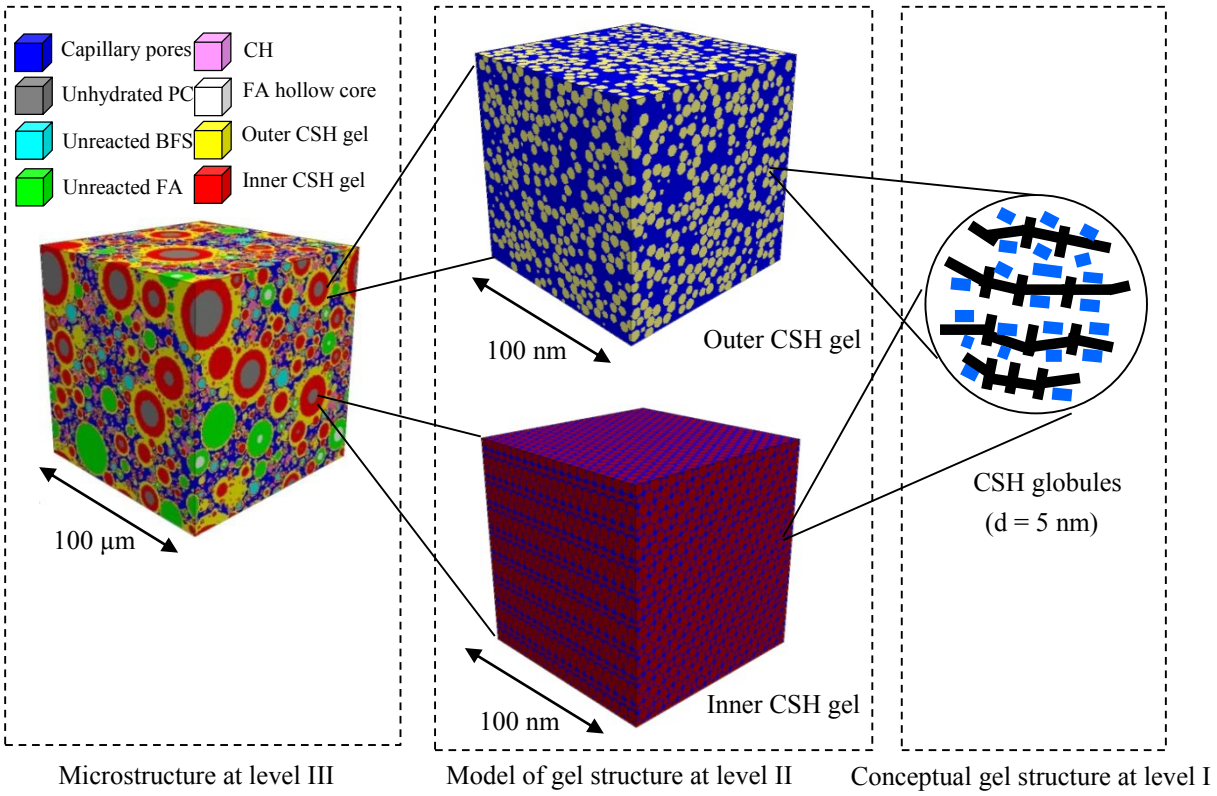

Fig. 4.18 Pore structure module for blended cement paste (w/b = 0.4, 60% PC, 20% BFS, 20% FA, see the properties of PC, BFS and FA in section 5.5, time = 28 days)

4.3.2.4 Pore structures of blended cement paste

As shown in Fig. 4.19a and Fig. 4.19b, the capillary pores and gel pores of blended cement paste at 1 day (w/b = 0.4, 60% PC, 20% BFS, 20% FA. For the properties of PC, BFS and FA, see section 5.5) are visualized by removing the solid voxels of the (multi-scale) virtual microstructure.

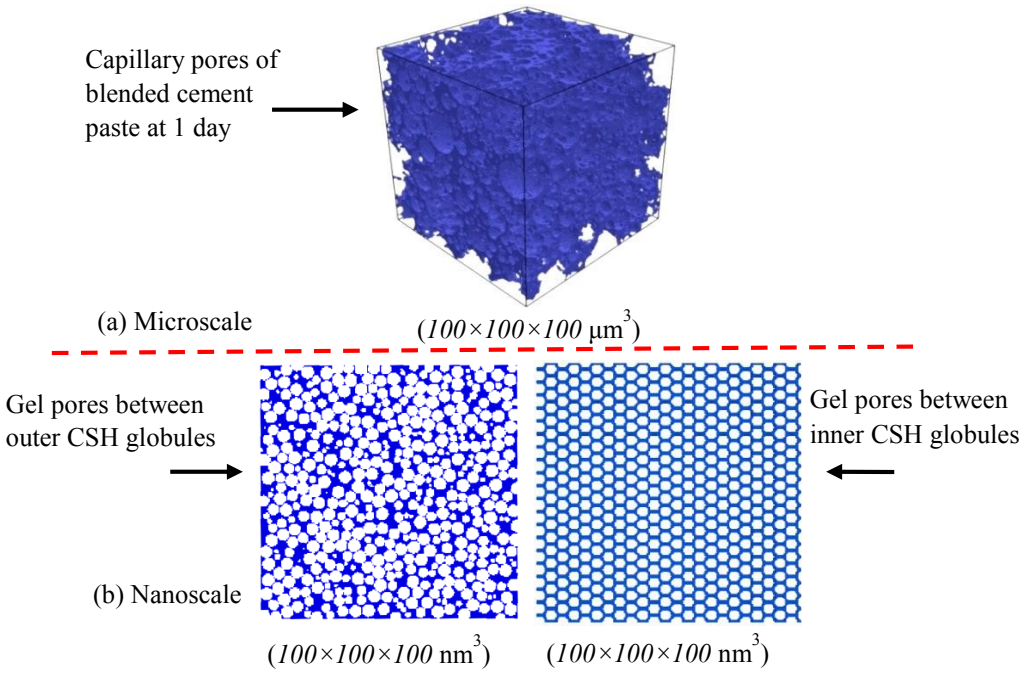

Fig. 4.19 An example of the capillary pores and gel pores of blended cement paste. Note: blue represents pore space, and the gel pore structures are visualized in 2D (w/b = 0.4, 60% PC, 20% BFS, 20% FA. For the properties of PC, BFS and FA, see section 5.5, time = 28days).

4.3.2.5 Pore size distribution

a. Capillary pore size distribution in the REV of cement paste

The capillary pore size distribution of cement paste is quantified as follows: First the simulated capillary pore structure of cement paste is segmented into $N_{slice,paste}$ slices (Fig. 4.20a). Then, each slice is digitalized into $N_{slice,paste} \times N_{slice,paste}$ voxels. Like the definition of pores in the pore analysis of SEM *[Lange et al., 1994]*, a pore is defined as a pore area (A_{pore}) that contains the neighbour connected pore voxels (Fig. 4.20b).

The diameter of a pore area is equal to $\sqrt{4A_{pore}/\pi}$. If the sum of the pore areas with diameter d in layer i is $A_{d,cap,i}$, the volume [μm^3] of the pores with diameter d [μm] in the 3D microstructure of cement paste is:

$$V_{d,cap} = \frac{L_{REV,paste}}{N_{slice,paste}} \times \sum_{i=1}^{n} A_{d,cap,i} \qquad [\mu m^3] \qquad (4.9)$$

where $L_{REV,paste}$ is the length of the REV of cement paste [μm]. $N_{slice,paste}$ is the number of slices. In HYMOSTRUC3D-E the number $N_{slice,paste}$ in Eq. (4.9) is set at 200 and the resolution, or the distance between two adjacent slices, is equal to $L_{REV,paste} / 200$ μm.

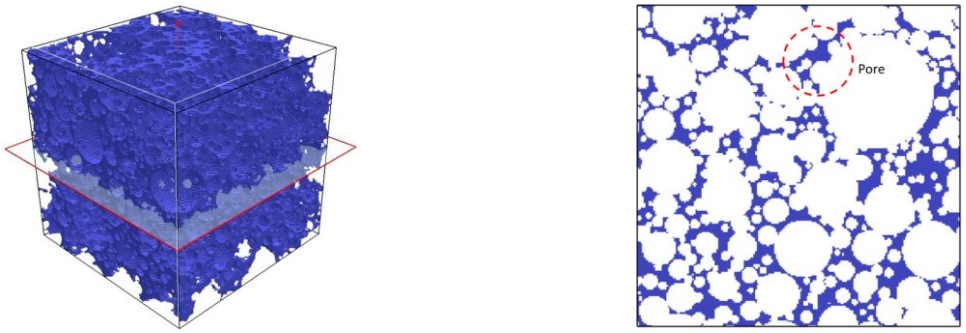

(a) Segmenting the capillary pore structure *(b) A slice obtained by the segmentation*

Fig. 4.20 Schematic representation of determination of the capillary pore structure

The volume fraction of the capillary pores with diameter d [μm] in the 3D microstructure of cement paste is calculated with Eq. (4.10):

$$V_{f,d,cap} = \frac{V_{d,cap}}{V_{REV,paste}} = \frac{V_{d,cap}}{{L_{REV,paste}}^3} \quad (4.10)$$

where $V_{REV,paste}$ is the total volume of 3D microstructure of cement paste [μm^3]

b. Gel pore size distribution

The gel pore size distribution are quantified at two levels: the pore size distribution in the REV of CSH gels (level II) and the gel pore distribution in the REV of cement paste (level III).

b1 Pore size distribution in the REV of CSH gels

To quantify the pore size distribution in the REV of CSH gels, the inner and outer CSH gel pore structures are segmented into $N_{slice,CSH}$ slices. Each slice is digitalized into $N_{slice,CSH} \times N_{slice,CSH}$ voxels. A pore is defined as a pore area (A_{pore}) that contains the neighbour connected pore voxels. An example of analysing the outer CSH gel is shown in Fig. 4.21.

Similar to Eq. (4.9) the volume [nm^3] of the pores with diameter d [nm] in the REV of CSH gels is:

$$V_{d,gel} = \frac{L_{REV,CSH}}{N_{slice,CSH}} \times \sum_{i=1}^{n} A_{d,gel,i} \quad [\text{nm}^3] \quad (4.11)$$

where $L_{REV,CSH}$ is the length of the REV of CSH gels [nm] and $N_{slice,CSH}$ is the number of slices. In HYMOSTRUC3D-E $N_{slice,CSH}$ in Eq. (4.11) is set at 100, and the resolution or the distance between two adjacent slices is equal to $L_{REV,CSH}$/100 nm.

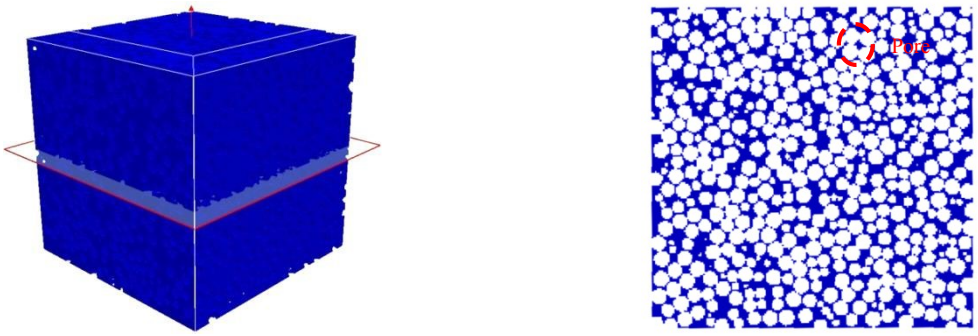

(a) Segmenting the gel pore structure *(b) A slice obtained by the segmentation*

Fig. 4.21 Schematic representation of determination of the gel pore structure. Note: blue is pore; white is solid.

The volume of the pores in the REV of CSH gels with diameter d [nm] is:

$$V_{f,d,gel} = \frac{V_{d,gel}}{V_{REV,CSH}} = \frac{V_{d,gel}}{L_{REV,CSH}{}^3} \quad (4.12)$$

where $V_{REV,CSH}$ is the volume of the REV of CSH gels [nm^3].

b2 Gel pore size distribution in the REV of cement paste

In HYMOSTRUC3D-E, the pore size distribution in the REV of CSH gels at the level II are upscaled to the simulated 3D microstructure of cement paste to obtain gel pore size distribution in the REV of cement paste. The upscaling process is detailed as follows.

Using Eq. (4.12), the volume fractions of gel pores with diameter d [nm] in the 3D microstructure of inner and outer CSH gels are $V_{f,d,in,gel}$ and $V_{f,d,ou,gel}$, respectively. The volume proportions of inner and outer CSH gels in the simulated 3D microstructure of cement paste (time = t_j), $f_{dig,j,in,gel}$ and $f_{dig,j,ou,gel}$, are calculated with Eq. (4.7) (see section 4.2.4). Accordingly, the volume proportion of the inner and outer CSH gels pores with diameter d [nm] in the simulated 3D microstructure of cement paste (time = t_j) can be obtained with (4.13) and (4.14):

$$V_{f,d,in,gel,j,paste} = V_{f,d,in,gel} \times f_{dig,j,in,gel} \quad (4.13)$$

$$V_{f,d,ou,gel,j,paste} = V_{f,d,ou,gel} \times f_{dig,j,ou,gel} \quad (4.14)$$

Fig. 4.22 shows an example of the calculated evolution of phases in the 3D microstructure of PC paste (w/c = 0.4, for the properties of PC, see section 5.2.1). With hydration proceeds from a degree of hydration (DoH) = 38% at 1 day to DoH = 77% at 28 days, the volume

fractions of inner and outer CSH gels increase from 0.17 to 0.35, and 0.14 to 0.23, respectively. Fig. 4.23 shows the calculated gel pore size distributions in PC paste at two ages.

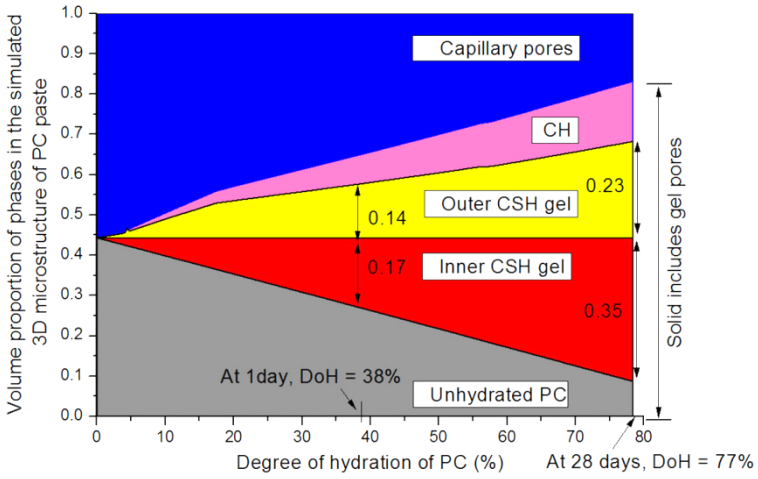

Fig. 4.22 Evolution of phases in the 3D microstructure of PC paste (w/c = 0.4). DoH = degree of hydration.

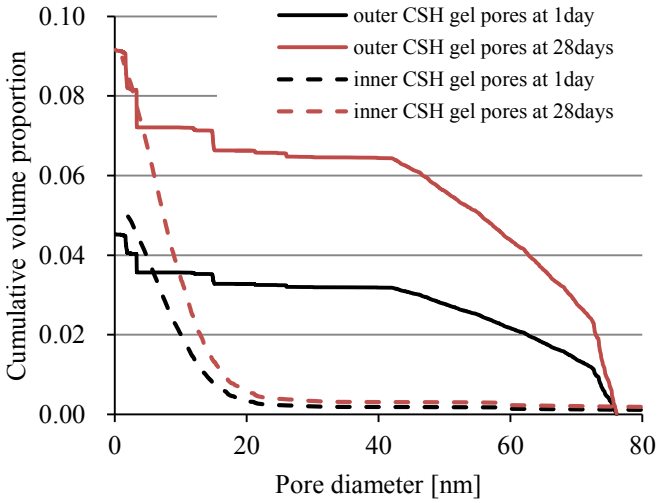

Fig. 4.23 Calculated volume proportion of gel pores in inner and outer CSH gels in the PC paste (w/c = 0.4).

4.4 Summary of HYMOSTRU3D-E

In Chapter 3 and Chapter 4 HYMOSTRUC3D is extended to simulate the hydration and microstructure development of blended cements (PC blended with BFS or/and FA). The extended model is called HYMOSTRU3D-E. HYMOSTRU3D-E model consists of two routes: *cement hydration route* and *microstructure development route*.

The *cement hydration route* represents the hydration-related extension of HYMOSTRUC3D. The reaction rate of a PC, BFS and FA particles in cement paste is simulated as a function of the water distribution and change in pore water chemistry and the temperature in the system.

The reaction rate of a PC particle is described with the formula:

$$\frac{\Delta\delta_{in,x_i,j+1,M_k}}{\Delta t_{j+1}} = K_{0,M_k} \times \Omega_1(.) \times \Omega_2(.) \times \Omega_3(.) \times F_1(.) \times \left[F_2(.) \times \left(\frac{\delta_{tr,M_k}}{\delta_{x_i,j,M_k}} \right)^{\beta_1} \right]^{\lambda_{M_k}} \qquad (4.15)$$

where $\Delta\delta_{in,x_i,j+1,M_k}$ is an incremental increase of the penetration depth of cement component M_k during a time increment $\Delta t_{j+1} = t_{j+1} - t_j$. $M_{k=1} = C_3S$, $M_{k=2} = C_2S$, $M_{k=3} = C_3A$, $M_{k=4} = C_4AF$. K_{0,M_k} is the initial penetration rate of the reaction front of hydrating cement component M_k [μm/hour]. Ω_1, Ω_2, Ω_3 are the reduction factors allowing for the change of water distribution and change in pore water chemistry in the system. F_1 represents the influence of temperature on the rate of reaction. F_2 accounts for the influence of temperature on the morphology and structure of hydration products. δ_{tr,M_k} is the transition thickness of the shell of hydration products when the hydration mechanism of M_k changes from *phase boundary reaction* to *diffusion-controlled reaction*. δ_{x_i,j,M_k} is the total thickness of inner product and outer product. λ_{M_k} is a coefficient to control reaction mechanisms (from *phase boundary reaction* ($\lambda_{M_k} = 0$) to *diffusion-controlled reaction* ($\lambda_{M_k} = 1$)). β_1 is a calibration parameter.

The reaction rate of a BFS or FA particle is described with the formula:

$$\frac{\Delta\delta_{in,x_i,j+1,S_k}}{\Delta t_{j+1}} = K_{0,S_k} \times \Omega_1(.) \times \Omega_2(.) \times \Omega_3(.) \times F_1(.) \times \left[F_2(.) \times \left(\frac{\sigma_{tr,S_k}}{\delta_{x_i,j,S_k}} \right)^{\beta_1} \right]^{\lambda_{S_k}} \times M_{pH,S_k} \qquad (4.16)$$

where $\Delta\delta_{in,x_i,j+1,S_k}$ is an incremental increase of the penetration depth of BFS or FA particle during a time increment $\Delta t_{j+1} = t_{j+1} - t_j$. $S_{k=1}$ = BFS, $S_{k=2}$ = FA. K_{0,S_k} is the initial penetration rate of the reaction part of BFS or FA [μm/hour], respectively. σ_{tr,S_k} is the transition thickness of the shell of hydration products when the hydration mechanism of BFS or FA particle changes from *phase boundary reaction* to *diffusion-controlled reaction*. M_{pH,S_k} represents the influence of pH on the reaction rate of BFS or FA.

The *microstructure development route* deals with the microstructure development-related extension of HYMOSTRUC3D. The microstructure development of blended cement paste is simulated by distributing inner product and outer product on the hydrating PC, BFS and FA particles, and the nucleation and growth of CH particles. In the algorithm for distributing inner product and outer product, the thickness of the shell of reaction product depends on the degree of hydration of reactive particles and the volume of inert particles embedded in growing outer shells simulated in the *cement hydration route*. The nucleation of CH particles is simulated by considering the initial pore solution chemistry and the number of gypsum particles in the system. The growth of CH particles is simulated by considering the pore structure development in the system. In addition, HYMOSTRUC3D-E contains a pore structure module in the *microstructure development route* for simulating the evolution of capillary porosity. Specific porosities are assigned to the inner and outer products. By determining the volume evolution of the inner and outer products, the evolution of gel porosity in cement paste is determined implicitly.

Table 4.3 lists the comparison between HYMOSTRUC3D and HYMOSTRUC3D-E. HYMOSTRU3D-E shows the following extensions:

1. Blended systems
In HYMOSTRUC3D is only able to simulate the hydration and microstructure development pure PC system. HYMOSTRU3D-E is able to simulate the hydration and microstructure development of several systems: mono system (PC), binary system (PC blended with BFS or FA), ternary system (PC blended with BFS and FA).

2. Pore solution chemistry
In HYMOSTRUC3D-E, the evolution of pore solution chemistry in cement paste is simulated, and the influence of the pore solution chemistry on the reaction rates of BFS and FA is quantified explicitly.

3. Nucleation and growth of CH particles
HYMOSTRUC3D-E contains a module to simulate the nucleation and growth of CH particles.

4. Evolution of gel porosity in cement paste
HYMOSTRU3D *only* gives the evolution of porosity of capillary pores in cement paste. However, HYMOSTRU3D-E determines the evolution of the pore structure, including the contribution of the gel pores to the total porosity of the cement paste. In this pore structure module, specific pore size distributions are assigned to the inner and outer products.

Table 4.3 Comparison between HYMOSTRUC3D and HYMOSTRUC3D-E

	HYMOSTRUC3D	HYMOSTRUC3D-E
Available systems	Mono system: PC paste	Mono system: PC paste Binary system: slag cement paste and fly ash cement paste Ternary system: PC blended with BFS and FA.
Degree of hydration of PC	Available	Available
Degree of the components of PC	Available	Available
Microstructure	Available	Available
Pore solution chemistry	Unavailable	Available
Nucleation and growth of CH particles	Unavailable	Available
Evolution of capillary porosity in cement paste	Available	Available
Evolution of gel porosity in cement paste	Gel volume was already calculated	Specific pore size distributions are assigned to the inner and outer products.

The next chapter will validate HYMOSTRU3D-E model by comparing simulation results and experimental data.

Chapter 5

Validation of the numerical model for hydration and microstructure of blended cements

5.1 Introduction

In Chapter 3 and Chapter 4 the extension of HYMOSTRUC3D regarding the simulation of the hydration process and microstructure development of blended cement pastes has been discussed. This extended HYMOSTRUC3D model was called HYMOSTRUC3D-E.

HYMOSTRUCD-E is able to simulate the hydration process and microstructure of PC paste with different components of PC and different w/c. In HYMOSTRUC3D-E the influence of different components of PC on the hydration of PC is quantified using the initial penetration rate K_0 and the transition thickness δ_{tr} for different components C_3S, C_2S, C_3A, C_4AF in PC particles. The influence of different w/c on the hydration of PC is quantified using the reduction factors, Ω_1, Ω_2 and Ω_3, allowing for the change of water distribution and change in pore water chemistry in the cement paste.

HYMOSTRUCD-E is also able to simulate the hydration process and microstructure of blended pastes with different contents of BFS and FA. In HYMOSTRUC3D-E the interactions between PC, BFS and FA are quantified using the aforementioned reduction factors, Ω_1, Ω_2 and Ω_3, allowing for the change of water distribution and change in pore water chemistry, *and* the factor M_{pH} allowing for determining the influence of pH on the reaction rate of BFS and FA particles.

As shown in Fig. 5.1, in this chapter the HYMOSTRUC3D-E model for simulating the hydration of PC and the pore structure of PC paste (section 5.2), the hydration of slag cements, the porosity and pore solution chemistry of slag cement pastes (section 5.2), the hydration of fly ash cements, the porosity and CH contents of fly ash cement pastes (section 5.3), the chemical shrinkage of PC, slag cement and fly ash cement (section 5.4) will be dealt with. It is noted that the simulation for ternary system could not be validated due to insufficient experimental data.

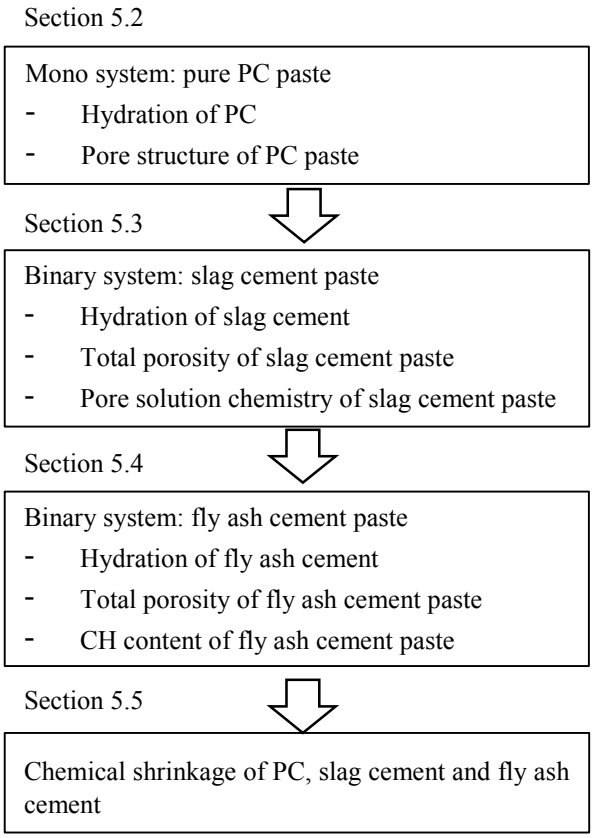

Fig. 5.1 Structure of Chapter 5

5.2 Mono system: pure PC

This section deals with the simulation of the hydration process and microstructure development of PC paste. The experimental data of Ye *[2003]* and Wang *[2013]* are used for comparison and validation. Their data concern the degree of hydration, total porosity and pore size distribution of PC pastes.

5.2.1 Input parameters

5.2.1.1 Raw materials and mixture design

The chemical composition of PC (CEM I 32.5N, produced by ENCI, Netherlands) is listed in Table 5.1. The mineral composition of PC calculated with the modified Bogue equation *[Taylor, 1997]* is: 63 % C_3S, 13 % C_2S, 8 % C_3A and 9 % C_4AF. The density of PC is 3.14 g/cm^3 *[Ye, 2003]*. The water-to-cement ratio (w/c) of the cement paste is 0.4. As shown in Fig. 5.2, the particle size distribution of PC follows the Rosin Rammler Bennett (RRB) distribution: $G(x) = 1 - exp(-bx^n)$. $G(x)$ is the cumulative weight, x is the particle diameter, n and b are fitting parameters.

Table 5.1 Chemical compositions of PC [Ye, 2003]

Raw materials	Chemical composition (wt. %)							
	CaO	SiO_2	Al_2O_3	Fe_2O_3	MgO	K_2O	Na_2O	SO_3
PC	63.4	21.0	5.03	2.83	2.0	0.65	0.24	3.0

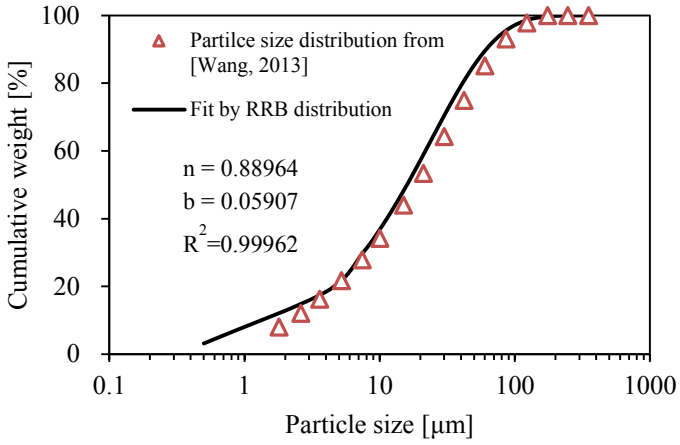

Fig. 5.2 Particle size distribution of PC (after Wang [2013]) Note: The PC used in the study of Ye [2003] is assumed to follow this particle size distribution.

5.2.1.2 Model parameters

In Eq. (3.22) and Eq. (3.23) K_0 and δ_{tr} are two important model parameters. K_0 is the initial penetration rate of the reaction front of hydrating PC-components, C_3S, C_2S, C_3A, C_4AF. δ_{tr} is the transition thickness when the hydration mechanism of C_3S, C_2S, C_3A, C_4AF change from *phase boundary reaction* to *diffusion-controlled reaction* (See the definitions of K_0 and δ_{tr} in section 3.2.2.1 and Appendix A.7.2). The values of K_0 and δ_{tr} of C_3S, C_2S, C_3A, C_4AF are calculated with the equations listed in Table 3.2. Table 5.2 lists the calculated values of K_0 and δ_{tr} for the PC presented in Table 5.1.

Table 5.2 Calculated hydration parameters K_0 and δ_{tr} for different components of PC particles (see the calculation method in section 3.2.2.1 and Appendix A.7.2)

No.	Phase	K_0 [μm/h]	δ_{tr} [μm]
1	C_3S	0.071	2.66
2	C_2S	0.005	3.08
3	C_3A	0.134	3.50
4	C_4AF	0.020	1.19

5.2.2 Reduction factors Ω_1, Ω_2 and Ω_3 in HYMOSTRUC3D and HYMOSTRUC3D-E

In HYMOSTRUC3D, the reduction factors Ω_1, Ω_2 and Ω_3, allowing for the change of water distribution and change in pore water chemistry in the cement paste, are important for simulating the hydration of PC (see the definition of the reduction factors Ω_1, Ω_2 and Ω_3 in 3.2.4). In the following paragraphs the values of reduction factors Ω_1, Ω_2 and Ω_3 HYMOSTRUC3D-E will be compared with the values used in the original HYMOSTRUC program *[Van Breugel, 1991]*.

5.2.2.1 Reduction factor Ω_1

The reduction factor Ω_1, allowing for the so called water withdrawal mechanism as explained in section 3.2.4.1, affects the reaction rate of PC particles. The value of Ω_1 will be different for particles with different size. In this section the value of Ω_1 for PC particles with diameter = 40 μm is used for the comparison between HYMOSTRUC and HYMOSTRUC3D-E. Fig. 5.3 shows the evolutions of reduction factor Ω_1 for the 40 μm PC particles in pure PC paste (w/c = 0.4) simulated with HYMOSTRUC and HYMOSTRUC3D-E. The value of Ω_1 simulated with HYMOSTRUC3D-E slightly differs from that simulated with HYMOSTRUC. This difference is caused by different values of the chemically bound water used in HYMOSTRUC3D-E and HYMOSTRUC. In HYMOSTRUC the chemically bound water for the hydration of PC was assumed to be 0.4 [g/g] (Fig. 5.3). In HYMOSTRUC3D-E the chemically bound water is calculated based on the stoichiometry of the hydration of the

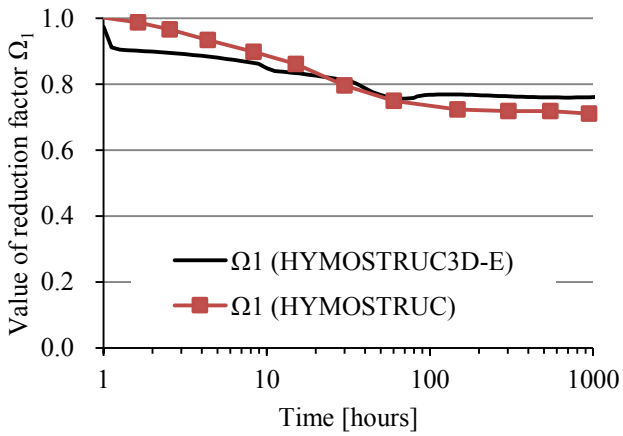

Fig. 5.3 The evolutions of reduction factor Ω_1 for the 40 μm PC particles in pure PC paste (w/c = 0.4) simulated with HYMOSTRUC and HYMOSTRUC3D-E

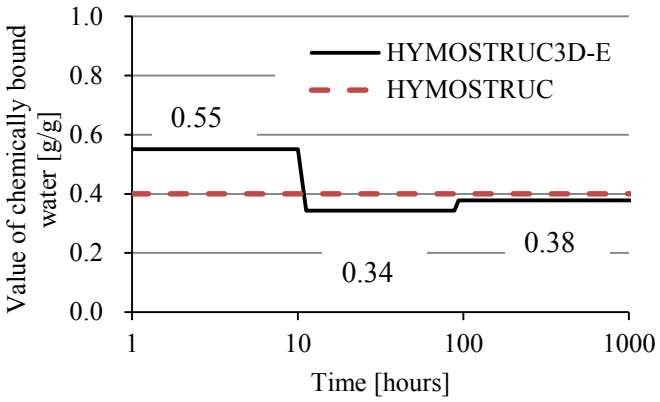

Fig. 5.4 The evolutions of chemically bound water of the hydration of PC in HYMOSTRUC and HYMOSTRUC3D-E

individual PC components (see Appendix C.1). Because the stoichiometry of the hydration of PC changes with progress of the hydration process (see section 3.2.1.1, the stoichiometry of the hydration of C_3A and C_4AF changes with progress of the hydration process), the chemically bound water for the hydration PC [g/g] will also change in HYMOSTRUC3D-E. As shown in Fig. 5.4, black line, in HYMOSTRUC3D-E the value of the chemical bound water for the hydration of PC decreases from 0.55 [g/g] to 0.34 [g/g] and then increases to 0.38 [g/g].

5.2.2.2 Reduction factor Ω_2

In both HYMOSTRUC and HYMOSTRUC3D-E, the reduction factor Ω_2 is used to quantify the influence of the water shortage in capillary pores on the reaction rate of PC particles. According to the concept of Ω_2 (see section 3.2.4.2 and Appendix A.7.4), the value of Ω_2 depends on the pore wall area of capillary pores filled with water $A_{wat}(\alpha)$ and the total capillary pore wall area $A_{por}(\alpha)$. Fig. 5.5 shows the evolutions of the reduction factor Ω_2 in pure PC paste (w/c = 0.4) simulated with HYMOSTRUC and HYMOSTRUC3D-E. The value of Ω_2 simulated with HYMOSTRUC3D-E slightly differs from that simulated with HYMOSTRUC. The difference between the values of Ω_2 in HYMOSTRUC and HYMOSTRUC3D-E has two reasons. The first reason is the difference in chemically bound water used in HYMOSTRUC3D-E and HYMOSTRUC (Fig. 5.4). The value of the chemically bound water will affect the amount of remaining capillary water and hence the value of $A_{wat}(\alpha)$ (see Appendix A.7.4). The second reason is the difference in pore structure simulated with HYMOSTRUC3D-E and HYMOSTRUC. The value of capillary pore volume $V_{por,j}$ will affect the values of both $A_{wat}(\alpha)$ and $A_{por}(\alpha)$. The value of Ω_2 in HYMOSTRUC3D-E is more realistic, as shown by the good agreement between the capillary porosity simulated with HYMOSTRUC3D-E and experimental results (Fig. 5.6).

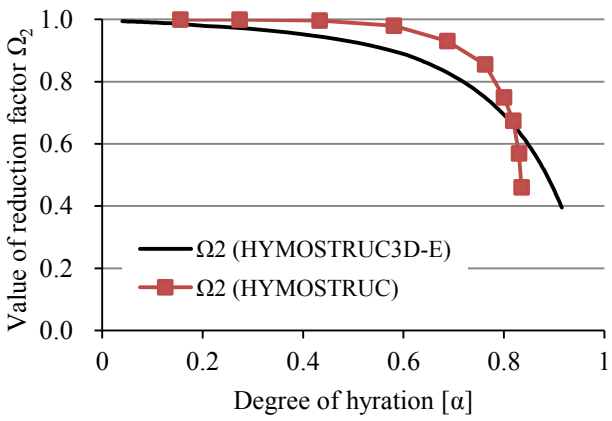

Fig. 5.5 Evolutions of Ω_2 in PC paste (w/c = 0.4) simulated with HYMOSTRUC and HYMOSTRUC3D-E. Note: Thickness of the adsorption layer = 9 Å.

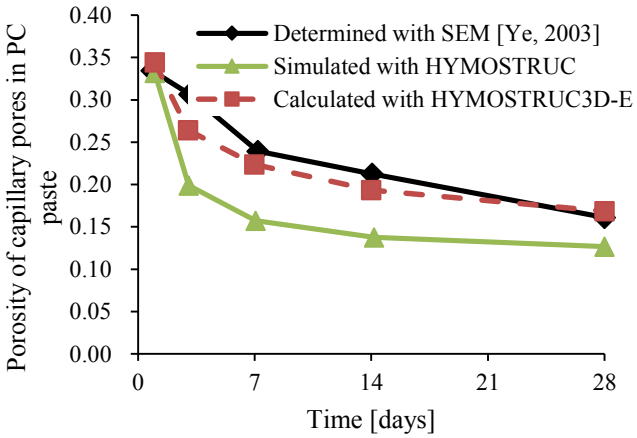

Fig. 5.6 Porosity of capillary pores in PC paste (w/c = 0.4) simulated with HYMOSTRUC and HYMOSTRUC3D-E, and obtained with SEM.

5.2.2.3 Reduction factor Ω_3

In both HYMOSTRUC and HYMOSTRUC3D-E the reduction factor Ω_3 is used to quantify the influence of the total amount of Ca^{2+} ions accommodated in capillary water on the reaction rate of PC particles (see section 3.2.4.3). Fig. 5.7 shows the evolution of the reduction factor Ω_3 in a pure PC paste (w/c = 0.4) simulated with HYMOSTRUC and HYMOSTRUC3D-E. The value of Ω_3 simulated with HYMOSTRUC3D-E slightly differs from that simulated with HYMOSTRUC. This difference is also caused by the difference in amounts of chemically bound water used in HYMOSTRUC3D-E and HYMOSTRUC (Fig. 5.4).

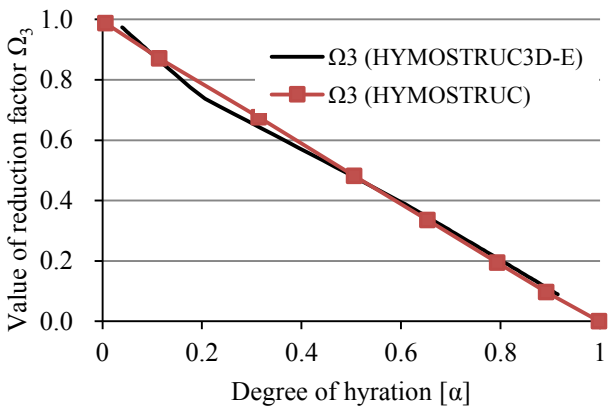

Fig. 5.7 Evolutions of Ω_3 in PC paste (w/c = 0.4) simulated with HYMOSTRUC and HYMOSTRUC3D-E

5.2.3 Degree of hydration of PC

The simulated hydration curve of PC paste is shown in Fig. 5.8, together with the degrees of hydration of PC calculated from non-evaporable water measurement *[Wang, 2013]* and SEM observations *[Ye, 2003]*. The simulated hydration curve is close to the experimental data. The degree of hydration (DoH) of PC increases rapidly at early age and then increases slowly. Fig. 5.9 shows the evolution of the degrees of hydration of C_3S, C_2S, C_3A and C_4AF. Similar to the simulation work of Tennis et al. *[2000]*, the simulated degrees of hydration of C_3S, C_2S, C_3A and C_4AF obtained with HYMOSTRUC3D-E follow: C_3A > C_3S > C_4AF > C_2S.

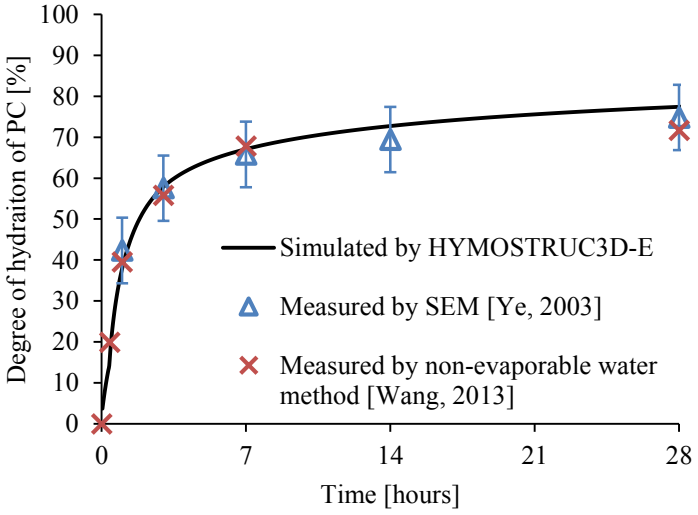

Fig. 5.8 Degree of hydration of PC obtained by simulation and experiments (w/c = 0.4)

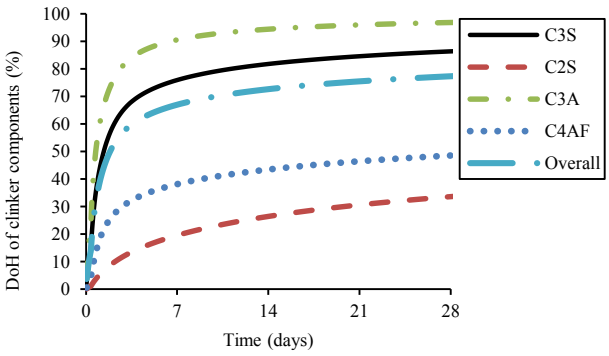

(a) DoH of clinker components obtained with HYMOSTRUC3D-E

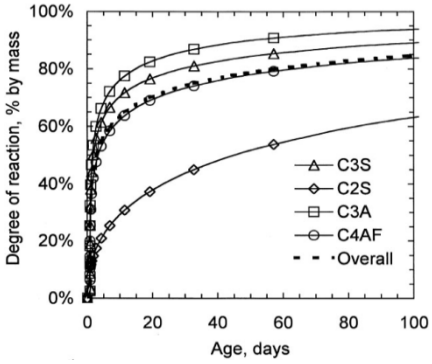

(b) DoH of clinker components obtained by Tennis et al. [2000]

Fig. 5.9 Degree of hydration of C_3S, C_2S, C_3A and C_4AF obtained by HYMOSTRUC3D-E and Tennis et al. [2000] Note: in (a) w/c = 0.4, and in (b) w/c = 0.5.

5.2.4 Microstructure development of PC paste

5.2.4.1 3D microstructure visualization

Fig. 5.10 shows four stages of the simulated microstructures of PC paste (0, 1, 7 and 28 days). These pictures show how the microstructure of PC paste becomes denser with time.

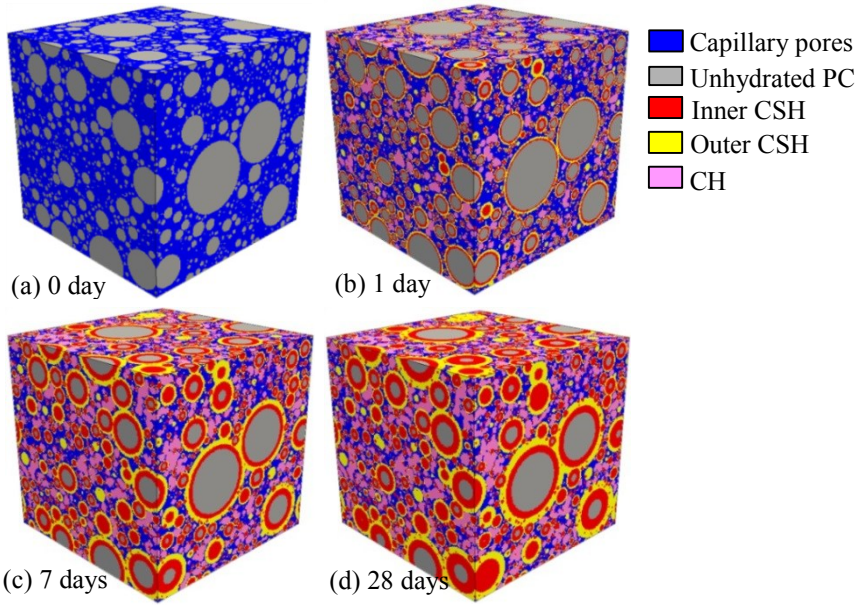

Fig. 5.10 Simulated 3D microstructures of PC at 0, 1, 7 and 28 days (Size = 100×100×100 μm^3)

5.2.4.2 Evolution of the volume phases in cement paste

Fig. 5.11a shows the volume evolution of phases calculated based on the stoichiometry of PC, while Fig. 5.11b shows the volume evolution of phases in the simulated 3D microstructure of PC paste. The volume evolution of CH and unhydrated PC in the simulated 3D microstructure (Fig. 5.11b) are close to those calculated based on the stoichiometry (Fig. 5.11a). The volume evolution of total solid phases in the simulated 3D microstructure (Fig. 5.11b) is also in good agreement with that calculated based on the stoichiometry (Fig. 5.11a). However, the volume of CSH gel in the simulated 3D microstructure (Fig. 5.11b) is larger than that calculated based on the stoichiometry (Fig. 5.11a). This is because the hydration products, such as AFt and AFm, etc., are considered as a part of CSH gel.

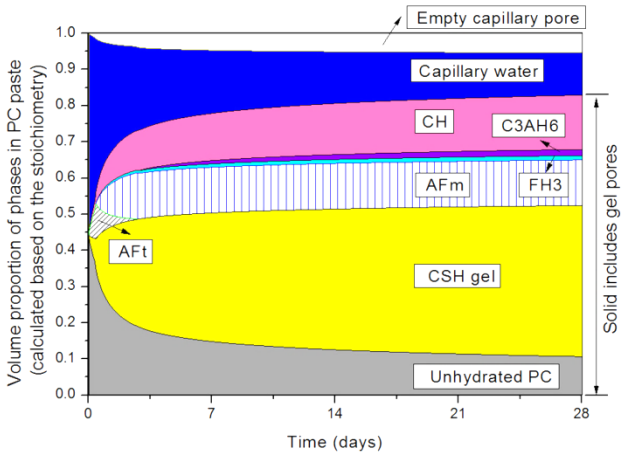

(a)

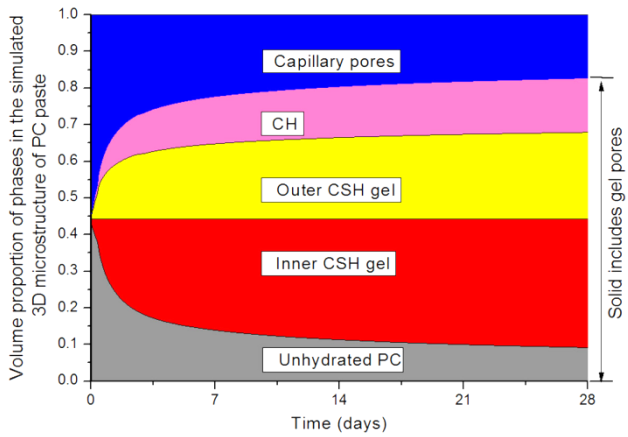

(b)

Fig. 5.11 Volume proportion of phases in PC paste, calculated based on the stoichiometry of PC hydration (Fig. 5.11a) and in the simulated 3D microstructure of PC paste (Fig. 5.11b)

5.2.4.3 Pore size distribution of PC paste

The simulated evolution of the capillary pore size distribution of PC paste from 1 day to 28 days is plotted in Fig. 5.12 and compared with the experimental data of MIP and SEM image analysis *[Ye, 2003]*. As shown in Fig. 5.12, the simulated capillary pore size distributions of PC paste at time from 1 day up to 28 days are close to the SEM observations *[Ye, 2003]*.

For pores larger than 0.1 μm the volume of capillary pores measured by MIP is much smaller than that determined by SEM and by simulation (e.g. Fig. 5.12d, 28 days). This is in good agreement with the experimental results of Diamond *[2000]* (see Fig. 5.13). According to Diamond the volume of big capillary pores is underestimated in the measurement of MIP because of the presence of "ink-bottle" pores.

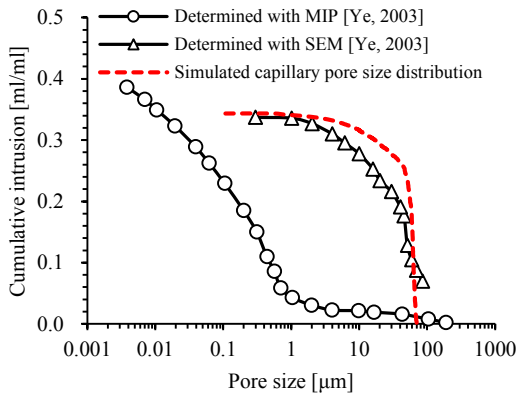

(a) Pore size distribution at 1 day

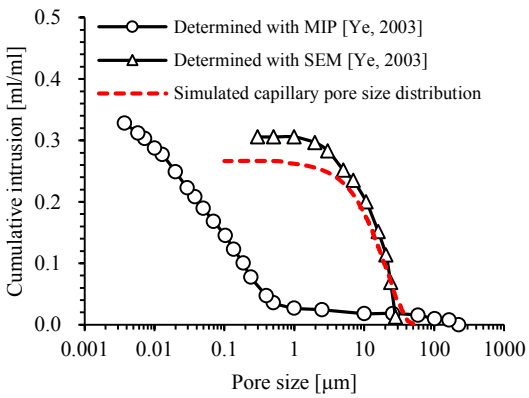

(b) Pore size distribution at 3 days

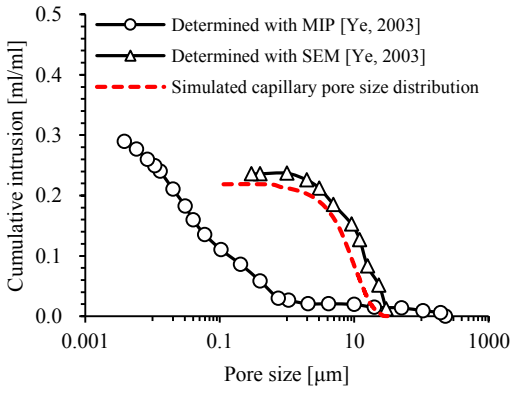

(c) Pore size distribution at 7 day

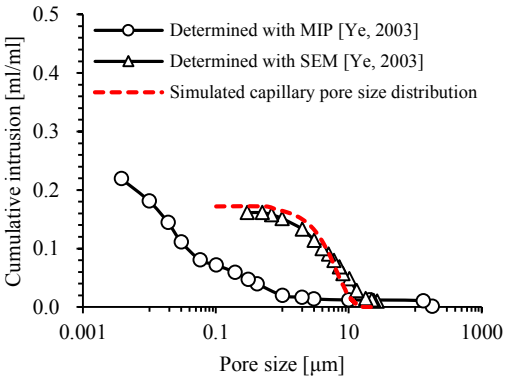

(d) Pore size distribution at 28 days

Fig. 5.12 Pore size distribution of PC paste from 1 to 28 days.

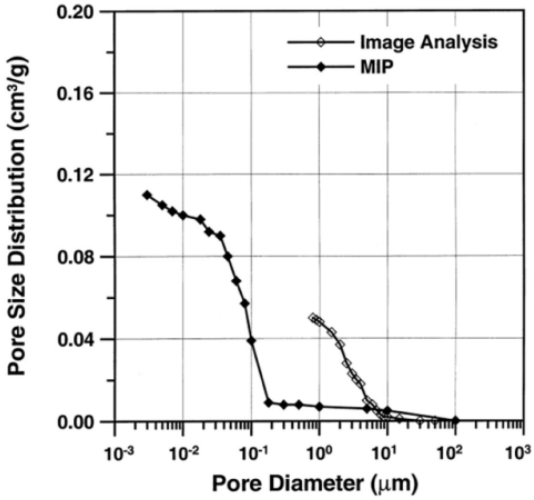

Fig. 5.13 Comparison of MIP and SEM pore size distribution plots for PC paste with w/c = 0.4 at 28 days (After Diamond [2000])

5.2.4.4 Porosity of PC paste

With progress of the hydration process, the capillary porosity of cement paste decreases and the gel porosity of cement paste increases. In HYMOSTRUC3D-E the porosity of inner and outer CSH gels are fixed, respectively. The volumes of inner and outer CSH gels increase with ongoing hydration. Hence, the volume of gel pores increases with increasing volumes of inner and outer CSH gels. Fig. 5.14 shows the determined capillary porosity, inner gel porosity and outer gel porosity in PC paste. Fig. 5.15 shows the porosity of cement paste, including capillary pores and gel pores obtained with MIP *[Ye, 2003]* and HYMOSTRUC3D-E. Similar to the total porosity obtained with MIP, the simulated total porosity decreases with progress of the hydration process. However, the simulated total porosity is larger than the total porosity obtained with MIP. There are two main reasons for this. First, it is quite difficult to use MIP to measure the small pores, such as pores smaller than 4 nm. However, in HYMOSTRUC3D-E all pores are simulated, also the very small ones. Second, it is not possible for MIP to detect the isolated pores. However, these isolated pores are simulated with HYMOSTRUC3D-E.

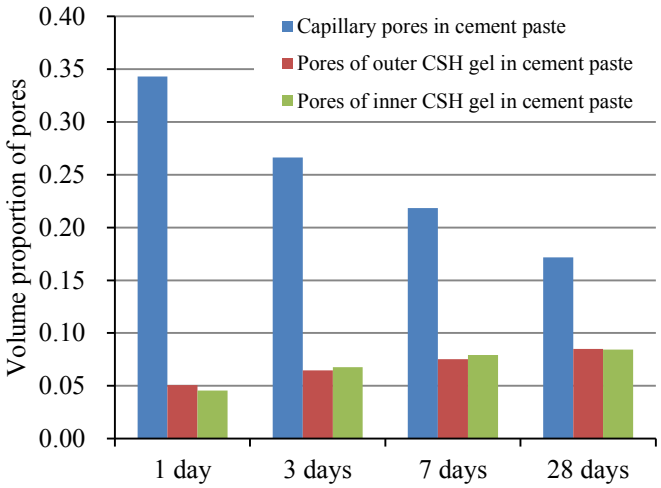

Fig. 5.14 Simulated volume proportion of capillary pores and pores of outer and inner CSH gels in cement paste.

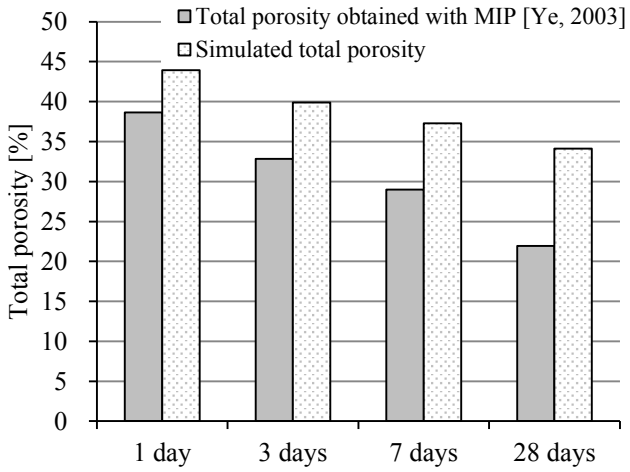

Fig. 5.15 Total porosity of PC paste obtained with MIP and HYMOSTRUC3D-E

5.3 Binary system: PC blended with BFS

In this section HYMOSTRUC3D-E is applied to simulate the hydration process, pore solution chemistry and microstructure development of slag cement pastes. The degree of hydration, total porosity, and pore solution chemistry of slag cement paste are simulated and compared with experimental data of Ye *[2006]*.

5.3.1 Input parameters

5.3.1.1 Raw materials and mixture design

Table 5.3 lists the chemical compositions of PC and BFS. The mineral composition of PC calculated with the modified Bogue equation *[Taylor, 1997]* is: 63.6 % C_3S, 9.7 % C_2S, 7.3 % C_3A and 9.7 % C_4AF. The densities of PC and BFS are 3.15 g/cm^3 and 2.85 g/cm^3, respectively *[Ye, 2006]*. As shown in Fig. 5.16, the particle size distributions of PC and BFS follow the Rosin Rammler Bennett (RRB) distribution: $G(x) = 1 - exp(-bx^n)$. $G(x)$ is the cumulative weight, x is the particle diameter, n and b are fitting parameters. Four mixtures will be considered. The mixture composition of pure PC and slag cement pastes are listed in Table 5.4.

Table 5.3 Chemical compositions of PC and BFS [Ye, 2006]

Raw materials	Chemical composition (wt. %)							
	CaO	SiO_2	Al_2O_3	Fe_2O_3	MgO	K_2O	Na_2O	SO_3
PC	64.1	20.1	4.8	3.2	0.0	0.52	0.28	2.7
BFS	40.8	35.4	13.0	0.53	8.0	0.49	0.21	0.1

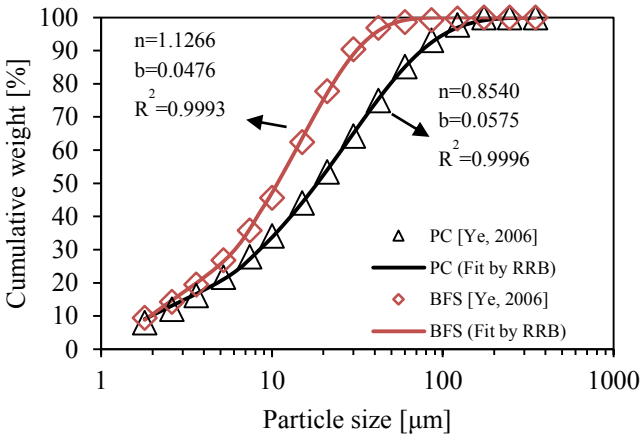

Fig. 5.16 Particle size distribution of PC and BFS. The particle size distributions of PC and BFS follow Rosin Rammler Bennett (RRB) distribution

Table 5.4 Mixture proportions of slag cement pastes [Ye, 2006]

Sample No.	PC (wt. %)	BFS (wt. %)	w/b
P100B0-0.4	100	0	0.4
P70B30-0.4	70	30	0.4
P50B50-0.4	50	50	0.4
P30B70-0.4	30	70	0.4

5.3.1.2 Model parameters

1. Hydration parameters K_0 and δ_{tr}

The penetration rate K_0 and transition thickness δ_{tr} for different minerals in PC are calculated with the equations listed in Table 3.2 (section 3.2.2.1). The model parameters K_0 *and* δ_{tr} for BFS particles are calculated with the method described in Appendix A.7.2. The results of the calculation are shown in Table 5.5.

Table 5.5 Calculated hydration parameters K_0 and δ_{tr} for different minerals of PC, and BFS particles (see the calculation method in section 3.2.2.1 and Appendix A.7.2)

No.	Phase	K_0 [μm/hour]	δ_{tr} [μm]
1	C_3S	0.0705	2.65
2	C_2S	0.0051	3.11
3	C_3A	0.1329	3.50
4	C_4AF	0.0200	1.19
5	BFS	0.0045	0.19

2. Effect of pH on the reaction rate of BFS particles

As mentioned in section 3.2.2.2, the dissolution rate of BFS particles increases with increasing pH of the pore solution. In HYMOSTRU3D-E the factor M_{pH} accounts for the effect of the pH on the dissolution rate of BFS particles (Eq. (5.1), see also Eq. (3.27)):

$$M_{pH,j,BFS} = 10^{A_{BFS}\times(pH_j - pH_{ref,BFS})} \tag{5.1}$$

where pH_j is the pH of the pore solution at time t_j. $pH_{ref,BFS}$ is the pH of the pore solution used to determine the initial penetration rate of the reaction front of a reacting BFS particle. A_{BFS} is the slope of the linear relationship between pH and the log dissolution of BFS. A_{BFS} is equal to 0.3 in HYMOSTRUC3D-E (see also Fig. 3.10).

3. Binding factors of Na^+ and K^+ ions

The binding factors b in Eq. (3.60) (Na^+ and K^+ bound by reaction products of PC and of blended cements are) important model parameters for simulating the pore solution chemistry (see section 3.3.2.2). These binding factors are listed in Table 3.4.

4. Stoichiometry of the pozzolanic reaction of BFS

The stoichiometry of the pozzolanic reaction of BFS is described with Eq. (5.2), which is from the research of Richardson et al. *[2002]* (see also Eq. (3.11) in section 3.2.1.2):

$$C_{7.88}S_{7.39}M_3A+2.6CH+31.5H \rightarrow 7.39C_{1.42}SH_{2.92}A_{0.046}+0.66M_{4.6}AH_{19} \quad (5.2)$$

where $C_{7.88}S_{7.39}M_3A$ represents BFS. $C_{1.42}SH_{2.92}A_{0.046}$ is the CSH gel produced in the reaction of BFS. $M_{4.6}AH_{19}$ is the hydrotalcite-like phase produced by the reaction of BFS.

5.3.2 Degree of hydration or pozzolanic reaction

5.3.2.1 Degree of hydration of PC in pure PC and slag cement pastes (50 and 70 % BFS)

Fig. 5.17a shows the measured degree of hydration of PC in pure PC and in slag cement pastes using SEM *[Ye, 2006]*. The experimental results show that the degree of hydration of PC is higher in the paste with higher BFS content. Because BFS reacts much slower than PC, there will be more space and more water for the hydration of PC in the paste with higher BFS content *[Lothenbach et al., 2011]*.

Fig. 5.17b shows the simulated degrees of hydration of PC in pure PC and in slag cement pastes. The simulated degrees of hydration of PC exhibit a trend similar to the experimental results. This trend (the addition of BFS increases the degree of hydration of PC) is simulated with the reduction factors Ω_1, Ω_2 and Ω_3, i.e. the factors that allow for the change of water distribution and change in pore water chemistry in the paste. If BFS is added in the paste, these reduction factors will be influenced. The following paragraphs will discuss the influence of BFS on the reductions factors in the paste.

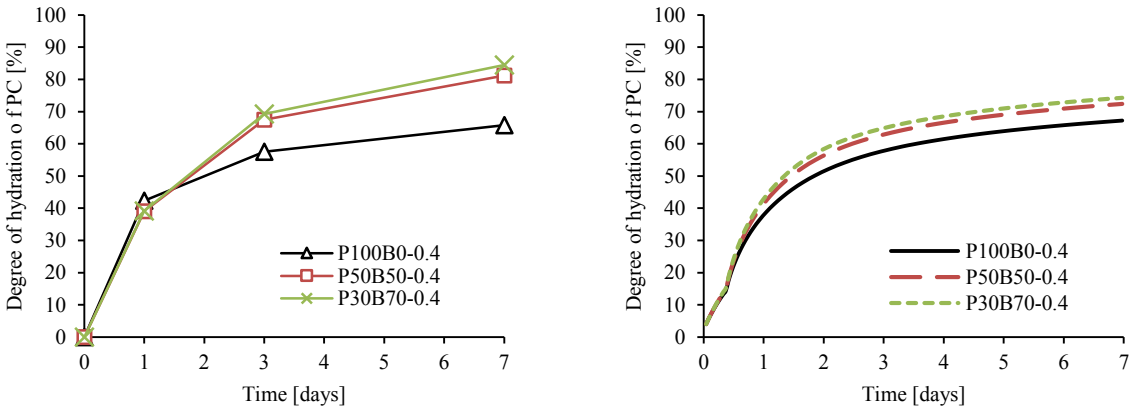

(a) DoH of PC obtained with SEM [Ye, 2006] *(b) DoH of PC simulated by HYMOSTRUC3D-E*

Fig. 5.17 Degree of hydration of PC in cement pastes with different BFS contents

1. Reduction factor Ω_1

In this section PC particles with diameter = 40 µm are considered to illustrate the influence of the addition of BFS on the evolution of the value Ω_1 for hydrating PC particles. The value of Ω_1 is calculated with (see also section 3.2.4.1):

$$\Omega_{1;x,j+1,PC} = \frac{\Delta w_{x,j,PC}}{\Delta w_{x,j,PC} + \Delta w_{em;x,j,PC,PC} + \Delta w_{em;x,j,BFS,PC}} \quad (5.3)$$

where $\Delta w_{x,j,PC}$ is the water consumption of this PC particle (x = 40 µm) in the time step from t_j to t_{j+1}. $\Delta w_{em;x,j,PC,PC}$ and $\Delta w_{em;x,j,BFS,PC}$ are the water consumption of embedded PC and BFS particles in this time step. It is noted that for each PC particle in the paste at a certain time the value of Ω_1 is assumed equal for all the minerals (C_3S, C_2S, C_3A and C_4AF) in this PC particle.

In comparison with the 40 µm particles in pure PC paste (P100B0-0.4), the 40 µm PC particles in the slag cement pastes (P50B50-0.4 and P30B70-0.4) show higher Ω_1-values during the period from mixing time up to 7 days (Fig. 5.18). This is because the addition of BFS will change the amount of water consumed by the reaction of embedded particles. For the 40 µm PC particles in the pure PC paste, only PC particles are embedded. For the 40 µm PC particles in the slag cement pastes, both PC particles and BFS particles are embedded. Because BFS particles react slower than PC particles at early age, the amount of water consumed by the particles in the outer shell of 40 µm PC particles in slag cement pastes will be smaller than the amount of water consumed by the particles in the outer shell of 40 µm PC particles in PC paste.

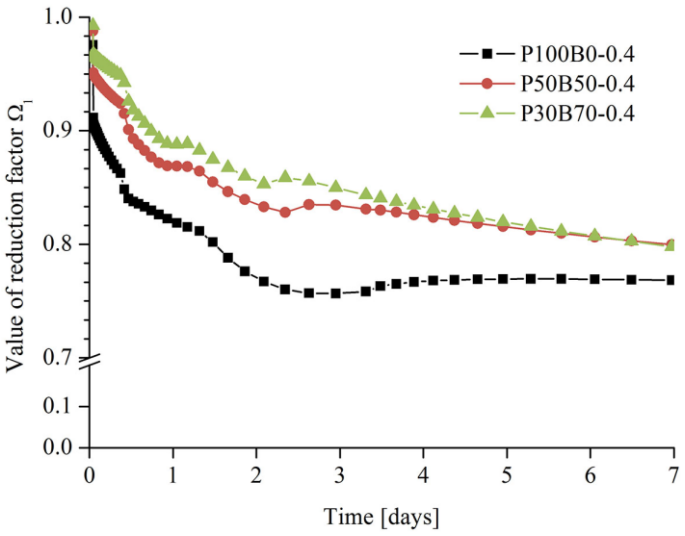

Fig. 5.18 The evolution of reduction factor Ω_1 *for the 40 µm PC particles in the paste*

2. Reduction factor Ω_2

With ongoing hydration the relative humidity (RH) in the pore system will decrease if the paste is sealed. As a result, the rate of reaction of cement particles will decrease. In HYMOSTRUC *[Van Breugel, 1991]* this effect of water shortage is allowed for with a reduction factor Ω_2 (see also section 3.2.4.2). It is calculated using Eq. (5.4).

$$\Omega_2(\alpha) = A_{wat}(\alpha)/A_{por}(\alpha) \tag{5.4}$$

where $A_{wat}(\alpha)$ is the pore wall area of capillary pores filled with water. $A_{por}(\alpha)$ is the total capillary pore wall area. The addition of slag will influence the pore structure of cement paste and the total amount of remaining capillary water. As a consequence, the addition of slag cement will influence both $A_{wat}(\alpha)$ and $A_{por}(\alpha)$.

The evolution of the value of Ω_2 with increasing hydration will be the same for all hydrating particles in a certain paste, irrespective the size of the particles. Fig. 5.19 shows the evolution of Ω_2 in PC and slag cement pastes. The values of Ω_2 in the slag cement pastes (P50B50-0.4 and P30B70-0.4) are higher than that in PC paste (P100B0-0.4). This is because the pore wall area of capillary pore filled with water ($A_{wat}(\alpha)$) in slag cement pastes is larger than that in PC paste.

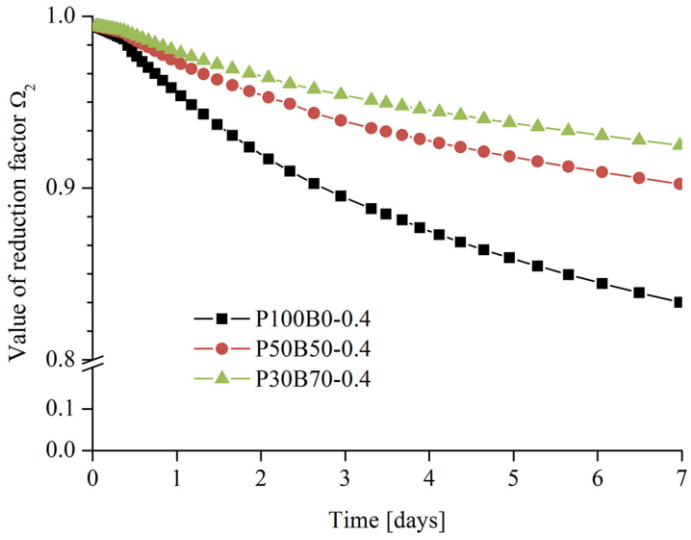

Fig. 5.19 Evolution of Ω_2 *in PC and slag cement pastes*

3. Reduction factor Ω_3

With continuing hydration the amount of capillary water available for accommodating Ca^{2+} ions will decrease. Assuming a constant concentration of Ca^{2+} ions, the total amount of Ca^{2+} ions in capillary water will decrease because of the decrease of the amount of capillary water. Because Ca^{2+} is important for the formation of hydration products, such as CSH gel and CH, etc., it was assumed that the rate of reaction in the paste will decrease because with decreasing amount of capillary water *[Van Breugel, 1991]*. In HYMOSTRUC3D-E model the reduction factor Ω_3 is calculated with Eq. (5.5) (see also section 3.2.4.3).

$$\Omega_3(\alpha) = V_{wat,j}/V_{wat,in} \tag{5.5}$$

where $V_{wat,in}$ is the initial water volume in the paste and $V_{wat,j}$ is the volume of capillary water at time t_j.

Similar to Ω_2, the value of Ω_3 with increasing hydration is identical for all hydrating particles in a certain paste. Fig. 5.20 shows the values of Ω_3 in PC and slag cement pastes as a function of time. The values of Ω_3 in the slag cement pastes (P50B50-0.4 and P30B70-0.4) are higher than that in the PC paste (P100B0-0.4). This is because at a given time the slag cement pastes contain more capillary water $V_{wat,j}$ (Fig. 5.21).

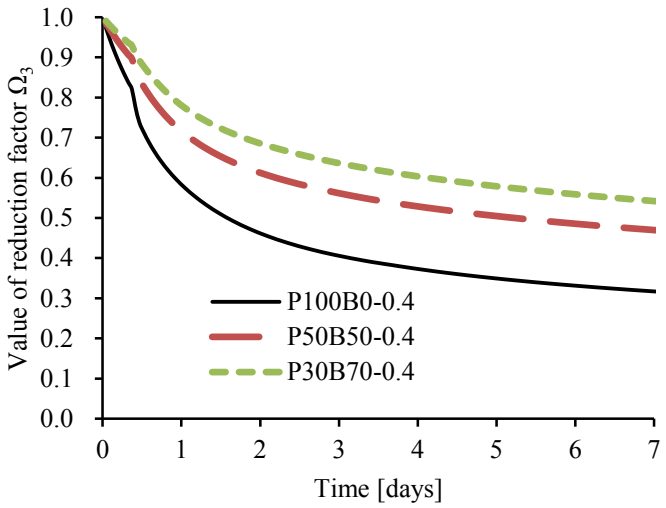

Fig. 5.20 Evolution of Ω_3 *in PC and slag cement pastes*

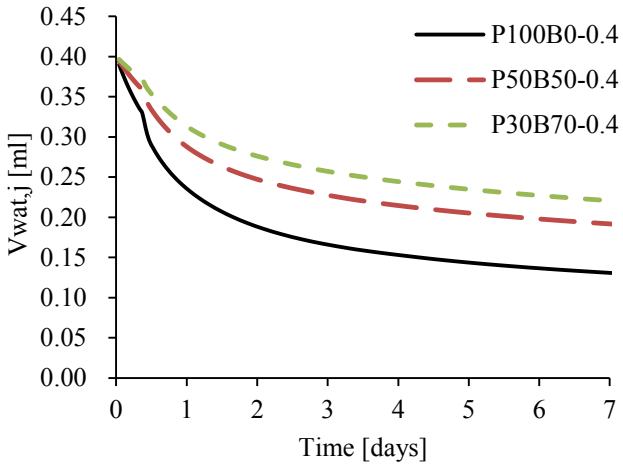

Fig. 5.21 Simulated evolution of capillary water $V_{wat,j}$ in PC and slag cement pastes

4. Joint effect of Ω_1, Ω_2 and Ω_3

For a PC particle, the simulated hydration rate is proportional to $\Omega_{1\cdot2\cdot3}$ ($\Omega_{1\cdot2\cdot3} = \Omega_1 \times \Omega_2 \times \Omega_3$) of this particle. Fig. 5.22 shows the evolutions of $\Omega_{1\cdot2\cdot3}$ for a 40 µm PC particle in pure PC and in slag cement pastes. The values of $\Omega_{1\cdot2\cdot3}$ for a 40 µm PC particle in slag cement pastes (P50B50-0.4 and P30B70-0.4) are higher than that for a 40 µm PC particle in the pure PC paste (P100B0-0.4). Note that a *higher* value of $\Omega_{1\cdot2\cdot3}$ means *less* reduction of the rate of hydration ($\Omega_{1\cdot2\cdot3} = 1$: no reduction; $\Omega_{1\cdot2\cdot3} = 0$: hydration stop). The $\Omega_{1\cdot2\cdot3}$-value for other PC particles in these pastes will exhibit a similar trend. As a consequence, the simulated degree of hydration of PC particles in the slag cement paste will be higher than that in the PC paste.

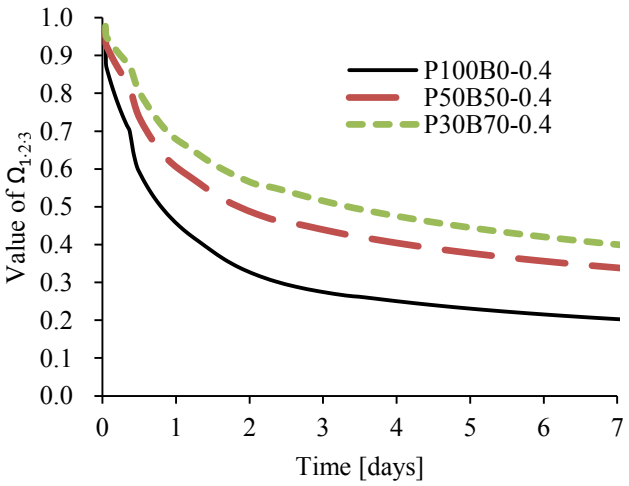

Fig. 5.22 Evolutions of $\Omega_{1\cdot2\cdot3}$ for a 40 µm PC particle in the paste

5.3.2.2 Degree of pozzolanic reaction of BFS in slag cement pastes

Fig. 5.23a and Fig. 5.23b show the degrees of pozzolanic reaction of BFS in slag cement pastes obtained by experiments and simulation, respectively. The simulations were performed with the function for simulating the reaction rate of BFS particles (Eq. (3.22), section 3.2.2.2). The SEM results (Fig. 5.23a) show that the degrees of pozzolanic reaction of BFS in P50B50 and P30B70 are close to each other. HYMOSTRUC3D-E gives a similar trend (Fig. 5.23a).

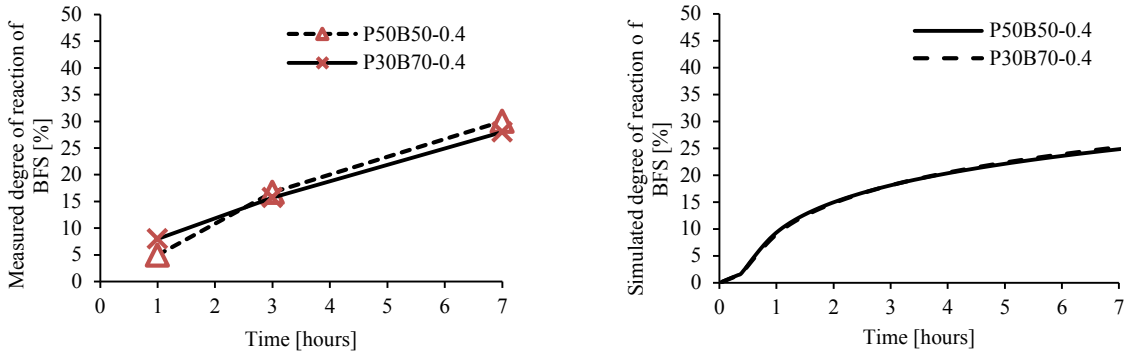

(a) Experimental results [Ye, 2006] *(b) Simulated by HYMOSTRUC3D-E*

Fig. 5.23 Degree of pozzolanic reaction of BFS in binary systems

In HYMOSTRUC3D-E, the reaction rate of a BFS particle is not only described with the reduction factors Ω_1, Ω_2 and Ω_3 allowing for the change of water distribution and change in pore water chemistry in the paste, but also depends on an additional factor M_{pH} for quantifying the effect of pH on the reaction rate of BFS. The following paragraphs will consider Ω_1, Ω_2, Ω_3 and M_{pH} for the 45 μm BFS particles to illustrate how HYMOSTRUC3D-E simulates the reaction process of BFS particles in pastes with different BFS contents.

1. The joint reduction factor $\Omega_{1\cdot2\cdot3}$ in mixtures with different BFS content

As shown in Fig. 5.24a the value of $\Omega_{1\cdot2\cdot3}$ for the 45 μm BFS particles in the mixture with higher BFS content (P30B70-0.4) is higher than that for the 45 μm BFS particles in the paste with lower BFS content (P50B50-0.4). A higher value of $\Omega_{1\cdot2\cdot3}$ means less reduction of the rate of hydration.

2. The factor M_{pH} in mixtures with different BFS content

As shown in Fig. 5.24b the value of the factor M_{pH} for the 45 μm BFS particles in the mixture with higher BFS content (P30B70-0.4) is lower than that for the 45 μm BFS particles in paste with lower BFS content (P50B50-0.4).

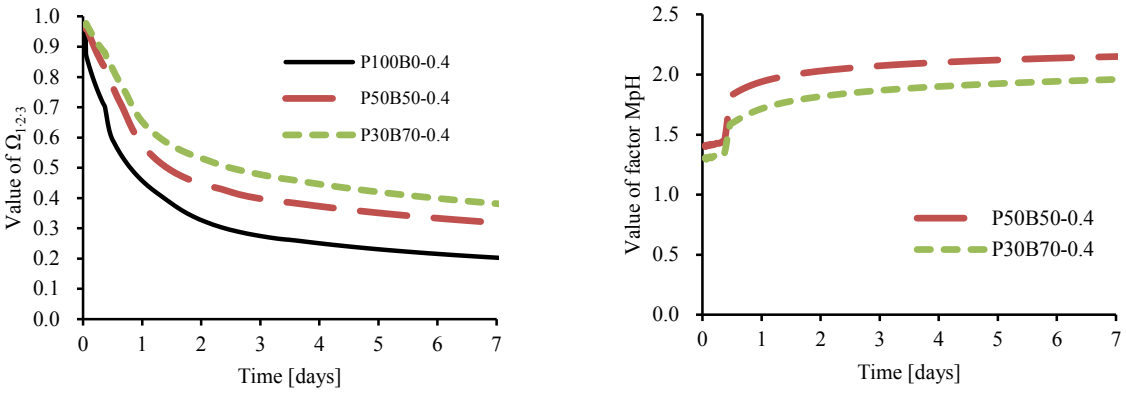

(a) value of $\Omega_{1\cdot2\cdot3}$ *(b) pH-factor* M_{pH}

Fig. 5.24 Joint reduction factor $\Omega_{1\cdot2\cdot3}$ *and factor* M_{pH} *for the 45 µm BFS particles in the pastes with different BFS content (see the maximum value of factor* M_{pH} *in Fig. 3.11, section 3.2.2.2)*

By combining the joint reduction factor $\Omega_{1\cdot2\cdot3}$ and the factor M_{pH} (Fig. 5.25), it is found that the value of $\Omega_{1\cdot2\cdot3} \times M_{pH}$ for the 45 µm BFS particles particle in the paste with higher BFS content (P30B70-0.4) is close to that for the 45 µm BFS particles in the paste with lower BFS content (P50B50-0.4). This means that the reaction rate of BFS particles in the pastes of P50B50 and P30B70 calculated with HYMOSTRUC3D-E will not alter very much.

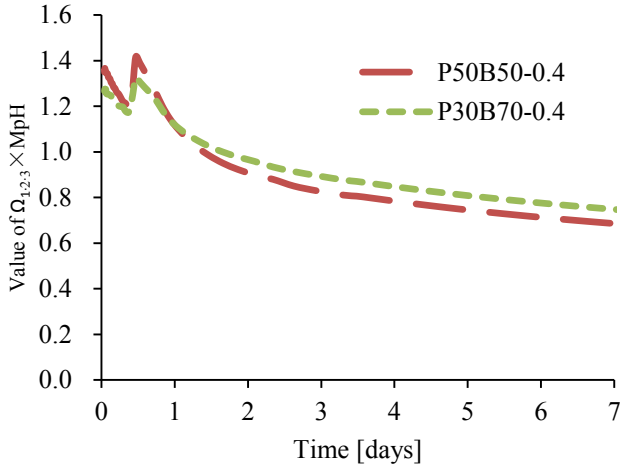

Fig. 5.25 Combination of $\Omega_{1\cdot2\cdot3}$ *and* M_{pH} *for the 45 µm BFS particles in the pastes with different BFS contents.*

5.3.3 Microstructure development of blended cement paste

5.3.3.1 3D microstructure visualization

Fig. 5.26 shows the pictures of the simulated 3D microstructures of slag cement paste with PC/BFS ratio 70/30 and water-to-binder ratio (w/b) 0.4 (P70B30-0.4) at an age of 0, 1 and 7 days. These pictures show how the simulated microstructure becomes denser with progress of the hydration process.

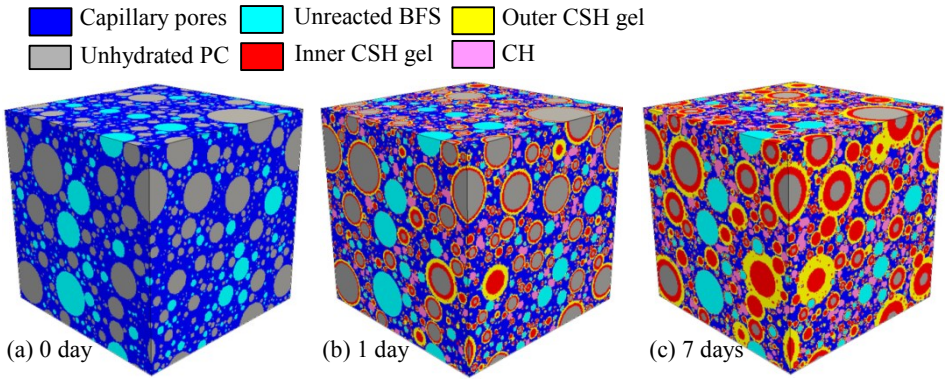

Fig. 5.26 Simulated microstructure of slag cement paste at an age of 0, 1 and 7 days (P70B30-0.4, 100×100×100 μm^3)

5.3.3.2 Evolution of the volume of phases in cement paste

Fig. 5.27a shows the evolution of the volume of individual phases calculated based on the stoichiometry of slag cement hydration. Fig. 5.27b shows the evolution of individual phases in the simulated 3D microstructure. The volumes of CH, unreacted PC and BFS in the simulated 3D microstructure are in good agreement with those calculated based on the stoichiometry of slag cement hydration, respectively. However, the volume of CSH gel in the simulated 3D microstructure (Fig. 5.27b) is larger than that calculated based on the stoichiometry (Fig. 5.27a). This is because the CSH gels produced by the pozzolanic reaction of BFS and the CSH gels produced by the hydration of PC are considered as one CSH gel phase. Besides, the hydration products, such as AFt, AFm, HT ($M_{4.6}AH_{19}$), etc., are also assumed to be part of this CSH gel phase.

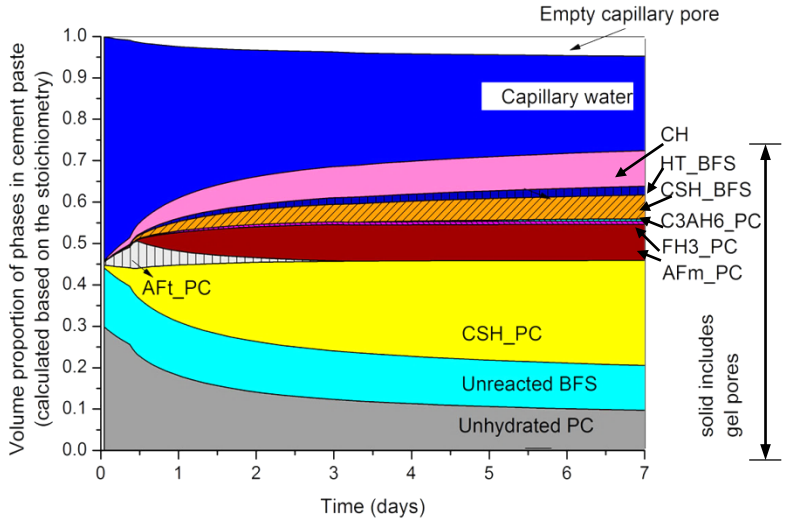

(a) Evolution of individual phases calculated based the stoichiometry of slag cement hydration (calculated in cement hydration route, Chapter 3)

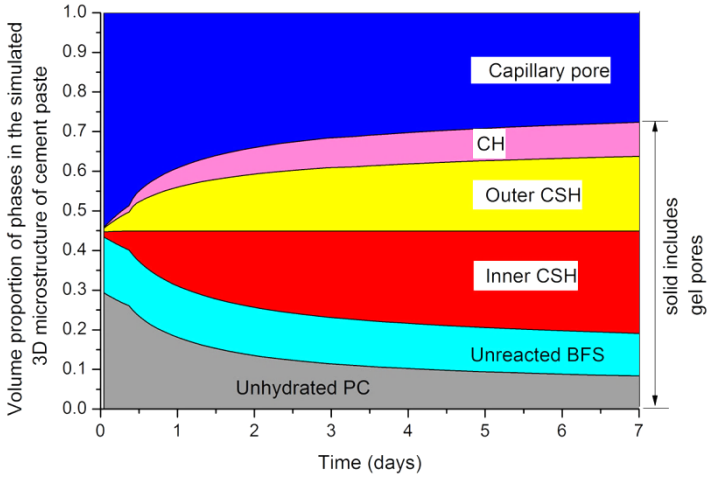

(b) Evolution of individual phases in the simulated 3D microstructure (simulated in microstructure development route, Chapter 4)

Fig. 5.27 Simulated evolution of phases in the slag cement paste (PC/BFS ratio = 70/30 and w/b = 0.4). Note: AFt_PC, AFm_PC, CSH_PC, FH3_PC, C3AH6 = AFt, AFm, CSH, FH_3, C_3AH_6 produced by the hydration of PC, respectively. CSH_BFS, HT_BFS = CSH, $M_{4.6}AH_{19}$ produced by the pozzolanic reaction of BFS, respectively.

5.3.3.3 Total porosity of slag cement pastes

Fig. 5.28 shows the total porosities of slag cement paste (BFS weight mass = 30 % and w/b = 0.4) obtained by MIP and HYMOSTRUC3D-E. According to the MIP data (grey columns), the total porosity of slag cement paste decreases with elapse of time. The simulated total porosity shows a similar trend (columns with dots). However, for the same age (e.g. 7 days), the simulated total porosity is larger than that measured by MIP. This is because the small gel pores, i.e. gel pores < 4 nm, are difficult to be measured by MIP, whereas all small gel pores have been taken into account in the simulation. Another reason is that MIP cannot detect the isolated pores, whereas in HYMOSTRUC3D-E all pores are considered (see also section 5.2.4.4).

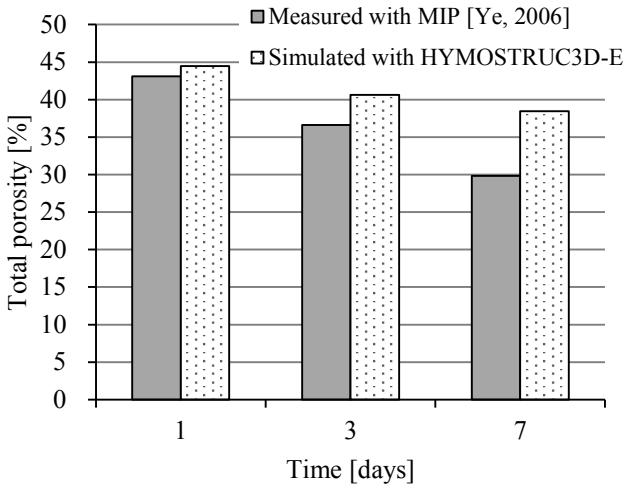

Fig. 5.28 Total porosities of the slag cement pastes (BFS weight mass = 30 % and w/b = 0.4) obtained by experiments (MIP) and HYMOSTRUC3D-E at an age of 1,3 and 7 days.

Fig. 5.29 shows the total porosities of PC and slag cement pastes (w/b = 0.4) at 7 days. According to the experimental data, the total porosity is higher for the cement paste with higher BFS content (the reason for this difference was described in the previous paragraph). The totally porosities simulated by HYMOSTRUC3D-E show a similar trend.

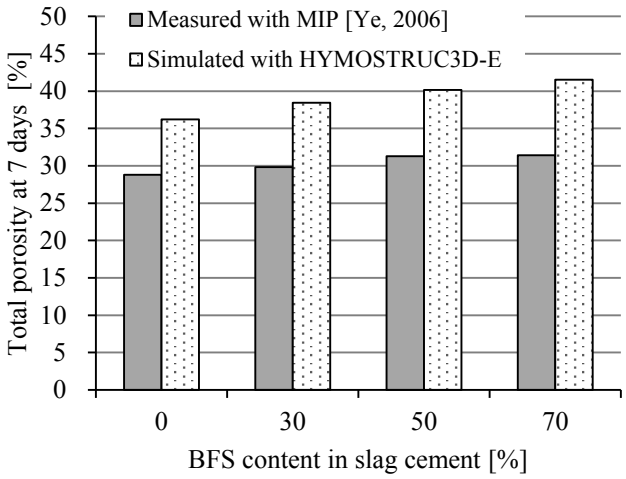

Fig. 5.29 Total porosities of the slag cement pastes at an age of 7 days (BFS weight mass = 30 % and w/b = 0.4) obtained with MIP and HYMOSTRUC3D-E

5.3.4 Pore solution chemistry

In HYMOSTRUC3D-E, the concentrations of Na^+ and K^+ ions in the pore solution were determined based on Taylor's method *[Taylor, 1987]*. The concentrations of Ca^{2+}, SO_4^{2-} and OH^- in the pore solution were determined using thermodynamic principles (see also section 3.3). The results of the simulation will be compared with experimental data in the following paragraphs.

5.3.4.1 Concentrations of alkali ions

Fig. 5.30a and Fig. 5.31a show the measured concentrations of the alkali ions Na^+ and K^+ in the pore solution of PC and slag cement pastes (w/b = 0.4) up to 7 days, respectively. The concentrations of both Na^+ and K^+ ions increase with ongoing hydration. Besides, the cement paste with higher BFS content shows lower concentrations of Na^+ and K^+ ions. In general, the alkali ions in the pore solution are continuously released from the PC and BFS particles with progress of the hydration process. Because PC reacts much faster than BFS, the alkali ions in the pore solution mainly come from the dissolution of PC. Hence, the concentrations of alkali ions in the pore solution will be lower in the paste with higher BFS content.

Fig. 5.30b and Fig. 5.31b show the simulated concentrations of Na^+ and K^+, respectively. The simulated evolutions of the concentrations of Na^+ and K^+ are close to the experimental data.

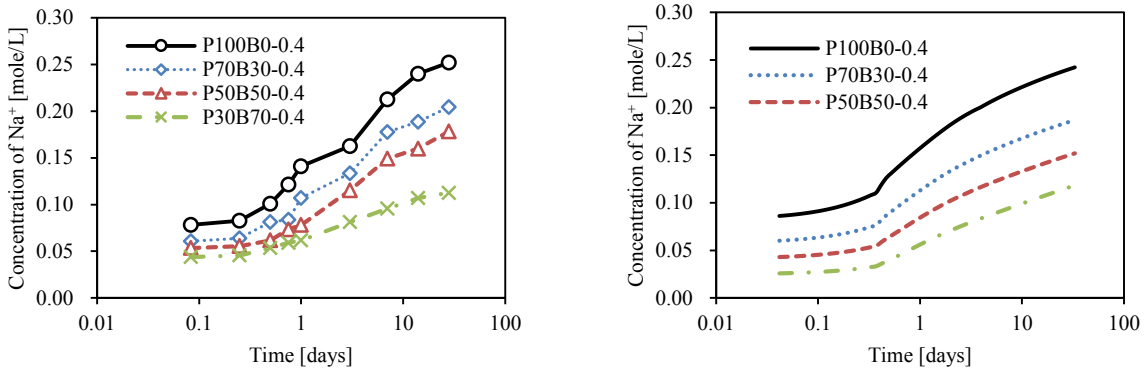

(a) [Na^+] measured by Ye [2006] *(b) [Na^+] simulated by HYMOSTRUC3D-E*

Fig. 5.30 Concentrations of Na^+ ions in pore solutions of PC and slag cement pastes

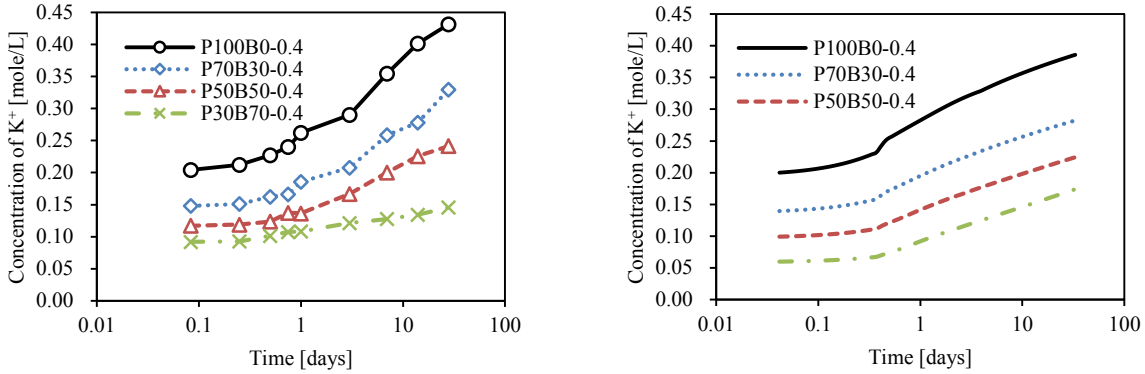

(a) [K^+] measured by Ye [2006] *(b) [K^+] simulated by HYMOSTRUC3D-E*

Fig. 5.31 Concentrations of K^+ ions in pore solutions of PC and slag cement pastes

5.3.4.2 Concentrations of Ca^{2+}

Fig. 5.32a and Fig. 5.32b show the concentrations of Ca^{2+} in the pore solution of PC and slag cement pastes obtained by experiments and HYMOSTRUC3D-E. It is found that:

1. The concentration of Ca^{2+} decreases with time

With ongoing hydration the concentrations of OH^- will increase because the concentrations of alkali ions will increase. According to the solubility equilibrium of CH, the concentration of Ca^{2+} will decrease if the concentration of OH^- increases. Besides, the concentrations of Ca^{2+} and SO_4^{2-} reach the solubility equilibrium of gypsum at very early age. This solubility equilibrium will also affect the concentration of Ca^{2+}. When gypsum is used up (after around 10 hours), the concentration of Ca^{2+} mainly depends on by the solubility equilibrium of CH. Both the results of experiments and simulations (Fig. 5.32a and Fig. 5.32b) show that the concentration of Ca^{2+} dramatically decreases at the moment the gypsum is used up.

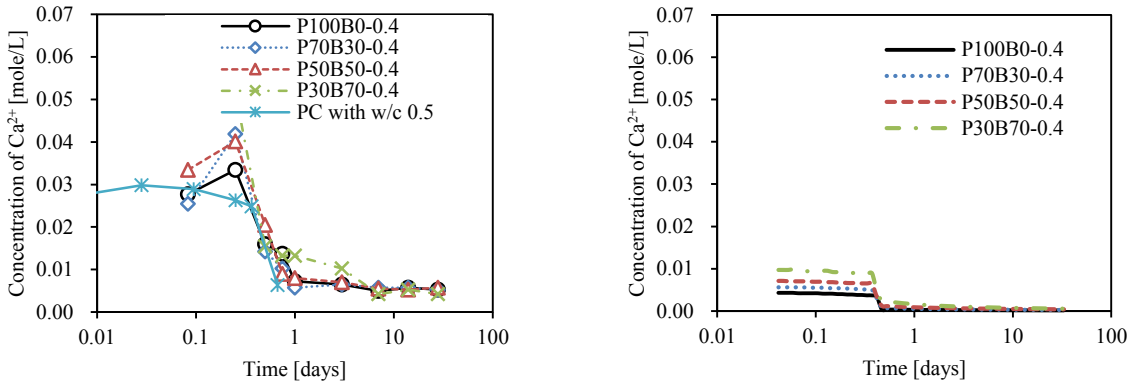

(a) [Ca^{2+}] measured by Ye [2006] *(b) [Ca^{2+}] simulated by HYMOSTRUC3D-E*

Fig. 5.32 Concentrations of Ca^{2+} ions in the pore solutions of PC and slag cement pastes. Note: PC with w/c 0.5 is the experimental data summarized in Taylor [1997]

2. The concentration of Ca^{2+} in BFS mixtures

As mentioned in the previous paragraph, the concentration of Ca^{2+} will decrease if the concentration of OH^- increases according to the solubility equilibrium of CH. The concentration of OH^- in the pore solution of cement-based materials mainly depends on the concentration of alkali ions. Because the concentration of alkali ions is lower in the paste with higher BFS content (see Fig. 5.30 and Fig. 5.31), the paste with higher BFS content will exhibit lower a concentration of OH^- and higher concentration of Ca^{2+}.

3. The simulated concentrations of Ca^{2+} are lower than experimental data

The simulated concentrations of Ca^{2+} for the cement paste with a certain BFS content (Fig. 5.32b) are lower than experimental data (Fig. 5.32a). There are two possible reasons for this. First, the actual Ca^{2+} and OH^- ions in pore solution are supersaturated at early age (see section 4.2.3), which cannot be accurately calculated with *only* the concept of solubility equilibrium. Another possible reason is from inadequate consideration of the solubility equilibria of hydration products containing calcium. In HYMOSTRUC3D-E it is assumed that the concentration of Ca^{2+} ions *only* depends on the solubility equilibria of gypsum and CH. In reality, the concentration of Ca^{2+} ions is also affected by the solubility equilibria of other phases in the cement paste, such as AFt, AFm, CSH.

5.3.4.3 Concentrations of SO_4^{2-}

Fig. 5.33a and Fig. 5.33b show the concentrations of SO_4^{2-} in the pore solution of PC and slag cement pastes obtained by experiments and HYMOSTRUC3D-E, respectively. In the pore solution of cement paste the concentration of SO_4^{2-} ions mainly depends on the solubility equilibrium of gypsum. With ongoing hydration the gypsum is gradually consumed by the

hydration of the components of PC, C_3A and C_4AF. As a consequence, the concentration of SO_4^{2-} decreases with ongoing hydration. For the system with higher BFS content, the gypsum content is smaller. As a result, the concentration of SO_4^{2-} will become lower.

As shown in Fig. 5.33b, the simulated concentration of SO_4^{2-} exhibits a sharp decline after 10 hours. In HYMOSTRUC3D-E it is assumed that the SO_4^{2-} ions are *only* released from the dissolution of gypsum. After 10 hours the gypsum is used up by hydration of the components of PC, C_3A and C_4AF. Hence, the concentration of SO_4^{2-} will decrease to zero. In reality the concentration of SO_4^{2-} ions is also related to the solubility equilibria of hydration products, such as AFt and AFm. As a result the measured concentration of SO_4^{2-} will not completely decrease to zero, as shown in Fig. 5.33a.

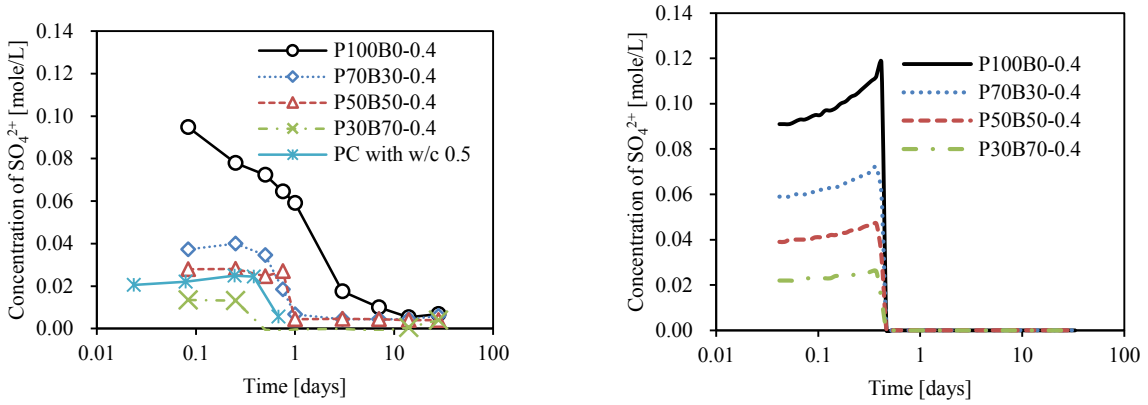

(a) $[SO_4^{2-}]$ measured by Ye [2006] *(b) $[SO_4^{2-}]$ simulated by HYMOSTRUC3D-E*

Fig. 5.33 Concentrations of SO_4^{2-} ions in pore solutions of PC and slag cement pastes
Note: PC with w/c 0.5 is the experimental data summarized in Taylor [1997]

5.3.4.4 Evolution of pH

Fig. 5.34a and Fig. 5.34b show the evolutions of pH in the pore solution of PC and slag cement pastes obtained by experiments and HYMOSTRUC3D-E, respectively. According to the experimental data (Fig. 5.34a), the value of pH in the pore solution of blended cement pastes is lower in the paste with higher BFS content. The simulated evolution of the pH in the pore solution (Fig. 5.34b) shows a sharp increase at around 10 hours. In the experiments a more gradual increase is observed. Except the difference in mode of change from low to high pH after about 0.5 to 1 days, the simulated evolution of the pH in the pore solution shows a trend similar to the experimental data.

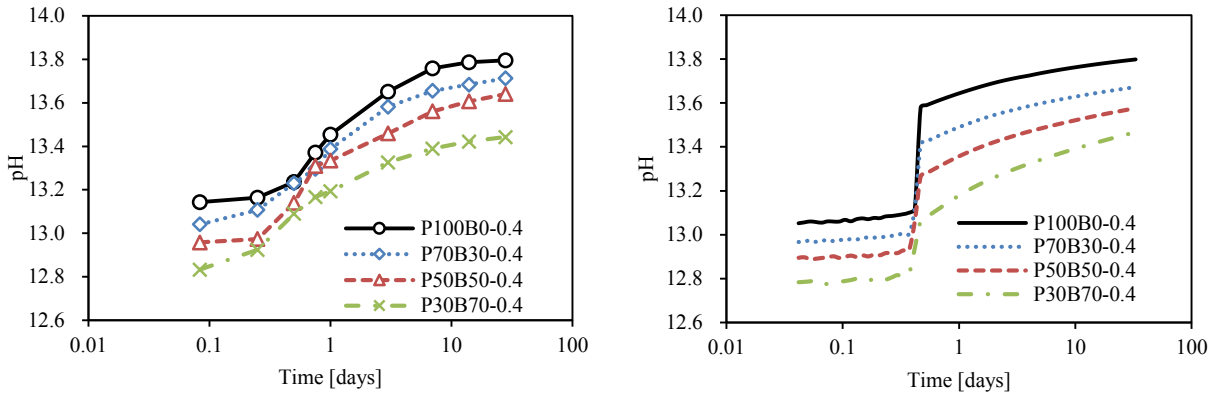

(a) pH measured by Ye [2006] *(b) pH simulated by HYMOSTRUC3D-E*

Fig. 5.34 Evolutions of pH in the pore solutions of PC and slag cement pastes

Fig. 5.35 shows the evolution of pH in the pore solution of PC paste simulated according to the method of Van Eijk et al. *[2000]* and by HYMOSTRUC3D-E, respectively. For both methods, the simulated evolution of pH is close to the experimental data measured after 3 days. From mixing time up to 10 hours, the evolution of pH simulated by HYMOSTRUC3D-E is close to the experimental data. From 10 hours to 3 days, the simulated values of the pH are higher than the experimental data. This discrepancy is caused by the sharp decrease of the concentration of SO_4^{2-} during this period. In HYMOSTRUC3D-E it is assumed that the concentration of SO_4^{2-} only depends on the solubility equilibrium of gypsum. Hence, when gypsum is used up in the cement paste the concentration of SO_4^{2-} will sharply decrease to zero and the pH will increase significantly. In reality, the concentration of SO_4^{2-} ions is also affected by the solubility equilibrium of hydration products like AFt and AFm. Hence, the simulated values of pH will be higher than the measured values.

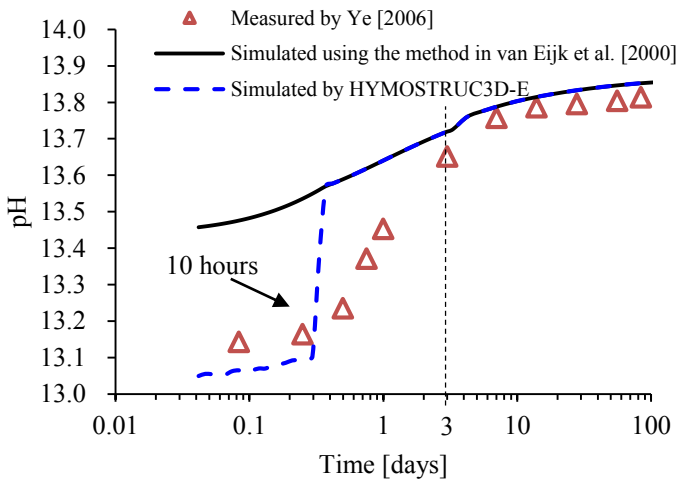

Fig. 5.35 Evolution of pH in the pore solution of PC paste with w/c = 0.4

5.4 Binary system: PC blended with FA

In this section the performance of HYMOSTRUC3D-E for simulating the hydration process and microstructure development of fly ash cement will be evaluated. The degree of hydration, total porosity and the content of calcium hydroxide (CH) of fly ash cement paste are simulated and compared with experimental data.

5.4.1 Input parameters

5.4.1.1 Raw materials and mixture design

Table 5.6 gives the chemical compositions of PC and FA determined by X-ray fluorescence (XRF). The mineral composition of PC calculated with the modified Bogue equation *[Taylor, 1997]* is: 67.1 % C_3S, 5.9 % C_2S, 7.8 % C_3A and 9.6 % C_4AF. The densities of PC and FA are 3.15 g/cm^3 and 2.31 g/cm^3, respectively *[Yu, 2015]*. As shown in Fig. 5.36, the particle size distributions of PC and FA follow the Rosin Rammler Bennett (RRB) distribution: $G(x) = 1 - exp(-bx^n)$. $G(x)$ is the cumulative weight, x is the particle diameter, n and b are the fitting parameters. The mixture proportions of pure PC and fly ash cement pastes are given in Table 5.7.

Table 5.6 Chemical compositions of PC and FA [Yu, 2015]

Raw materials	Chemical composition (%)							
	CaO	SiO_2	Al_2O_3	Fe_2O_3	MgO	K_2O	Na_2O	SO_3
PC	64.4	20.36	4.96	3.17	2.09	0.64	0.14	2.57
FA	7.14	48.40	31.40	0.0	1.35	1.64	0.72	1.18

Table 5.7 Mixture proportions of fly ash cement pastes [Yu, 2015]

Sample No.	PC (wt. %)	FA (wt. %)	w/b
P100F0-0.4	100	0	0.4
P70F30-0.4	70	30	0.4
P70F30-0.5	50	50	0.5
P50F50-0.4	30	70	0.4

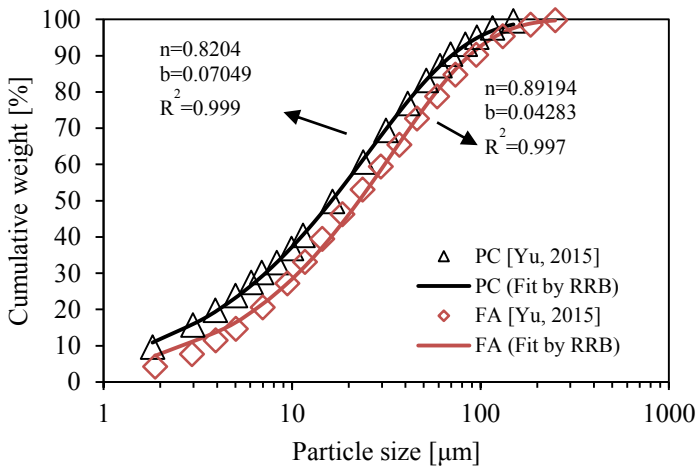

Fig. 5.36 Particle size distribution of PC and FA

5.4.1.2 Model parameters

1. Hydration parameters K_0 and δ_{tr}

The penetration rate K_0 and transition thickness δ_{tr} for different minerals in PC are calculated with the equations listed in Table 3.2 (section 3.2.2.1). For FA particles the model parameters K_0 *and* δ_{tr} are calculated according to the method in Appendix A.7.2. The results of the calculation are listed in Table 5.8.

Table 5.8 Calculated hydration parameters K_0 and δ_{tr} for different minerals of PC, and FA particles (see the calculation method in section 3.2.2.1 and Appendix A.7.2)

No.	Phase	K_0 [µm/h]	δ_{tr} [µm]
1	C_3S	0.070	2.60
2	C_2S	0.005	3.16
3	C_3A	0.132	3.50
4	C_4AF	0.020	1.19
5	FA	0.001	3.60

2. Volume proportion of the hollow cores of FA particles

The mean density of FA particles are determined by the solid glass phase and the hollow cores. The density of the solid glass phase in FA particles is 2.5 to 2.7 g/cm^3 *[Taylor, 1997]*. The density of the FA particles including their hollow core is 2.3 g/cm^3 *[Yu, 2015]*. The volume proportion of the hollow core of the FA particles, $\phi_{hollow,FA}$, can be calculated from the density of the glass phase ρ_{glass} and the density of the FA particles ρ_{FA} including hollow core (Eq. (5.6)):

$$\phi_{hollow,FA} = 1 - \rho_{FA}/\rho_{glass} \quad (5.6)$$

For ρ_{glass}s = 2.5 to 2.7 g/cm^3, ρ_{FA} = 2.3 g/cm^3, Eq. (5.6) gives $\phi_{hollow,FA}$ = 0.08 to 0.15. In this section, $\phi_{hollow,FA}$ is set at (0.08+0.15)/2 = 0.12.

3. Factor for determining the effect of pH on the reaction rate of FA particles

The factor M_{pH} is used to quantify the effect of the pH of the pore solution on the reaction rate of FA particles. The factor M_{pH} is calculated using Eq. (5.7) (see also Eq. (3.28)):

$$M_{pH,j,FA} = 10^{A_{FA}\times(pH_j - pH_{ref,FA})} \quad (5.7)$$

where $pH_{ref,FA}$ is the pH of the pore solution used to determine the initial penetration rate of the reaction front of a reacting FA particle. pH_j is the pH of the pore solution at time t_j. A_{FA} is the slope in the linear relationship between pH and the log dissolution rate of FA. In HYMOSTRUC3D-E the value of A_{FA} is assumed to be 0.3, which is the same as the value of A_{BFS} for the slag cement paste (see also Fig. 3.10).

4. Binding factors for Na^+ and K^+ ions

The binding factors b in Eq. (3.60) (Na^+ and K^+ bound by reaction products of PC and of blended cements) are important model parameters for simulating the pore solution chemistry (see section 3.3.2.2). These binding factors are listed in .

5. Stoichiometry of the pozzolanic reaction of FA

The stoichiometry of pozzolanic reactions of FA is described with Eq. (5.8), which is from the research of Bentz et al. *[1997]* (see also section 3.2.1.3):

$$AS{\cdot}xS{\cdot}yC+(2+1.1x-y)CH+(6+2.8x+y)H \rightarrow xC_{1.1}SH_{3.9}+C_2ASH_8 \quad (5.8)$$

where $AS{\cdot}xS{\cdot}yC$ is the chemical formula of FA. x and y are stoichiometry coefficients. x and y can be calculated from the chemical composition of FA. For the chemical compositions of FA listed in Table 5.7, the values of x and y in Eq. (5.8) are 1.62 and 0.43, respectively. Accordingly, Eq. (5.8) is rewritten as:

$$AS{\cdot}1.62S{\cdot}0.43C+3.35CH+11H \rightarrow 1.62C_{1.1}SH_{3.9}+C_2ASH_8 \quad (5.9)$$

5.4.2 Degree of hydration or pozzolanic reaction

5.4.2.1 Degrees of hydration of PC in pure PC paste and fly ash cement pastes

The degrees of hydration of pure PC and fly ash cement pastes obtained by experiments (SEM) and HYMOSTRUC3D-E are shown in Fig. 5.37a and Fig. 5.37b, respectively.

1. Pure PC paste (P100F30-0.4) versus fly ash cement paste (P70F30-0.4)

According to the experimental data (Fig. 5.37a), the degree of hydration of PC in the fly ash cement paste (P70F30-0.4) is higher than that in the pure PC paste (P100F0-0.4). This is caused by the "dilution effect" of FA. Because FA reacts relatively slowly, there will be more extra space and water available for the distributing of hydration products of PC. In consequence, the rate of hydration of PC will increase. However, with ongoing pozzolanic reaction of FA, the water available for the hydration of PC will gradually decrease. As a result, the degree of hydration of PC in the fly ash cement paste will finally become close to that in the pure PC paste.

The simulated degrees of hydration of PC exhibit a trend similar to the experimental results (Fig. 5.37b). In HYMOSTRUC3D-E the incorporation of FA will change the joint reduction factor $\Omega_{1\cdot2\cdot3}$ ($\Omega_{1\cdot2\cdot3} = \Omega_1 \times \Omega_2 \times \Omega_3$) allowing for the change of water distribution and change in pore water chemistry in the paste. In Fig. 5.38 the evolution of $\Omega_{1\cdot2\cdot3}$ for the 40 μm PC particles is used to illustrate the effect of FA on the evolution of reduction factors Ω_1, Ω_2 and Ω_3. The value of $\Omega_{1\cdot2\cdot3}$ for the 40 μm PC particles is higher in the fly ash cement paste (P70F30-0.4). As a result, the rate of hydration of PC in the fly ash cement paste (P70F30-0.4) will be faster.

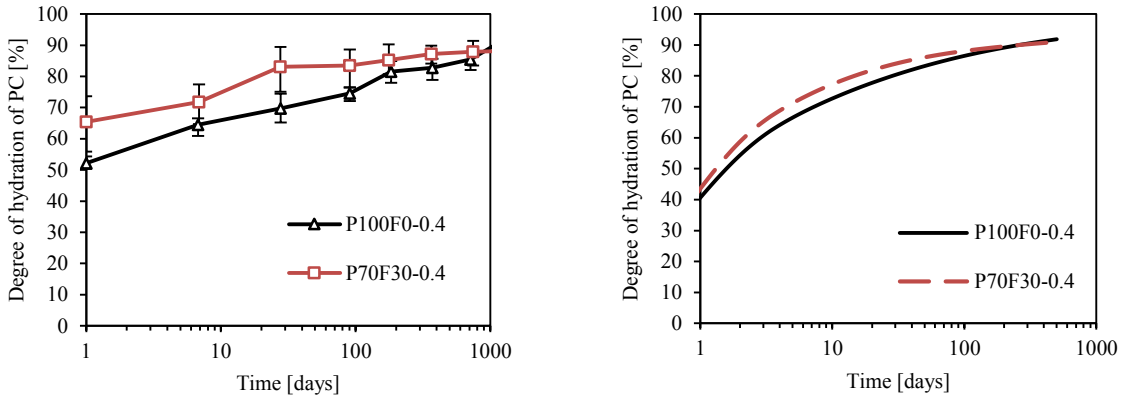

(a) DoH of PC measured by Yu [2015] *(b) DoH of PC simulated by HYMOSTRUC3D-E*

Fig. 5.37 Degree of hydration of PC in pure PC paste and fly ash cement pastes (see mixture composition in Table 5.7, section 5.4.1.1)

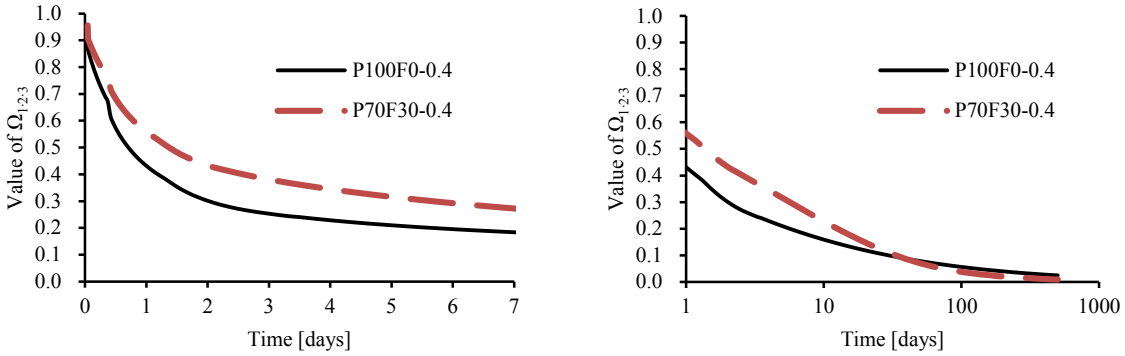

(a) $\Omega_{1\cdot2\cdot3}$ presented at linear scale *(b) $\Omega_{1\cdot2\cdot3}$ presented at log scale*

Fig. 5.38 Evolutions of $\Omega_{1\cdot2\cdot3}$ for the 40 μm PC particles in pure PC paste and fly ash cement pastes

2. Fly ash cement pastes with different w/b

The SEM results (Fig. 5.39a) show that the degree of hydration of PC in paste with higher w/b (P70F30-0.5) is higher than that of PC in paste with lower w/b (P70F30-0.4). This is because both the space and the amount of water available for distributing hydration products of PC is larger in the paste with higher w/b.

As shown in Fig. 5.39b, the values of the degree of hydration of PC given by HYMOSTRUC3D-E show a trend similar to the experimental data. In HYMOSTRUC3D-E the change of w/b in the paste will affect the joint reduction factor $\Omega_{1\cdot2\cdot3}$, which will alter the rate of hydration of PC. Fig. 5.40 shows the evolutions of the value of $\Omega_{1\cdot2\cdot3}$ for the 40 μm PC particles in different pastes. The value of $\Omega_{1\cdot2\cdot3}$ in the paste with higher w/b (P70F30-0.5) is larger than that in the paste with lower w/b (P70F30-0.4). As a consequence, the simulated degree of hydration of PC is higher in the paste with higher w/b (P70F30-0.5).

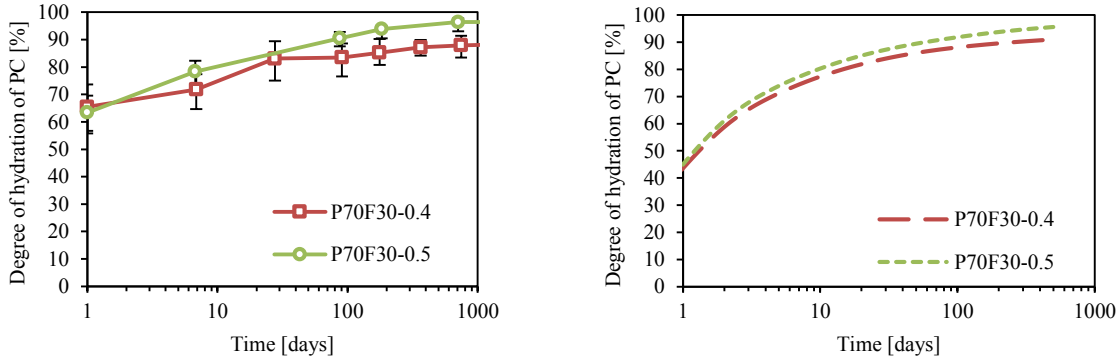

(a) DoH of PC measured by Yu [2015] *(b) DoH of PC simulated by HYMOSTRUC3D-E*

Fig. 5.39 Degree of hydration of PC in fly ash cement pastes with different w/b

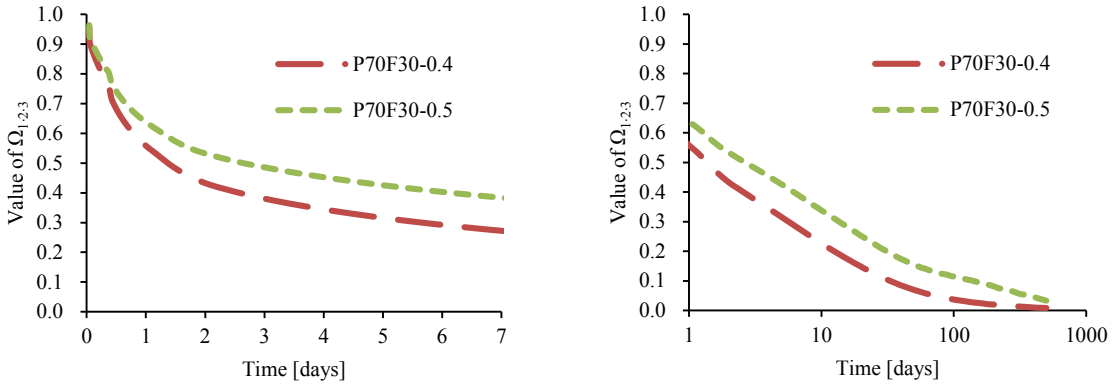

(a) $\Omega_{1\cdot2\cdot3}$ presented at linear scale *(b) $\Omega_{1\cdot2\cdot3}$ presented at log scale*

Fig. 5.40 Evolutions of $\Omega_{1\cdot2\cdot3}$ for the 40 μm PC particles in fly ash cement pastes with different w/b

5.4.2.2 Degree of reaction of FA in binary system

Fig. 5.41a shows the simulated degree of pozzolanic reaction of FA in fly ash cement pastes with different w/b (w/b = 0.4 and 0.5). The simulation results of HYMOSTRUC3D-E show a trend similar to the reports by Lam et al. *[2000]* (Fig. 5.41b): the degree of pozzolanic reaction of FA is higher in the fly ash cement paste with higher w/b. However the absolute value of the simulated degree of pozzolanic reaction of FA is different from the results from Lam et al. *[2000]*. This difference is probably caused by the difference between the properties of FA in this thesis and in the research of Lam et al. *[2000]*.

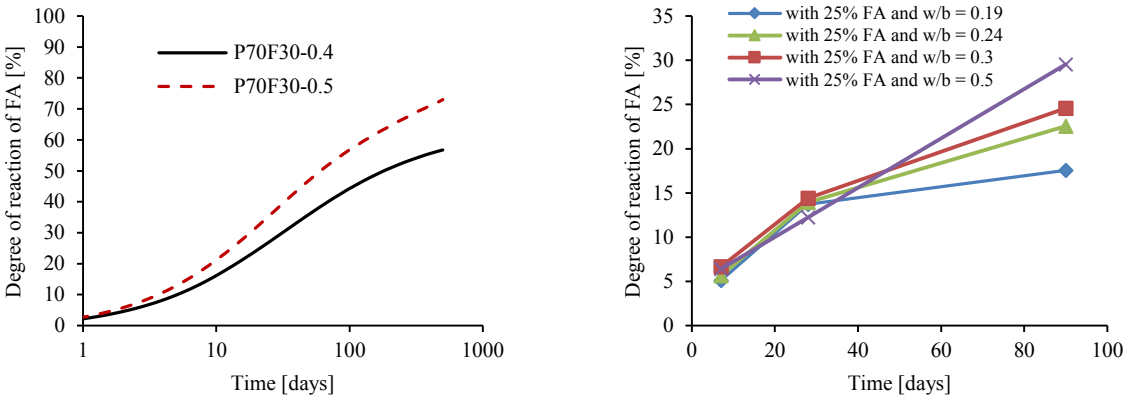

(a) Results obtained with HYMOSTRUC3D-E *(b) Results from Lam et al. [2000]*

Fig. 5.41 Degree of hydration of FA in fly ash cement pastes with different w/b obtained with HYMOSTRUC3D-E and experiments [Lam et al., 2000]

5.4.3 Microstructure development of fly ash cement paste

5.4.3.1 3D microstructure visualization

Fig. 5.42 visualizes the simulated 3D microstructures of fly ash paste with PC/FA ratio = 70/30 and w/b = 0.4 (P70F30-0.4) at time t = 0, 1, 7 and 28 days. These microstructures consist of capillary pores, unhydrated PC, unreacted FA, hollow core of FA particles, inner and outer CSH gels, and CH.

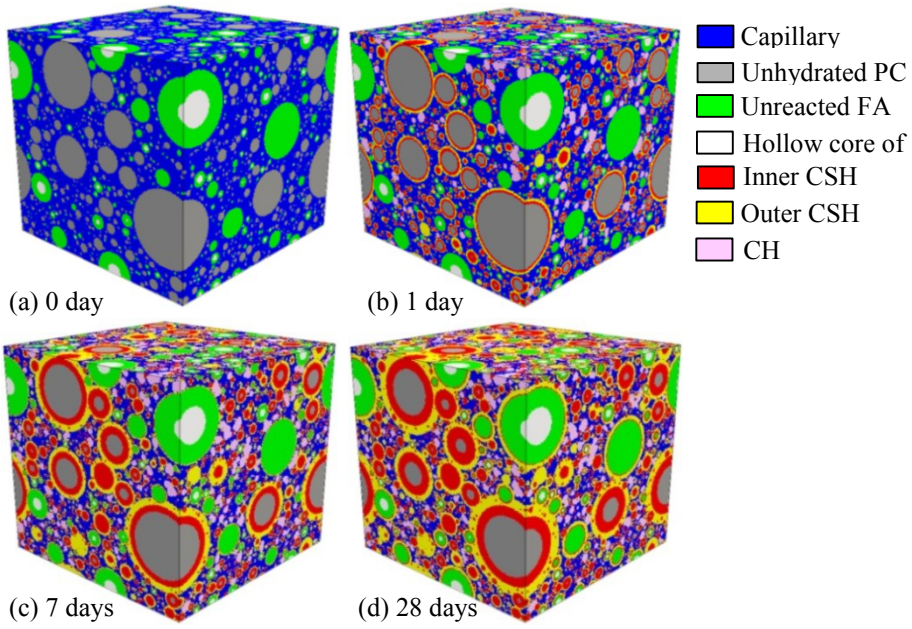

Fig. 5.42 Simulated 3D microstructures of fly ash cement paste (P70F30-0.4) (Size = 100×100×100 μm^3)

Fig. 5.43a displays the evolution of the volume of individual phases in the fly ash cement paste P70B30-0.4 calculated based on the stoichiometry of fly ash cement hydration. Fig. 5.43b shows the evolution of the volume of individual phases in the simulated 3D microstructures. The volume proportions of CH, unhydrated PC and FA in the simulated 3D microstructure (Fig. 5.43b) are in good agreement with those calculated based on the stoichiometry (Fig. 5.43a). The volume proportion of total solid phases in the simulated 3D microstructure (Fig. 5.43b) is also in good agreement with that calculated based on the stoichiometry (Fig. 5.43a). However, the volume proportion of CSH gel in the simulated 3D microstructure (Fig. 5.43b) is larger than that calculated based on the stoichiometry (Fig. 5.43a). This is because the hydration products, such as AFt and AFm, etc., are not considered separately, but as a part of CSH gel in the 3D microstructure.

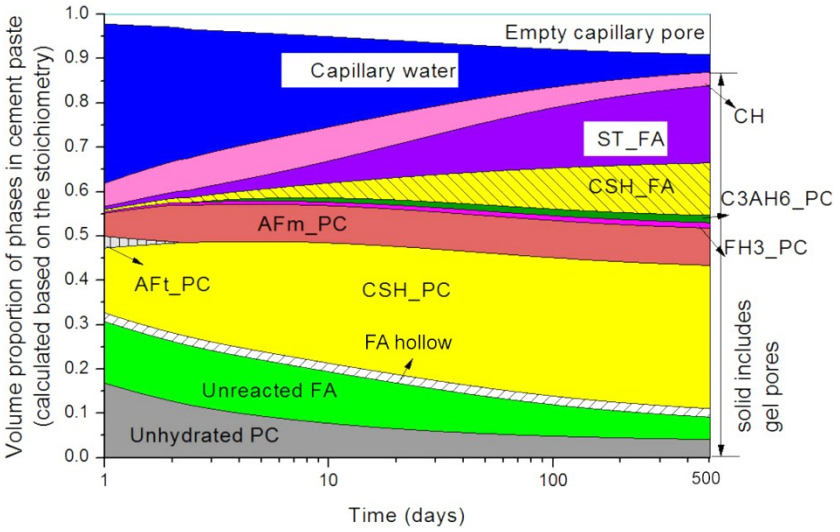

(a) Evolution of individual phases calculated based the stoichiometry of fly ash cement hydration (calculated in cement hydration route, Chapter 3)

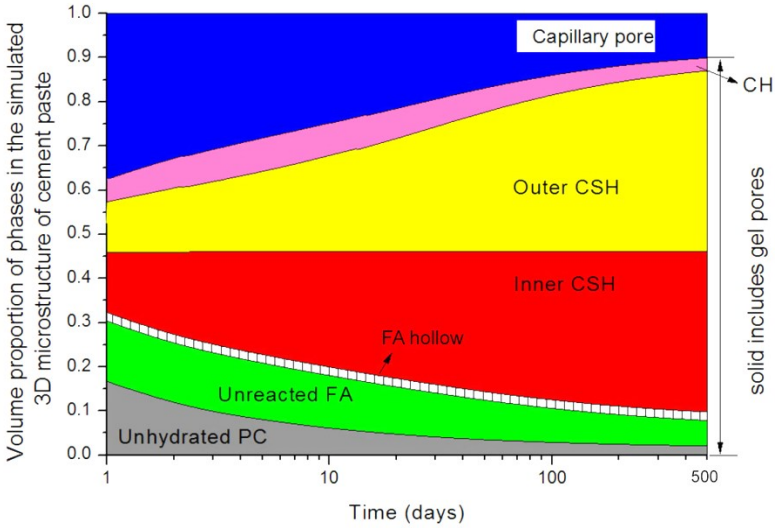

(b) Evolution of individual phases in the simulated 3D microstructure (simulated in microstructure development route, Chapter 4)

Fig. 5.43 Evolution of individual phases in the fly ash cement paste (P70B30-0.4) Note: AFt_PC, AFm_PC, CSH_PC, FH3_PC, C3AH6 = AFt, AFm, CSH, FH_3, C_3AH_6 produced by the hydration of PC, respectively. CSH_FA, ST_FA = CSH, C_2ASH_8, produced by the pozzolanic reaction of FA, respectively.

5.4.3.2 Total porosity of PC paste and fly ash cement pastes

Fig. 5.44a and Fig. 5.44b show the total porosity of PC and fly ash cement pastes obtained by MIP and HYMOSTRUC3D-E, respectively. According to the MIP data (Fig. 5.44a), the cement paste with higher FA content shows higher total porosity during the measuring period from 1 to 1000 days. The main reason is that the reaction rate of FA is slow in comparison to that of PC. Hence, the growth rate of the solid phase in the paste is also slow. As shown in Fig. 5.44b, HYMOSTRUC3D-E gives a similar trend as the MIP data. However, for the same FA content the simulated total porosity is larger than that determined by MIP. This is because the small gel pores, i.e. gel pores < 4 nm, are difficult to measure by MIP, whereas all small gel pores can be considered in the simulation. Another reason is that MIP cannot detect the isolated pores, whereas in HYMOSTRUC3D-E all pores are simulated (see also section 5.2.4.4).

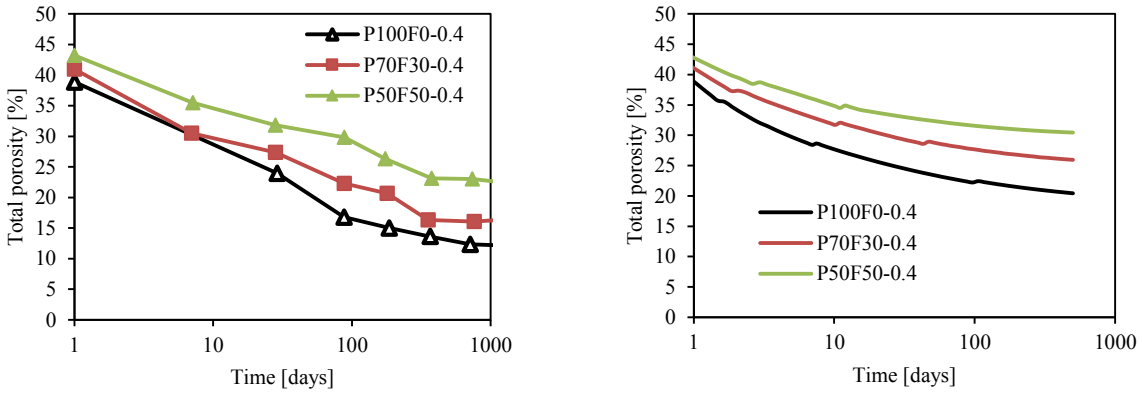

(a) MIP data [Yu, 2015] *(b) Simulated by HYMOSTRUC3D-E*

Fig. 5.44 Total porosity of PC/fly ash cement pastes Note: the porosity of the hollow cores of FA are not taken into account.

5.4.4 CH content in cement paste

In HYMOSTRUC3D-E, the CH content is calculated based on the stoichiometry of the chemical reactions in the paste. The CH content is presented as the ratio of CH mass [g] to initial cement mass [g]. Fig. 5.45a and Fig. 5.45b show the CH contents in pure PC and fly ash cement pastes obtained by Thermogravimetric analysis (TGA) and HYMOSTRUC3D-E, respectively. According to the TGA data of Yu *[2015]* (Fig. 5.45a), the paste with higher FA content shows lower CH content. As shown in Fig. 5.45b, HYMOSTRUC3D-E gives the same trend as TGA data of Yu *[2015]*. However, the values of the simulated CH content differ from that of the measured CH. A possible reason comes from the existence of amorphous and

microcrystalline CH in cement paste *[Gallucci et al., 2007]*. In the TGA measurement the dehydration temperature for this amorphous and microcrystalline CH might differ from that for crystalline CH. Therefore, this amorphous or microcrystalline CH might be underestimated in TGA measurement. The CH content of cement paste can also be measured by SEM. As shown in Fig. 5.46, the CH content in pure PC paste with w/c = 0.4 simulated with HYMOSTRUC3D-E is in good agreement with SEM observations.

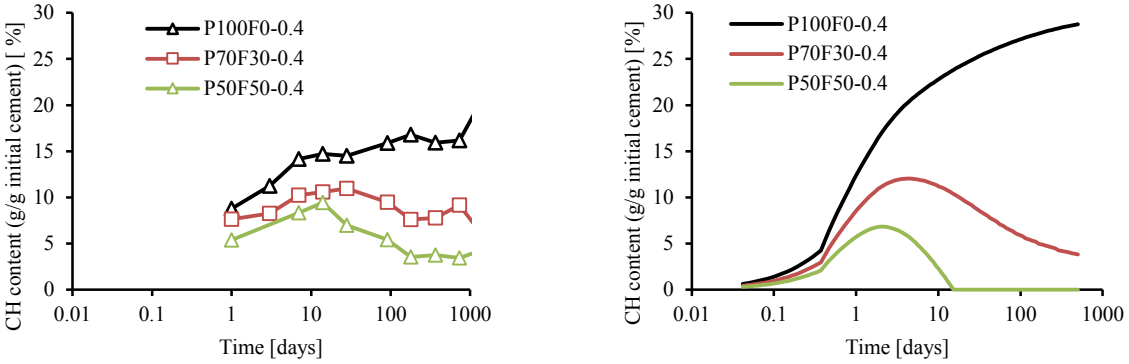

(a) measured CH content [Yu, 2015] *(b) simulated CH content*

Fig. 5.45 CH content in pure PC and fly ash cement pastes. Note: CH content means the ratio of CH weight [g] to initial cement mass [g].

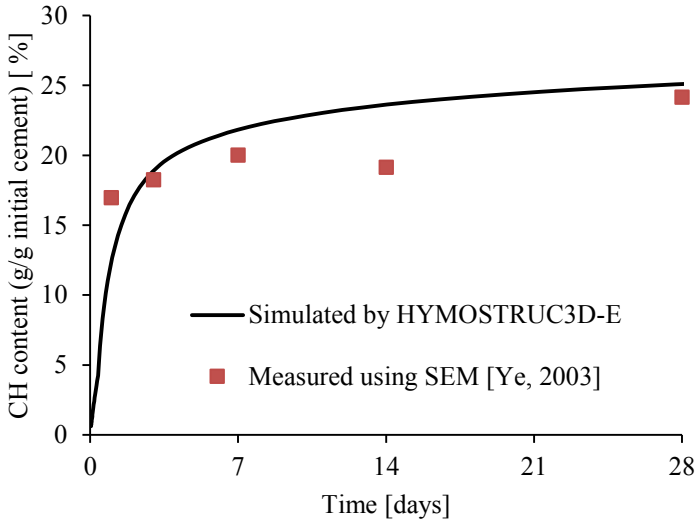

Fig. 5.46 CH content in pure PC paste with w/c = 0.4 as function of time (The standard deviations of SEM are from 0.2 to 0.36, which are too small to be visualized in this figure)

5.5 Chemical shrinkage of PC and blended cements

In this section HYMOSTRUC3D-E is applied to simulate the chemical shrinkage of pure PC paste, slag cement paste and fly ash cement paste. The experimental data, including the degree of hydration and chemical shrinkage, will be used for comparison and discussion. The simulation for ternary system could not be validated due to insufficient experimental data.

5.5.1 Raw materials and mixture design

Table 5.9 shows the chemical compositions of PC, BFS and FA measured by X-ray fluorescence (XRF). The mineral composition of PC calculated with the modified Bogue equation *[Taylor, 1997]* is: C_3S (62.0 %), C_2S (10.5 %), C_3A (7.3 %), C_4AF (10.2 %). The particle size distributions of PC, BFS and FA are plotted in Fig. 5.47a, Fig. 5.47b, and Fig. 5.47c, respectively. The densities of PC, BFS and FA measured with gravity sedimentation are 3.15 g/cm^3, 2.89 g/cm^3, 2.26 g/cm^3, respectively.

The chemical shrinkage of PC pastes with w/c = 0.3 and 0.4 (PC-0.3 and PC-0.4), slag cement paste with w/b = 0.31 (BFS-0.31), and fly ash cement paste with w/b = 0.33 (FA-0.33) will be dealt with. Table 5.10 lists the mixture compositions of the cement pastes.

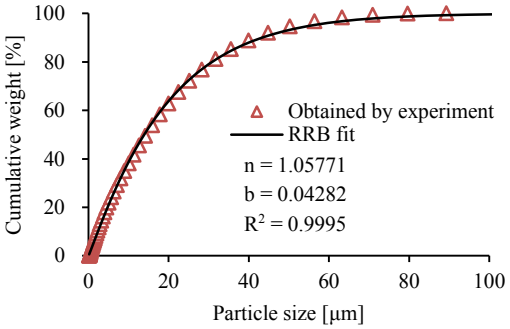

(a) Particle size distribution of PC

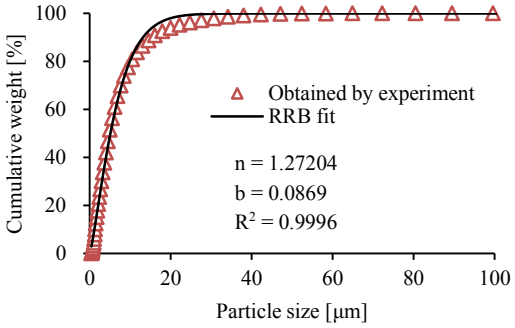

(b) Particle size distribution of BFS

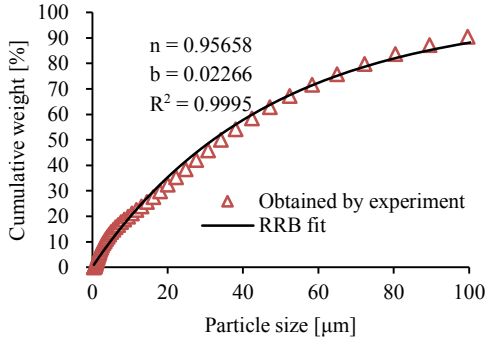

(c) Particle size distribution of FA

Fig. 5.47 Particle size distributions of PC, BFS and FA particles

Table 5.9 Chemical compositions of PC, BFS and FA particles

	CaO	SiO_2	Al_2O_3	Fe_2O_3	SO_3	MgO	K_2O	Na_2O	Others	LOI
PC	63.28	20.07	4.98	3.65	2.75	1.1	0.44	0.1	0.74	2.89
BFS	39.93	35.28	15.4	0.39	0.86	5.12	0.68	0.38	2.93	-0.97
FA	6.17	58.84	21.63	6.65	0.42	1.37	1.63	0.78	1.87	0.64

Table 5.10 Mixture compositions of pure PC and blended cement pastes

Name	Mass ratio of cement-BFS-FA	Volume ratio of cement-BFS-FA	w/b (mass ratio)	w/b (volume ratio)
PC-0.3	100 %-0 %-0 %	100 %-0 %-0 %	0.30	0.93
PC-0.4	100 %-0 %-0 %	100 %-0 %-0 %	0.40	1.25
BFS-0.31	68 %-32 %-0 %	67 %-33 %-0 %	0.31	0.93
FA-0.33	73 %-0 %-27 %	67 %-0 %-33 %	0.33	0.93

5.5.2 Experiments

5.5.2.1 Chemical shrinkage of PC and blended cements

The cement paste for determining chemical shrinkage was prepared in a three-litre Hobart mixer at a room temperature of 20±2 °C. After 3 minutes mixing, the cement paste was weighed (accuracy 0.01 g) and put into a 250 ml conical flask (Fig. 5.48). The thickness of cement paste in the conical flask was around 7 mm. The conical flask was vibrated several times by hand, and the conical flask was carefully filled with distilled water. After that the rubber plug with a 5 ml capillary tube was used to seal the conical flask. Then paraffin oil was added into the capillary tube to prevent water evaporation. The conical flask was placed in an isothermal water (20±0.5 °C) container. The paraffin oil level in the capillary tube was periodically recorded up to 7 days. The chemical shrinkage is equal to the level change in the capillary tube. The standard deviation of measurement was no more than 0.3 [ml/100 g].

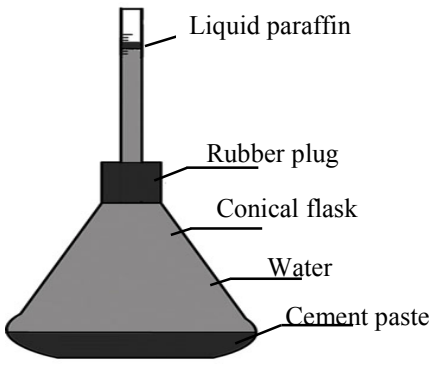

Fig. 5.48 Schematic representation of the set up for measuring the chemical shrinkage of cement paste

5.5.2.2 Degree of reactions of PC, BFS and FA

1. Degree of hydration of PC in pure PC pastes

The PC pastes for destemming the degree of hydration were prepared in a three-litre Hobart mixer at room temperature around 20±2 °C. After 3 minutes mixing, the specimens were poured in a plastic bottle (ϕ 33×70 mm). Then the specimens were sealed and cured at 20±2 °C. At the age of testing the hydration of cement pastes was stopped using ethanol. The specimens were crushed and then vacuum-oven-dried. Next the specimens were ground to powder. This method for obtaining the powder was also applied for determining the degree of pozzolanic reaction of BFS and FA in binary systems.

After crushing the powder placed in a furnace at 105 °C for 24 hours. After that the calcined powder was weighed and placed in the furnace at 1005 °C for 2 hours. The degree of hydration (α) was calculated with Eq. (5.10):

$$\alpha = \frac{W_{105} - W_{1005} - LOI \times W_{1005}/(1 - LOI)}{W_{1005} \times W_{complete}} \tag{5.10}$$

where W_{105} is the weight mass of specimen after heating at 105 °C, W_{1005} the weight mass of specimen after heating at 1005 °C, LOI the loss on ignition of raw Portland cement. $W_{complete}$ is the non-evaporable water of 1g PC for complete hydration. $W_{complete}$ is calculated from the proportions of the minerals of PC with the equation proposed by Molina *[1992]*:

$$W_{complete} = 0.24\times[C_3S] + 0.21\times[C_2S] + 0.40\times[C_3A] + 0.37\times[C_4AF] \tag{5.11}$$

where $[C_3S]$, $[C_2S]$, $[C_3A]$ and $[C_4AF]$ are the mass fraction of C_3S, C_2S, C_3A and C_4AF, respectively.

2. Degree of reaction of BFS in slag cement paste

The degree of pozzolanic reaction of BFS in slag cement paste was determined with the selective dissolution method proposed by Lumley et al. *[1995]*. Unreacted BFS is insoluble in EDTA solution, while other phases, such as unhydrated PC, hydration products of PC and reaction products of BFS, can be dissolved in EDTA solution.

The EDTA solution was prepared as proposed by Lumley et al. *[1995]*. The disodium EDTA·$2H_2O$ (93.0 g), the triethanolamine (250 ml) and the distilled water (500 ml) were mixed in a 1000 ml conical flask. After that, extra distilled water was added in the conical flask until the total volume of this EDTA solution reached 1000 ml. The prepared EDTA solution (25 ml) was added in a 400 ml conical flask. Then, the diluted EDTA solution was obtained by adding the extra distilled water in this conical flask until the total volume of the solution reached 400 ml.

The dried powder of slag cement pastes (around 0.25 g) was added into a 500 ml conical flask. The diluted EDTA solution (400 ml) was poured out in this conical flask. This mixture

was stirred in the conical flask for 2 hours. During the stirring process, the solid phases in the cement paste, such as unhydrated PC, hydration products of PC and reaction products of BFS, were dissolved. The undissolved solid residue was obtained by filtering the solution under vacuum and washing it 5 times. After that the undissolved solid residue was weighed (accuracy is 0.0001 g). The undissolved solid residue R_{BFS} [g] contains three phases: unreacted BFS, unreacted PC (small amount) and hydrotalcite produced by the reaction of BFS. R_{BFS} is calculated as:

$$R_{BFS} = 100f_{BFS}(1-\alpha_{BFS}) + R_p(1-f_{BFS}) + 100f_{BFS} \times h \times \alpha \times M_s \quad (5.12)$$

where R_{BFS} is the residue of 100 g of dried slag cement paste [g], f_{BFS} the mass fraction of the BFS in slag cement, α_{BFS} the degree of reaction of BFS in slag cement pastes, R_p the weight mass [g] of the residue of 100 g of blended cement after being dissolved in EDTA solution [g], h the mass [g] of hydrotalcite for 1 g of MgO in BFS, and M_s mass content of MgO in BFS (mass percent).

The degree of pozzolanic reaction of BFS (α_{BFS}) in binary system is calculated as:

$$\alpha_{BFS} = \frac{R_{BFS} - 100f_{BFS} - R_p(1-f_{BFS})}{100f_{BFS} \times h \times M_s - 100f_{BFS}} \quad (5.13)$$

3. Degree of reaction of FA in fly ash cement paste

The degree of pozzolanic reaction of FA in fly ash cement paste was determined by the selective dissolution method proposed by Haha et al. *[2010]*. Unreacted FA is insoluble in the solution of EDTA-NaOH, while other phases, such as unreacted PC, products of PC hydration and products of FA reaction, are soluble.

The EDTA-NaOH solution was prepared as follows: The disodium EDTA·$2H_2O$ (8.206 g) and the NaOH (2 g) were put in a 500 ml conical flask, followed by adding distilled water until the volume of the solution reaches 500 ml. In addition, a solution was obtained by mixing the distilled water (500 ml), the triethanolamine solution (volume ratio of trithanolamine: distilled water = 1 : 1, 50 ml), the NaOH solution (1 mole/L, 125 ml).

The dried powder of fly ash cement paste (around 0.2500 g) was added in a 500 ml conical flash. After that the EDTA-NaOH solution (125 ml), the distilled water (125 ml), the triethanolamine solution (12.5 ml) and the NaOH solution (31.25 ml) were mixed in this conical flash. The mixture in the conical flask was stirred for 2 hours. By stirring, the solid phases, such as unreacted PC, products of PC hydration and products of FA reaction, are dissolved. The undissolved solid residue was obtained by filtering the solution under vacuum and washing it 5 times. After that the undissolved solid residue was weighed (accuracy is 0.1 mg). The undissolved solid residue R_{FA} [g] is the unreacted FA. It is calculated as:

$$R_{FA} = 100 f_{FA}(1 - \alpha_{FA}) - F_S \times f_{FA} \quad (5.14)$$

where R_{FA} is residue of 100 g of dried fly ash cement paste [g], f_{FA} the mass fraction of the FA in fly ash cement, α_{FA} the degree of reaction of FA in fly ash cement pastes, and F_S the weight mass [g] of residue of 100 g of fly ash cement after being dissolved in EDTA-NaOH solution.

The degree of reaction of FA (α_{FA}) in the fly ash cement pastes is calculated as:

$$\alpha_{FA} = 1 - \frac{R_{FA} + F_S \times f_{FA}}{100 f_{FA}} \quad (5.15)$$

5.5.3 Modelling with HYMOSTRUC3D-E

1. Model parameters K_0 and δ_{tr}

The penetration rate K_0 and transition thickness δ_{tr} for different minerals in PC are calculated with the equations listed in Table 3.2 (section 3.2.2.1). The K_0 *and* δ_{tr} for BFS and FA particles are calculated with the method described in Appendix A.7.2. Table 5.11 gives the calculated values of the model parameters.

Table 5.11 Calculated model parameters K_0 and δ_{tr} for different minerals of PC, BFS and FA particles (see the calculation method in section 3.2.2 and Appendix A.7.2)

Phase	K_0 [μm/hour]	δ_{tr} [μm]
C_3S	0.701	3.48
C_2S	0.005	3.22
C_3A	0.126	3.44
C_4AF	0.020	1.19
BFS	0.0045	0.188
FA	0.001	3.60

2. Volume proportion of the hollow cores of FA particles

The volume proportion of the hollow cores in the FA particles $\phi_{hollow,FA}$ is calculated with Eq. (5.6). For ρ_{glass} = 2.5 to 2.7 g/cm^3, ρ_{FA} = 2.26 g/cm^3, Eq. (5.6) gives $\phi_{hollow,FA}$ = 0.096 to 0.163. In this section, $\phi_{hollow,FA}$ is calculated at (0.096+0.163)/2 = 0.13.

3. Factor for determining the effect of pH on the reaction rate of BFS particles

As mentioned in section 3.2.2.2, the factors A_{BFS} and A_{FA} are important for quantifying the effect of pH of pore solution on dissolution rates of BFS and FA particles. In HYMOSTRUC3D-E, both the factors A_{BFS} and A_{FA} are set at 0.3 (see also section 3.2.2.2).

4. Binding factors for Na^+ and K^+ ions

The binding factors b in Eq. (3.60) (Na^+ and K^+ bound by reaction products of PC and of blended cements) are important model parameters for simulating the pore solution chemistry. These binding factors are listed in Table 3.4 (section 3.3.2.2).

5. Stoichiometry of the pozzolanic reactions of BFS and FA

The stoichiometry of the pozzolanic reaction of BFS is described with Eq. (5.16), which is from the research of Richardson et al. *[2002]* (see also Eq. (3.11) in section 3.2.1.2):

$$C_{7.88}S_{7.39}M_3A+2.6CH+31.5H\rightarrow 7.39C_{1.42}SH_{2.92}A_{0.046}+0.66M_{4.6}AH_{19} \quad (5.16)$$

where $C_{7.88}S_{7.39}M_3A$ represents BFS. $C_{1.42}SH_{2.92}A_{0.046}$ is the CSH gel produced by the reaction of BFS with water and CH. $M_{4.6}AH_{19}$ is the hydrotalcite-like phase produced by the reaction of BFS with water and CH.

The stoichiometry of pozzolanic reactions of FA is described with Eq. (5.17), which is from the research of Bentz et al. *[1997]* (see also Eq. (3.20) in section 3.2.1.3):

$$AS\cdot xS\cdot yC+(2+1.1x-y)CH+(6+2.8x+y)H \rightarrow xC_{1.1}SH_{3.9}+C_2ASH_8 \quad (5.17)$$

where $AS\cdot xS\cdot yC$ is the chemical formula of FA. x and y are stoichiometry coefficients. x and y can be calculated from the chemical composition of FA. For the chemical compositions of FA listed in Table 5.9, the values of x and y in Eq. (5.17) are 3.62 and 0.56, respectively. Accordingly, Eq. (5.17) is rewritten as:

$$AS\cdot 3.62S\cdot 0.56C+5.42CH+16.68H \rightarrow 3.62C_{1.1}SH_{3.9}+C_2ASH_8 \quad (5.18)$$

5.5.4 Degree of hydration and chemical shrinkage of PC pastes

Fig. 5.49 shows the simulated degrees of hydration of PC together with the experimental values. The simulated degree of hydration is close to the experimental data. Fig. 5.50 shows the chemical shrinkage of cement pastes with w/c = 0.3 and 0.4 (PC-0.3 and PC-0.4), obtained by simulation and experiments. During the first day, the simulated chemical shrinkage of PC pastes with w/c = 0.3 and 0.4 is in good agreement the experimental data. After 1 day, the simulated chemical shrinkage of both cement pastes is larger than the experimental data. In the chemical shrinkage test set up, as schematically shown in Fig. 5.48, the cement paste at the bottom of the conical flask will become dense with progress of the hydration process. As a result transport of water into the cement paste becomes difficult. Consequently, the measured chemical shrinkage will be smaller than the real chemical shrinkage.

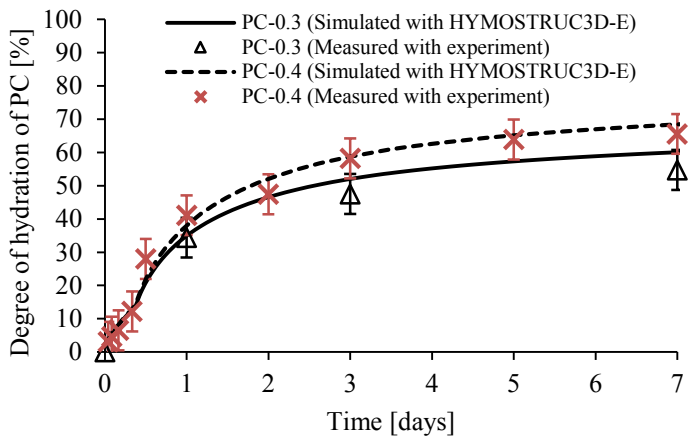

Fig. 5.49 Degrees of hydration of PC in PC pastes with w/c = 0.3 and 0.4

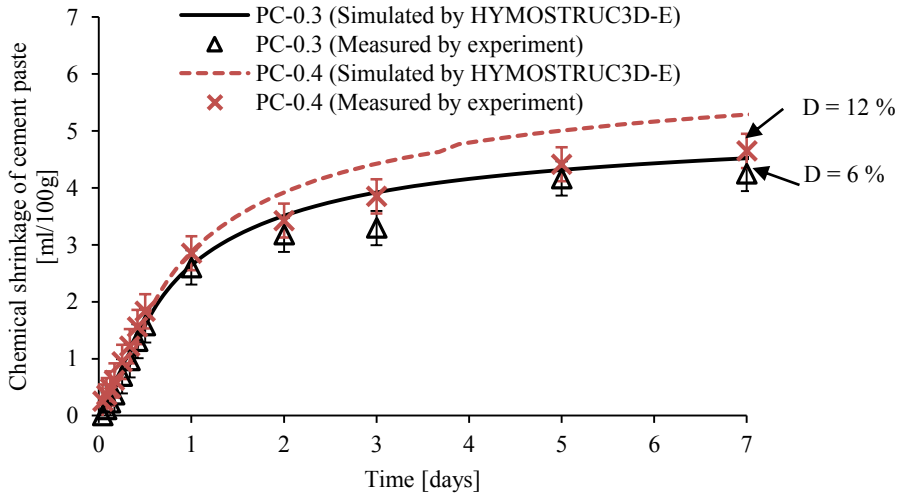

Fig. 5.50 Chemical shrinkage of PC pastes with w/c = 0.3 and 0.4. D represents the difference between the results of simulation and measurement

5.5.5 Degree of hydration and chemical shrinkage of blended cement pastes

The simulated degrees of hydration of PC in the binary systems (BFS-0.31 and FA-0.33) are shown in Fig. 5.51. In comparison with the degree of hydration of PC in the pure PC paste (PC-0.3), the degrees of hydration of PC in BFS-0.31 and FA-0.3 are slightly higher. In this numerical model, the effect of incorporating BFS and FA on the hydration of PC is simulated with the reduction factors Ω_1, Ω_2, and Ω_3, allowing for the change of water distribution and change in pore water chemistry in the cement paste. As discussed in sections 5.3 and 5.4, the values of the joint reduction factor $\Omega_{1\cdot2\cdot3}$ for the PC particles are higher in case BFS and FA are incorporated (Note: $0 < \Omega_{1\cdot2\cdot3} < 1$). Higher $\Omega_{1\cdot2\cdot3}$ value of PC particles means a higher rate of hydration of PC particle. As a result, the rate degree of hydration of PC will be higher.

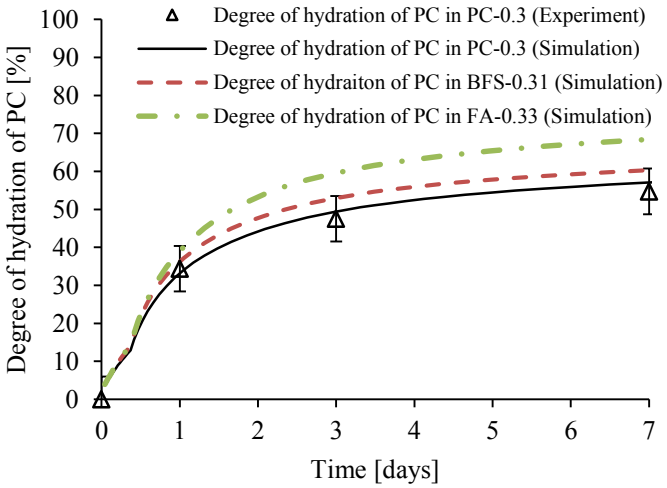

Fig. 5.51 Degree of hydration of PC in PC, slag and fly ash cement pastes BFS-0.31 = slag cement paste with w/b = 0.31 and BFS mass content = 32 %; FA-0.33 = fly ash cement paste with w/b = 0.33 and FA mass content = 27 %.

Fig. 5.52 shows the degrees of the pozzolanic reaction of BFS and FA up to 7 days obtained by HYMOSTRUC3D-E and experiments. The simulated degrees of pozzolanic reaction of BFS and FA are close to the experimental data.

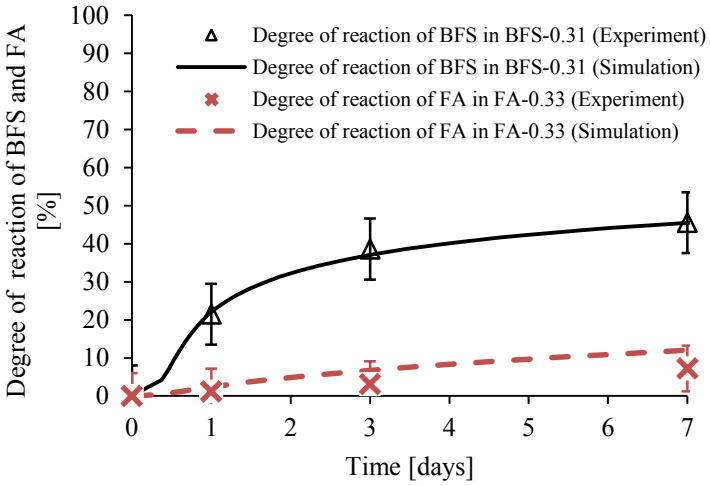

Fig. 5.52 Degrees of pozzolanic reaction of BFS and FA in blended cement pastes: BFS-0.31 = slag cement paste with w/b = 0.31 and BFS mass content = 32 %; FA-0.33 = fly ash cement paste with w/b = 0.33 and FA mass content = 27 %.

Fig. 5.53 shows the chemical shrinkage of slag cement paste with w/b = 0.31 (BFS-0.31) and fly ash cement paste with w/b = 0.33 (FA-0.33), respectively. At a given age the chemical shrinkage of slag cement paste is larger than that of fly ash cement paste due to the faster reaction of BFS compared to FA.

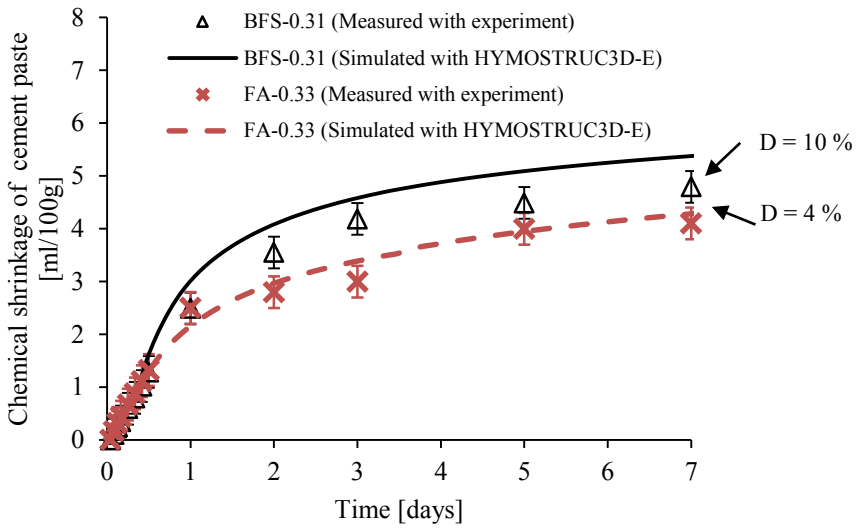

Fig. 5.53 Chemical shrinkage of slag and fly ash cement pastes: BFS-0.31 = slag cement paste with w/b = 0.31 and BFS mass content = 32 %; FA-0.33 = fly ash cement paste with w/b = 0.33 and FA mass content = 27 %. D represents the relative difference between the results of simulation and measurement

Fig. 5.54 shows the total degree of hydration of cement versus the chemical shrinkage of cement paste. For the same total degree of hydration of the cement, slag cement paste (BFS-0.31) and fly ash cement paste (FC-0.33) show larger chemical shrinkage than pure PC paste (PC-0.3). This is because the chemical shrinkage of PC is smaller than that of BFS and FA (Table 5.12). The chemical shrinkage of PC for complete hydration is normally around 6 ml/100g *[Geiker et al., 1982; Tazawa et al., 1995; Thomas et al., 2012]*. The chemical shrinkage of BFS (BFS reacts with water and CH) for complete reaction ranges from 11.5 to 18 ml/100g *[Chen et al., 2007a, b; Bentz, 2007]*. The chemical shrinkage of FA (FA reacts with water and CH) for complete reaction ranges from 10 to 16 ml *[Bentz, 2007]*.

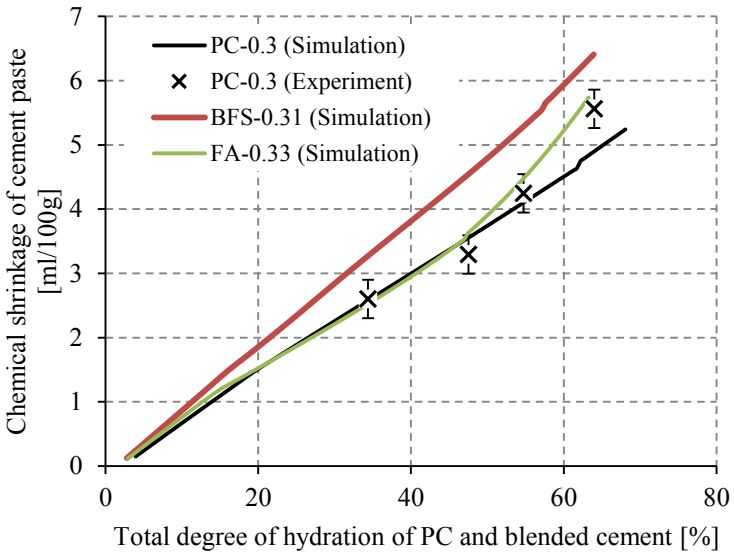

Fig. 5.54 Total degree of hydration of PC and blended cement versus chemical shrinkage of cement paste. Note: total degree of hydration of PC and blended cement is calculated as $\alpha_{PC} \times W_{PC} + \alpha_{BFS} \times W_{BFS} + \alpha_{FA} \times W_{FA}$. α_{PC}, α_{BFS} *and* α_{FA} *are the degree of reaction of PC, BFS and FA, respectively.* W_{PC}, W_{BFS} *and* W_{FA} *represent the weight fraction of PC, BFS and FA, respectively*

Table 5.12 Chemical shrinkage of PC, BFS and FA for complete hydration or reaction

Materials	Chemical shrinkage [ml/100g]	Reference
PC	6	Geiker et al.*[1982]* Tazawa et al. *[1995]* Thomas et al. *[2012]*
BFS	11.5-14	Chen et al. *[2007a,b]*
	18	Bentz *[2007]*
FA	10-16	Bentz *[2007]*

5.6 Concluding remarks

In this chapter the performance of HYMOSTRUC3D-E is evaluated for simulating the hydration, microstructure, pore solution chemistry and chemical shrinkage of pure PC and blended cement pastes. The following conclusions can be drawn:

1. Mono system: pure PC

In section 5.2 the hydration process and microstructure development of PC paste (w/c = 0.4) are simulated. The simulated degree of hydration of PC, pore size distributions of PC paste are compared with experimental data of Ye *[2003]* and Wang *[2013]*. The simulated pore size distributions of the capillary pores of PC paste at the age of 1 day to 28 days are in good agreement with the measured pore size distributions of capillary pores of PC paste using SEM image analysis. The simulated total porosity of cement paste is higher than the porosity measured using MIP (Fig. 5.15). This is because the small gel pores, i.e. gel pores< 4 nm, cannot be measured by MIP, whereas in HYMOSTRUC3D-E all pores are considered. The second reason is that MIP cannot detect the isolated pores, whereas HYMOSTRUC3D-E gives all pores. This difference also occurs in slag cement pastes and fly ash cement pastes as will be summarized in below *2. Binary system: PC blended with BFS* and *3. Binary system: PC blended with FA.*

2. Binary system: PC blended with BFS

In section 5.3 the hydration process, pore solution chemistry and microstructure development of slag cement pastes (w/b = 0.4, BFS content up to 70 %) are simulated. The simulated degree of hydration of slag cements is in good agreement with experimental data of *[Ye, 2006]*. The simulated concentrations of alkali ions (Na^+ and K^+) in the pore solution of slag cement pastes are close to the experimentally obtained data. The simulated concentrations of Ca^{2+} and SO_4^{2-} differ from the results of experiments, probably because the actual Ca^{2+} and OH^- ions in pore solution are supersaturated at early age (see section 4.2.3), which cannot be accurately calculated with *only* the concept of solubility equilibrium. Another possible reason for this is the actual concentrations of Ca^{2+} and SO_4^{2-} ions is also affected by the solubility equilibria of other phases in the cement paste, such as AFt, AFm, CSH (see section 3.3.2.3). The simulated evolution of the pH of the pore solution shows a trend similar to the experimental results. This is because the concentrations of Ca^{2+} and SO_4^{2-} are much lower than those of alkali ions. The relatively low accuracy of the simulated concentrations of Ca^{2+} and SO_4^{2-} did not significantly influence the accuracy of the simulated evolution of the pH.

3. Binary system: PC blended with FA

In section 5.4 the hydration process and microstructure development of fly ash cement pastes (w/b = 0.4 and 0.5, FA contents up to 70 %) are simulated. The simulated degree of hydration of PC in fly ash cements is in good agreement with the experimental results of Yu *[2015]*. The simulated degree of hydration of FA in fly ash cements shows similar trend with the

experimental results of Lam et al. *[2000]*. However the absolute value of the simulated degree of pozzolanic reaction of FA is different from the results from Lam et al. *[2000]*. This difference is probably caused by the difference between the properties of FA in this thesis and in the research of Lam et al. *[2000]*. The simulated CH contents of fly ash cement pastes differ from the measured CH contents of fly ash cement pastes using TGA measurement *[Yu, 2015]*. This is probably because the amorphous and microcrystalline CH are underestimated in the TGA measurement.

4. Chemical shrinkage of PC and blended cements

In section 5.5 the chemical shrinkage of PC pastes with w/c = 0.3 and 0.4, slag cement paste with w/b = 0.31 and fly ash cement with w/b = 0.33 is simulated with HYMOSTRUC3D-E. At early age, i.e. during the first 1 day, the simulated chemical shrinkage of PC pastes, slag cement paste and fly ash cement paste is in good agreement with the experimental results. At later age, i.e. after 1 day, the simulated chemical shrinkage of PC pastes, slag cement paste and fly ash cement paste is larger than the experimental results (differences are from 4 % to 12 %). In the chemical shrinkage test set up, as schematically shown in Fig. 5.48, the cement paste at the bottom of the conical flask will become dense with progress of the hydration process. As a result transport of water into the cement paste becomes difficult. Consequently, the measured chemical shrinkage will be smaller than the real chemical shrinkage. For the same total degree of hydration of cement, both slag cement and fly ash cement show larger chemical shrinkage than pure PC. The reason for this is the chemical shrinkage of PC for complete hydration is smaller than the chemical shrinkage BFS and FA for complete reaction (see Table 5.12)

Chapter 6

Conclusions and outlooks

6.1 Conclusions

For optimization of the use of SCMs in cementitious system, such as blast furnace slag (BFS) and fly ash (FA), a numerical model for simulating the hydration and microstructure development of blended cements is needed. A lot of models, like those of Wang et al. *[2009, 2010a, 2010b]*, Kolani et al. *[2012]*, Merzouki et al. *[2013]* and Tan *[2015]*, have been proposed in recent years to simulate the hydration and microstructure of blended cements. However these models need further development. For example, the nucleation and growth of CH particles were not simulated in these models. Moreover, the influence of pore solution chemistry on the reaction rate of SCMs was not quantified (see also Chapter 2). To overcome the limitations of these models, this study aims to extend HYMOSTRUC3D to simulate the hydration and microstructure development of systems of Portland cement (PC) blended with blast furnace slag (BFS) or/and fly ash (FA). The extended HYMOSTRUC3D is called HYMOSTRUC3D-E.

HYMOSTRUC3D-E comprises two routes: the *cement hydration route* and the *microstructure development route*. The *cement hydration route* deals with the hydration-related extension of HYMOSTRUC3D. The reaction rate of a PC, BFS and FA particles is simulated as a function of the water distribution and change in pore water chemistry in the system. The pore solution chemistry of blended cement pastes and its influence on the reaction of BFS or/and FA are specifically dealt with. The *microstructure development route* deals with the microstructure development-related extension of HYMOSTRUC3D. The microstructure development of blended cement paste is simulated by growing hydrating particles, and nucleation and growth of CH particles. To differentiate between the volume of the capillary porosity and gel porosity, a pore structure module is also proposed in the *microstructure development route* for simulating the evolution of capillary porosity. Specific porosities are assigned to the inner and outer products. By determining the volume evolution of the inner and outer products, the evolution of gel porosity in cement paste is determined.

In comparison with HYMOSTRUC3D, HYMOSTRU3D-E shows the following extensions (Table 6.1):

1. Blended systems

HYMOSTRUC3D is only able to simulate the hydration and microstructure development pure PC system. HYMOSTRU3D-E is able to simulate the hydration and microstructure

Table 6.1 Comparison between HYMOSTRUC3D and HYMOSTRUC3D-E (see also Table 4.3)

	HYMOSTRUC3D	HYMOSTRUC3D-E
Available systems	Mono system: PC paste	Mono system: PC paste Binary system: slag cement paste and fly ash cement paste Ternary system: PC blended with BFS and FA.
Degree of hydration of PC	Available	Available
Degree of the components of PC	Available	Available
Microstructure	Available	Available
Pore solution chemistry	Unavailable	Available
Nucleation and growth of CH particles	Unavailable	Available
Evolution of capillary porosity in cement paste	Available	Available
Evolution of gel porosity in cement paste	Gel volume was already calculated	Specific pore size distributions are assigned to the inner and outer products.

development of several systems: mono system (PC), binary system (PC blended with BFS or FA), ternary system (PC blended with BFS and FA).

2. Pore solution chemistry

In HYMOSTRUC3D-E, the evolution of pore solution chemistry in cement paste is simulated, and the influence of the pore solution chemistry on the reaction rates of BFS and FA is quantified explicitly.

3. Nucleation and growth of CH particles

HYMOSTRUC3D-E contains a module to simulate the nucleation and growth of CH particles.

4. Evolution of gel porosity in cement paste

In HYMOSTRU3D-E a pore structure module is proposed to determine the pore structure of cement paste, including the contribution of gel pores to the total porosity. In this pore structure module, specific pore size distributions are assigned to the inner and outer products.

HYMOSTRUC3D-E is used to simulate the hydration process, microstructure, pore solution chemistry and chemical shrinkage of pure PC and blended cement pastes. By comparing the results of simulation and experiments, the following conclusions can be drawn:

1. Degree of hydration

For systems with different w/c and different initial content of BFS and FA, the simulated degrees of hydration (or reaction) of PC, BFS and FA are validated with experimental data. In HYMOSTRUC3D-E the influence of the mineral composition of PC on the hydration of PC is

taken into account using the initial penetration rate (K_0) and the transition thickness (δ_{tr}) for different minerals (C_3S, C_2S, C_3A, C_4AF) in PC particles. The influence of BFS or/and FA on the hydration of PC and the effect of the w/b on the hydration or reaction of PC, BFS, and FA are quantified by further detailing of the reduction factors Ω_1, Ω_2 and Ω_3, which allow for the changes of the water distribution and changes in pore water chemistry in the system. The effect of pore solution chemistry on the pozzolanic reaction of BFS and FA is quantified using the pH-factor M_{pH} allowing for the effect pH on the reaction rate of BFS and FA particles. With these extensions of the original simulation model, the hydration process of the cements with different components, such as different contents of PC, BFS and FA, and different w/b, could be simulated.

2. Pore structure

For pure Portland cement paste (w/c = 0.4), the simulated capillary pore size distributions at the age from 1 day to 28 days are in good agreement with those obtained using SEM image analysis. The simulated total porosity is larger than the porosity measured using MIP. This is because the small gel pores, i.e. gel pores< 4 nm, cannot be measured by MIP, whereas in HYMOSTRUC3D-E all gel pores are given. A second reason is that MIP cannot detect the isolated pores, whereas HYMOSTRUC3D-E gives all pores. This difference also occurs in slag cement systems (w/b = 0.4 and BFS content from 30% to 70%), fly ash cement systems (w/b = 0.4 and FA content ranging from 30% to 50%).

3. Pore solution chemistry

For a pure Portland cement system (w/c = 0.4) and slag cement systems (w/b = 0.4, BFS content ranging from 30% to 70%), the simulated concentrations of alkali ions (Na^+ and K^+), and the evolution of pH in the pore solution are validated with the experimental data. The simulated concentrations of Ca^{2+} and SO_4^{2-} differ from the experimental data. The possible reason for this is in HYMOSTRUC3D-E the concentrations of Ca^{2+} and SO_4^{2-} ions are considered to *only* depend on the solubility equilibria of gypsum and CH, whereas the actual concentrations of Ca^{2+} and SO_4^{2-} ions are also affected by other phases in the cement paste, such as AFt, AFm, CSH. Besides the actual Ca^{2+} ions in pore solution are supersaturated at early age (see section 4.2.3), which cannot be accurately calculated *only* with the concept of solubility equilibrium.

4. Chemical shrinkage

The chemical shrinkage of PC pastes with w/c = 0.3 and 0.4, slag cement paste with w/b = 0.31 and fly ash cement with w/b = 0.33 are simulated with HYMOSTRUC3D-E. For PC pastes, the simulated chemical shrinkage of these cement pastes is in good agreement with the experimental results at early age, i.e. during the first 1 day. At later age, i.e. after 1 day, the simulated chemical shrinkage is larger than the experimental results. The reason for this is the transport of water into the actual cement paste becomes difficult at later age (see section 5.5.4). This difference also occurs in the slag cement paste and the fly ash cement paste. For

the same total degree of hydration of cement, both slag cement and fly ash cement show larger chemical shrinkage than pure PC, because the chemical shrinkage of PC for complete hydration is smaller than the chemical shrinkage BFS and FA for complete reaction (see Table 5.12).

5. Nucleation and growth of CH particles

For a pure Portland cement system (w/c = 0.4), the cumulative size distribution of CH particles simulated by HYMOSTRUC3D-E is close to the experimental data, at least for small particle sizes, i.e. < 3.4 μm. For large particle sizes, i.e. > 3.4 μm, the cumulative size distribution of CH particles simulated by HYMOSTRUC3D-E differs from the experimental data. This is because the pore structure simulated by HYMOSTRUC3D-E using a REV = $100\times100\times100$ μm^3 doesn't contain the big pores, i.e. the pores > 10 μm (the limitation due to the size of the REV of cement paste). In reality these big pores exist in the cement paste, and they provide room for the growth of large CH particles.

6.2 Outlooks

6.2.1 Potentials of HYMOSTRUC3D-E

HYMOSTRUC3D has been successfully used to predict the properties of cement-based materials, such as the transport properties of cement pastes *[Ye, 2006; Zhang, 2013]* and the tensile strength of cement pastes *[Qian et al., 2010]*, etc. HYMOSTRUC3D-E is an extension of HYMOSTRUC3D model. HYMOSTRUC3D-E can also be used to predict the properties of cement-based materials, such as the transport properties of cement pastes, the tensile strength of cement pastes, etc. In addition to the applications, HYMOSTRUC3D-E has more potentials. There are five examples:

1. Prediction of adiabatic hydration curves of blended cement concrete structures

HYMOSTRUC can be used to simulate the hydration process of PC as a function of cement composition, particle size distribution, w/c ratio and temperature to produce adiabatic hydration curves *[Van Breugel, 1991]*. The obtained adiabatic hydration curves can serve as the starting point for dealing with the thermal stresses of concrete structures. In the *cement hydration route* of HYMOSTRUC3D-E, the hydration process of blended cements is simulated, which can be used to calculate the adiabatic hydration curves of blended cements. The obtained adiabatic hydration curves of blended cements can be to investigate the thermal stress of blended cement concrete structures.

2. Corrosion of steel in concrete

The corrosion of steel in concrete is an electrochemical process. If the pH of the pore solution in concrete is low, the corrosion of steel is apt to occur *[Taylor, 1997]*. For concretes incorporating supplementary cementitious materials (SCM), like BFS and FA, the pH of the

pore solution in these concretes is normally lower than in pure PC concretes. HYMOSTRUC3D-E can be used as a tool to evaluate the evolution of pH in systems incorporating BFS or/and FA, and has the potential to investigate corrosion of steel in the concretes blended with BFS or/and FA.

3. Creep

Creep of cement-based materials originate from the deformation of hydration products, such as CSH gel. HYMOSTRUC3D-E contains a pore structure module to determine the evolution of the pore structure of cement paste, including the contribution of gel pores to total porosity. The evolution of inner CSH gel porosity and outer CSH gel porosity are also distinguished in this pore structure module. Differentiation between the porosity of inner CSH gel and outer CSH gel may provide us a stronger basis for creep studies.

4. Drying shrinkage

Being exposed to the atmosphere at air temperature, the relative humidity (RH) of cement-based materials can drop from 100% to 50%. Both the capillary pores and the large gel pores will dry out at this RH range. In HYMOSTRUC3D-E the evolution of the pore structure of cement paste is determined by considering the contribution of gel pores to total porosity, which can be helpful to describe the drying process of cement-based materials.

5. Carbonation process

In blended cement systems, CH formed in the hydration of PC will be consumed by the pozzolanic reactions of SCMs. This consumption of CH will alter the performance of cement-based materials. For instance, the carbonation resistance of blended cement concretes will decrease if the CH content in the systems decreases. In HYMOSTRUC3D-E, the nucleation and growth of CH particles in pore structure are simulated, which can be helpful to investigate the carbonation process of blended cement-based materials.

6.2.2 Recommendations for further research

There is still room to improve and further extend HYMOSTRUC3D-E model:

1. Simulation of pore solution chemistry

The concentrations of Na^+, K^+, OH^- simulated by HYMOSTRUC3D-E show trends similar to experimental data. However, the accuracy of the simulation of the concentrations of Ca^{2+} and SO_4^{2-} is relatively low. Moreover, the concentrations of the ions, such as Mg^{2+}, $Al(OH)_4^-$, $SiO(OH)_3^-$, are not simulated in HYMOSTRUC3D-E. It is recommended to further consider the equilibrium of hydration products, such as AFt, AFm and CSH gel etc., in the pore solution to simulate the concentrations of the ions like Ca^{2+}, SO_4^{2-}, Mg^{2+}, $Al(OH)_4^-$, $SiO(OH)_3^-$, etc.

2. Simulation of relative humidity

The evolution of relative humidity (RH) in cement paste is an important parameter to investigate autogenous shrinkage of cement paste. In our preliminary studies, the RH in cement paste was calculated from the 3D pore structure and the volume of empty capillary pore simulated with HYMOSTRUC3D-E. The influence of alkali ions, i.e. Na^+, K^+ on the evolution of RH in cement paste was also quantified. However the calculated value of RH differs from the experimental data. The reason for this difference is not clear yet. In further study, it is recommended to further proposed a module to simulate the RH in cement paste.

3. Nucleation and growth of hydration products, such as AFt and AFm

In the 3D microstructure simulated by HYMOSTRUC3D, the hydration products, such as CSH gel, CH, AFt, AFm, etc., are considered as one gel phase. In comparison with HYMOSTRUC3D, HYMOSTRUC3D-E distinguishes between CSH and CH, and simulates the nucleation and growth of CH particles in the pore space. In further study, it is recommended to simulate the nucleation and growth of AFt and AFm particles in pore space.

Reference

[1] Abraitis, P.K., Livens, F.R., Monteith, J.E., Small, J.S., Trivedi, D.P., Vaughan, D.J. and Wogelius, R.A. (2000). The kinetics and mechanisms of simulated British Magnox waste glass dissolution as a function of pH, silicic acid activity and time in low temperature aqueous systems. Applied Geochemistry, 15(9), pp.1399-1416.

[2] Ahmaruzzaman M. (2010). A review on the utilization of fly ash. Progress in energy and combustion science,36(3), pp.327-363.

[3] Bentur, A., Berger, R.L., Kung, J.H., Milestone, N.B. and Young, J.F. (1979). Structural properties of calcium silicate pastes: II, effect of curing temperature. Journal of the American Ceramic Society, 62(7-8), pp.362-366.

[4] Bentz, D.P. (1995). A three-dimensional cement hydration and microstructure program: I. hydration rate, heat of hydration, and chemical shrinkage. Building and Fire Research Laboratory, National Institute of Technology.

[5] Bentz, D.P. (1997). Three-Dimensional Computer Simulation of Portland Cement Hydration and Microstructure Development. Journal of the American Ceramic Society, 80(1), pp.3-21.

[6] Bentz, D.P., 'CEMHYD3D: a three-dimensional cement hydration and microstructure development modeling package. Version 3.0', NISTIR 7232. US Department of Commerce. (2005).

[7] Bentz, D.P. (2007). Internal curing of high-performance blended cement mortars. ACI Materials Journal, 104(4), p.408.

[8] Bentz, D.P. (2014). Activation energies of high-volume fly ash ternary blends: hydration and setting. Cement and Concrete Composites, 53, pp.214-223.

[9] Bentz, D.P. and Garboczi, E.J. (1991). Digitized simulation model for microstructural development. Ceramic Transactions, 16 pp., 211.

[10] Bentz, D.P., Coveney, P.V., Garboczi, E.J., Kleyn, M.F. and Stutzman, P.E. (1994). Cellular automaton simulations of cement hydration and microstructure development. Modelling and Simulation in Materials Science and Engineering, 2(4), pp.783-808.

[11] Bentz, D.P. and Remond, S. (1997). Incorporation of fly ash into a 3-D cement hydration microstructure model. National Institute of Standards and Technology, Technology Administration, US Department of Commerce.

[12] Bentz, D.P., Jensen, O.M., Coats, A.M. and Glasser, F.P. (2000). Influence of silica fume on diffusivity in cement-based materials: I. Experimental and computer modeling studies on cement pastes. Cement and Concrete Research, 30(6), pp.953-962.

[13] Bentz, D.P., Jensen, O.M., Hansen, K.K., Olesen, J.F., Stang, H. and Haecker, C.J. (2001). Influence of Cement Particle-Size Distribution on Early Age Autogenous

Strains and Stresses in Cement-Based Materials. Journal of the American Ceramic Society, 84(1), pp.129-135.

[14] Biernacki, J.J., Williams, P.J. and Stutzman, P.E. (2001). Kinetics of reaction of calcium hydroxide and fly ash. ACI Materials Journal, 98(4), pp.340-349.

[15] Biernacki, J.J., Richardson, J.M., Stutzman, P.E. and Bentz, D.P. (2002). Kinetics of slag hydration in the presence of calcium hydroxide. Journal of the American Ceramic Society, 85(9), pp.2261-2267.

[16] Bishnoi, S. and Scrivener, K.L. (2009a). μic: A new platform for modelling the hydration of cements. Cement and Concrete Research, 39(4), pp.266-274.

[17] Bishnoi, S. and Scrivener, K.L. (2009b). Studying nucleation and growth kinetics of alite hydration using μic. Cement and Concrete Research, 39(10), pp.849-860

[18] Blanc, P., Bourbon, X., Lassin, A. and Gaucher, E.C. (2010). Chemical model for cement-based materials: Thermodynamic data assessment for phases other than C–S–H. Cement and Concrete Research, 40(9), pp.1360-1374.

[19] Brantley, S.L. (2008). Kinetics of mineral dissolution. In: SL. Brantley, J.D. Kubicki, and A.F. White, eds. Kinetics of water-rock interaction. Springer.

[20] Bullard, J.W. (2007a). A three-dimensional microstructural model of reactions and transport in aqueous mineral systems. Modelling and Simulation in Materials Science and Engineering, 15(7), p.711.

[21] Bullard, J.W. (2007b). Approximate rate constants for nonideal diffusion and their application in a stochastic model. The Journal of Physical Chemistry A, 111(11), pp.2084-2092.

[22] Cement Statistics and Information (USGS, 2015); URL: http://minerals.usgs.gov/minerals/pubs/commodity/cement/index.html

[23] Chen, W. and Brouwers, H.J.H. (2007a). The hydration of slag, part 1: reaction models for alkali-activated slag. Journal of Materials Science, 42(2), pp.428-443.

[24] Chen, W. and Brouwers, H.J.H. (2007b). The hydration of slag, part 2: reaction models for blended cement. Journal of Materials Science, 42(2), pp.444-464.

[25] Chen, W., Brouwers, H.J.H. and Shui, Z.H. (2007c). Three-dimensional computer modeling of slag cement hydration. Journal of Materials Science, 42(23), pp.9595-9610.

[26] Damidot, D., Lothenbach, B., Herfort, D. and Glasser, F.P. (2011). Thermodynamics and cement science. Cement and Concrete Research, 41(7), pp.679-695.

[27] Diamond, S. (2000). Mercury porosimetry: an inappropriate method for the measurement of pore size distributions in cement-based materials. Cement and Concrete Research, 30(10), pp.1517-1525.

[28] Diamond, S. (2001). Calcium hydroxide in cement paste and concrete- a microstructural appraisal. Materials Science of Concrete Special, pp.37-58.

[29] Diamond, S. (2007). Particle arrangements in freshly-mixed mortars: Basis for modeling. Journal of Advanced Concrete Technology, 5(3), pp.277-283.

[30] Dolado, J.S. and van Breugel, K. (2011). Recent advances in modeling for cementitious materials. Cement and Concrete Research, 41(7), pp.711-726.

[31] Fernandez-Jimenez, A., Puertas, F. and Arteaga, A. (1998). Determination of kinetic equations of alkaline activation of blast furnace slag by means of calorimetric data. Journal of thermal analysis and calorimetry, 52(3), pp.945-955.

[32] Fonseca, P.C., Jennings, H.M. and Andrade, J.E. (2011). A nanoscale numerical model of calcium silicate hydrate. Mechanics of Materials, 43(8), pp.408-419.

[33] Gallucci, E. and Scrivener, K. (2007). Crystallisation of calcium hydroxide in early age model and ordinary cementitious systems. Cement and Concrete Research, 37(4), pp.492-501.

[34] Geiker, M. and Knudsen, T. (1982). Chemical shrinkage of Portland cement pastes. Cement and Concrete Research, 12(5), pp.603-610.

[35] Haha, M.B., De Weerdt, K. and Lothenbach, B. (2010). Quantification of the degree of reaction of fly ash. Cement and Concrete Research, 40(11), pp.1620-1629.

[36] Hales, T.C. (1998). An overview of the Kepler conjecture. arXiv preprint math/9811071.

[37] Harutyunyan, V.S., Kirchheim, A.P., Monteiro, P.J.M., Aivazyan, A.P. and Fischer, P., 2009. Investigation of early growth of calcium hydroxide crystals in cement solution by soft X-ray transmission microscopy. Journal of materials science, 44(4), pp.962-969.

[38] Helmuth, R. (1987). Fly ash in cement and concrete. Portland Cement Association.

[39] Hong, S.Y. and Glasser, F.P. (1999). Alkali binding in cement pastes: Part I. The CSH phase. Cement and Concrete Research, 29(12), pp.1893-1903.

[40] Hong, S.Y. and Glasser, F.P. (2002). Alkali sorption by CSH and CASH gels: Part II. Role of alumina. Cement and Concrete Research, 32(7), pp.1101-1111.

[41] Hummel, W., Berner, U., Curti, E., Pearson, F.J. and Thoenen, T. (2002). Nagra/PSI chemical thermodynamic data base 01/01. National Cooperative for the Disposal of Radioactive Waste, Switzerland.

[42] Jawed, I. and Skalny, J. (1978). Alkalies in cement: a review: II. Effects of alkalies on hydration and performance of Portland cement. Cement and Concrete Research, 8(1), pp.37-51.

[43] Jennings, H.M. (2000). A model for the microstructure of calcium silicate hydrate in cement paste. Cement and Concrete Research, 30(1), pp.101-116.

[44] Jennings, H.M. (2004) .Colloid model of C−S−H and implications to the problem of creep and shrinkage. Materials and Structures, 37(1), pp.59-70.

[45] Jennings, H.M. (2008). Refinements to colloid model of CSH in cement: CM-II. Cement and Concrete Research, 38(3), pp.275-289.

[46] Jennings, H.M. and Johnson, S.K. (1986) Simulation of microstructure development during the hydration of a cement compound. Journal of the American Ceramic Society, 69(11), pp.790-795.

[47] Jennings, H.M., Thomas, J.J., Gevrenov, J.S., Constantinides, G. and Ulm, F.J. (2007). A multi-technique investigation of the nanoporosity of cement paste. Cement and Concrete Research, 37(3), pp.329-336.

[48] Kishi, T. and Maekawa, K. (1995). Thermal and mechanical modelling of young concrete based on hydration process of multi-component cement minerals. In: the Proceedings of the International RILEM symposium on Thermal Cracking in Concrete at Early Age. Munich, E&FN Spon, London: pp.11-18.

[49] Kjellsen, K.O. and Justnes, H. (2004). Revisiting the microstructure of hydrated tricalcium silicate-a comparison to Portland cement. Cement and Concrete Composites, 26(8), pp.947-956.

[50] Klein, D.H. and Smith, M.D. (1968). Homogeneous nucleation of calcium hydroxide. Talanta, 15(2), pp.229-231.

[51] Koenders, E.A.B. (1997). Simulation of volume changes in hardening cement-based materials, PhD Thesis, Delft University of Technology, Delft, The Netherlands.

[52] Kolani, B., Buffo-Lacarrière, L., Sellier, A., Escadeillas, G., Boutillon, L. and Linger, L. (2012). Hydration of slag-blended cements. Cement and Concrete Composites, 34(9), pp.1009-1018.

[53] Kumar, A., Sant, G., Patapy, C., Gianocca, C. and Scrivener, K.L. (2012). The influence of sodium and potassium hydroxide on alite hydration: Experiments and simulations. Cement and Concrete Research, 42(11), pp.1513-1523.

[54] Lam, L., Wong, Y.L. and Poon, C.S. (2000). Degree of hydration and gel/space ratio of high-volume fly ash/cement systems. Cement and Concrete Research, 30(5), pp.747-756.

[55] Lange, D.A., Jennings, H.M. and Shah, S.P. (1994). Image analysis techniques for characterization of pore structure of cement-based materials. Cement and Concrete Research, 24(5), pp.841-853.

[56] Le, N.L., Stroeven, M., Sluys, L.J. and Stroeven, P. (2013). A novel numerical multi-component model for simulating hydration of cement. Computational Materials Science, 78, pp.12-21.

[57] Lothenbach, B. and Winnefeld, F. (2006). Thermodynamic modelling of the hydration of Portland cement. Cement and Concrete Research, 36(2), pp.209-226.

[58] Lothenbach, B., Scrivener, K. and Hooton, R.D. (2011). Supplementary cementitious materials. Cement and Concrete Research, 41(12), pp.1244-1256.

[59] Lumley, J.S., Gollop, R.S., Moir, G.K. and Taylor, H.F.W. (1996). Degrees of reaction of the slag in some blends with Portland cements. Cement and Concrete Research, 26(1), pp.139-151.

[60] Maeda, T., Baba, T. and Mizuno, T. (2004). Effects of basicity and leachant pH on the dissolution rates of molten slag. Waste Manage Experts (In Japanese), 15, pp.45-51.

[61] Maekawa, K., Chaube, R. and Kishi, T. (1999). Modelling of concrete performance hydration, microstructure formation and transport, London: E & FN SPON.

[62] Maekawa, K., Ishida, T. and Kishi, T. (2003). Multi-scale modeling of concrete performance. Journal of Advanced Concrete Technology, 1(2), pp.91-126.

[63] Masoero, E., Del Gado, E., Pellenq, R.M., Ulm, F.J. and Yip, S. (2012). Nanostructure and nanomechanics of cement: polydisperse colloidal packing. Physical review letters, 109(15), p.155503.

[64] McGrail, B.P., Ebert, W.L., Bakel, A.J. and Peeler, D.K. (1997). Measurement of kinetic rate law parameters on a Na-Ca-Al borosilicate glass for low-activity waste. Journal of Nuclear Materials, 249(2), pp.175-189.

[65] Mehta, P. K., (1989). 3rd International Conference on Fly Ash, Silica Fume, and Natural Pozzolans in Concrete, Tronheim, Norway, pp. 1–43.

[66] Merzouki, T., Bouasker, M., Khalifa, N.E.H. and Mounanga, P. (2013). Contribution to the modeling of hydration and chemical shrinkage of slag-blended cement at early age. Construction and Building Materials, 44, pp.368-380.

[67] Mindess, S., Young, J.F. and Darwin, D. (2003). Concrete. 2nd ed. Prentice Hall.

[68] Molina, L. (1992). On predicting the influence of curing conditions on the degree of hydration. Swedish Cement and Concrete Research Institute.

[69] Navi, P. and Pignat, C. (1996). Simulation of cement hydration and the connectivity of the capillary pore space. Advanced Cement Based Materials, 4(2), pp.58-67.

[70] Nguyen, V.T. (2011). Rice husk ash as a mineral admixture for ultra high performance concrete. PhD Thesis, Delft, Delft University of Technology, The Netherlands.

[71] Nothnagel, R. and Budelmann, H. (2008). Model for the formation of microstructure in cement paste during hydration. In International RILEM Symposium on Concrete Modelling-ConMod'08 (pp. 361-368). RILEM Publications SARL.

[72] Oelkers, E.H. (2001). General kinetic description of multioxide silicate mineral and glass dissolution. Geochimica et Cosmochimica Acta, 65(21), pp.3703-3719.

[73] Oelkers, E.H., Schott, J. and Devidal, J.L. (1994) .The effect of aluminum, pH, and chemical affinity on the rates of aluminosilicate dissolution reactions. Geochimica et Cosmochimica Acta, 58(9), pp.2011-2024.

[74] Papadakis, V.G. (1999). Effect of fly ash on Portland cement systems: Part I. Low-calcium fly ash. Cement and Concrete Research, 29(11), pp.1727-1736.

[75] Papadakis, V.G. (2000). Effect of fly ash on Portland cement systems: Part II. High-calcium fly ash. Cement and Concrete Research, 30(10), pp.1647-1654.

[76] Pignat, C., Navi, P. and Scrivener, K. (2005). Simulation of cement paste microstructure hydration, pore space characterization and permeability determination. Materials and structures, 38(4), pp.459-466.

[77] Qian, Z.W. Schlangen, E., Ye, G. and Van Breugel, K. (2010). Prediction of mechanical properties of cement paste at microscale. Materiales de Construccion, 60(297), pp.7-18.

[78] Ramezanianpour, A.A. (2014). Cement Replacement Materials: Properties, Durability, Sustainability. Springer.

[79] Richardson, I.G. (1999). The nature of CSH in hardened cements. Cement and Concrete Research, 29(8), pp.1131-1147.

[80] Richardson, J.M., Biernacki, J.J., Stutzman, P.E. and Bentz, D.P. (2002). Stoichiometry of slag hydration with calcium hydroxide. Journal of the American Ceramic Society, 85(4), pp.947-953.

[81] Rosin, P. and Rammler, E. (1933). The laws governing the fineness of powdered coal. Journal of the Institute of Fuel., 7, pp.29-36.

[82] Scherer, G.W. (2002). September. Factors affecting crystallization pressure. In International RILEM TC 186-ISA Workshop on Internal Sulfate Attack and Delayed Ettringite Formation, Villars, Switzerland (pp. 139-154).

[83] Siddique, R. and Khan, M.I. (2011). Supplementary cementing materials. Springer.

[84] Skoge, M., Donev, A., Stillinger, F.H. and Torquato, S. (2006). Packing hyperspheres in high-dimensional Euclidean spaces. Physical Review E, 74(4), p.041127.

[85] Škvára, F., Kopecký, L., Šmilauer, V. and Bittnar, Z. (2009). Material and structural characterization of alkali activated low-calcium brown coal fly ash. Journal of Hazardous Materials, 168(2), pp.711-720.

[86] Song, S. and Jennings, H.M. (1999). Pore solution chemistry of alkali-activated ground granulated blast-furnace slag. Cement and Concrete Research, 29(2), pp.159-170.

[87] Steiger, M. (2005). Crystal growth in porous materials—II: Influence of crystal size on the crystallization pressure. Journal of crystal growth, 282(3), pp.470-481.

[88] Stroeven, M. (1999). Discrete numerical modelling of composite materials-application to cementitious materials, PhD Thesis, Delft, Delft University of Technology, The Netherlands.

[89] Tan, Z.J. (2015). Experimental study and numerical simulation of hydration and microstructure development of ternary cement-based materials. PhD thesis, Ghent, Ghent University, Belgium.

[90] Tan, Z.J., De Schutter, G., Ye, G., Gao, Y. and Machiels, L. (2014). Influence of particle size on the early hydration of slag particle activated by Ca(OH)2 solution. Construction and Building Materials, 52, pp.488-493.

[91] Taylor, H.F.W. (1987). A method for predicting alkali ion concentrations in cement pore solutions. Advances in Cement Research, 1(1), pp.5-17.

[92] Taylor, H.F.W. (1997). Cement Chemistry. 2nd ed. London: Thomas Telford Publishing.

[93] Tazawa, E.I., Miyazawa, S. and Kasai, T. (1995). Chemical shrinkage and autogenous shrinkage of hydrating cement paste. Cement and concrete research, 25(2), pp.288-292.

[94] Tennis, P.D. and Jennings, H.M. (2000). A model for two types of calcium silicate hydrate in the microstructure of Portland cement pastes. Cement and Concrete Research, 30(6), pp.855-863.

[95] Thomas, J.J., Jennings, H.M., and Allen, A.J. (2010). Relationships between composition and density of tobermorite, jennite, and nanoscale $CaO{-}SiO_2{-}H_2O$. The Journal of Physical Chemistry C, 114(17), 7594-7601.

[96] Thomas, J.J., Biernacki, J.J., Bullard, J.W., Bishnoi, S., Dolado, J.S., Scherer, G.W. and Luttge, A. (2011). Modeling and simulation of cement hydration kinetics and microstructure development. Cement and Concrete Research, 41(12), pp.1257-1278.

[97] Thomas, J.J., Allen, A.J. and Jennings, H.M. (2012). Density and water content of nanoscale solid C–S–H formed in alkali-activated slag (AAS) paste and implications for chemical shrinkage. Cement and Concrete Research, 42(2), pp.377-383.

[98] Torquato, S., Truskett, T.M. and Debenedetti, P.G. (2000). Is random close packing of spheres well defined?. Physical review letters, 84(10), p.2064.

[99] Van Breugel, K. (1991). Simulation of hydration and formation of structure in hardening cement-based materials, PhD Thesis, Delft, Delft University of Technology, The Netherlands.

[100] Van Breugel, K. (2004). Modelling of cement-based systems—the alchemy of cement chemistry. Cement and Concrete Research, 34(9), pp.1661-1668.

[101] Van Eijk, R.J. and Brouwers, H.J.H. (2000). Prediction of hydroxyl concentrations in cement pore water using a numerical cement hydration model. Cement and Concrete Research, 30(11), pp.1801-1806.

[102] Wang, X.Y., Lee, H.S. and Park, K.B. (2009). Simulation of low-calcium fly ash blended cement hydration. Materials Journal, 106(2), pp.167-175.

[103] Wang, X.Y. and Lee, H.S. (2010a). Modeling the hydration of concrete incorporating fly ash or slag. Cement and concrete Research, 40(7), pp.984-996.

[104] Wang, X.Y., Lee, H.S., Park, K.B., Kim, J.J. and Golden, J.S. (2010b). A multi-phase kinetic model to simulate hydration of slag–cement blends. Cement and Concrete Composites, 32(6), pp.468-477.

[105] Wang, Y. (2013). Performance assessment of cement-based materials blended with micronized sand: microstructure, durability and sustainability, PhD Thesis, Delft, Delft University of Technology, The Netherlands.

[106] Witmann, F.H. (1983). Structure of Concrete with respect to Crack formation, Fracture Mechanics of Concrete.

[107] Worrell, E., Price, L., Martin, N., Hendriks, C. and Meida, L.O. (2001). Carbon dioxide emissions from the global cement industry 1. Annual Review of Energy and the Environment, 26(1), pp.303-329.

[108] Ye, G. (2003). Experimental Study and Numerical Simulation of the Development of the microstructure and permeability of cementitious materials, PhD Thesis, Delft, Delft University of Technology, The Netherlands.

[109] Ye, G. (2006). Numerical simulation of connectivity of individual phases in hardening cement-based systems made of blended cement with and without admixtures, VENI report, Delft, Delft University of Technology, the Netherlands.

[110] Ye, G., Lura, P. and van Breugel, K. (2006). Modelling of water permeability in cementitious materials. Materials and Structures, 39(9), pp.877-885.

[111] Young, J.F. and Hansen, W. (1986). Volume relationships for CSH formation based on hydration stoichiometries. In MRS proceedings (Vol. 85, p. 313). Cambridge University Press.

[112] Yu, Z.Q. (2015). Microstructure development and transport properties of Portland Cement-fly ash binary systems-in view of service life predictions, PhD Thesis, Delft, Delft University of Technology, The Netherlands.

[113] Zhang, M.Z. (2013) Multiscale Lattice Boltzmann-Finite Element Modelling of Transport Properties in Cement-based Materials, PhD Thesis, Delft, Delft University of Technology, The Netherlands.

[114] Zuo, Y.B, Qian, Z.W, Garboczi, E.D., Ye, G. (2018) Numerical simulation of the initial particle parking structure of cement/geopolymer paste and the dissolution of amorphous silica using real-shape particles, Cement and Concrete Research, submitted.

List of Abbreviations

AFm ($C_4A\bar{S}H_{12}$)	monosulphate aluminate hydrate
AFt ($C_6A\bar{S}_3H_{32}$)	ettringite
Al_2O_3 (A)	aluminium oxide
AS	aluminosilicate
BFS	ground granulated blast furnace slag
C_2ASH_8	strätlingite
C_2S	dicalcium silicate
C_3A	tricalcium aluminate
C_3AH_6	hydrogarnet
C_3S	tricalcium silicate
C_4AF	tetracalcium alumino ferrite
CaO (C)	calcium oxide
CAS_2	calcium aluminosilicate
CH	calcium hydroxide
CO_2	carbon dioxide
CSH	calcium silicate hydrate
EDTA	ethylene diamine tetraacetic acid
FA	fly ash
FH_3	iron hydroxide
H_2O (H)	water
K_2O	potassium oxide
MgO (M)	Magnesium oxide
M_5AH_{13}	hydrotalcite-like phase
MIP	mercury intrusion porosimetry
Na_2O	sodium oxide
NaOH	Sodium hydroxide
PC	Portland cement
REV	representative elementary volume
SCM	supplementary cementitious materials
SiO_2 (S)	silicon dioxide
SO_3 ($\bar{S}$)	sulfur trioxide
TGA	thermogravimetric analysis
USGS	U.S. Geological Survey
w/b	water-to-binder ratio
w/c	water-to-cement ratio
XRF	X-ray fluorescence

List of Symbols

$K_{sp,CH}$	solubility constant of CH	
$K_{sp,gyp}$	solubility constant of gypsum	
N_{dig,X_k}	number of voxels of X_k in the simulated 3D microstructure	
$V_{ou,central,j,PC}$	growth caused by hydration of central PC particle	[μm^3]
$V_{ou,tot;x_i,j,PC}$	total outer product volume of central particle (extra growth is taken into account) at time t_j	[μm^3]
$V_{paste,0}$	volume of cement paste for 1 g initial cement	[cm^3]
$\alpha_{<x_i,j,tot,M_k}$	total degree of hydration of clinker components at time t_j for PC particles with diameters $< x_i$	
$\alpha_{<x_i,j,tot,A}$	total degree of hydration (or reaction)of A particles with diameters of $< x_i$ at time t_j. A can be PC, BFS and FA.	
α_{x_i,j,M_k}	degree of hydration of clinker components at time t_j for a PC particle with diameter x_i	
$\alpha_{x_i,j,A}$	degree of hydration of A particle with diameter x_i at time t_j. A can be PC, BFS and FA.	
α_{j,M_k}	total degree of hydration of clinker components in all PC particles at time t_j.	
$\alpha_{j,A}$	degree of hydration of all A particles. A can be PC, BFS and FA.	
δ_{in,x_i,j,M_k}	total penetration depth of reaction front of clinker components at time t_j for a PC particle with diameter x_i	[μm]
$\delta_{in,x_i,j,A}$	average penetration depth of the reaction front of clinker components at time t_j for A particle with diameter x_i. A can be PC, BFS and FA.	[μm]
$\{CH^0\}$	activities of CH	
$\{Ca^{2+}\}$	activities of Ca^{2+} ions	
$\{OH^-\}$	activities of OH^- ions	
$h_{1st,C_3A/C_4AF}$	ratio of $\alpha_{1st,C_3A}/\alpha_{1st,C_4AF}$ in the previous time t_{j-1} in stage 1.	
$h_{2nd,C_3A/C_4AF}$	ratio of α_{j,C_3A} to α_{j,C_4AF}at the last time in stage 2	
$A_{BFS(or\ FA)}$	coefficients to calculate the dissolution rate of BFS (or FA)	
AE_{T,α,C_3S}	activation energy of C_3S with degree of hydration α at temperature T	[kJ/mole]
$A_{d,cap,i}$	capillary pore areas with diameter d on layer i	
$A_{d,gel,i}$	gel pore areas with diameter d on layer i	
$A_{por}(\alpha)$	total capillary pore wall area	
$A_{wat}(\alpha)$	pore wall area of capillary pore filled with water	
$B_{BFS(or\ FA)}$	coefficient to calculate the dissolution rate of BFS (or FA)	
C_D	constant in Davies equations	
$D_{Ca,OH}$	mean diffusion coefficient of Ca^{2+} and OH^- ions in the solution	
$E_{a,BFS}$	activation energy of BFS	[kJ/mole]
$E_{a,FA}$	activation energy of FA	
F_1	factor to quantify the influence of temperature on the reaction activity	
F_2	factor to quantify the influence of temperature on the morphology and structure of hydration products	
I_m	ionic strength of pore solutions	

K_0	basic penetration rate of the reaction front of a hydrating particle PC [μm/hour]	[μm/hour]
$L_{REV,CSH}$	length of the 3D microstructure of CSH gel	[μm]
$L_{REV,paste}$	length of the 3D microstructure of cement paste	[μm]
M_A	molar mass of A. A can be C_3AH_6, K_2O, Na_2O, C_3S, C_2S, C_3A, C_4AF, AFm, AFt, AS, BFS, C, CH, CSH, FH_3, FA, HT, S, water.	[g/mole]
M_{pH}	factor that represents the influence of pH on the penetration rates of BFS and FA particle	
$N_{x_i,A}$	number of particles in fraction i for each 1 g A. A can be PC, BFS, FA and CH.	
$N_{x_i,REV,A}$	number of A particles in fraction i in the 3D microstructure. A can be PC, BFS and FA.	[mole]
$N_{dig,tot}$	total number of voxels in the simulated 3D microstructure	
N_{frac}	number of fractions for particle size	[mole]
N_{gyp}	number of gypsum particles	
$N_{ou,globule}$	number of mono-size spheres for the nanostructure of outer CSH gel in the REV of outer CSH gel	
$N_{slice,CSH}$	number of slices to digitalize the 3D microstructure of CSH gel	
$N_{slice,paste}$	number of slices to digitalize the 3D microstructure of cement paste	
$R_{ou;x_i,j}$	radius of the outer product of a central particle	[μm]
$V_{REV,Bk}$	initial volume of PC, BFS and FA in the simulated 3D microstructure	[μm^3]
$V_{x_i,PC}$	volume of central PC particle	[μm^3]
$V_{REV,CSH}$	volume of the 3D structure of outer CSH gel	[nm^3]
$V_{ad,j}$	volume of water adsorbed by CSH gel for 1g initial cement at time t_j	[cm^3]
$V_{chsh,j,A}$	chemical shrinkage of hydrating (or reacting) A. A can be PC, BFS and FA	[cm^3]
$V_{chsh,j,tot}$	value of the chemical shrinkage of blended cement paste at time t_j	[cm^3]
$V_{con,j,A}$	volume of reacted A at time t_j. A can be C_3S, C_2S, C_3A, C_4AF, AS, BFS, C, CH, S, gypsum, PC, FA, water.	
$V_{em,x_i,A,B}$	embedded volumes of A for the central B particle. A and B can be PC, BFS and FA	[μm^3]
$V_{f,d,cap}$	volume fraction the pores with diameter d in the 3D microstructure of cement paste	
$V_{f,d,gel}$	volume fraction the pores with diameter d in the 3D microstructure of CSH gel	
$V_{f,d,in,gel,j,paste}$	volume fraction of inner gel pores with diameter d in the 3D microstructure of cement paste	
$V_{f,d,in,gel}$	volume fraction of gel pores with diameter d in the 3D microstructure of inner CSH gel	
$V_{f,d,ou,gel,j,paste}$	volume fraction of outer gel pores with diameter of d in the 3D microstructure of cement paste	
$V_{f,d,ou,gel}$	volume fraction of gel pores with diameter of d in the 3D microstructure of outer CSH gel	
$V_{fr,j,wat,tot}$	volume of free water in capillary pore at time t_j	[cm^3]
$V_{globule}$	volume of CSH globule	[nm^3]
V_{gyp}	volume of gypsum particles	[cm^3]
$V_{j,CH,tot}$	volume of total CH in the system at time t_j	[cm^3]

$V_{ou,<x_i,j,A}$	expansion caused by embedding A for a central PC particle. A can be PC, BFS, FA and CH.	[µm^3]
$V_{ou,tot;x,j,A}$	total outer product volume of A particle (extra growth is taken into account) at time t_j. A can be PC, BFS and FA	[µm^3]
$V_{ou;x_i,j}$	volume of outer product for the central particle with diameter x_i at time t_j	[cm^3]
$V_{por,j}$	volume of capillary pore for 1 g initial cement at time t_j	[cm^3]
$V_{product,j,tot,A}$	total volume of products produced by the pozzolanic reaction of A at time t_j. A can be PC, BFS and FA	[µm^3]
V_{ratio,B_k}	initial volume fraction of PC, BFS and FA in the cement paste; B_1 = PC; B_2 = BFS; B_3 = FA	
$V_{re,j,A}$	volume of remaining phase A in the system at time t_j	[cm^3]
$V_{solid,j}$	total volume of solid phase in the system at time t_j	[µm^3]
$V_{unre,x_i,PC}$	volume of unreacted phase of PC particle with a diameter of x_i	[cm^3]
$V_{wat,in}$	volume of capillary water at mixing time	[cm^3]
$V_{wat,j}$	volume of wet capillary pore at time t_j	[cm^3]
$V_{wet,in}$	volume of capillary pore filled with water at mixing time	[cm^3]
$W_{x_i,A}$	mass of particles in fraction i for each 1 g A. A can be PC, BFS and FA.	[g]
$W_{x_i,cal,A}$	recalculated mass of particles in fraction i for 1 g A. A can be PC, BFS and FA.	[g]
$W_{CSH,FA}$	molar mass of CSH produced by pozzolanic reaction of FA	[g/mole]
W_{tot,B_k}	total mass of particles between minimum and maximum diameters	[g]
$b_{A,B}$	binding factors (A bound by hydration products B). A can be Na^+ and K^+ for AFm produced by the hydration of PC	[ml/g]
$c_{A,S}$	concentration of A in the supersaturated pore solution. A can be Na^+, K^+ Ca^{2+} and OH^-.	[mole/L]
c_A	concentration of A in the pore solution. A can be Na^+, K^+ Ca^{2+}, OH^- and SO_4^{2-}.	[mole/L]
d_{CH}	mean diameter of $Ca[OH]_2$ unit in the nucleus	
$f_{A,B}$	mass fraction of A in B. A can be Na_2O and K_2O. B can be PC, BFS and FA.	
f_A	weight fraction of A in PC. A can be C_3S, C_2S, C_3A, C_4AF and gypsum	
$f_{dig,j,A}$	volume fraction of A in the simulated 3D microstructure at time t_j. A can be hollow core, PC, BFS, FA, CH, capillary pore, inner product, outer product, solid phase.	
$k_{K_2O,PC}$	mass fraction of K_2O in the form of sulphate in PC	
$k_{Na_2O,PC}$	mass fraction of Na_2O in the form of sulphate in PC	
$m_{A,j,B}$	weight of products formed by hydrating (or reacting) B at time t_j. B can be PC, BFS and FA	[g]
m_{F1}	coefficients to calculate the activation energy of PC	
$m_{con,j,A,B}$	mass of A consumed by hydrating (or reacting) B at time t_j. B can be C_3S, C_2S, C_3A, C_4AF, PC, BFS and FA	[g]
n_{F1}	coefficients to calculate the activation energy of PC	
$n_{con,1st,C_3A}$	amount of reacted C_3A from initial time to first boundary time	[mole]
$n_{con,1st,C_4AF}$	amount of reacted C_4AF from initial time to first boundary time	[mole]

$n_{con,1st,wat,C_3A}$	amount of water consumed by the hydration of C_3A up to the first boundary time	[mole]
$n_{con,1st,wat,C_4AF}$	amount of water consumed by the hydration of C_4AF up to the first boundary time	[mole]
$n_{con,2nd,C_3A}$	amount of reacted C_3A from the first boundary time to the second boundary time	[mole]
$n_{con,2nd,C_4AF}$	amount of reacted C_4AF from the first boundary time to the second boundary time	[mole]
$n_{con,2nd,wat,C_3A}$	amount of water consumed by the hydration of C_3A from the first boundary time to the second boundary time	[mole]
$n_{con,2nd,wat,C_4AF}$	amount of water consumed by the hydration of C_4AF from the first boundary time to the second boundary time	[mole]
$n_{con,j,A,B}$	amount of A consumed by hydrating (or reacting) B at time t_j. B can be C_3S, C_2S, C_3A, C_4AF, PC, BFS and FA.	[mole]
$n_{con,j,A}$	amount of hydrated (or reacted) A. A can be C_3S, C_2S, C_3A, C_4AF, PC, BFS and FA.	[mole]
$n_{j,CH,tot}$	amount of total CH in the system	[mole]
$n_{re,0,gyp}$	amount of gypsum at mixing time	
$n_{re,1st,AFt,PC}$	amount of AFt produced by the hydration of C_3A and C_4AF up to the first boundary time	[mole]
$n_{re,in,gyp}$	initial amount of gypsum in 1 g initial blended cement	[mole]
$n_{re,j,A}$	amount of remaining A in the system.	[mole]
$n_{wat,A}$	amount of water consumed by the reaction of 1 mole A. A can be BFS and FA.	[mole]
$pH_{ref,A}$	pH in the pore solution to determine the initial penetration rate of the reaction front of A particles. A can be BFS and FA	
w_{REV,B_k}	mass of PC, BFS and FA in the simulated 3D microstructure	[g]
$w_{chem,j,A}$	chemical bound water of the products for 1 g A. A can be PC, BFS and FA	[g]
$\Delta\delta_{in,x_i,j+1}$	incremental increase of the penetration depth of a PC, BFS or FA particle x_i during a time increment $\Delta t_{j+1} = t_{j+1} - t_j$	[µm]
$\Omega_1,\ \Omega_2,\ \Omega_3$	reduction factors allowing for the change of water distribution and change in pore water chemistry in the system	
α_{1st,C_3A}	degree of hydration of C_3A at first boundary time	
α_{1st,C_4AF}	degree of hydration of C_4AF at first boundary time	
α_{2nd,C_3A}	increase of the degree of hydration of C_3A and C_4AF up to the second boundary time.	
α_{2nd,C_4AF}	increase of the degree of hydration of C_4AF up to the second boundary time.	
α_{j,C_2S}	degree of hydration of C_2S at time t_j	
α_{j,C_3A}	degree of hydration of C_3A at time t_j	
α_{j,C_3S}	degree of hydration of C_3S at time t_j	
α_{j,C_4AF}	degree of hydration of C_4AF at time t_j	
$\alpha_{j,gyp}$	degree of hydration of gypsum at time t_j	
$\gamma_{Ca^{2+}}$	activity coefficients of Ca^{2+} ions	
$\gamma_{Ca^{2+}}$	activity coefficients of OH^- ions	
γ_{BFS}	dissolution rate of BFS	[kg·m^{-2}day^{-1}]

γ_{FA}	dissolution rate of FA	[kg·m^{-2}day^{-1}]
$\gamma_{cal,RRB}$	correction factor to recalculate the mass of particle size in each fraction for RRB distribution	
$\gamma_{cal,log}$	correction factor to recalculate the mass of particle size in each fraction for RRB distribution	
$\delta_{ou;x,j}$	thickness of the outer shell	[µm]
δ_{tr}	transition thickness of the shell of hydration products when the hydration mechanism of PC particle changes from phase boundary reaction to diffusion-controlled reaction	[µm]
$\zeta_{sh,x_i,A,B}$	shell density of A for a central B particle. A and B can be PC, BFS, FA and CH.	
$\zeta_{x_i,A}$	cell density of A with diameter of x_i. A can be PC, BFS, FA and CH.	
κ_T	coefficient to quantify the influence of temperature on the volume change of hydration products	
$\nu_{j,20,PC,excl\ CH}$	volume increase ratio of PC hydration at temperature 20 ºC and time t_j (CH is not taken into account).	
$\nu_{j,T,Bk}$	volume increase ratio of PC, BFS and FA at time t_j and temperature T	
ρ_A	density of a phase A.	[g/cm^3]
ω_0	water-to-binder ratio of cement paste	
ϕ_0	minimum diameter of pore	
$\phi_{hollow,FA}$	volume fraction of hollow core in FA particles	
$\phi_{por;\alpha}$	maximum diameter of pore	[µm]
$\phi_{wat;\alpha}$	diameter of wet pore	[µm]
A	constant in Davies equations	
$m(C_3S)$	weight of reacted C_3S	[g]
$\Delta w_{x_i,j,A}$	water consumed by the pozzolanic reaction of central A particle between time t_{j-1} and t_j. A can be PC, BFS and FA.	[g]
$\Delta w_{em;x_i,j,BFS,BFS}$	water consumption of embedded A in B particle between time t_{j-1} and t_j. A and B can be PC, BFS and FA.	[g]
$\Delta\alpha_{x_i,j,A}$	increase of the degree of pozzolanic reactions of A particle with diameter x_i from time increment $\Delta t_j = t_j - t_{j-1}$. A can be C_3S, C_2S, C_3A, C_4AF, PC, BFS and FA	
ζ	shell density	
λ	coefficient to control reaction mechanisms (phase boundary diffusion controlled reactions)	
χ	stereometric conversion factor in HYMOSTRUC3D	

Appendix

A: Reactions of PC, BFS and FA particles in the system

The following steps are used to simulate the reactions of PC, BFS and FA particles:

1. Definition of representative elementary volume (REV) of cement paste.
2. Calculation of weight of PC, BFS and FA in REV.
3. Description of particle size distribution of PC, BFS and FA.
4. Calculation of number of PC, BFS and FA particles in REV.
5. Diameter of hollow core in FA particles.
6. Definition of cell and shell.
7. Reaction rates of PC, BFS and FA particles.

A.1 Definition of representative elementary volume of cement paste

A representative elementary volume (REV) of cement paste is defined as a cube with size $100 \times 100 \times 100$ μm^3 (Fig. A.1). No initial air bubble is contained in this cube. To simulate the spatial distribution of particles in the REV of cement paste, the number of PC, BFS and FA particles are calculated first. In HYMOSTRUC3D-E, the number of PC, BFS and FA particles in the REV of cement paste is calculated from the mixture compositions and properties of cements, including water-to-binder ratio (w/b), contents and particle size distribution of PC, BFS and FA. The following sections A.2 to A.4 will describe the calculation process.

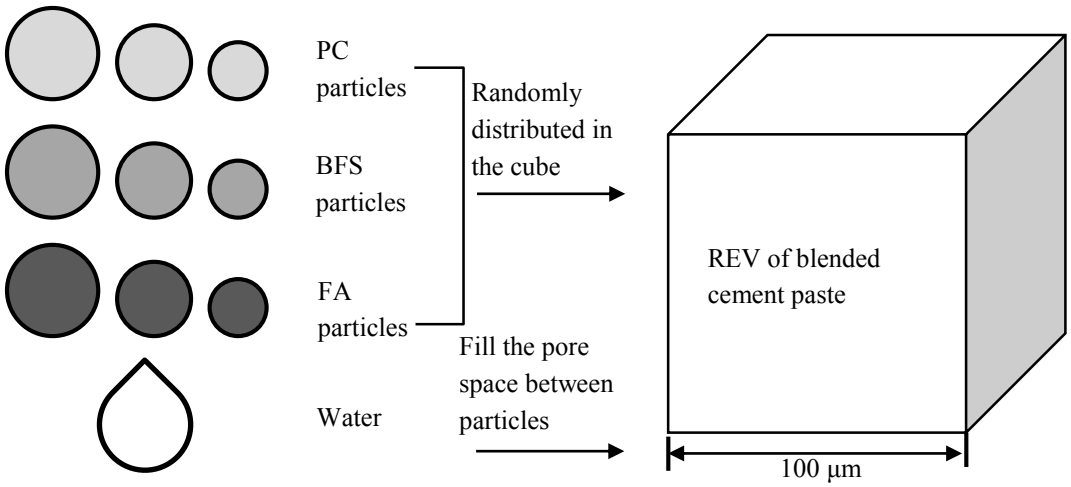

Fig. A.1 Schematic picture of simulating spatial distribution of PC, BFS and FA particles in the REV of cement paste (REV means representative elementary volume of cement paste)

A.2 Calculation of weight of PC, BFS, and FA in REV

The weight of PC, BFS and FA in the REV of cement paste is calculated from the mixture composition of blended cement paste. For a blended cement paste with 1g blended cement and a given w/b, the volume of the blended cement paste $V_{paste,0}$ is:

$$V_{paste,0} = f_{PC}/\rho_{PC} + f_{BFS}/\rho_{BFS} + f_{FA}/\rho_{FA} + \omega_0/\rho_{wa} \quad [cm^3] \quad (A.1)$$

where f_{PC}, f_{BFS}, f_{FA} are the weight of PC, BFS and FA in 1g blended cement [g], respectively. ρ_{PC}, ρ_{BFS}, ρ_{FA}, ρ_{wa} are the density of PC, BFS, FA and water [g/cm^3], respectively. ω_0 is the water-to-binder ratio (w/b).

The volumes V_{ratio,B_k} of PC, BFS and FA at mixing time in the cement paste are:

$$V_{ratio,B_k} = f_{B_k}/(\rho_{B_k} \times V_{paste,0}) \quad [cm^3/cm^3] \quad (A.2)$$

where $B_{k=1} = PC$, $B_{k=2} = BFS$, $B_{k=3} = FA$

The volumes V_{REV,B_k} of PC, BFS, and FA in the REV of cement paste are:

$$V_{REV,B_k} = V_{ratio,B_k} \times L^3_{REV,paste} \quad [\mu m^3] \quad (A.3)$$

where $L_{REV,paste}$ is the length of the REV of cement paste.

The weight of PC, BFS, and FA w_{REV,B_k} in the REV of cement paste are:

$$w_{REV,B_k} = V_{REV,B_k} \times 10^{-12} \times \rho_{B_k} \quad [g] \quad (A.4)$$

A.3 Description of particle size distribution of PC, BFS and FA

In 1933, Rosin and Rammler proposed a mathematical expression to describe the particle size distribution of materials obtained by cracking *[Rosin et al., 1933]*. This mathematical expression is called RRB distribution:

$$G(x) = 1 - exp(-bx^n) \quad [g] \quad (A.5)$$

where $G(x)$ is the cumulative weight of particle $G(x)$. x is the diameter of particle. n and b are fitting parameters.

In HYMOSTRUC3D-E, RRB distribution is used to describe the particle size distribution of PC, BFS and FA particles. In Eq. A.5, x arranges from 0 μm to ∞ μm. It is difficult to place all the particles that arrange from 0 μm to ∞ μm the REV of cement paste. To solve this

Table A.1 Fractions of diameters of particles for RRB distribution

Diameters	Fraction sequence	Fraction boundary
x_1 (x_{min})	1	x_1 to x_2
x_2	2	
x_3	3	
…	…	…
x_n (x_{max})	N_{frac}	x_{n-1} to x_{n-2}

problem the minimum and maximum diameters are introduced in HYMOSTRUC3D-E. Only the particles between the minimum and maximum diameter will be placed in the REV of cement paste. To place these particles in the REV of cement paste conveniently, N_{frac} fractions between the minimum and maximum diameters are introduced (Table A.1).

For each 1 g PC, BFS and FA particles, the weight of particles W_{x_i,B_k} in fraction *i* is:

$$W_{x_i,B_k} = G(x_{i+1}) - G(x_i) \quad [g] \qquad (A.6)$$

The total weight of particles W_{tot,B_k} between minimum and maximum diameters is:

$$W_{tot,B_k} = \sum_{i=1}^{n} W_{x_i,B_k} \quad [g] \qquad (A.7)$$

Because the particles in the range outside the minimum size and the maximum size are not placed in the REV of cement paste, the weight of the particles in the REV will be smaller than the weight of the particles in cement paste. In HYMOSTRUC3D-E, a correction factor $\gamma_{cal,RRB}$ is introduced to compensate these underestimated particles (Eq.(A.8)):

$$\gamma_{cal,RRB} = \frac{G(\infty) - G(0)}{G(max) - G(min)} = \frac{1}{G(max) - G(min)} \quad [g] \qquad (A.8)$$

The weight of particles W_{x_i,cal,B_k} in a fraction *i* is recalculated:

$$W_{x_i,cal,B_k} = (G(x_{i+1}) - G(x_i)) \times \gamma_{cal,RRB} \quad [g] \qquad (A.9)$$

A.4 Calculation of number of PC, BFS and FA particles in the REV of cement paste

For each 1 g PC, BFS and FA, the number N_{x_i,B_k} of particles in fraction *i* is:

$$N_{x_i,B_k} = W_{x_i,r,B_k} \times 10^{12} / \left(\frac{\pi x_i^3}{6} \times \rho_{B_k} \right) \quad \text{(A.10)}$$

For a fraction *i*, the number N_{x_i,REV,B_k} of PC, BFS and FA particles in the REV of cement paste is:

$$N_{x_i,REV,B_k} = w_{REV,B_k} \times N_{x_i,B_k} \quad \text{(A.11)}$$

A.5 Diameter of hollow core in FA particles

In HYMOSTRUC3D-E, it is assumed that all FA particles have hollow cores, and for each FA particle the volume fraction of hollow cores is equal to $\phi_{hollow,FA}$. For the diameter of the hollow cores of FA particles $x_{i,hollow,FA}$, it holds:

$$x_{i,hollow,FA} = x_i \times \left(\phi_{hollow,FA}\right)^{1/3} \quad \mu m \quad \text{(A.12)}$$

A.6 Definition of cell and shell

With progress of the hydration process, a number of PC, BFS and FA particles can become embedded in the outer product of other particles (Fig. A.2). These particles are defined as embedded particles *[Van Breugel, 1991]*. These embedded particles will affect the hydration process and the morphology of hydration products. To quantify these two effects, Van Breugel *[1991]* introduced the concept of cell and shell of particles.

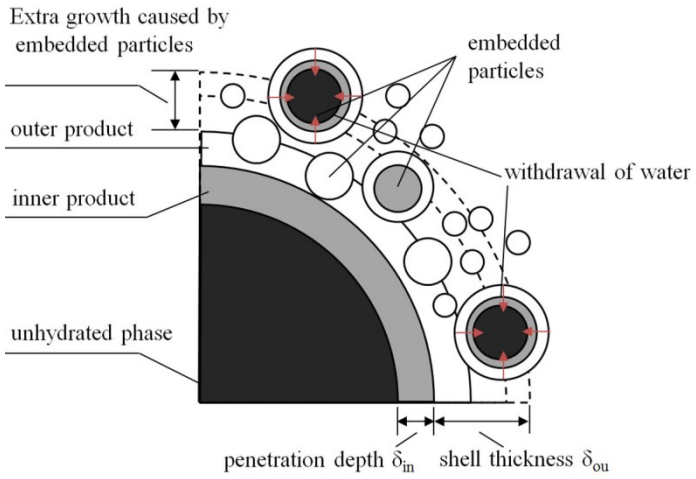

Fig. A.2 Schematic representation of the embedding particle concept [after Van Breugel, 1991]

a. Definition of cell

A cell I_x^c is defined as a cubic space in which the diameter of the largest particle is x_i (Fig. A.3). This cell contains the particles from fraction *1* to fraction *i*. There is only one particle of fraction *i* in this cell and this particle is located in the centre of cell. Accordingly, this particle is defined as *central particle*. Other particles in each fraction (<*i*) are assumed to be homogenously distributed in the cell.

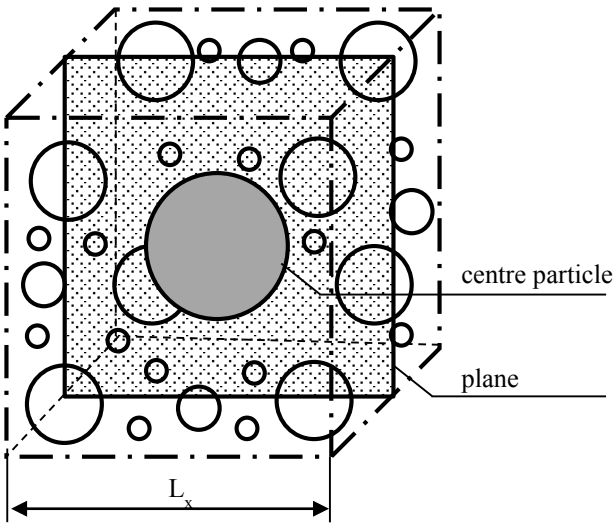

Fig. A.3 Schematic representation of the definition of cell in HYMOSTRUC3D (after van Breugel [1991])

In HYMOSTRUC, the volume of cell I_x^C is:

$$I_x^C = (V_w + V_{\leq x})/N_x \quad \text{cm}^3 \qquad \text{(A.13)}$$

where N_x is the number of particles in the fraction with a diameter x μm. V_w is the volume of water for 1 g cement. $V_{\leq x}$ is the volume of particles $\leq x$.

The cell density ζ_x is defined as the ratio of the cement volume to the cell volume:

$$\zeta_x = V_{\leq x}/(V_w + V_{\leq x}) \qquad \text{(A.14)}$$

In HYMOSTRUC3D-E the concept of cell is also used. Since there are four kinds of *central particles* (PC, BFS, FA and CH), four categories of cells are defined. In addition, the volumes of the cells of four categories, i.e. $I_{x_i,PC}^C, I_{x_i,BFS}^C, I_{x_i,FA}^C, I_{x_i,CH}^C$, for the same fraction is equal to each other. It holds:

$$I_{x_i,PC}^C = I_{x_i,BFS}^C = I_{x_i,FA}^C = I_{x_i,CH}^C =$$

$$\frac{V_w + V_{\leq x_i,PC} \times f_{PC} + V_{\leq x_i,BFS} \times f_{BFS} + V_{\leq x_i,FA} \times f_{FA}}{N_{x_i,PC} \times f_{PC} + N_{x_i,BFS} \times f_{BFS} + N_{x_i,FA} \times f_{FA}} \quad \text{cm}^3 \qquad \text{(A.15)}$$

where $V_{\leq x_i,PC} = W_{\leq x_i,cal,PC}/\rho_{PC}$, $V_{\leq x_i,BFS} = W_{\leq x_i,cal,BFS}/\rho_{BFS}$, $V_{\leq x_i,FA} = W_{\leq x_i,cal,FA}/\rho_{FA}$.

Similar to (A.13), four categories of cell density are introduced:

a1. For the cell density of PC, it holds:

$$\zeta_{x_i,PC} = \frac{V_{\leq x_i,PC} \times f_{PC}}{N_x \times I_{x_i,PC}^C} \qquad \text{(A.16)}$$

where $N_x = N_{x_i,PC} \times f_{PC} + N_{x_i,BFS} \times f_{BFS} + N_{x_i,FA} \times f_{FA}$

a2. For the cell density of BFS, it holds:

$$\zeta_{x_i,BFS} = \frac{V_{\leq x_i,BFS} \times f_{BFS}}{N_x \times I_{x_i,BFS}^C} \qquad \text{(A.17)}$$

a3. For the cell density of FA, it holds:

$$\zeta_{x_i,FA} = \frac{V_{\leq x_i,FA} \times f_{FA}}{N_x \times I_{x_i,FA}^C} \qquad \text{(A.18)}$$

a4. For the cell density of CH, it holds:

$$\zeta_{x_i,CH} = \frac{V_{\leq x_i,CH} \times f_{CH}}{N_x \times I^C_{x_i,CH}} \quad \text{(A.19)}$$

b. Definition of shell

Shell is defined as the space surrounds a *central particle*. This space is considered to contain the particles with diameters smaller than *central particle*. The ratio of the smaller particles volume to the total shell volume is defined as *shell density*. Because there are four categories of *central particle* and four kinds of particles in the cell of *central particle*, sixteen shell densities are defined as follows.

If the central particle is PC:

b1. For the shell density of PC particle, it holds:

$$\zeta_{sh,x_i,PC,PC} = \frac{\zeta_{x_i,PC} \times I^C_{x_i,PC} - V_{x_i,PC}}{I^C_{x_i,PC} - V_{x_i,PC}} \quad \text{(A.20)}$$

b2. For the shell density of BFS particles, it holds:

$$\zeta_{sh,x_i,BFS,PC} = \frac{\zeta_{x_i,BFS} \times I^C_{x_i,PC}}{I^C_{x_i,PC} - V_{x_i,PC}} \quad \text{(A.21)}$$

b3. For the shell density of FA particles, it holds:

$$\zeta_{sh,x_i,FA,PC} = \frac{\zeta_{x_i,FA} \times I^C_{x_i,PC}}{I^C_{x_i,PC} - V_{x_i,PC}} \quad \text{(A.22)}$$

b4. For the shell density of CH particles, it holds:

$$\zeta_{sh,x_i,CH,PC} = \frac{\zeta_{x_i,CH} \times I^C_{x_i,PC}}{I^C_{x_i,PC} - V_{x_i,PC}} \quad \text{(A.23)}$$

If the central particle is BFS:

b5. For the shell density of PC particles, it holds:

$$\zeta_{sh,x_i,PC,BFS} = \frac{\zeta_{x_i,PC} \times I^C_{x_i,BFS}}{I^C_{x_i,BFS} - V_{x_i,BFS}} \quad \text{(A.24)}$$

b6. For the shell density of BFS particles, it holds:

$$\zeta_{sh,x_i,BFS,BFS} = \frac{\zeta_{x_i,BFS} \times I^C_{x_i,BFS} - V_{x_i,BFS}}{I^C_{x_i,BFS} - V_{x_i,BFS}} \quad \text{(A.25)}$$

b7. For the shell density of FA particles, it holds:

$$\zeta_{sh,x_i,FA,BFS} = \frac{\zeta_{x_i,FA} \times I^C_{x_i,BFS}}{I^C_{x_i,BFS} - V_{x_i,BFS}} \quad \text{(A.26)}$$

b8. For the shell density of CH particles, it holds:

$$\zeta_{sh,x_i,CH,BFS} = \frac{\zeta_{x_i,CH} \times I^C_{x_i,BFS}}{I^C_{x_i,BFS} - V_{x_i,BFS}} \quad \text{(A.27)}$$

If the central particle is FA:

b9. For the shell density of PC particles, it holds:

$$\zeta_{sh,x_i,PC,FA} = \frac{\zeta_{x_i,PC} \times I^C_{x_i,FA}}{I^C_{x_i,FA} - V_{x_i,FA}} \quad \text{(A.28)}$$

b10. For the shell density of BFS particles, it holds:

$$\zeta_{sh,x_i,BFS,FA} = \frac{\zeta_{x_i,BFS} \times I^C_{x_i,FA}}{I^C_{x_i,FA} - V_{x_i,FA}} \quad \text{(A.29)}$$

b11. For the shell density of FA particles, it holds:

$$\zeta_{sh,x_i,FA,FA} = \frac{\zeta_{x_i,FA} \times I^C_{x_i,FA} - V_{x_i,FA}}{I^C_{x_i,FA} - V_{x_i,FA}} \quad \text{(A.30)}$$

b12. For the shell density of CH particles, it holds:

$$\zeta_{sh,x_i,CH,FA} = \frac{\zeta_{x_i,CH} \times I^C_{x_i,FA}}{I^C_{x_i,FA} - V_{x_i,FA}} \tag{A.31}$$

If the central particle is CH:

b13. For the shell density of PC particles, it holds:

$$\zeta_{sh,x_i,PC,CH} = \frac{\zeta_{x_i,PC} \times I^C_{x_i,CH}}{I^C_{x_i,CH} - V_{x_i,CH}} \tag{A.32}$$

b14. For the shell density of BFS particles, it holds:

$$\zeta_{sh,x_i,BFS,CH} = \frac{\zeta_{x_i,BFS} \times I^C_{x_i,CH}}{I^C_{x_i,CH} - V_{x_i,CH}} \tag{A.33}$$

b15. For the shell density of FA particles, it holds:

$$\zeta_{sh,x_i,FA,CH} = \frac{\zeta_{x_i,FA} \times I^C_{x_i,CH}}{I^C_{x_i,CH} - V_{x_i,CH}} \tag{A.34}$$

b16. For the shell density of CH particles, it holds:

$$\zeta_{sh,x_i,CH,CH} = \frac{\zeta_{x_i,CH} \times I^C_{x_i,CH} - V_{x_i,CH}}{I^C_{x_i,CH} - V_{x_i,CH}} \tag{A.35}$$

Fig. A.4 shows the calculated density of PC particles embedded in the shell of central PC, BFS, FA and CH particles. For the central BFS, FA and CH particles with the same diameter, the shell density of embedded PC is the same. For the central PC particles, the shell density of embedded PC is smaller. The reason for this is the volume of central PC particle $V_{x_i,PC}$ is not taken into account to calculate the volume of PC particles embedded in the shell of central particle if the central particle is PC (see Eq. (A.20)), whereas the volume of all PC particles is taken into account to calculate the volume of PC particles embedded in the shell of central particle if the central particle is BFS, FA and CH (see Eq. (A.24), Eq. (A.28) and Eq. (A.32)).

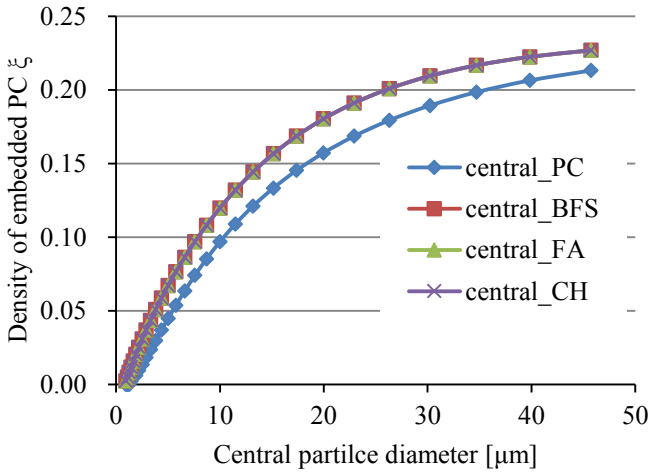

Fig. A.4 Calculated value of density of embedded PC in the shell of different central partilces. (60% wt. PC blended with 20% wt. BFS and 20% wt. FA. For the properties of PC, BFS and FA, see section 5.5)

A.7 Reactions rates of PC, BFS and FA

A.7.1 Function of reaction rates

In HYMOSTRUC3D-E the clinker components, i.e. C_3S, C_2S, C_3A and C_4AF, in PC are assumed to hydrate independently. The reaction rates of these components are described with:

$$\frac{\Delta\delta_{in,x_i,j+1,M_k}}{\Delta t_{j+1}} = K_{0,M_k} \times \Omega_1(.) \times \Omega_2(.) \times \Omega_3(.) \times F_1(.) \times \left[F_2(.) \times \left(\frac{\delta_{tr,M_k}}{\delta_{x_i,j,M_k}}\right)^{\beta_1}\right]^{\lambda_{M_k}} \quad \text{(A.36)}$$

where $\Delta\delta_{in,x_i,j+1,M_k}$ [μm] is an incremental increase of the penetration depth of the reaction front of PC components M_k during a time increment $\Delta t_{j+1} = t_{j+1} - t_j$ [hour]. $M_{k=1} = C_3S$, $M_{k=2} = C_2S$, $M_{k=3} = C_3A$, $M_{k=4} = C_4AF$. K_{0,M_k} is the basic penetration rate of M_k [μm/hour]. Ω_1, Ω_2, Ω_3 are the reduction factors allowing for the change of water distribution and change in pore water chemistry in the system. F_1 represents the influence of temperature on the rate of reaction. F_2 represents the influence of temperature on the morphology and structure of hydration products. δ_{tr} is the transition thickness of the shell of hydration products when the hydration mechanism of a PC particle changes from a *phase boundary reaction* to a *diffusion-controlled reaction*. λ_{M_k} is a coefficient to control the reaction mechanisms (from *phase boundary reaction* ($\lambda_{M_k} = 0$) to *diffusion-controlled reaction* ($\lambda_{M_k} = 1$)). β_1 is a calibration parameter.

The reaction rate of a BFS or FA particle is described as:

$$\frac{\Delta\delta_{in,x_i,j+1,S_k}}{\Delta t_{j+1}} = K_{0,S_k} \times \Omega_1(.) \times \Omega_2(.) \times \Omega_3(.) \times F_1(.) \times \left[F_2(.) \times \left(\frac{\delta_{tr,S_k}}{\delta_{x_i,j,S_k}}\right)^{\beta_1}\right]^{\lambda} \times M_{pH,S_k} \quad \text{(A.37)}$$

where $\Delta\delta_{in,x_i,j+1,S_k}$ [μm] is an incremental increase of the penetration depth of S_k ($S_{k=1}$ = BFS; $S_{k=2}$ = FA) particle during a time increment $\Delta t_{j+1} = t_{j+1} - t_j$ [hour]. K_{0,S_k} is the initial penetration rate of the reaction front of BFS and FA particle [μm/hour], respectively. δ_{tr,S_k} is the transition thickness of the shell of hydration products when the hydration mechanism of BFS and FA particle changes from *phase boundary reaction* to *diffusion-controlled reaction*. M_{pH,S_k} is the factor that represents the influence of pH on the penetration rate of BFS and FA

A.7.2 Initial penetration rate and transition thickness

(1) Method to calculate the penetration rate and the transition thickness

The penetration rate K_0 of the reaction front of a hydrating (or reacting) PC, BFS and FA particle can be determined with the particle size distribution and the measured degree of hydration (or reaction) of PC, BFS and FA particle at early age.

For a particle with a diameter x_i, and a penetration depth δ_{in,x_i}, the degree of hydration α_{x_i} is:

$$\alpha_{x_i} = 1 - \left(1 - \frac{2\delta_{in,x_i}}{x_i}\right)^3 \quad \text{(A.38)}$$

The total degree of hydration of particles α_{tot} is:

$$\alpha_{tot} = \sum_{i=1}^{i=Max} W_{x_i,cal,Bk} \times \alpha_{x_i} = \sum_{i=1}^{i=Max} \left[W_{x_i,cal,Bk} \times \left(1 - \left(1 - \frac{2\delta_{in,x_i}}{x_i}\right)^3\right)\right] \quad \text{(A.39)}$$

It is assumed that all the particles with different diameters have same penetration depth at early age. It holds:

$$\delta_{in,x_1} = \delta_{in,x_2} = \delta_{in,x_3} = \cdots = \delta_{in,x_i} \quad \text{(A.40)}$$

α_{tot} can be obtained from experiments. By combining Eq. (A.39) and Eq. (A.40), the

penetration depth of particles δ_{in} can be calculated from the total degree of hydration of particles α_{tot}. The penetration rate K_0 of the reaction front of a hydrating (or reacting) PC, BFS and FA particle is:

$$K_0 = \delta_{in}/t \tag{A.41}$$

where t is the time.

The transition thickness δ_{tr} can be calculated from the penetration depth of particles δ_{in}:

$$\delta_{tr} = \sum W(x_i) \times \left\{ \delta_{in} + \left\{ \left(\frac{x_i}{2}\right)^3 + (\nu - 1)\left[\left(\frac{x_i}{2}\right)^3 - \left(\frac{x}{2} - \delta_{in}\right)^3 \right] \right\}^{1/3} - \frac{x_i}{2} \right\} \tag{A.42}$$

where ν is the volume increase ratio of a hydrating particle.

(2) Hydration parameters for PC particles

Van Breugel *[1991]* calculated and summarized the penetration rate K_0 and transition thickness δ_{tr} for PC with different clinker compositions. He found that the values of K_0 and δ_{tr} for PC particles depend on the clinker compositions of PC:

$$K_0 = 0.02 + 6.6 \times 10^{-6} \times [C_3S\%]^2 \quad \text{[μm/hour]} \tag{A.43}$$

$$\delta_{tr} = -0.02 \times [C_2S\%] + 4 \quad \text{[μm]} \tag{A.44}$$

Nguyen *[2011]* summarized the values of K_0 and δ_{tr} for C_3S, C_2S, C_3A, C_4AF in PC particles with different clinker compositions. He found that the values of K_0 and δ_{tr} for C_3S, C_2S, C_3A, C_4AF depend on the mass fraction of clinker components in PC particles. Using linear regression he obtained the equations listed in Table A.2 to calculate the values of K_0 and δ_{tr} for C_3S, C_2S, C_3A, C_4AF in PC particles. These equations are adopted in HYMOSTRUC3D-E to calculate the values of K_0 and δ_{tr} for C_3S, C_2S, C_3A, C_4AF in PC particles.

Table A.2 Equations to calculate K_0 and δ_{tr} for different clinker components of PC [after Nguyen, 2011]

No.	Phase	K_0 [μm/h]	δ_{tr} [μm]
1	C_3S	0.064 + 0.020×(1 - % C_3S)	2.12 + 1.47×(1 - % C_3S)
2	C_2S	0.003 + 0.002×(1 - % C_2S)	2.07 + 1.15×(1 - % C_2S)
3	C_3A	1.212 - 1.171×(1 - % C_3A)	2.33 + 1.28×(1 - % C_3A)
4	C_4AF	0.02	1.19

(3) Hydration parameters for BFS and FA particles

In HYMOSTRUC3D-E, the K_0 for BFS and FA particles is calculated with the method described in A.7.2 *(1) Basic method to calculate penetration rate and transition thickness.* First, the degrees of reaction of BFS and FA with of CH and water were determined. BFS and FA were mixed with the saturated CH solution to prepare BFS paste and FA paste, respectively. The initial pH of solution was 12.5. The water-to-binder ratio was fixed at 0.4. Then, the heat release of these pastes was measured at 25 °C. To calculate the degree of reaction of BFS and FA, the maximum heat release of BFS and FA were set at 460 J/g and 800 J/g according to the reports of Kishi et al. *[1995]*, and Bentz et al. *[1997]*, respectively. The particle size distributions of BFS and FA were measured using a laser particle size analyser. Based on Eq. (A.38) to Eq. (A.42), the penetration depth can be calculated. Two examples are shown in Fig. A.5. As shown in Fig. A.4, the K_0 for BFS particles is 0.0045 μm/hours and the K_0 for FA is 0.001 μm/hour. According to the calculation using Eq. (A.42), the δ_{tr} of BFS is 0.188 μm. The δ_{tr} of FA is assumed to be close to that of PC.

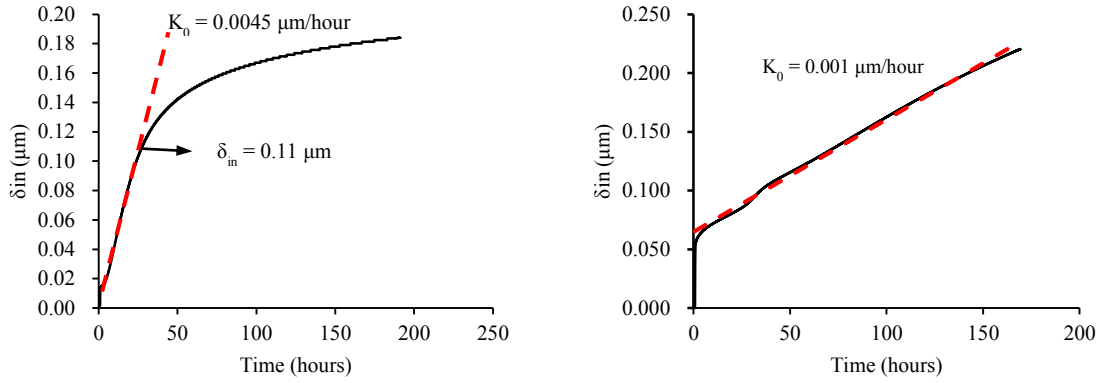

(a) K_0 for BFS particles *(b) K_0 for FA particles*

Fig. A.5 Initial penetration rate of the reaction front of a reacting BFS or FA particle

A.7.3 Reduction factor Ω_1

In HYMOSTRUC, small particles are assumed to become embedded in the growing outer shell of bigger particles. If the embedded small particles are not fully hydrated yet, they will further react, consuming water. In consequence, the amount of water for further reaction of the bigger particles will reduce. As a result, the rate of reaction of the bigger particles will decrease. This so called water withdrawal effect is accounted for the reduction factor Ω_1. The factor Ω_1 is also considered in HYMOSTRUC3D-E for the hydration of blended cements (Fig. A.6).

(1) Reduction factor Ω_1 for the hydration of a PC particle:

$$\Omega_{em;x_i,j+1,PC} = \frac{\Delta w_{x_i,j,PC}}{\Delta w_{x_i,j,PC} + \Delta w_{em;x_i,j,PC,PC} + \Delta w_{em;x_i,j,BFS,PC} + \Delta w_{em;x_i,j,FA,PC}} \quad \text{(A.45)}$$

where $\Omega_{em;x_i,j+1,PC}$ is the reduction factor Ω_1 at time t_{j+1} of a PC particle with diameter of x_i μm. $\Delta w_{x_i,j,PC}$ is the water consumption of this PC particle between time t_{j-1} and t_j. $\Delta w_{em;x_i,j,PC,PC}$, $\Delta w_{em;x_i,j,BFS,PC}$, $\Delta w_{em;x_i,j,FA,PC}$ are the water consumption of embedded PC,

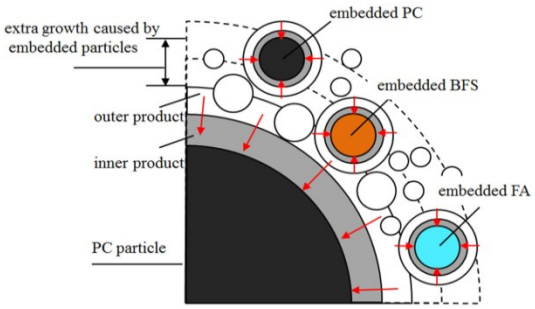

(a) the reduction factor Ω_1 for the hydration of a PC particle

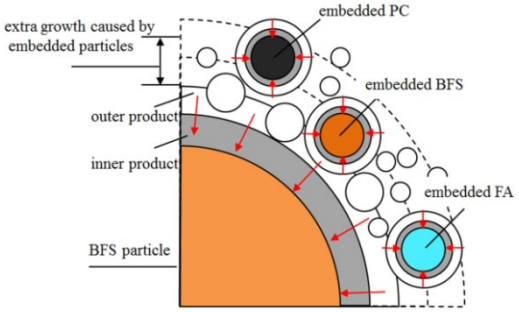

(b) the reduction factor Ω_1 for the hydration of a BFS particle

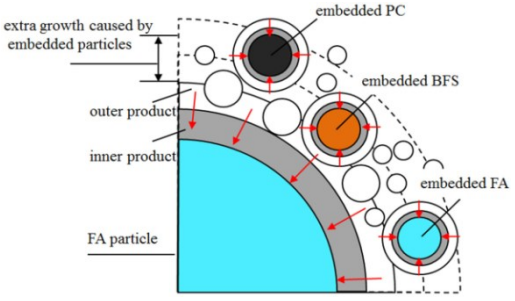

(c) the reduction factor Ω_1 for the hydration of a FA particle

Fig. A.6 Schematic pictures of the reduction factor Ω_1 for the hydration of a PC, BFS or FA particle

BFS, and FA particles between time t_{j-1} and t_j, respectively. For the calculation of $\Delta w_{x_i,j,PC}$, $\Delta w_{em;x_i,j,PC,PC}$, $\Delta w_{em;x_i,j,BFS,PC}$, $\Delta w_{em;x_i,j,FA,PC}$ see Appendix E.1.

(2) Reduction factor Ω_1 for the reaction of a BFS particle:

$$\Omega_{em;x_i,j+1,BFS} = \frac{\Delta w_{x_i,j,BFS}}{\Delta w_{x_i,j,BFS} + \Delta w_{em;x_i,j,PC,BFS} + \Delta w_{em;x_i,j,BFS,BFS} + \Delta w_{em;x_i,j,FA,BFS}} \quad \text{(A.46)}$$

where $\Omega_{em;x_i,j+1,BFS}$ is the reduction factor Ω_1 at time t_{j+1} of a BFS particle with diameter of x_i μm. $\Delta w_{x_i,j,BFS}$ is the water consumption of this BFS particle between time t_{j-1} and t_j. $\Delta w_{em;x_i,j,PC,BFS}$, $\Delta w_{em;x_i,j,BFS,BFS}$, $\Delta w_{em;x_i,j,FA,BFS}$ are the water consumption of embedded PC, BFS, and FA particles between time t_{j-1} and t_j, respectively. For the calculation of $\Delta w_{x_i,j,BFS}$, $\Delta w_{em;x_i,j,PC,BFS}$, $\Delta w_{em;x_i,j,BFS,BFS}$ and $\Delta w_{em;x_i,j,FA,BFS}$ see Appendix E.2.

(3) Reduction factor Ω_1 for the reaction of a FA particle:

$$\Omega_{em;x_i,j+1,FA} = \frac{\Delta w_{x_i,j,FA}}{\Delta w_{x_i,j,FA} + \Delta w_{em;x_i,j,PC,FA} + \Delta w_{em;x_i,j,BFS,FA} + \Delta w_{em;x_i,j,FA,FA}} \quad \text{(A.47)}$$

where $\Omega_{em;x_i,j+1,FA}$ is the reduction factor Ω_1 at time t_{j+1} of a FA particle with diameter of x_i μm. $\Delta w_{x_i,j,FA}$ is the water consumption of this FA particle time t_{j-1} and t_j. $\Delta w_{em;x_i,j,PC,FA}$, $\Delta w_{em;x_i,j,BFS,FA}$, $\Delta w_{em;x_i,j,FA,FA}$ are the water consumption of embedded PC, BFS, and FA particles time t_{j-1} and t_j, respectively. For the calculation of $\Delta w_{x_i,j,FA}$, $\Delta w_{em;x_i,j,PC,FA}$, $\Delta w_{em;x_i,j,BFS,FA}$ and $\Delta w_{em;x_i,j,FA,FA}$ see Appendix E.3.

A.7.4 Reduction factor Ω_2

With ongoing hydration water is continuously consumed and the internal relative humidity (RH) will decrease if the system is sealed (Fig. A.7). As a result, the rate of reaction of the cement particles will decrease. In HYMOSTRUC this effect of water shortage is allowed for with the reduction factor: Ω_2.

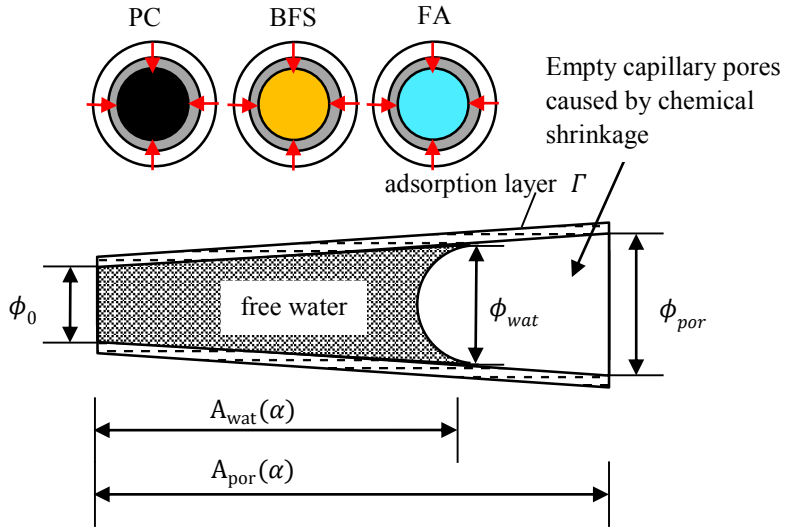

Fig. A.7 Schematic representation of the reduction factor Ω_2 for the hydration of a PC, BFS or FA particle. Note: ϕ_0 is the minimum diameter of capillary pore, and ϕ_{por} is the maximum diameter of capillary pore. ϕ_{wat} is the maximum diameter of water-filled capillary pore.

For a given system, Ω_2 is identical for all particles in the system:

$$\Omega_2(\alpha) = \frac{A_{wat}(\alpha)}{A_{por}(\alpha)} \tag{A.48}$$

where $A_{wat}(\alpha)$ and $A_{por}(\alpha)$ are the total wet capillary pore wall area and total capillary pore wall area.

To calculate $A_{wat}(\alpha)$ and $A_{por}(\alpha)$, both the pore size distribution of cement paste and the remaining water in the capillary pore should to be known. As summarized by Van Breugel *[1991]* the cumulative porosity of cement paste was approximately proportional to the log pore diameter. Using this linear relationship, both the cumulative porosity and pore size can be calculated:

$$V_{\leq\phi} = k \times V\left(ln\frac{\phi}{\phi_0}\right)^n \tag{A.49}$$

where n is set at 1, ϕ_0 is the minimum diameter of pore. k is the slope. V is the volumetric unit. k is set at 36×10^9 μm. ϕ_0 is assumed to be 0.002 μm.

$$\phi = \phi_0 \times exp\left\{\frac{V_\phi}{a}\right\} \quad [\mu m] \tag{A.50}$$

where V_ϕ is the cumulative porosity for pore diameter ϕ. a is constant which depends on type and fineness of the cement and the w/c ratio.

The maximum capillary pore size is:

$$\phi_{por} = \phi_0 \times exp\left\{\frac{V_{por}}{a}\right\} \quad [\mu m] \quad (A.51)$$

where V_{por} is the volume of total capillary pores for 1 cm^3 cement paste.

The size of the capillary pores filled with water is:

$$\phi_{wat} = \phi_0 \times exp\left\{\frac{V_{wat}}{a}\right\} \quad [\mu m] \quad (A.52)$$

where V_{wet} is the volume of total wet capillary pores for 1 cm^3 cement paste.

The volume of total capillary pores at time t_j is:

$$V_{por,j} = \frac{V_{paste,0} - V_{solid,j}}{V_{paste,0}} \quad (A.53)$$

where $V_{solid,j}$ is the volume of solid phase at time t_j in the cement paste with g blended cement.

The volume of total capillary pores filled water at time t_j is:

$$V_{wat,j} = \frac{V_{paste,0} - V_{solid,j} - V_{chsh,j} - V_{ab,j,wat}}{V_{paste,0}} \quad (A.54)$$

where $V_{cshsh,j}$ is the chemical shrinkage at time t_j for 1 g blended cement. $V_{ab,j,wat}$ is water adsorbed by CSH gel at time t_j in the cement paste with 1 g blended cement.

$A_{wat}(\alpha)$ and $A_{por}(\alpha)$ are:

$$A_{wat}(\alpha) = -4 \times k \times V \times \left\{\phi_{wat;\alpha}^{-1} - \phi_0^{-1}\right\} \quad [\mu m^2] \quad (A.55)$$

$$A_{por}(\alpha) = -4 \times k \times V \times \left\{\phi_{por;\alpha}^{-1} - \phi_0^{-1}\right\} \quad [\mu m^2] \quad (A.56)$$

Similar to that in HYMOSTRUC, $\Omega_2(\alpha)$ in HYMOSTRUC3D-E is:

$$\Omega_2(\alpha) = \frac{A_{wat}(\alpha)}{A_{por}(\alpha)} = \frac{\phi_{wat;\alpha} - \phi_0}{\phi_{por;\alpha} - \phi_0} \times \frac{\phi_{por;\alpha}}{\phi_{wat;\alpha}} \quad \text{(A.57)}$$

A.7.5 Reduction factor Ω_3

With continuing hydration the amount of capillary water available for accommodating Ca^{2+} ions will decrease. Even the assumption of a constant concentration of Ca^{2+} ions, the total amount of Ca^{2+} ions in capillary water will decrease because of the shortage of capillary water. Because Ca^{2+} is important for the formation of hydration products, such as CSH gel and CH, etc., it was estimated that the rate of reaction in the paste will decrease because of the decreasing total amount of Ca^{2+} ions in capillary water *[Van Breugel, 1991]*. In HYMOSTRUC this effect is described with Ω_3:

$$\Omega_3(\alpha) = \frac{V_{wat,j}}{V_{wat,in}} \quad \text{(A.58)}$$

where $V_{wat,in}$ is the initial volume of capillary water and $V_{wat,j}$ is the capillary water at time t_j. This reduction factor Ω_3 is also considered in HYMOSTRUC3D-E for the hydration of blended cements.

A.7.6 Temperature factor F_1

In HYMOSTRUC, F_1 is used to describe the influence of temperature on the reaction rate of PC particles. It was considered that temperature influences the activation energy of PC, which could change the reaction rate of PC particles. The activation energy of PC is:

$$AE_{T,\alpha,C_3S} = p_0 \times \alpha \times e^{-\left(m_{F1} \times [C_3S]^{n_{F1}} + 0.025 \times T^{1.5}\right)} + 0.33 \times [C_3S] + 30 \quad \text{[kJ/mole]} \quad \text{(A.59)}$$

where m_{F1} (2.52×10^{-11}), n_{F1} (6.15) are coefficients, p_0 (76 kJ/mole) is the activation energy of cement with C_3S of 0 %.

Based on Arrhenius function, F_1 is:

$$F_1 = exp\left\{\frac{AE_{T_{20},\alpha,C_3S}}{R \times (273 + T_{20})} - \frac{AE_{T,\alpha,C_3S}}{R \times (273 + T)}\right\} \quad \text{(A.60)}$$

where T_{20} is the reference temperature (20 ºC).

In HYMOSTRUC3D-E, the influence of temperature is considered as follows:

(1) Temperature factor F_1 for a hydrating PC particle

Eq. A.64 is used to calculate the F_1 for C_3S, C_2S, C_3A, and C_4AF.

(2) Temperature factor F_1 for a reacting BFS particle

Biernacki et al. *[2002]* indicated that for the system of BFS mixed with CH and water, the temperature dependence of the rate of reaction of BFS could be described by the Arrhenius function:

$$k_{BFS} = A_{F1} \times exp(-E_a/RT) \quad \text{(A.61)}$$

where k_{BFS} is the rate constant, A_{F1} is the pre-exponential factor, E_a is the apparent activation energy. The activation energy ranged from 14.5 to 22.6 kJ/mole for different weight ratios of BFS to CH. In the work of Fernandez-Jimenez et al. *[1998]*, for the system of BFS mixed with NaOH solution, the activation energy was 50 to 58 kJ/mole.

In HYMOSTRUC3D-E, F_1 is obtained based on Arrhenius function. The activation energy is assumed to be constant for different degrees of pozzolanic reaction of BFS and temperature. Thus, the factor F_1 for a reacting BFS particle is:

$$F_1 = exp\left\{\frac{E_{a,BFS}}{R \times (273 + T_{20})} - \frac{E_{a,BFS}}{R \times (273 + T)}\right\} \quad \text{(A.62)}$$

where $E_{a,BFS}$ is the activation energy of BFS. It is set at 58 kJ/mole.

(3) Temperature factor F_1 for a reacting FA particle

Bentz *[2014]* found that the activation energy of fly ash cements (FAcontents: 10%, 40%, 60%) ranges from 33.2 to 47.2 kJ/mole. Škvára et al. *[2009]* tested the activation energy of FA activated by NaOH solution (16 mole/L). The activation energy of FA was 86.2 kJ/mole, being twice times as that of PC. The activation energy of FA reported by Škvára et al. *[2009]* is used in HYMOSTRUC3D-E. Hence, the factor F_1 for a reacting FA particle is:

$$F_1 = exp\left\{\frac{E_{a,FA}}{R \times (273 + T_{20})} - \frac{E_{a,FA}}{R \times (273 + T)}\right\} \quad \text{(A.63)}$$

where $E_{a,FA}$ is the activation energy of FA particles. It is set at 86.2 kJ/mole.

A.7.7 Temperature factor F_2

F_2 is a factor used to quantify the influence of temperature on the morphology of CSH gel in HYMOSTRUC3D. Bentur et al. *[1979]* found that both the capillary porosity and the hydration products volume decreased with the increase of curing temperature for the C_3S paste. Gallucci et al. *[2013]* also found that the density of CSH gel increased with temperature. Van Breugel *[1991]* summarized that the decrease of the volume of hydration

products decreases the thickness of the product layer. Consequently the reaction rate at diffusion controlled period increases. In contrast, with increasing the density of CSH gel, the reaction rate at diffusion controlled period decreases.
In HYMOSTRUC3D, the influence of temperature on the volume ratio of hydration product to reactant is quantified as:

$$\nu_T = \nu_{20} \times exp(-28 \times 10^{-6} \times T^2) \quad \text{(A.64)}$$

where ν_{20} is the volume ratio of hydration product to reactant at 20 ºC. It is set at 2.2 in HYMOSTRUC3D.

The influence of temperature on the morphology of CSH gel is quantified as:

$$F_2(T) = \left(\frac{\nu_T}{\nu_{20}}\right)^{\beta_2} \quad \text{(A.65)}$$

where β_2 is a calibration parameter.

In HYMOSTRUC3D-E, the influence of temperature on the morphology of hydration product of blended cement is also considered:

$$\nu_{j,T,B_k} = \nu_{j,20,B_k} \times exp(-28 \times 10^{-6} \times T^2) \quad \text{(A.66)}$$

where $\nu_{j,20,B_k}$ is the volume ratio of hydration (or reaction) product to reactant for B_k at 20 ºC, and at time t_j.

The factor F_2 for the hydration (or reaction) of PC, BFS and FA is:

$$F_2(T)_{B_k} = \left(\frac{\nu_{j,T,B_k}}{\nu_{j,20,B_k}}\right)^{\beta_2} \quad \text{(A.67)}$$

Fig. A.8 shows the calculated value of F_2 for a hydrating PC, BFS and FA particle as a function of temperature.

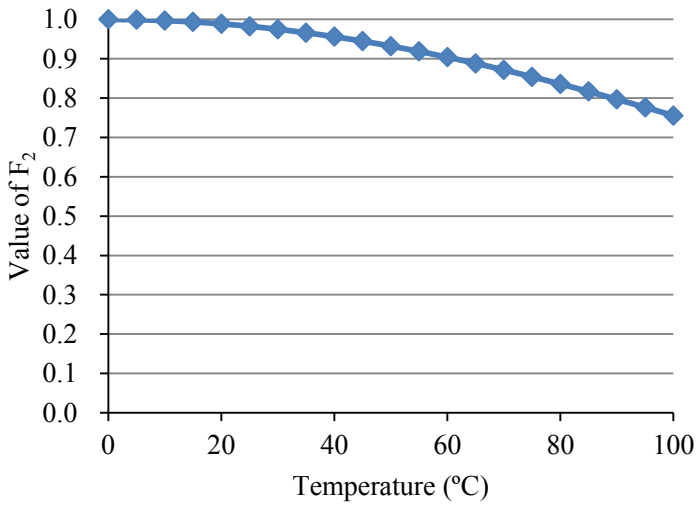

Fig. A.8 The value of F_2 for a hydrating PC, BFS and FA particle as a function of temperature

A.7.8 pH factor M_{pH}

In HYMOSTRUC3D-E, a pH factor M_{pH} is used to quantify the effect of pH on the dissolution rates of BFS and FA particles.

(1) The value of M_{pH} at time t_j or the reaction of PC particles

Jawed et al. *[1978]* summarized that the alkalis slightly accelerate the hydration of C_3S and C_2S, and remarkably reduce the acceleration period of C_3S and C_2S. The hydration of C_3A was decreased with the content of Na_2O in the system. Recently, Kumar et al. *[2012]* found that the pH increases the rate of hydration in the accelerate period, and reduces the duration of the induction, acceleration, and deceleration periods. Because the dissolution rate of PC particles is relatively high at low pH, such as pH of 7.0, the influence of pH on the penetration rate of PC particles is neglected in this study.

(2) The value of M_{pH} for the reaction of BFS particles at time t_j

For the pH from 7 up to 14, the log dissolution rate of BFS particles linearly increases with increasing the pH:

$$log(\gamma_{BFS}) = A_{BFS} \times pH + B_{BFS} \quad \text{(A.68)}$$

where γ_{BFS} is the dissolution rate of BFS, A_{BFS} and B_{BFS} are the coefficients of the linear relationship between $log(\gamma_{BFS})$ and pH.

According to Eq. (A.68), the dissolution rate of BFS particles ($\gamma_{BFS,j}$) in the pore solution

with a certain pH value at time t_j is:

$$\gamma_{BFS,j} = 10^{A_{BFS} \times pH + B_{BFS}} \quad \text{(A.69)}$$

The dissolution rate of BFS particles ($\gamma_{BFS,ref}$) in the pore solution that is used to determine the initial penetration rate of the reaction front of BFS particles ($K_{0,BFS}$) also follows Eq. (A.69):

$$\gamma_{BFS,ref} = 10^{A_{BFS} \times pH_{ref,BFS} + B_{BFS}} \quad \text{(A.70)}$$

where $pH_{ref,BFS}$ is the pH in the pore solution that is used to determine the initial penetration rate of the reaction front of BFS particles.

By combining Eq. (A.69) and (A.70), it holds:

$$\gamma_{BFS,j}/\gamma_{BFS,ref} = 10^{A_{BFS} \times (pH_j - pH_{ref,BFS})} \quad \text{(A.71)}$$

where $\gamma_{BFS,j}/\gamma_{BFS,ref}$ is introduced as the factor $M_{pH,j,BFS}$ for determining the effect of pH on the reaction rate of a BFS particle at time t_j.

(3) The value of M_{pH} for the reaction of FA particles at time t_j

Like the calculation for BFS particles, the factor M_{pH} for determining the effect of pH on the reaction rate of FA particles at time t_j is:

$$M_{pH,j,FA} = 10^{A_{FA} \times (pH_j - pH_{ref,FA})} \quad \text{(A.72)}$$

where $pH_{ref,FA}$ is the pH of pore solution used to determine $K_{0,BFS}$. A_{FA} is the slope in the linear relationship between log dissolution rate of FA and pH.

B: Degree of hydration of blended cements

Degrees of hydration of PC, and degrees of pozzolanic reaction of BFS and FA are calculated from the penetration depth of PC, BFS and FA particles:

B.1 Degree of hydration of PC

The increase of the degree of hydration $\Delta\alpha_{x_i,j,M_k}$ of C_3S, C_2S, C_3A, and C_4AF in a PC particle with diameter x_i for time increment $\Delta t_j = t_j - t_{j-1}$ is:

$$\Delta\alpha_{x_i,j,M_k} = \left(\frac{x_i/2 - \delta_{in,x_i,j-1,M_k}}{x_i/2}\right)^3 - \left(\frac{x_i/2 - \delta_{in,x_i,j-1,M_k} - \Delta\delta_{in,x_i,j,M_k}}{x_i/2}\right)^3 \quad \text{(B.1)}$$

where $\delta_{in,x_i,j-1,M_k}$ is the penetration depth of the reaction front of C_3S, C_2S, C_3A, and C_4AF at time t_{j-1}, respectively.

The total degree of hydration α_{x_i,j,M_k} of C_3S, C_2S, C_3A, and C_4AF at time t_j is:

$$\alpha_{x_i,j,M_k} = \sum_{n=1}^{j} \Delta\alpha_{x_i,n,M_k} \quad \text{(B.2)}$$

The total penetration depth δ_{in,x_i,j,M_k} of the reaction front of C_3S, C_2S, C_3A, and C_4AF at time t_j is:

$$\delta_{in,x_i,j,M_k} = (x_i/2) \times \left(1 - \left(1 - \alpha_{x_i,j,M_k}\right)^{1/3}\right) \quad \text{(B.3)}$$

The average penetration depth $\delta_{in,x_i,j,PC}$ of the reaction front of the clinker components of a PC particle with diameter x_i at time t_j is:

$$\delta_{in,x_i,j,PC} = x_i/2 - \left(\frac{V_{unre,x_i,PC}}{4\pi/3}\right)^{1/3} \quad \text{(B.4)}$$

where $V_{unre,x_i,PC}$ is the volume of the unreacted phase of a PC particle with diameter of x_i.

The total degree of hydration $\alpha_{x_i,j,PC}$ of the PC particle with diameter x_i at time t_j is:

$$\alpha_{x_i,j,PC} = 1 - \left(\frac{x_i/2 - \delta_{in,x_i,j,PC}}{x_i/2} \right)^3 \quad \text{(B.5)}$$

The increase of the total degree of hydration $\Delta\alpha_{x_i,j,PC}$ of the PC particle with diameter x_i at time t_j is:

$$\Delta\alpha_{x_i,j,PC} = \alpha_{x_i,j,PC} - \alpha_{x_i,j-1,PC} \quad \text{(B.6)}$$

The total degree of hydration $\alpha_{<x_i,j,tot,PC}$ of PC particles with diameters $< x_i$ at time t_j is:

$$\alpha_{<x_i,j,tot,PC} = \sum_{x=x_{min}}^{x=x_{i-1}} \alpha_{x_{i-1},j,PC} \times W_{x_{i-1},cal,PC} \quad \text{(B.7)}$$

The total degree of hydration $\alpha_{j,PC}$ of all PC particles at time t_j is:

$$\alpha_{j,PC} = \sum_{x=x_{min}}^{x=x_{max}} \alpha_{x_i,j,PC} \times W_{x_i,cal,PC} \quad \text{(B.8)}$$

The total degrees of hydration $\alpha_{<x_i,j,tot,M_k}$ of C_3S, C_2S, C_3A, and C_4AF at time t_j in PC particles with diameters $< x_i$ are:

$$\alpha_{<x_i,j,tot,M_k} = \sum_{x=x_{min}}^{x=x_{i-1}} \alpha_{x_{i-1},j,Mk} \times W_{x_{i-1},cal,PC} \quad \text{(B.9)}$$

The total degree of hydration α_{j,M_k} of C_3S, C_2S, C_3A, and C_4AF at time t_j in all PC particles is:

$$\alpha_{j,M_k} = \sum_{x=x_{min}}^{x=x_{max}} \alpha_{x_i,j,M_k} \times W_{x_i,cal,PC} \quad \text{(B.10)}$$

B.2 Degrees of pozzolanic reactions of BFS and FA

The increase of the degree of pozzolanic reaction $\Delta\alpha_{x_i,j,BFS}$ of a BFS particle with diameter x_i at time t_j is:

$$\Delta\alpha_{x_i,j,BFS} = \left(\frac{x_i/2 - \delta_{in,x_i,j-1,BFS}}{x_i/2}\right)^3 - \left(\frac{x_i/2 - \delta_{in,x_i,j-1,BFS} - \Delta\delta_{in,x_i,j,BFS}}{x_i/2}\right)^3 \quad \text{(B.11)}$$

where $\delta_{in,x_i,j-1,BFS}$ is the penetration depth of the reaction front of BFS particle at time t_{j-1}.

The increase of the degree of pozzolanic reaction $\Delta\alpha_{x_i,j,FA}$ of a FA particle with diameter x_i at time t_j is:

$$\Delta\alpha_{x_i,j,FA} = \frac{\left(x_i/2 - \delta_{in,x_i,j-1,FA}\right)^3 - \left(x_i/2 - \delta_{in,x_i,j-1,FA} - \Delta\delta_{in,x_i,j,FA}\right)^3}{(x_i/2)^3 - \left(x_{i,hollow,FA}/2\right)^3} \quad \text{(B.12)}$$

where $\delta_{in,x_i,j-1,FA}$ is the penetration depth of the reaction front of FA particle at time t_{j-1}.

The degree of pozzolanic reaction α_{x_i,j,S_k} of a BFS and FA particle with diameter x_i at time t_j is:

$$\alpha_{x_i,j,S_k} = \sum_{n=1}^{j} \Delta\alpha_{x_i,n,S_k} \quad \text{(B.13)}$$

where $S_{k=1}$ = BFS, $S_{k=2}$ = FA

The degree of pozzolanic reaction $\alpha_{<x_i,j,tot,S_k}$ of the BFS and FA particles with diameter $<$ x_i at time t_j is:

$$\alpha_{<x_i,j,tot,S_k} = \sum_{x=x_{min}}^{x=x_{i-1}} \alpha_{x_{i-1},j,S_k} \times W_{x_{i-1},cal,S_k} \quad \text{(B.14)}$$

The degree of pozzolanic reaction α_{j,S_k} of all BFS and FA particles from x_{min} to x_{max} is:

$$\alpha_{j,S_k} = \sum_{x=x_{min}}^{x=x_{max}} \alpha_{x_i,j,S_k} \times W_{x_i,cal,S_k} \quad \text{(B.15)}$$

C: Volume of individual phases calculated based on stoichiometry

The amount (in mole) of each phase in the cement paste with 1 g blended cement and a given w/b ratio is calculated at first. Then the volume of each phase is calculated based on mole weight and density. The mole weight and densities of individual phases in the system are listed in Appendix G.

C.1 Volume evolution of hydrating PC

The amount n_{con,j,M_k} (in mole) of reacted C_3S, C_2S, C_3A and C_4AF at time t_j is:

$$n_{con,j,M_k} = f_{PC} \times f_{M_k} \times \alpha_{j,M_k} / M_{M_k} \quad (C.1)$$

where f_{M_k} is the weight [g] of C_3S, C_2S, C_3A, C_4AF in 1 g PC, respectively. f_{PC} is the weight [g] of PC in 1 g blended cement. M_{M_k} is the molar mass of C_3S, C_2S, C_3A, C_4AF. α_{j,M_k} is the degree of hydration of C_3S, C_2S, C_3A, C_4AF.

The amount $n_{con,j,gyp}$ (in mole) of reacted (consumed) gypsum at time t_j is:

$$n_{con,j,gyp} = 3 \times \left(n_{con,j,C_3A} + n_{con,j,C_4AF}\right) \quad if \quad n_{con,j,C_3A} + n_{con,j,C_4AF} \le n_{re,in,gyp} \quad (C.2)$$

$$n_{con,j,gyp} = n_{re,in,gyp} \quad if \quad n_{con,j,C_3A} + n_{con,j,C_4AF} > n_{re,in,gyp} \quad (C.3)$$

where $n_{re,in,gyp}$ is initial amount (in mole) of gypsum in 1 g blended cement [mole].

The amount n_{re,j,M_k} (in mole) of remaining C_3S, C_2S, C_3A, and C_4AF at time t_j is:

$$n_{re,j,M_k} = f_{PC} \times f_{M_k} \times \left(1 - \alpha_{j,M_k}\right) / M_{M_k} \quad (C.4)$$

The amount $n_{re,j,gyp}$ (in mole) of remaining gypsum at time t_j is:

$$n_{re,j,gyp} = n_{re,in,gyp} - n_{con,j,gyp} \quad (C.5)$$

The amount $n_{re,j,CSH,PC}$ (in mole) of CSH produced by the hydration of PC at time t_j is:

$$n_{re,j,CSH,PC} = n_{con,j,C_3S} + n_{con,j,C_2S} \quad (C.6)$$

The amount $n_{re,j,CH,PC}$ (in mole) of CH produced by the hydration of PC at time t_j is:

$$n_{re,j,CH,PC} = 1.3 \times n_{con,j,C_3S} + 0.3 \times n_{con,j,C_2S} + 1 \times n_{con,j,C_4AF} \quad \text{(C.7)}$$

where 1.3, 0.3 and 1 are the stoichiometric coefficients for the hydration of C_3S, C_2S and C_4AF.

The amount $n_{re,j,FH_3,PC}$ (in mole) of FH_3 produced by the hydration of PC at time t_j is:

$$n_{re,j,FH_3,PC} = n_{con,j,C_4AF} \quad \text{(C.8)}$$

The progresses of the hydration process of C_3A and C_4AF are divided into three stages depending on the amount of remaining gypsum and AFt (Fig. C.1). The water consumed by the hydration of PC, and the remaining AFt, AFm, and C_3AH_6 are also divided into three stages.

(1) In stage 1: if gypsum exits in the system

The condition of stage 1 is $n_{con,j,C_3A} + n_{con,j,C_4AF} < n_{re,in,gyp}$. The amount (in mole) $n_{con,j,wat,PC}$ of water consumed by the hydration of PC at time t_j is:

$$n_{con,j,wat,PC} = \begin{pmatrix} 5.3 \times n_{con,j,C_3S} + 4.3 \times n_{con,j,C_2S} + \\ 26 \times n_{con,j,C_3A} + 30 \times n_{con,j,C_4AF} \end{pmatrix} \quad \text{(C.9)}$$

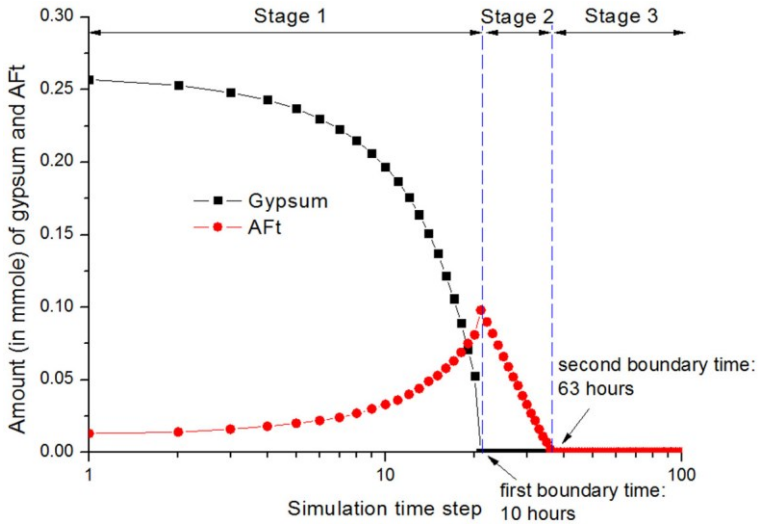

Fig. C.1 Schematic representation of three stages to calculate the volume evolution of phases of hydrating C_3A and C_4AF as a function of the amount of gypsum and AFt.

The chemical bound water $w_{chem,j,PC}$ [g] of the hydration product for 1 g PC is:

$$w_{chem,j,PC} = \left(\frac{5.3 \times f_{C_3S}}{M_{C_3S}} + \frac{4.3 \times f_{C_2S}}{M_{C_2S}} + \frac{26.0 \times f_{C_3A}}{M_{C_3A}} + \frac{30.0 \times f_{C_4AF}}{M_{C_4AF}}\right) \times M_{wat} \quad \text{(C.10)}$$

where M_{wat} is the molar mass of H_2O.

The amount $n_{re,j,AFt,PC}$ (in mole) of remaining AFt at time t_j is:

$$n_{re,j,AFt,PC} = n_{con,j,gyp}/3.0 \quad \text{(C.11)}$$

The amount $n_{re,j,AFm,PC}$ (in mole) of AFm produced by the hydration of PC at time t_j is:

$$n_{re,j,AFm,PC} = 0 \quad \text{(C.12)}$$

The amount $n_{re,j,C_3AH_6,PC}$ (in mole) of C_3AH_6 produced by the hydration of PC at time t_j is:

$$n_{re,j,C_3AH_6,PC} = 0 \quad \text{(C.13)}$$

(2) At the first boundary time (between stage 1 to stage 2)

The condition of the first boundary time (see Fig. C.1) is $n_{con,1st,C_3A} + n_{con,1st,C_4AF} = n_{re,in,gyp}$. Accordingly, it holds that:

$$n_{re,in,gyp} = f_{PC} \times \left(\frac{3.0 \times \alpha_{1st,C_3A} \times f_{C_3A}}{M_{C_3A}} + \frac{3.0 \times \alpha_{1st,C_4AF} \times f_{C_4AF}}{M_{C_4AF}}\right) \quad \text{(C.14)}$$

where α_{1st,C_3A} and α_{1st,C_4AF} are the degrees of hydration of C_3A and C_4AF at first boundary time. $n_{con,1st,C_3A}$ and $n_{con,1st,C_4AF}$ are the amounts (in mole) of reacted C_3A and C_4AF at first boundary time.

To calculate α_{1st,C_3A} and α_{1st,C_4AF}, it is assumed that the ratio of α_{1st,C_3A} to α_{1st,C_4AF} is close to $\alpha_{1st,C_3A}/\alpha_{1st,C_4AF}$ at the previous time t_{j-1} in stage 1. Accordingly, it holds that:

$$\alpha_{1st,C_4AF} = \frac{n_{re,0,gyp}}{3.0 \times f_{PC} \times \left(h_{1st,C_3A/C_4AF} \times \frac{f_{C_3A}}{W_{C_3A}} + \frac{f_{C_4AF}}{W_{C_4AF}}\right)} \quad \text{(C.15)}$$

$$\alpha_{1st,C_3A} = h_{1st,C_3A/C_4AF} \times \alpha_{1st,C_4AF} \quad \text{(C.16)}$$

where $h_{1st,C_3A/C_4AF}$ is the ratio of $\alpha_{1st,C_3A}/\alpha_{1st,C_4AF}$ in the previous time t_{j-1} in stage 1.

The amounts (in mole) of reacted (consumed) C_3A and C_4AF at the first boundary time are:

$$n_{con,1st,C_3A} = f_{PC} \times f_{C_3A} \times \alpha_{1st,C_3A}/M_{C_3A} \quad \text{(C.17)}$$

$$n_{con,1st,C_4AF} = f_{PC} \times f_{C_4AF} \times \alpha_{1st,C_4AF}/M_{C_4AF} \quad \text{(C.18)}$$

The amount $n_{con,1st,wat,C_3A}$ (in mole) of water consumed by the hydration of C_3A up to the first boundary time is:

$$n_{con,1st,wat,C_3A} = 26.0 \times n_{con,1st,C_3A} \quad \text{(C.19)}$$

The amount $n_{con,1st,wa,C_4AF}$ (in mole) of water consumed by the hydration of C_4AF up to the first boundary time is:

$$n_{con,1st,wat,C_4AF} = 30.0 \times n_{con,1st,C_4AF} \quad \text{(C.20)}$$

The amount $n_{re,1st,AFt,PC}$ (in mole) of AFt produced by the hydration of C_3A and C_4AF up to the first boundary time is:

$$n_{re,1st,AFt,PC} = n_{re,0,gyp}/3.0 \quad \text{(C.21)}$$

(3) In stage 2: If gypsum is used up and if ettringite exists in the system

The condition of stage 2 is $n_{con,j,C_3A} + n_{con,j,C_4AF} > n_{re,in,gyp}$ and $n_{re,j,AFt,PC} > 0$. The AFt consumed by the hydration of C_3A and C_4AF $n_{con,j,AFt,PC}$ in stage 2 is:

$$n_{con,j,AFt,PC} = 0.5 \times f_{PC} \times \left[\left(\alpha_{j,C_3A} - \alpha_{1st,C_3A} \right) \times \frac{f_{C_3A}}{M_{C_3A}} + \left(\alpha_{j,C_4AF} - \alpha_{1st,C_4AF} \right) \times \frac{f_{C_4AF}}{M_{C_4AF}} \right] \quad \text{(C.22)}$$

The amount $n_{re,j,gyp}$ (in mole) of remaining gypsum is:

$$n_{re,j,gyp} = 0 \quad \text{(C.23)}$$

The amount $n_{con,j,wat,PC}$ (in mole) of water consumed by the hydration of PC is:

$$n_{con,j,wat,PC} = 5.3 \times n_{con,j,C_3S} + 4.3 \times n_{con,j,C_2S} + n_{con,1st,wat,C_3A} + n_{con,1st,wat,C_4AF} + 2.0 \times \left(n_{con,j,C_3A} - n_{con,1st,C_3A}\right) + 6.0 \times \left(n_{con,j,C_4AF} - n_{con,1st,C_4AF}\right) \quad \text{(C.24)}$$

The chemical bound water $w_{chem,j,PC}$ of the hydration product for 1 g PC is:

$$w_{chem,j,PC} = \left(\frac{5.3 \times f_{C_3S}}{M_{C_3S}} + \frac{4.3 \times f_{C_2S}}{M_{C_2S}} + \frac{2.0 \times f_{C_3A}}{M_{C_3A}} + \frac{6.0 \times f_{C_4AF}}{M_{C_4AF}}\right) \times M_{wat} \quad \text{(C.25)}$$

The amount $n_{re,j,AFt,PC}$ (in mole) of remaining AFt is:

$$n_{re,j,AFt,PC} = n_{re,1st,AFt,PC} - n_{con,j,AFt,PC} \quad \text{(C.26)}$$

The amount $n_{re,j,AFm,PC}$ (in mole) of AFm produced by the hydration of PC is:

$$n_{re,j,AFm,PC} = 1.5 \times \left(n_{con,j,C_3A} - n_{con,1st,C_3A}\right) + 1.5 \times \left(n_{con,j,C_4AF} - n_{con,1st,C_4AF}\right) \quad \text{(C.27)}$$

The amount $n_{re,j,C_3AH_6,PC}$ (in mole) of C_3AH_6 produced by the hydration of PC is:

$$n_{re,j,C_3AH_6,PC} = 0.0 \quad \text{(C.28)}$$

(4) At the second boundary time (between stage 2 to stage 3)

The condition of the second boundary time (see Fig. C.1) is $n_{re,1st,AFt,PC} - n_{con,2nd,AFt,PC} = 0$. Accordingly, it holds:

$$n_{re,1st,AFt,PC} = n_{con,2nd,AFt,PC} = 0.5 \times f_{PC} \times \left(\alpha_{2nd,C_3A} \times \frac{f_{C_3A}}{M_{C_3A}} + \alpha_{2nd,C_4AF} \times \frac{f_{C_4AF}}{M_{C_4AF}}\right) \quad \text{(C.29)}$$

where α_{2nd,C_3A} and α_{2nd,C_4AF} are the increase of the degree of hydration of C_3A and C_4AF up to the second boundary time.

To calculate α_{2nd,C_3A} and α_{2nd,C_4AF}, it is assumed that the ratio of $(\alpha_{1st,C_3A} + \alpha_{2nd,C_3A})$ to $(\alpha_{1st,C_4AF} + \alpha_{2nd,C_4AF})$ is equal to $\alpha_{j,C_3A}/\alpha_{j,C_4AF}$ in the last time in stage 2. By combining Eq. (C.29), it holds:

$$\alpha_{2nd,C_4AF} = \frac{\begin{pmatrix} 2n_{re,1st,AFt,PC}/f_{PC} + \alpha_{1st,C_3A} \times f_{C_3A}/M_{C_3A} - \\ h_{2nd,C_3A/C_4AF} \times \alpha_{1st,C_4AF} \times f_{C_3A}/M_{C_3A} \end{pmatrix}}{h_{2nd,C_3A/C_4AF} \times \frac{f_{C_3A}}{M_{C_3A}} + \frac{f_{C_4AF}}{M_{C_4AF}}} \quad \text{(C.30)}$$

where $h_{2nd,C_3A/C_4AF}$ is the ratio of α_{j,C_3A} to α_{j,C_4AF} at the last time in stage 2.

$$\alpha_{2nd,C_3A} = h_{2nd,C_3A/C_4AF} \times \left(\alpha_{2nd,C_4AF} + \alpha_{1st,C_4AF}\right) - \alpha_{1st,C_3A} \quad \text{(C.31)}$$

The amounts (in mole) of water consumed by the hydration of C_3A and C_4AF from the first boundary time to the second boundary time are:

$$n_{con,2nd,wat,C_3A} = 2.0 \times n_{con,2nd,C_3A} \quad \text{(C.32)}$$

$$n_{con,2nd,wat,C_4AF} = 6.0 \times n_{con,2nd,C_4AF} \quad \text{(C.33)}$$

(5) In stage 3: After AFt is used up

The condition of stage 3 is $n_{re,1st,AFt,PC} - n_{con,j,AFt,PC} < 0$. The remaining amount $n_{re,j,AFt,PC}$ (in mole) of AFt is:

$$n_{re,j,AFt,PC} = 0 \quad \text{(C.34)}$$

The remaining amount (in mole) $n_{re,j,C_3AH_6,PC}$ of C_3AH_6 is:

$$\begin{aligned} n_{re,j,C_3AH_6,PC} &= n_{con,j,C_3A} - n_{con,1st,C_3A} - n_{con,1st,C_3A} + \\ & n_{con,j,C_4AF} - n_{con,1st,C_4AF} - n_{con,1st,C_4AF} \end{aligned} \quad \text{(C.35)}$$

The amount $n_{con,j,wat,PC}$ (in mole) of water consumed by the hydration of PC is:

$$\begin{aligned} n_{con,j,wat,PC} &= 5.3 \times n_{con,j,C_3S} + 4.3 \times n_{con,j,C_2S} + n_{con,1st,wat,C_3A} + \\ & n_{con,1st,wat,C_4AF} + n_{con,2nd,wat,C_3A} + n_{con,2nd,wat,C_4AF} + \\ & 6.0 \times \left(n_{con,j,C_3A} - n_{con,1st,C_3A} - n_{con,1st,C_3A}\right) + \\ & 10.0 \times \left(n_{con,j,C_4AF} - n_{con,1st,C_4AF} - n_{con,1st,C_4AF}\right) \end{aligned} \quad \text{(C.36)}$$

The chemical bound water $w_{chem,j,PC}$ [g] of the hydration product for 1 g PC is:

$$w_{chem,j,PC} = \left(\frac{5.3 \times f_{C_3S}}{M_{C_3S}} + \frac{4.3 \times f_{C_2S}}{M_{C_2S}} + \frac{6.0 \times f_{C_3A}}{M_{C_3A}} + \frac{10.0 \times f_{C_4AF}}{M_{C_4AF}}\right) \times M_{wat} \quad \text{(C.37)}$$

The evolution (in mole) of individual phase of hydrating PC is calculated in the above three stages. The volume evolution of individual phase of hydrating PC can be obtained as follows:

The consumed volumes of reactants (C_3S, C_2S, C_3A, C_4AF, gypsum and water) by the hydration of PC are:

$$V_{con,j,M_k} = n_{con,j,M_k} \times M_{M_k}/\rho_{M_k} \quad \text{(C.38)}$$

$$V_{con,j,gyp} = n_{con,j,gyp} \times M_{gyp}/\rho_{gyp} \quad \text{(C.39)}$$

$$V_{con,j,wat,PC} = n_{con,j,wat,PC} \times M_{wat}/\rho_{wat} \quad \text{(C.40)}$$

The total volume $V_{con,j,tot,PC}$ of reactants for the hydration of PC is:

$$V_{con,j,tot,PC} = V_{con,j,C_3S} + V_{con,j,C_2S} + V_{con,j,C_3A} + V_{con,j,C_4AF} + V_{con,j,gyp} + V_{con,j,wat,PC} \quad \text{(C.41)}$$

The volume $V_{re,j,PC}$ of unreacted PC is:

$$V_{re,j,PC} = f_{PC}/\rho_{PC} - V_{con,j,tot,PC} \quad \text{(C.42)}$$

The volume $V_{re,j,product}$ of products of components, CSH, CH, AFt, AFm, C_3AH_6 and FH_3, produced by the hydration of PC is:

$$V_{re,j,product} = n_{re,j,product} \times M_{product}/\rho_{product} \quad \text{(C.43)}$$

The total volume $V_{product,j,tot,PC}$ of products for the hydration of PC is:

$$V_{product,j,tot,PC} = V_{re,j,CSH,PC} + V_{re,j,CH,PC} + V_{re,j,AFt,PC} + V_{re,j,AFm,PC} + V_{re,j,C_3AH_6,PC} + V_{re,j,FH_3,PC} \quad \text{(C.44)}$$

The volume ratio $v_{j,20,PC}$ of products to reactants for the hydration of PC is:

$$v_{j,20,PC} = \left(V_{product,j,tot,PC} - V_{re,j,CH,PC}\right)/\left(V_{con,j,tot,PC} - V_{con,j,wat,PC}\right) \quad \text{(C.45)}$$

The chemical shrinkage $V_{chsh,j,PC}$ of hydrating PC is:

$$V_{chsh,j,PC} = V_{con,j,tot,PC} - V_{product,j,tot,PC} \quad \text{(C.46)}$$

C.2 Volume evolution of reacting BFS

HYMOSTRUC3D-E uses the stoichiometry of the reaction of BFS with CH and water based on the report of Richardson et al. *[2002]:*

$$C_{7.88}S_{7.39}M_3A+2.6CH+31.5H \rightarrow 7.39C_{1.42}SH_{2.92}A_{0.046}+0.66M_{4.6}AH_{19} \quad \text{(C.47)}$$

The amount $n_{con,j,BFS}$ (in mole) of reacted BFS is:

$$n_{con,j,BFS} = f_{BFS} \times \alpha_{j,BFS}/M_{BFS} \quad \text{(C.48)}$$

where M_{BFS} is the molar mass of BFS ($C_{7.88}S_{7.39}M_3A$). f_{BFS} is the weight [g] of BFS in 1 g blended cement. $\alpha_{j,BFS}$ is the degree of pozzolanic reaction of BFS at time t_j.

The amount $n_{con,j,CH,BFS}$ (in mole) of CH consumed by the pozzolanic reaction of BFS is:

$$n_{con,j,CH,BFS} = n_{con,j,BFS} \times n_{CH,BFS} \quad \text{(C.49)}$$

where $n_{CH,BFS}$ is the amount (in mole) of CH that consumed by the reaction of 1 mole BFS. It is equal to 2.6 based on the report of Richardson et al. *[2002]*.

The amount $n_{con,j,wat,BFS}$ (in mole) of water consumed by the pozzolanic reaction of BFS is:

$$n_{con,j,wat,BFS} = n_{con,j,BFS} \times n_{wat,BFS} \quad \text{(C.50)}$$

where $n_{wat,BFS}$ is the amount of water consumed by the reaction of 1 mole BFS. It is equal to 31.5 using the stoichiometry of the reaction of BFS mentioned in Chapter 3 (Eq. 3.10).

The amounts in mole) of CSH gel and HT ($M_{4.6}AH_d$) produced by the pozzolanic reaction of BFS are:

$$n_{re,j,CSH,BFS} = n_{con,j,BFS} \times n_{CSH,BFS} \quad \text{(C.51)}$$

$$n_{re,j,CSH,BFS} = n_{con,j,BFS} \times n_{HT,BFS} \quad \text{(C.52)}$$

where $n_{CSH,BFS}$ and $n_{HT,BFS}$ are the amount (in mole) of CSH and HT produced by the full reaction of 1 mole BFS, respectively.

The volumes of reactants (BFS, CH and water) are:

$$V_{con,j,BFS} = n_{con,j,BFS} \times M_{BFS}/\rho_{BFS} \quad \text{(C.53)}$$

$$V_{con,j,CH} = n_{con,j,CH} \times M_{CH}/\rho_{CH} \quad \text{(C.54)}$$

$$V_{con,j,wat} = n_{con,j,wat} \times M_{wat}/\rho_{wat} \quad \text{(C.55)}$$

The total volume $V_{con,j,tot,BFS}$ of reactants for the pozzolanic reaction of BFS is:

$$V_{con,j,tot,BFS} = V_{con,j,BFS} + V_{con,j,CH,BFS} + V_{con,j,wat,BFS} \quad \text{(C.56)}$$

The volume $V_{re,j,BFS}$ of unreacted BFS is:

$$V_{re,j,BFS} = f_{BFS}/\rho_{BFS} - V_{con,j,BFS} \quad \text{(C.57)}$$

The volumes of products (CSH gel and HT) produced by the pozzolanic reactions of BFS are:

$$V_{re,j,CSH,BFS} = n_{re,j,CSH,BFS} \times M_{CSH,BFS}/\rho_{CSH,BFS} \quad \text{(C.58)}$$

$$V_{re,j,HT,BFS} = n_{re,j,HT,BFS} \times M_{HT,BFS}/\rho_{HT,BFS} \quad \text{(C.59)}$$

The total volume $V_{product,j,tot,BFS}$ of products produced by the pozzolanic reaction of BFS is:

$$V_{product,j,tot,BFS} = V_{re,j,CSH,BFS} + V_{re,j,HT,BFS} \quad \text{(C.60)}$$

The volume ratio $v_{j,20,BFS}$ of products to reactants for the pozzolanic reaction of BFS is:

$$v_{j,20,BFS} = \frac{V_{product,j,tot,BFS}}{V_{con,j,tot,BFS} - V_{con,j,CH,BFS} - V_{con,j,wat,BFS}} \quad \text{(C.61)}$$

The chemical shrinkage $V_{chsh,j,BFS}$ of reacting BFS is:

$$V_{chsh,j,BFS} = V_{con,j,tot_{BFS}} - V_{product,j,tot_{BFS}} \quad \text{(C.62)}$$

The chemical bound water $w_{chem,j,BFS}$ of the pozzolanic reaction product for 1 g BFS is:

$$w_{chem,j,BFS} = n_{wa,BFS} \times M_{wat}/M_{BFS} \quad \text{(C.63)}$$

C.3 Volume evolution of reacting FA

The stoichiometry of the reaction of FA with CH and water is:

$$AS{\cdot}xS{\cdot}yC+(2+1.1x-y)CH+(6+2.8x+y)H \rightarrow xC_{1.1}SH_{3.9}+C_2ASH_8 \quad \text{(C.64)}$$

where $AS{\cdot}xS{\cdot}yC$ is the chemical formula of FA. x and y are stoichiometry coefficients. x and y can be calculated from the chemical composition of FA.

The amounts (in mole) of reacted AS, S and C in FA are:

$$n_{con,j,AS,FA} = n_{AS,FA} \times f_{FA} \times \alpha_{j,FA}/M_{FA} \quad \text{(C.65)}$$

$$n_{con,j,s,FA} = n_{S,FA} \times f_{FA} \times \alpha_{j,FA}/M_{FA} \quad \text{(C.66)}$$

$$n_{con,j,C,FA} = n_{C,FA} \times f_{FA} \times \alpha_{j,FA}/M_{FA} \quad \text{(C.67)}$$

where $n_{AS,FA}$, $n_{s,FA}$ and $n_{C,FA}$ are the amount (in mole) of AS, S, C that consumed by the reaction of 1 mole FA. They are obtained based on the stoichiometry of the pozzolanic reactions of FA in the blended system. M_{FA} is the molar mass of FA (A·xS·yC).

The amounts (in mole) of CH and H consumed by the pozzolanic reaction of FA are:

$$n_{con,j,CH,FA} = n_{CH,FA} \times f_{FA} \times \alpha_{j,FA}/M_{FA} \quad \text{(C.68)}$$

$$n_{con,j,wat,FA} = n_{wat,FA} \times f_{FA} \times \alpha_{j,FA}/M_{FA} \quad \text{(C.69)}$$

where $n_{CH,FA}$ and $n_{wat,FA}$ are the amount (in mole) of CH and water that consumed by the reaction of 1 mole FA. They are obtained based on the stoichiometry of the pozzolanic reactions of FA in the blended system.

The amounts (in mole) of CSH and ST produced by the pozzolanic reaction of fly ash are:

$$n_{re,j,CSH,FA} = n_{CSH,FA} \times f_{FA} \times \alpha_{j,FA}/M_{FA} \quad \text{(C.70)}$$

$$n_{re,j,ST,FA} = n_{ST,FA} \times f_{FA} \times \alpha_{j,FA}/M_{FA} \quad \text{(C.71)}$$

where $n_{CSH,FA}$ $n_{ST,FA}$ are the amount (in mole) of CSH, ST (C_2ASH_8) that produced by the reaction of 1 mole FA. They are obtained based on the stoichiometry of the pozzolanic reactions of FA in the blended system.

The volumes of consumed reactants (AS, S, C, CH, and water) by the pozzolanic reaction of FA are:

$$V_{con,j,AS,FA} = n_{AS,FA} \times M_{AS,FA}/\rho_{AS,FA} \quad \text{(C.72)}$$

$$V_{con,j,S,FA} = n_{S,FA} \times M_{S,FA}/\rho_{S,FA} \quad \text{(C.73)}$$

$$V_{con,j,C,FA} = n_{C,FA} \times M_{C,FA}/\rho_{C,FA} \quad \text{(C.74)}$$

$$V_{con,j,CH,FA} = n_{CH,FA} \times M_{CH}/\rho_{CH} \quad \text{(C.75)}$$

$$V_{con,j,wat,FA} = n_{wat,FA} \times M_{wat}/\rho_{wat} \quad \text{(C.76)}$$

where $n_{CH,FA}$ and $n_{wat,FA}$ are the amount (in mole) of CH and water for the full pozzolanic reaction of 1 mole FA.

For the total volume $V_{con,j,tot,FA}$ of consumed reactants for the pozzolanic reaction of FA, it holds:

$$V_{con,j,tot,FA} = V_{con,j,AS,FA} + V_{con,j,S,FA} + V_{con,j,C,FA} + V_{con,j,CH,FA} + V_{con,j,wat,FA} \quad \text{(C.77)}$$

The volume $V_{re,j,FA}$ of unreacted FA is:

$$V_{re,j,FA} = f_{FA}/\rho_{FA} - V_{con,j,AS,FA} - V_{con,j,S,FA} - V_{con,j,C,FA} \quad \text{(C.78)}$$

The volumes of products (CSH and ST) produced by the pozzolanic reaction of fly ash are:

$$V_{re,j,CSH,FA} = n_{re,j,CSH,FA} \times M_{CSH,FA}/\rho_{CSH,FA} \quad \text{(C.79)}$$

$$V_{re,j,ST,FA} = n_{re,j,ST,FA} \times M_{ST,FA}/\rho_{ST,FA} \quad \text{(C.80)}$$

The total volume $V_{product,j,tot,FA}$ of products produced by the pozzolanic reaction of FA is:

$$V_{product,j,tot,FA} = V_{re,j,CSH,FA} + V_{re,j,ST,FA} \quad \text{(C.81)}$$

The volume ratio $v_{j,20,FA}$ of products to reactants for the pozzolanic reaction of FA is:

$$v_{j,20,FA} = \frac{V_{product,j,tot,FA}}{V_{con,j,tot,FA} - V_{con,j,CH,FA} - V_{con,j,wat,FA}} \quad \text{(C.82)}$$

The chemical shrinkage $V_{chsh,j,FA}$ of reacting FA is:

$$V_{chsh,j,FA} = V_{con,j,tot,FA} - V_{product,j,tot,FA} \quad \text{(C.83)}$$

The chemical bound water $w_{chem,j,FA}$ of the pozzolanic reaction product for 1 g FA is:

$$w_{chem,j,FA} = n_{wat,FA} \times M_{wat}/M_{FA} \quad \text{(C.84)}$$

C.4 Total volume evolution in the system

The amount $n_{j,CH,tot}$ (in mole) of total CH is:

$$n_{j,CH,tot} = n_{re,j,CH,PC} - n_{con,j,CH,BFS} - n_{con,j,CH,FA} \quad \text{(C.85)}$$

The volume $V_{j,CH,tot}$ of total CH is:

$$V_{j,CH,tot} = n_{j,CH,tot} \times M_{CH}/\rho_{CH} \quad \text{(C.86)}$$

The total volume $V_{solid,j}$ of solid phase is:

$$V_{solid,j} = V_{re,j,PC} + V_{re,j,BFS} + V_{re,j,FA} + V_{product,j,tot,PC} + V_{product,j,tot,BFS} + V_{product,j,tot,FA} - V_{con,j,CH,BFS} - V_{con,j,CH,FA} \quad \text{(C.87)}$$

As mentioned above, the volume of product is affected by the temperature in the system. This influence is quantified as:

$$V_{re,j,solid_{system}} = V_{re,j,PC} + V_{re,j,BFS} + V_{re,j,FA} + \left(V_{product,j,tot_{PC}} + V_{product,j,tot_{BFS}} + V_{product,j,tot_{FA}} - V_{con,j,CH_{BFS}} - V_{con,j,CH_{FA}}\right) \times \kappa_T \quad \text{(C.88)}$$

where κ_T is equal to $\exp(-28\times10^{-6}\times T^2)$.

The chemical shrinkage $V_{chsh,j,tot}$ of blended cement paste is:

$$V_{chsh,j,tot} = V_{chsh,j,PC} + V_{chsh,j,BFS} + V_{chsh,j,FA} \quad \text{(C.89)}$$

According to Thomas et al. *[2012]*, 1 mole CSH gel produced by the hydration of PC could absorb 0.3 mole water. Also in this study, 1 mole the CSH gels produced by the hydration of PC, and the pozzolanic reaction of BSF and FA are assumed to be able to absorb 0.3 mole water. Accordingly, the total absorbed water $V_{ab,j,wat}$ is calculated:

$$V_{ab,j,wat} = 0.3 \times (n_{re,j,CSH,PC} + n_{re,j,CSH,BFS} + n_{re,j,CSHFA} \times M_{wat}/\rho_{wat}) \quad \text{(C.90)}$$

The volume fraction $f_{solid,j}$ of solid phase is:

$$f_{solid,j} = V_{solid,j}/V_{paste,0} \quad \text{(C.91)}$$

D: Volume ratio of products to reactants

Van Breugel *[1991]* calculated the volume ratio of hydration product to reactant of PC (ν_{PC}) from experimental data *[Bentur, et al., 1979]*, and found that ν_{PC} decreased from 2.2 to 1.86 with increase of hydration degree up to 0.9. In this model, the ratios for PC, BFS and FA are calculated based on the stoichiometry of chemical reactions in the system.

D.1 Volume increase ratio of a PC particle

If all hydration products are taken into account, the volume increase ratio $\nu_{j,20,PC}$ of a PC particle is:

$$\nu_{j,20,PC} = \frac{V_{re,j,CSH,PC} + V_{re,j,AFt,PC} + V_{re,j,AFm,PC} + V_{re,j,FH_3,PC} + V_{re,j,C_3AH_6,PC} + V_{re,j,CH,PC}}{V_{con,j,C_3S} + V_{con,j,C_2S} + V_{con,j,C_3A} + V_{con,j,C_4AF} + V_{con,j,gyp}} \quad \text{(D.1)}$$

where $V_{re,j,CSH,PC}$, $V_{re,j,AFt,PC}$, $V_{re,j,AFm,PC}$, $V_{re,j,FH_3,PC}$, $V_{re,j,C_3AH_6,PC}$ and $V_{re,j,CH,PC}$ are the volumes of CSH, AFt, AFm, FH_3, and C_3AH_6 produced by the hydration of PC at time t_j, respectively. V_{con,j,C_3S}, V_{con,j,C_2S}, V_{con,j,C_3A}, V_{con,j,C_4AF} and $V_{con,j,gyp}$, are the volumes of remaining C_3S, C_2S, C_4AF, C_3A and $C\bar{S}H_2$ at time t_j, respectively.

If CH is excluded in the hydration product, the volume increase ratio $\nu_{j,20,excl.,PC}$ of a PC particle is:

$$\nu_{j,20,excl.,PC} = \frac{V_{re,j,CSH,PC} + V_{re,j,AFt,PC} + V_{re,j,AFm,PC} + V_{re,j,FH_3,PC} + V_{re,j,C_3AH_6,PC}}{V_{con,j,C_3S} + V_{con,j,C_2S} + V_{con,j,C_3A} + V_{con,j,C_4AF} + V_{con,j,gyp}} \quad \text{(D.2)}$$

D.2 Volume increase ratio of a BFS particle

$$\nu_{j,20,BFS} = \frac{V_{re,j,CSH,BFS} + V_{re,j,HT,BFS}}{V_{con,j,BFS}} \quad \text{(D.3)}$$

where $V_{re,j,CSH,BFS}$ and $V_{re,j,HT,BFS}$ are the volumes of CSH and $M_{4.6}AH_{19}$ produced by the reaction of BFS at time t_j, respectively. $V_{con,j,BFS}$ is the consumed BFS volume at time t_j.

D.3 Volume increase ratio of a FA particle

$$\nu_{j,20,FA} = \frac{V_{re,j,CSH,FA} + V_{re,j,ST,FA}}{V_{con,\,j,\,FA}} \quad \text{(D.4)}$$

where $V_{re,j,CSH,FA}$ and $V_{re,j,ST,FA}$ are the volumes of CSH, C_2ASH_8 produced by the reaction of FA at time t_j, respectively. $V_{con,j,FA}$ is the consumed FA volume at time t_j.

E: Extra growth thickness of particles

The radius $R_{ou;x_i,j}$ of the outer product of a *central particle* x_i is:

$$R_{ou;x_i,j} = \left(\frac{V_{ou;x_i,j}}{4\pi/3} + \left(\frac{x_i}{2}\right)^3\right)^{1/3} \quad \text{(E.1)}$$

where $V_{ou;x_i,j}$ is the volume of outer product for the *central particle* with diameter x_i at time t_j. With progress of the hydration process, small particles may become embedded in the shell of the hydration products of big particles. Due to the effect of embedded particles, the big particles will exhibit an extra growth. An algorithm is proposed in the HYMOSTRUC3D-E to calculate the total outer product volume of a particle by considering the embedded particles.

E.1 Extra growth thickness of a PC particle

The total outer product volume at time t_j $V_{ou,tot;x_i,j,PC}$ is:

$$V_{ou,tot;x_i,j,PC} = V_{ou,central,j,PC} + V_{ou,<x_i,j,PC} + V_{ou,<x_i,j,BFS} + V_{ou,<x_i,j,FA} + V_{ou,<x_i,j,CH} \quad \text{(E.2)}$$

where $V_{ou,central,j,PC}$ is the growth of the shell caused by hydration of the *central particle*. $V_{ou,<x_i,j,PC}$, $V_{ou,<x_i,j,BFS}$, $V_{ou,<x_i,j,FA}$, $V_{ou,<x_i,j,CH}$ are the growth of the shell caused by embedding of PC, BFS, FA, and CH, respectively. The diameters of embedded particles are assumed to be $< x_i$.

For $V_{ou,central,j,PC}$, it holds:

$$V_{ou,central,j,PC} = V_{x_i,PC} \times \alpha_{x_i,j,PC} \times (\nu_{j,T,PC} - 1) \quad \text{(E.3)}$$

where $V_{x_i,PC}$ is the volume of the *central particle*, $\alpha_{x_i,j,PC}$ is the degree of hydration of the *central particle*, and $\nu_{j,T,PC}$ is the volume increase ratio of hydration products to reactants of PC. CH is not taken into account in the outer shell of the *central particle*.

For $V_{ou,<x_i,j,PC}$, it holds:

$$V_{ou,<x_i,j,PC} = V_{ou,tot;x_i,j,PC} \times \zeta_{sh,x_i,PC,PC} \times \left[\alpha_{<x_i,j,tot,PC} \times \left(\nu_{j,T,PC} - 1\right) + 1\right] \quad \text{(E.4)}$$

where $V_{ou,tot;x_i,j,PC}$ is the total outer product volume of the *central particle* (extra the growth of the shell is taken into account). $\zeta_{sh,x_i,PC,PC}$ is the shell density of PC particles ($< x_i$) in the cell of the *central particle*. $\alpha_{<x_i,j,tot,PC}$ is the degree of hydration of the PC particles ($< x_i$) in the cell of the *central particle*. $\nu_{j,T,BFS}$ is the volume increase ratio of reaction products to reactants of BFS.

For $V_{ou,<x_i,j,BFS}$, it holds:

$$V_{ou,<x_i,j,BFS} = V_{ou,tot;x_i,j,PC} \times \zeta_{sh,x_i,BFS,PC} \times \left[\alpha_{<x_i,j,tot,BFS} \times \left(\nu_{j,T,BFS} - 1\right) + 1\right] \quad \text{(E.5)}$$

where $\zeta_{sh,x_i,BFS,PC}$ is the shell density of BFS particles ($< x_i$) in the cell of the *central particle*. $\alpha_{<x_i,j,tot,BFS}$ is the degree of reaction of the BFS particles ($< x_i$) in the cell of the *central particle*. $\nu_{j,T,BFS}$ is the volume increase ratio of reaction products to reactants of BFS.

$V_{ou,<x_i,j,FA}$ is:

$$V_{ou,<x_i,j,FA} = V_{ou,tot;x_i,j,PC} \times \zeta_{sh,x_i,FA,PC} \times \left[\alpha_{<x_i,j,tot,FA} \times \left(\nu_{j,T,FA} - 1\right) + 1\right] \quad \text{(E.6)}$$

where $\zeta_{sh,x_i,FA,PC}$ is the shell density of FA particles ($< x_i$) in the cell of the *central particle*. $\alpha_{<x_i,j,tot,FA}$ is the degree of reaction of the FA particles ($< x_i$) in the cell of the *central particle*. $\nu_{j,T,FA}$ is the volume increase ratio of reaction products to reactants of FA.

$V_{ou,<x_i,CH}$ is:

$$V_{ou,<x_i,CH} = V_{ou,tot;x_i,j,PC} \times \zeta_{sh,x_i,CH,PC} \quad \text{(E.7)}$$

where $\zeta_{sh,x_i,CH,PC}$ is the shell density of CH particles ($< x_i$) in the cell of the *central particle*.

By solving Eq. E.1 to E.7, the total outer product volume at time t_j, $V_{ou,tot;x,j,PC}$ is:

$$V_{ou,tot;x,j,PC} = \frac{V_{x_i,PC} \times \alpha_{x_i,j,PC} \times (\nu_{j,T,PC} - 1)}{\begin{Bmatrix} 1 - \zeta_{sh,x_i,PC,PC} \times \left[\alpha_{<x_i,j,tot,PC} \times \left(\nu_{j,T,PC} - 1\right) + 1\right] \\ -\zeta_{sh,x_i,BFS,PC} \times \left[\alpha_{<x_i,j,tot,BFS} \times \left(\nu_{j,T,BFS} - 1\right) + 1\right] \\ -\zeta_{sh,x_i,FA,PC} \times \left[\alpha_{<x_i,j,tot,FA} \times \left(\nu_{j,T,FA} - 1\right) + 1\right] - \zeta_{sh,x_i,CH,PC} \end{Bmatrix}} \quad \text{(E.8)}$$

The embedded volumes of PC, BFS, FA and CH for the *central particle* of PC are:

$$V_{em,x_i,j,PC,PC} = V_{ou,tot;x_i,j,PC} \times \zeta_{sh,x_i,PC,PC} \quad \text{(E.9)}$$

$$V_{em,x_i,j,BFS,PC} = V_{ou,tot;x_i,j,PC} \times \zeta_{sh,x_i,BFS,PC} \quad \text{(E.10)}$$

$$V_{em,x_i,j,FA,PC} = V_{ou,tot;x_i,j,PC} \times \zeta_{sh,x_i,FA,PC} \quad \text{(E.11)}$$

$$V_{em,x_i,j,CH,PC} = V_{ou,tot;x_i,j,PC} \times \zeta_{sh,x_i,CH,PC} \quad \text{(E.12)}$$

Fig. E.1 shows the embedded cement volume in outer shells of hydrating particles obtained with HYMOSTRUC (Fig. E.1a) and HYMOSTRUC3D-E (Fig. E.1b). For the PC particle with larger size, the embedded cement volume in outer shells is larger. For the same particle size, the embedded cement volume in outer shells obtained with HYMOSTRUC is larger than that obtained with HYMOSTUC3D-E. The reason for this is in HYMOSTRUC3D-E CH phase is not taken into account to calculate the volume increase ratio $\nu_{j,T,PC}$ of products to reactants of hydrating PC. As a result, the thickness of the shell of hydrating PC particles in HYMOSTRUC3D-E is smaller than that of the shell of hydrating PC particles in HYMOSTRUC.

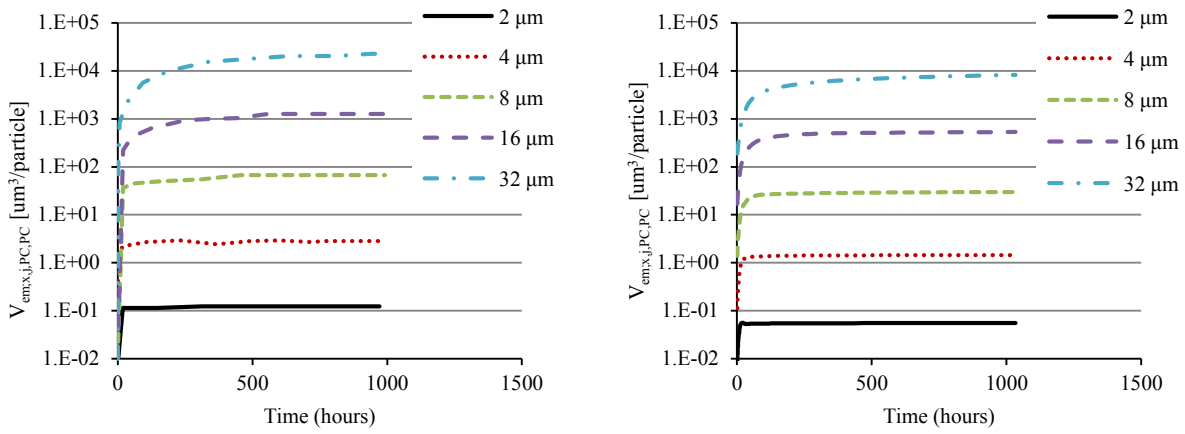

(a) *(b)*

Fig. E.1 Embedded cement volume in outer shells of hydrating particles obtained with HYMOSTRUC (a) and HYMOSTRUC3D-E (b). (w/c = 0.5, for the properties of PC see Table 8.2 in [Van Breugel, 1991])

The increase of weight $\Delta w_{x_i,j,PC}$ of water consumed by the hydration of central PC particle is:

$$\Delta w_{x_i,j,PC} = w_{chem,j,PC} \times \Delta\alpha_{x_i,j,PC} \times \pi(x_i)^3 \times \rho_{PC}/(6 \times \rho_{wa}) \quad \text{(E.13)}$$

The increase of weight of water consumed by the hydration (or reaction) of embedded PC, BFS and FA are:

$$\Delta w_{em;x_i,j,PC,PC} = w_{chem,j,PC} \times \Delta\alpha_{<x_i,j,tot,PC} \times V_{em,x_i,j,PC,PC} \times \rho_{PC}/\rho_{wa} \quad \text{(E.14)}$$

$$\Delta w_{em;x_i,j,BFS,PC} = w_{chem,j,BFS} \times \Delta\alpha_{<x_i,j,tot,BFS} \times V_{em,x_i,j,BFS,PC} \times \rho_{BFS}/\rho_{wa} \quad \text{(E.15)}$$

$$\Delta w_{em;x_i,j,FA,PC} = w_{chem,j,FA} \times \Delta\alpha_{<x_i,j,tot,FA} \times V_{em,x_i,j,FA,PC} \times \rho_{FA}/\rho_{wa} \quad \text{(E.16)}$$

E.2 Extra growth thickness of a BFS particle

The extra growth thickness of a BFS particle is calculated with an algorithm similar to that for a PC particle. The total outer product volume $V_{ou,tot;x,j,BFS}$ of a BFS particle (extra growth is taken into account) at time t_j is:

$$V_{ou,tot;x,j,BFS} = \frac{V_{x_i,BFS} \times \alpha_{x_i,j,BFS} \times (\nu_{j,T,FA} - 1)}{\left\{\begin{matrix} 1 - \zeta_{sh,x_i,PC,BFS} \times \left[\alpha_{<x_i,j,tot,PC} \times (\nu_{j,T,PC} - 1) + 1\right] \\ -\zeta_{sh,x_i,BFS,BFS} \times \left[\alpha_{<x_i,j,tot,BFS} \times (\nu_{j,T,BFS} - 1) + 1\right] \\ -\zeta_{sh,x_i,FA,BFS} \times \left[\alpha_{<x_i,j,tot,FA} \times (\nu_{j,T,FA} - 1) + 1\right] - \zeta_{sh,x_i,CH,BFS} \end{matrix}\right\}} \quad \text{(E.17)}$$

where $V_{x_i,BFS}$ is the volume of the *central particle*. $\alpha_{x_i,j,BFS}$ is the degree of hydration of the central BFS particle. $\zeta_{sh,x_i,PC,BFS}$, $\zeta_{sh,x_i,BFS,BFS}$, $\zeta_{sh,x_i,FA,BFS}$, $\zeta_{sh,x_i,CH,BFS}$ are the shell density of embedded PC, BFS, FA and CH ($< x_i$) in the cell of central BFS particle.

The embedded volumes of PC, BFS, FA and CH for central BFS particle are:

$$V_{em,x_i,PC,BFS} = V_{ou,tot;x_i,j,BFS} \times \zeta_{sh,x_i,PC,BFS} \quad \text{(E.18)}$$

$$V_{em,x_i,BFS,BFS} = V_{ou,tot;x_i,j,BFS} \times \zeta_{sh,x_i,BFS,BFS} \quad \text{(E.19)}$$

$$V_{em,x_i,FA,BFS} = V_{ou,tot;x_i,j,BFS} \times \zeta_{sh,x_i,FA,BFS} \quad \text{(E.20)}$$

$$V_{em,x_i,CH,BFS} = V_{ou,tot;x_i,j,BFS} \times \zeta_{sh,x_i,CH,BFS} \quad \text{(E.21)}$$

The increase of weight of water consumed by the hydration of central BFS particle $\Delta w_{x_i,j,BFS}$ is:

$$\Delta w_{x_i,j,BFS} = w_{chem,j,BFS} \times \Delta\alpha_{x_i,j,BFS} \times \pi(x_i)^3 \times \rho_{BFS}/(6 \times \rho_{wa}) \quad \text{(E.22)}$$

The increase of weight of water consumed by the hydration (or reaction) of embedded PC, BFS and FA for the central BFS particle are:

$$\Delta w_{em;x_i,j,PC,BFS} = w_{chem,j,PC} \times \Delta\alpha_{<x_i,j,PC} \times V_{em,x_i,j,PC,BFS} \times \rho_{PC}/\rho_{wa} \quad \text{(E.23)}$$

$$\Delta w_{em;x_i,j,BFS,BFS} = w_{chem,j,BFS} \times \Delta\alpha_{<x_i,j,BFS} \times V_{em,x_i,j,BFS,BFS} \times \rho_{BFS}/\rho_{wa} \quad \text{(E.24)}$$

$$\Delta w_{em;x_i,j,FA,BFS} = w_{chem,j,FA} \times \Delta\alpha_{<x_i,j,FA} \times V_{em,x_i,j,FA,BFS} \times \rho_{FA}/\rho_{wa} \quad \text{(E.25)}$$

E.3 Extra growth thickness of a FA particle

The extra growth thickness of a FA particle is calculated with an algorithm similar to that for a PC particle. The total outer product volume $V_{ou,tot;x,j,FA}$ of FA at time t_j is:

$$V_{ou,tot;x,j,FA} = \frac{V_{x_i,FA} \times \alpha_{x_i,j,FA} \times (\nu_{j,T,FA} - 1)}{\begin{Bmatrix} 1 - \zeta_{sh,x_i,PC,FA} \times [\alpha_{<x_i,j,tot,PC} \times (\nu_{j,T,PC} - 1) + 1] \\ -\zeta_{sh,x_i,BFS,FA} \times [\alpha_{<x_i,j,tot,BFS} \times (\nu_{j,T,BFS} - 1) + 1] \\ -\zeta_{sh,x_i,FA,FA} \times [\alpha_{<x_i,j,tot,FA} \times (\nu_{j,T,FA} - 1) + 1] - \zeta_{sh,x_i,CH,FA} \end{Bmatrix}} \quad \text{(E.26)}$$

where $V_{x_i,FA}$ is the volume of the *central particle*. $\alpha_{x_i,j,FA}$ is the degree of reaction of the *central particle*. $\zeta_{sh,x_i,PC,FA}$, $\zeta_{sh,x_i,BFS,FA}$, $\zeta_{sh,x_i,FA,FA}$, $\zeta_{sh,x_i,CH,FA}$ are the shell density of embedded PC, BFS, FA and CH ($< x_i$) in the cell of central FA particle.

The embedded volumes of PC, BFS, FA and CH for the central FA particle are:

$$V_{em,x_i,j,PC,FA} = V_{ou,tot;x_i,j,FA} \times \zeta_{sh,x_i,PC,BFS} \quad \text{(E.27)}$$

$$V_{em,x_i,BFS,FA} = V_{ou,tot;x_i,j,FA} \times \zeta_{sh,x_i,BFS,BFS} \quad \text{(E.28)}$$

$$V_{em,x_i,FA,FA} = V_{ou,tot;x_i,j,FA} \times \zeta_{sh,x_i,FA,BFS} \quad \text{(E.29)}$$

$$V_{em,x_i,CH,FA} = V_{ou,tot;x_i,j,FA} \times \zeta_{sh,x_i,CH,BFS} \quad \text{(E.30)}$$

The increase of weight of water consumed by the hydration of central FA particle $\Delta w_{x_i,j,FA}$ is:

$$\Delta w_{x_i,j,FA} = w_{chem,j,FA} \times \Delta\alpha_{x_i,j,FA} \times \pi(x_i)^3 \times \rho_{FA}/(6 \times \rho_{wa}) \quad \text{(E.31)}$$

The increase of weight of water consumed by the hydration (or reaction) of embedded PC, BFS and FA are:

$$\Delta w_{em;x_i,j,PC,FA} = w_{chem,j,PC} \times \Delta\alpha_{<x_i,j,PC} \times V_{em,x_i,j,PC,FA} \times \rho_{PC}/\rho_{wa} \quad \text{(E.32)}$$

$$\Delta w_{em;x_i,j,BFS,FA} = w_{chem,j,BFS} \times \Delta\alpha_{<x_i,j,BFS} \times V_{em,x_i,j,BFS,FA} \times \rho_{BFS}/\rho_{wa} \quad \text{(E.33)}$$

$$\Delta w_{em;x_i,j,FA,FA} = w_{chem,j,FA} \times \Delta\alpha_{<x_i,j,FA} \times V_{em,x_i,j,FA,FA} \times \rho_{FA}/\rho_{wa} \quad \text{(E.34)}$$

F: Thermodynamic equations of ions in the pore solution

If the solid phase of CH is present in the system, the concentrations of Ca^{2+} and OH^- in the pore solution depends on the solubility product constant of CH (according to thermodynamic principles *[Damidot et al., 2011]*). It holds:

$$\frac{\{CH^0\}}{\{Ca^{2+}\} \times \{OH^-\}^2} = \frac{1}{c_{Ca^{2+}} \times \gamma_{Ca^{2+}} \times (c_{OH^-})^2 \times (\gamma_{OH^-})^2} = K_{sp,CH} \quad \text{(F.1)}$$

where $\{CH^0\}$, $\{Ca^{2+}\}$, $\{OH^-\}$ are the activities of ions, $\gamma_{Ca^{2+}}$ and γ_{OH^-} are the activity coefficients of ions (The activity coefficients of ions is a factor used in thermodynamics to account for deviations from ideal behaviour in a mixture of chemical substances). $K_{sp,CH}$ is the solubility product constant of CH. Its value is $10^{5.2}$ calculated from the thermodynamic data summarized by Blanc et al. *[2010]*.

Similarly, if the solid phase of gypsum is present in the system, the concentrations of Ca^{2+} and SO_4^{2-} in the pore solution depend on the solubility product constant of gypsum. It holds:

$$\frac{\left\{C\bar{S}H_2{}^0\right\}}{\{Ca^{2+}\} \times \{SO_4^{2-}\} \times \{H_2O\}^2} = \frac{1}{c_{Ca^{2+}} \times \gamma_{Ca^{2+}} \times c_{SO_4^{2-}} \times \gamma_{SO_4^{2-}}} = K_{sp,gyp} \quad \text{(F.2)}$$

where $K_{sp,gyp}$ is the solubility product constant of gypsum. Its value is $10^{4.65}$ using the thermodynamic data in Blanc et al. *[2010]*.

The activity coefficients of ions are calculated with Davies equation *[Hummel et al., 2002]*:

$$log_{10}\gamma_{Ca^{2+}} = 4 \times A \times \left(C_D \times I_m - \frac{\sqrt{I_m}}{1+\sqrt{I_m}}\right) \quad \text{(F.3)}$$

$$log_{10}\gamma_{OH^-} = A \times \left(C_D \times I_m - \frac{\sqrt{I_m}}{1+\sqrt{I_m}}\right) \quad \text{(F.4)}$$

$$log_{10}\gamma_{SO_4^{2-}} = 4 \times A \times \left(C_D \times I_m - \frac{\sqrt{I_m}}{1+\sqrt{I_m}}\right) \quad \text{(F.5)}$$

where A is a constant (0.510 $kg^{1/2} \cdot mol^{-1/2}$), C_D is a constant (0.2), I_m is the strength of ions in the pore solutions.

Based on the charge balance between positive and negative ions in the pore solution, it holds:

$$c_{Na^+} + c_{K^+} + 2 \times c_{Ca^{2+}} = 2 \times c_{SO_4^{2-}} + c_{OH^-} \quad \text{(F.6)}$$

According to the definition of ions strength, it holds:

$$I_m = 0.5 \times \left(c_{Na^+} + c_{K^+} + 4 \times c_{Ca^{2+}} + 4 \times c_{SO_4^{2-}} + c_{OH^-}\right) \quad \text{(F.7)}$$

As shown in Table F.1, four cases are used to solve the thermodynamic equations of the concentrations of Ca^{2+}, SO_4^{2-}, and OH^-.

Table F.1 Four cases of the simulation of pore solution chemistry of cement paste

Case No.	status of CH	status of gypsum
Case 1	solid CH is present	solid gypsum is present
Case 2	solid CH is present	solid gypsum not present
Case 3	solid CH is not present	solid gypsum is present
Case 4	solid CH is not present	solid gypsum not present

Accordingly, the equations used to calculate the concentration of Ca^{2+}, SO_4^{2-}, and OH^- should be different. These equations are summarized as follows.

(1) Thermodynamic equations: case 1

In this case solid gypsum and CH are present in the system. By combining Eq. (F.1) to Eq. (F.5) it holds:

$$c_{Ca^{2+}} \times 10^{4 \times A \times \left(C_D \times I_m - \frac{\sqrt{I_m}}{1+\sqrt{I_m}}\right)} \times (c_{OH^-})^2 \times 10^{2 \times A \times \left(C_D \times I_m - \frac{\sqrt{I_m}}{1+\sqrt{I_m}}\right)} = \frac{1}{K_{sp,CH}} \quad \text{(F.8)}$$

$$c_{Ca^{2+}} \times 10^{4 \times A \times \left(C_D \times I_m - \frac{\sqrt{I_m}}{1+\sqrt{I_m}}\right)} \times \left(c_{SO_4^{2-}}\right)^2 \times 10^{4 \times A \times \left(C_D \times I_m - \frac{\sqrt{I_m}}{1+\sqrt{I_m}}\right)} = \frac{1}{K_{sp,gyp}} \quad \text{(F.9)}$$

By solving Eq. (F.6) to Eq. (F.9), the concentrations of Ca^{2+}, SO_4^{2-}, and OH^- can be obtained. Since both solid gypsum and CH are present in the system, two conditions should be checked: 1) The amount of CH and gypsum in the system should larger than the amount of Ca^{2+} dissolved in the solution; 2) The amount of gypsum in the system should be larger than the amount of SO_4^{2-} dissolved in the solution. If the calculated concentrations of Ca^{2+} and SO_4^{2-} do not fit the above two conditions, case 2 will be checked.

(2) Thermodynamic equations: case 2

In this case only solid CH is present in the system. By combining Eq. (F.1), (F.3) and (F.4) it

holds:

$$c_{Ca^{2+}} \times 10^{4\times A\times\left(C_D\times I_m-\frac{\sqrt{I_m}}{1+\sqrt{I_m}}\right)} \times (c_{OH^-})^2 \times 10^{2\times A\times\left(C_D\times I_m-\frac{\sqrt{I_m}}{1+\sqrt{I_m}}\right)} = \frac{1}{K_{sp,CH}} \quad \text{(F.10)}$$

Solid gypsum is not present in the system in Case 2. It means all the gypsum in the system is dissolved. Thus, $c_{SO_4^{2-}}$ can be calculated from the remaining gypsum in the system:

$$c_{SO_4^{2-}} = \frac{n_{re,j,gyp}}{V_{fr,j,wat,tot}} \quad \text{(F.11)}$$

where $n_{re,j,gyp}$ is the amount (in mole) of remaining gypsum in the system.

By solving Eq. (F.6), Eq. (F.7), Eq. (F.10) and Eq. (F.11), the concentrations of Ca^{2+}, SO_4^{2-}, and OH^- can be obtained. Since only solid CH is present in the system, there will be two conditions: 1) The amount of CH and gypsum in the system should be larger than the amount of Ca^{2+} dissolved in the solution; 2) The saturated amount of SO_4^{2-} in the solution should be larger than the amount SO_4^{2-} dissolved in the solution. If the calculated concentrations of Ca^{2+} and SO_4^{2-} do not fit the above two conditions, case 3 will be checked.

(3) Thermodynamic equations: case 3

In this case, only solid gypsum is present in the system. By combining Eq. (F.2), Eq. (F.3) and Eq. (F.5), it holds:

$$c_{Ca^{2+}} \times 10^{4\times A\times\left(C_D\times I_m-\frac{\sqrt{I_m}}{1+\sqrt{I_m}}\right)} \times c_{SO_4^{2-}} \times 10^{4\times A\times\left(C_D\times I_m-\frac{\sqrt{I_m}}{1+\sqrt{I_m}}\right)} = \frac{1}{K_{sp,gyp}} \quad \text{(F.12)}$$

CH is not present in the system in Case 3. It means all the CH in the system is dissolved. Thus, the concentration of Ca^{2+} can be calculated from the remaining CH in the system:

$$c_{Ca^{2+}} = \frac{n_{j,CH,tot}}{V_{fr,j,wat,tot}} + c_{SO_4^{2-}} \quad \text{(F.13)}$$

where $n_{j,CH,tot}$ is the amount (in mole) of remaining CH in the system.

By solving Eq. (F.6), Eq. (F.7), Eq. (F.12) and Eq. (F.13), the concentrations of Ca^{2+}, SO_4^{2-}, and OH^- can be obtained. Since only solid gypsum is present in the system, there will be two conditions: 1) The amount of gypsum in the system should be larger than the amount of SO_4^{2-}dissolved in the solution; The saturated amount of Ca^{2+} in the solution should be larger than the amount of Ca^{2+} dissolved in the solution. If the calculated concentrations of Ca^{2+} and SO_4^{2-} do not fit the above two conditions, case 4 will be checked.

(4) Thermodynamic equations: case 4

In this case either solid CH or gypsum is present in the system. Because solid gypsum is not present in the system in Case 4, all the gypsum in the system is dissolved. Thus, the concentration of SO_4^{2-} can be calculated from the amount of remaining gypsum in the system:

$$c_{SO_4^{2-}} = \frac{n_{re,j,gyp}}{V_{fr,j,wa,tot}} \quad \text{(F.14)}$$

Because solid CH is not present in the system in Case 4, all the CH in the system is dissolved. Hence, the concentration of Ca^{2+} can be calculated from the amount of remaining CH in the system:

$$c_{Ca^{2+}} = \frac{n_{j,CH,tot}+n_{re,j,gyp}}{V_{fr,j,wa,tot}} \quad \text{(F.15)}$$

By solving Eq. (F.6), Eq. (F.7), Eq. (F.14) and Eq. (F.15), the concentrations of Ca^{2+}, SO_4^{2-}, and OH^- can be obtained. Since either solid CH or gypsum is present in the system, there will be two conditions: 1) The saturated amount of SO_4^{2-} in the solution should be larger than the amount of SO_4^2 dissolved in the solution. 2) The saturated amount of Ca^{2+} in the solution should be larger than the amount of Ca^{2+} dissolved in the solution. If the calculated concentrations of Ca^{2+} and SO_4^{2-} do not fit the above two conditions, case 4 will be not right.

G: Densities and molar mass of phases in the simulation

Table G.1 Densities and molar mass of cementitious materials in the simulation

Name	Formula	Densities [g/cm^3]	Molar mass [g/mole]
Tricalcium silicate	C_3S	3.21 *	228.3
Dicalcium silicate	C_2S	3.28 *	172.2
Tricdcium aluminate	C_3A	3.03 *	270.2
Tetracalcium aluminoferrite	C_4AF	3.73 *	485.9
Gypsum	$C\bar{S}H_2$	2.32 *	172.1
CSH (PC)	$C_{1.7}SH_4$	2.05 $^{\Delta}$	227.4
Calcium hydroxide	CH	2.24 *	74.10
Ettringite	$C_6A\bar{S}_3H_{32}$	1.75 *	1254.4
Monosulphaste	$C_4A\bar{S}H_{12}$	1.99 *	622.2
Hydrogarnet	C_3AH_6	2.52 *	378.8
Iron hydroxide	FH_3	2.2 *	214
CSH (BFS)	$C_{1.42}SH_{2.92}A_{0.046}$	2.27	197.0
Hydrotalcite	$M_{4.6}AH_{19}$	1.80 -	629.3
Tetracalcium aluminate hydrate	C_4AH_{19}	1.80 -	668.4
Strätlingite	C_2ASH_8	1.94 -	418.2
CSH (FA)	$C_{1.1}SH_{3.9}$	2.12 *	191.9

*Note: * is from Bentz et al. [1994]. ¯ is from Chen et al. [2007a]. CSH (PC), CSH (BFS), CSH (FA) means the CSH produced the hydration (or reaction) of PC, BFS, FA, respectively. $^{\Delta}$ is from Thomas et al. [2010]*

Propositions

1. Simulating the pore structure is crucial for simulating the growth of CH crystals in cementitious materials, because the growth of CH crystals is hindered by the pore wall.
2. A PhD candidate doing modelling work must be familiar with two languages. First is the natural language used to communicate with supervisors and colleagues. Second is the programming language used to communicate with computers.
3. Ignoring unexpected simulation results may keep us going in the wrong direction.
4. A good numerical model for a complex phenomenon should leave its room for extension.
5. On the road to success persistence is your best friend.
6. Discussion sparks new ideas.
7. An idea is only valuable after being realized.
8. Living without an aim, is like sailing without a compass (John Ruskin).
9. Working smart is better than working hard. However, working hard provides fertile soil for smart ideas.
10. All knowledge of reality starts from experience and ends in it (Albert Einstein).

These propositions are regarded as opposable and defendable, and have been approved as such by the promotors Prof. dr. ir. Klaas van Breugel and Prof. Jiang Xiong Wei.

Curriculum Vitae

Personal information

Name	Peng Gao (高鹏)
Birth date	28 June 1986
Birth place	Chongqing, China
Email	p.gao@foxmail.com

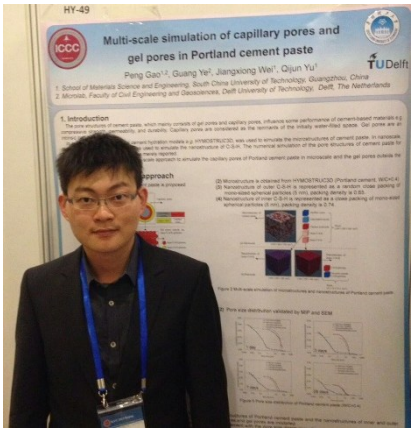

Education background

10/2013-06/2018

Dual PhD in Delft University of Technology (The Netherlands) and South China University of Technology (China)

09/2010-10/2013

PhD candidate in South China University of Technology (China)

09/2009-07/2010

Master of Material Science in South China University of Technology (China)

09/2005-07/2009

Bachelor of Material Science and Engineering in South China University of Technology (China)

Publications – Journal paper

[1] **P. Gao**, T.S Zhang, J.X. Wei, Q.J. Yu, *Evaluation of RRSB distribution and lognormal distribution for describing the particle size distribution of graded cementitious materials*, Powder Technology, 2018, 331: 137–145.

[2] **P. Gao**, T.S Zhang, R.F. Luo, J.X. Wei, Q.J. Yu, *Improvement of autogenous shrinkage measurement for cement paste at very early age: Corrugated tube method using non-contact sensors*, Construction and Building Materials, 2014,55: 57-62.

[3] X.W. Ouyang, **P. Gao**, G. Ye, K. van Breugel, *Effect of filler-hydrates adhesion properties on cement paste strength*, ACI Materials Journal, In press.

[4] H. Dong, H.Z. Zhang, Y.B. Zuo, **P. Gao**, Guang. Ye, *Relationship between the size of the samples and the interpretation of the mercury intrusion results of an artificial sandstone*, *Materials*, 2018, 11, 201.

[5] H. Dong, **P. Gao**, G. Ye, *Characterization and comparison of capillary pore structures of digital cement pastes*, Materials and Structures, 2017,50(2):154.

[6] G. Sherzer, **P. Gao**, E. Schlangen, G. Ye, E. Gal, *Upscaling Cement Paste Microstructure to Obtain the Fracture, Shear, and Elastic Concrete Mechanical LDPM Parameters*, Materials, 2017,10(3): 242.

[7] M. Wyrzykowski, J. Sanahuja, L. Charpin, M. Königsberger, C. Hellmich, B. Pichler, L. Valentini, T. Honório, V. Smilauer, K. Hajkova, G. Ye, **P.Gao**, C. Dunant, A. Hilaire, S. Bishnoi, *M. Azenha, Numerical benchmark campaign of COST Action TU1404–microstructural modelling,* RILEM technical letters, 2017,2: 99–107.

[8] T.S. Zhang, **P. Gao**, R.F. Luo, J.X. Wei, Q.J. Yu, *Volumetric deformation of gap-graded blended cement pastes with large amount of supplementary cementitious materials*, Construction and Building Materials, 2014,54:339–347.

[9] T.S. Zhang, **P. Gao**, R.F. Luo, J.X. Wei, Q.J. Yu, *Effectiveness of novel and traditional methods to incorporate industrial wastes in cementitious materials-An overview*. Resources, Conservation and Recycling, 2013, 74: 134–143.

[10] T.S. Zhang, **P. Gao**, R.F. Luo, Y.Q. Guo, J.X. Wei, Q.J. Yu, *Measurement of chemical shrinkage of cement paste: Comparison study of ASTM C 1608 and an improved method*, Construction and Building Materials, 2013, 48, 662-669.

Publications – Conference paper

[11] **P. Gao**, G. Ye, J.X. Wei, Q.J. Yu, *Numerical simulation of the autogenous shrinkage of hardening Portland cement paste*, ECCOMAS Congress 2016, VIT European Congress of Computational Methods in Applied Sciences and Engineering, Crete Island, Greece, 2016.

[12] **P. Gao**, G. Ye, J.X. Wei, Q.J. Yu, *Simulation of the autogenous shrinkage of slag cement paste in microscale*, 3rd International RILEM Conferences on Microstructure Related Durability of Cementitious Composites, Nanjing, China, 2016.

[13] **P. Gao**, G. Ye, J.X. Wei, Q.J. Yu, Multi-scale simulation of capillary pores and gel pores in Portland cement paste, International Congress on the chemistry of Cement, Beijing, China, 2015.

[14] **P. Gao**, G. Ye, J.X. Wei, Q.J. Yu, *Simulation of the development of pH in the pore solution of slag cement paste at early age*, RILEM International Symposium on Concrete Modelling, Beijing, China, 2014.

[15] **P. Gao**, G. Ye, J.X. Wei, Q.J. Yu, *Investigation of the performance of graded slag cements*, 3rd International Conference on Service Life Design for Infrastructure, Zhuhai, China, 2014.

[16] G. Sherzer, **P. Gao**, G. Ye and E. Gal, *Evaluation of the LDPM Elastic and Fracture Parameters by Up-Scaling Procedure*, Conference segment on Service Life of Cement-Based Materials and Structures, Lyngby, Denmark, 2016.

[17] G. Sherzer, **P. Gao**, G. Ye and E. Gal, *Upscaling Micro Chemical and Mechanical Models to Obtain the LDPM Parameters*, 3rd International Conferences on Microstructure Related Durability of Cementitious Composites, Nanjing, China, 2016.

[18] G. Sherzer, **P. Gao**, E. Schlangen, G. Ye, E. Gal, *Upscaling of the Cement Paste Microstructure response to Obtain the Compressive Mechanical LDPM Parameter*, 4th MC meeting of the COST Action TU1404 will take place in Brussels, Belgium on 12-14 September, 2017 in conjonction with the 2nd International RILEM/COST Conference on Early Age Cracking and Serviceability in Cement-based Materials and Structures.

[19] G. Sherzer, **P. Gao**, E. Schlangen, G. Ye, E. Gal, *Upscaling Cement Paste Microstructure to Obtain the Mechanical LDPM Parameter,* EURO-C 2018 Conference – Computational Modelling of Concrete Structures, will take place in Bad Hofgastein, Austria, 2018.

[20] A. Susanto, **P. Gao**, D.A. Koleva, K. van Breugel, *Electrical Current Flow and Cement Hydration: Implications on Cement-Based Microstructure, 2nd International Conference on Architecture*, Materials and Construction 2016 (ICAMC 2016), Dubai, UAE, 3-5 December, 2016.

[21] H. Dong, **P. Gao**, G. Ye., *Simulation of drying processes in early age cement pastes, 9th international symposium on cement and concrete*, 9th International Symposium on Cement and Concrete, Wuhan, China, 2017.

[22] Z.M. Li, **P. Gao**, G. Ye, *Experimental study on autogenous deformation of metakaolin based geopolymer*, 2nd International RILEM/COST Conference on Early Age Cracking and Serviceability in Cement-based Materials and Structures (EAC2), Belgium, 2017.

Lecture

HYMOSTRUC3D-E training lecture for UltraTech Cement Ltd. (India) during 4-6, April, 2018 in Microlab, TUDelft.

Computer language

C ++ (operation system: windows and Linux)